## THESIS / THÈSE

**DOCTOR OF SCIENCES**

**Rational design, synthesis, molecular modeling and evaluation of -carboline and 5H-indeno[1,2-c]pyridazin-5-one derivatives as potential MAO and IDO inhibitors**

Reniers, Jérémy

*Award date:*
2011

*Awarding institution:*
University of Namur
Chemistry Department
Unit of theoretical and structural physico-chemistry

Link to publication

Facultés
Universitaires
Notre-Dame
de la Paix

# Rational design, synthesis, molecular modeling and evaluation of β-carboline and 5*H*-indeno[1,2-*c*]pyridazin-5-one derivatives as potential MAO and IDO inhibitors

## Faculté des Sciences

DÉPARTEMENT DE CHIMIE

Dissertation présentée par
Jérémy RENIERS
en vue de l'obtention du grade
de Docteur en Sciences

Octobre 2011

FUNDP
Faculté des Sciences
Département de Chimie

# Rational design, synthesis, molecular modeling and evaluation of β-carboline and 5*H*-indeno[1,2-*c*]pyridazin-5-one derivatives as potential MAO and IDO inhibitors

Dissertation présentée par
**Jérémy RENIERS**
en vue de l'obtention du grade
de Docteur en Sciences

Composition du jury :

Prof. S. Vincent (FUNDP, Namur, président du jury)
Prof. R. Kiss (ULB, Bruxelles)
Prof. C. Michiels (FUNDP, Namur)
Dr. R. Frédérick (FUNDP, Namur)
Prof. J. Wouters (FUNDP, Namur, promoteur)

2011

# Conception rationnelle, synthèse, modélisation moléculaire et évaluation de dérivés β-carbolines et 5*H*-indéno[1,2-*c*]pyridazin-5-ones comme inhibiteurs potentiels de la MAO et d'IDO

Par Jérémy Reniers

Résumé:

La monoamine oxydase A (MAO-A) et −B (MAO-B) sont des cibles intéressantes pour une large gamme de thérapies contre des pathologies telles que la dépression, l'anxiété et les maladies de Parkinson et d'Alzheimer. La plupart des inhibiteurs actuels mènent à des effets secondaires par un manque d'affinité et de sélectivité envers une des isoformes. Récemment, les structures cristallographiques de hMAO-A et −B en complexe avec des inhibiteurs ont ouvert le chemin vers la découverte de nouveaux inhibiteurs plus sélectifs et plus puissants. En conséquence, l'objectif principal de ce travail, fut la conception de nouveaux inhibiteurs plus puissants, réversibles et sélectifs de MAO-A ou −B à partir des motifs β-carbolines et 5*H*-indéno[1,2-*c*]pyridazin-5-ones respectivement, en suivant une stratégie classique comprenant une approche expérimentale (synthèse et évaluation biologique) et théorique (modélisation moléculaire). Les pouvoirs d'inhibition sur la MAO ont montré que la substitution du groupe méthoxy de l'harmine par des groupes plus lipophiles augmente l'inhibition de MAO-A. Des études sur les 5*H*-indéno[1,2-*c*]pyridazin-5-ones substituées à la fois aux positions 3 et 8 par des groupes lipophiles ont montré que la substitution en position 3 influence significativement les propriétés d'inhibition de la MAO-B.

De plus, l'implication à travers une même voie métabolique et la similarité dans les propriétés structurales de la MAO avec l'indoléamine 2,3-dioxygénase (IDO) et la lysine spécifique déméthylase 1 (LSD1) respectivement, nous ont amené à l'investigation des β-carbolines et 5*H*-indéno[1,2-*c*]pyridazin-5-ones comme inhibiteurs potentiels d'IDO et de LSD1. Cependant, les deux series n'inhibent pas ces deux systèmes enzymatiques et sont donc sélectives de MAO.

Finalement, en partant de la même stratégie utilisée pour la MAO, nous nous sommes aussi intéressés à la synthèse de deux nouvelles β-carbolines substitutées en position 3 par des groupements aminés et directement dérivées du 3-butyl-β-carboline, un inhibiteur connu d'IDO. Ces deux composés présentent en effet une charge positive à pH physiologique laquelle pourrait établir une interaction coulombienne supplémentaire avec le 7-propionate de l'hème comparé au 3-butyl-β-carboline. Cependant, les premiers résultats tendent à démontrer que l'introduction d'une charge positive abolit l'inhibition d'IDO.

# Rational design, synthesis, molecular modeling and evaluation of β-carboline and 5*H*-indeno[1,2-*c*]pyridazin-5-one derivatives as potential MAO and IDO inhibitors

By Jérémy Reniers

Abstract:

Monoamine oxidase A (MAO-A) and –B (MAO-B) are attractive targets for a broad range of treatments against pathologies including depression, anxiety disorders, Parkinson's and Alzheimer's diseases. Most current MAO inhibitors lead to side effects by a lack of affinity and selectivity towards one of the isoforms. Recently, the crystal structures of hMAO-A and –B in complex with inhibitors opened the way towards the discovery of new, more selective and potent inhibitors. Thus, the main objective of this work, was the design of new, more potent, reversible and selective MAO-A or –B inhibitors derived from β-carboline and 5*H*-indeno[1,2-*c*]pyridazin-5-one scaffolds respectively, following a classical strategy including experimental (synthesis and biological evaluation) and theoretical (molecular modeling) approaches. The MAO inhibitory potencies showed that the replacement of the methoxy group of harmine by more lipophilic groups increases the inhibition for MAO-A. Studies on 5*H*-indeno[1,2-*c*]pyridazin-5-one scaffold bearing lipophilic groups in the 3 and 8-positions showed that the substitution in the 3-position dramatically influences the MAO-B-inhibiting properties.

Furthermore, the involvement through a same metabolic pathway and the similarity in the structural properties of MAO with indoleamine 2,3-dioxygenase (IDO) and lysine specific demethylase 1 (LSD1) respectively, led us to the investigation of the β-carboline and 5*H*-indeno[1,2-*c*]pyridazin-5-one derivatives as potential IDO and LSD1 inhibitors. However, the two series show no inhibition of those two enzymes and are thus selective of MAO.

Finally, starting from the same strategy used for MAO, we are also interested in the synthesis of two new 3-substituted-β-carboline derivatives with amino groups and directly derived from 3-butyl-β-carboline, a known IDO inhibitor. Indeed, these two compounds display a positive charge at physiological pH which might establish an additional coulomb interaction with 7-propionate of the heme compared to 3-butyl-β-carboline. Howerver, first results tend to demonstrate that the introduction of a positive charge abolishes the inhibition of IDO.

Au terme de ces quatre années de thèse passées au sein du laboratoire de Chimie Biologique Structurale, je tiens à exprimer mes remerciements les plus sincères à toutes les personnes qui ont contribué, de près ou de loin, par leur aide et/ou leur soutien, à l'élaboration de ce travail, parmi eux :

" Ne jamais conclure au-delà de ce que

les expériences présentent " et

" Ne jamais suppléer au silence des faits "


*Lavoisier*

## ABBREVIATIONS

| | |
|---|---|
| AChE | Acetylcholinesterase |
| AD | Alzheimer's disease |
| ADHP | 10-Acetyl-3,7-dihydroxyphenoxazine |
| ALS | Amyotrophic lateral sclerosis |
| AOD | Amine oxidase domain |
| BChE | Butyrylcholinesterase |
| CHES | 2-(*N*-cyclohexylamino)ethane sulfonic acid |
| CNS | Central nervous system |
| CSD | Cambridge structural database |
| DA | Dopamine |
| DCM | Dichloromethane |
| p-DMAB | *para*-Dimethylaminobenzaldehyde |
| DMF | Dimethylformamide |
| DMSO | Dimethylsulfoxide |
| ESI | Electron spray ionization |
| FAD | Flavin adenin dinucleotide |
| GOLD | Genetic optimization for ligand docking |
| HDMs | Histone demethylases |
| HMTs | Histone methyltransferases |
| HPLC | High performance liquid chromatography |
| HRP | Horseradish peroxidase |
| 5-HT | 5-Hydroxytryptamine, serotonin |
| IDO | Indoleamine 2,3-dioxygenase |
| LAH | Lithium aluminium hydride |
| LDR | Luciferin detection reagent |
| LSD1 | Lysine specific demethylase 1 |
| baMAO | Baboon monoamine oxidase |
| boMAO | Bovine monoamine oxidase |
| hMAO | Human monoamine oxidase |
| rMAO | Rat monoamine oxidase |
| MAO-A | Monoamine oxidase type A |
| MAO-B | Monoamine oxidase type B |

| | |
|---|---|
| MAOI | Monoamine oxidase inhibitor |
| MEP | Molecular electrostatic potential |
| MS | Mass spectrometry |
| 1MT | 1-Methyltryptophan |
| NFK | *N*-formylkynurenine |
| NMR | Nuclear magnetic resonance |
| PD | Parkinson's disease |
| PDB | Protein databank |
| Ph | Phenyl |
| PIM | 4-Phenylimidazole |
| Pyr | Pyridine |
| RFU | Relative fluorescence unit |
| RIMAs | Reversible MAO-A inhibitors |
| RLU | Relative luminescence unit |
| RMSD | Root mean square deviation |
| ROS | Reactive oxygen species |
| RP-HPLC | Reverse phase high performance liquid chromatography |
| R.T. | Room temperature |
| SET | Single electron transfer |
| SI | Selectivity index |
| TCA | Trichloroacetic acid |
| TDO | Tryptophan 2,3-dioxygenase |
| TFA | Trifluoroacetic acid |
| THF | Tetrahydrofurane |
| TMS | Tetramethylsilane |
| D-Trp | D-Tryptophan |
| L-Trp | L-Tryptophan |
| UV | Ultraviolet |
| XRD | X-ray diffraction |

**AMINO ACIDS**
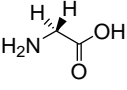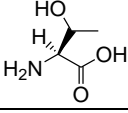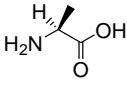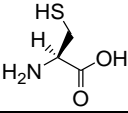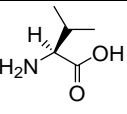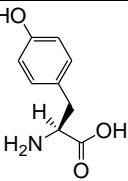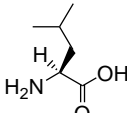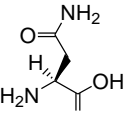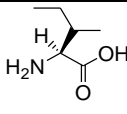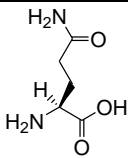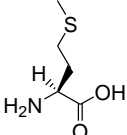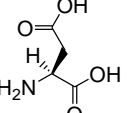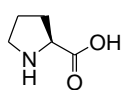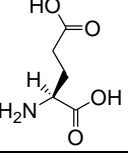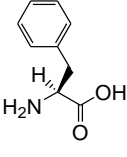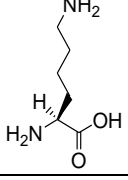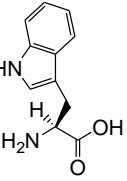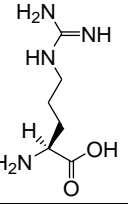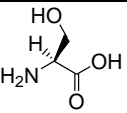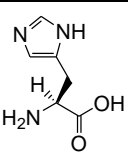
| Amino acid | 3-Letter | 1-Letter | Structure | Amino acid | 3-Letter | 1-Letter | Structure |
|---|---|---|---|---|---|---|---|
| Glycine | Gly | G | | Threonine | Thr | T | |
| Alanine | Ala | A | | Cysteine | Cys | C | |
| Valine | Val | V | | Tyrosine | Tyr | Y | |
| Leucine | Leu | L | | Asparagine | Asn | N | |
| Isoleucine | Ile | I | | Glutamine | Gln | Q | |
| Methionine | Met | M | | Aspartic acid | Asp | D | |
| Proline | Pro | P | | Glutamic acid | Glu | E | |
| Phenylalanine | Phe | F | | Lysine | Lys | K | |
| Tryptophan | Trp | W | | Arginine | Arg | R | |
| Serine | Ser | S | | Histidine | His | H | |

**TABLE OF CONTENTS**

# INTRODUCTION

The discovery in the 1950s of the antidepressant properties of monoamine oxidase inhibitors (MAOIs) was the major finding that led to the monoamine theory of depression [1]. Earlier MAOIs introduced into clinical practice for the treatment of depression were abandoned due to adverse side effects, such as hepatotoxicity, orthostatic hypotension and the so called 'cheese effect' characterized by hypertensive crises. These side effects were hypothesized to be related to non-selective and irreversible monoamine oxidase inhibition.

Since the 1950s, monoamine oxidase A (MAO-A) and –B (MAO-B) have been extensively studied with approximately 20000 published papers listed in databases such as PubMed [2]. This long-term interest stems from their roles in the oxidative catabolism of important amine neurotransmitters. The identification of two isoforms (MAO-A and –B) and the recent determination of the crystal structures of hMAO-A [3] and –B [4] have led to renewed interest in the rational design of potent, specific inhibitors with therapeutic potential and no undesirable side effects.

Nowadays, the therapeutic interest of MAOIs falls into two major categories. Selective MAO-A inhibitors are used as anti-depressant and anti-anxiety drugs whereas selective MAO-B inhibitors are used alone or in combination in the therapy of Alzheimer's and Parkinson's diseases [5].


# 1. MONOAMINE OXIDASE (MAO)

## 1.1 Biological actions of MAO

MAO is a flavoenzyme with the flavin adenine dinucleotide (FAD) covalently bound to a cysteine residue by an 8α-(S-cysteinyl)-flavin linkage. The enzyme is anchored to the mitochondrial outer membrane of neuronal, glial and several other cell types. It catalyzes the oxidative deamination of biogenic and xenobiotic amines to the corresponding aldehyde and ammonia in the periphery as well as in the central nervous system (CNS) (Scheme 1.I) [6-7]. MAO is involved in the biodegradation of aromatic monoamines, including classical neurotransmitters, such as serotonin (5-HT), adrenaline and dopamine, and appears to play a central role in several psychiatric and neurological disorders.

MAO first transforms the amino substrate into imine derivative which is hydrolysed spontaneously to yield the corresponding aldehyde and ammonia. Reoxidation of the cofactor by molecular oxygen produces hydrogen peroxide ($H_2O_2$).

$$H_2O_2 \quad\nwarrow\quad\nearrow\quad MAO\text{-}FAD \quad\nwarrow\quad\nearrow\quad R'CH_2\text{-}NHR''$$
$$\xrightarrow{H_2O}$$
$$O_2 \quad\swarrow\quad\searrow\quad MAO\text{-}FADH_2 \quad\swarrow\quad\searrow\quad R'HC{=}NR'' \qquad\qquad R'CHO + H_2NR''$$
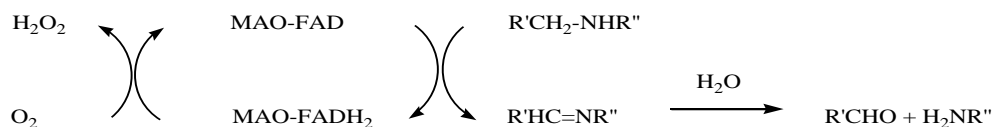
**Scheme 1.I.** Oxidative deamination pathway of monoamines by MAO [7].

## 1.2 MAO subtypes

In mammals, MAO exists in two isoforms, MAO-A and −B. They are encoded by separate genes. MAO-B shares 70% of the amino acid sequence of MAO-A and, in particular, the active center of both enzymes is very similar (RMSD = 0.40 Å) [8]. However, they differ with respect to distribution in body's tissues, and substrate/inhibitor specificity.

### 1.2.1 MAO distribution and localization

MAO-A and −B are tightly associated with the mitochondrial outer membrane. MAO is present in most tissues, but the proportions of the two isoenzymes vary from tissue to tissue. Although in humans they are both expressed in most peripheral tissues and organs, MAO-A is prevalent in fibroblasts and placental tissue [9], while MAO-B is the only isoform in platelets and lymphocytes. In the human brain, there are regional differences in MAO activity: the basal ganglia (striatum) and hypothalamus show the highest levels activity, whereas low levels of activity are observed in the cerebellum and neocortex [10]. The two isoenzymes are not evenly distributed in the human brain, and the main form in the basal ganglia is MAO-B. Immunohistochemical and autoradiographic studies have established that, in the brain, MAO-A is predominantly localized in catecholaminergic neurons, whereas MAO-B is mainly expressed in serotonergic and histaminergic neurons, as well as in astrocytes [9]. This finding, albeit well documented by several laboratories, is in apparent contrast with the pharmacological evidence that serotonin levels are enhanced only following MAO-A, but not MAO-B, inhibition. The reasons of this mismatch, however, are still mostly elusive.

MAO-A levels have also been found to dramatically increase (~9-fold) in the heart of aged rats, thereby suggesting the probability of age-dependent increases in MAO-A levels in humans [2].

### 1.2.2 MAO substrates

The main substrates of the MAO-A and –B isoforms are aromatic monoamines, including the classical neurotransmitters (i.e., 5-HT, dopamine, noradrenaline and adrenaline). Several studies showed that no definite subdivision into substrates highly specific for one or the other isoforms of MAO can be made, and that most natural substrates can be metabolized by both MAO-A and –B [7]. The deamination of the substrates by MAO-A and/or –B in living organisms depends on several factors. These include the kinetic constants ($K_m$ and $k_{cat}$), characteristic for each enzyme form in relation to its various substrates, the ratio between the amount of MAO-A and –B in the tissues and the specific localization of the two enzymes in the different cells. MAO-A preferentially catalyzes the deamination of serotonin (5HT), adrenaline, and noradrenaline [9]. Noradrenaline is considered to be mainly a substrate for MAO-A while it also appears to be metabolized by MAO-B, particularly in tissues expressing high amounts of this isoform [11]. MAO-B preferentially catalyzes the deamination of β-phenylethylamine and benzylamine. *In vitro*, dopamine and other monoamines (such as tryptamine and tyramine) are deaminated by both isoforms, but dopamine *in vivo* is preferentially metabolized by MAO-B [9]. Apart from the substrates already mentioned, MAO-A and –B are able to oxidize a large variety of primary, secondary and tertiary amines [12]. As a general rule primary and secondary amine derivatives are usually deaminated by both forms while tertiary amines seem to be selective MAO-B substrates [13]. This ability to oxidize tertiary amines is thus thought to be a selective feature of MAO-B.

### 1.2.3 Three-dimensional structures

The three dimensional structures of hMAO-A [3] and hMAO-B [4] have been determined and are shown in figure 1.I.
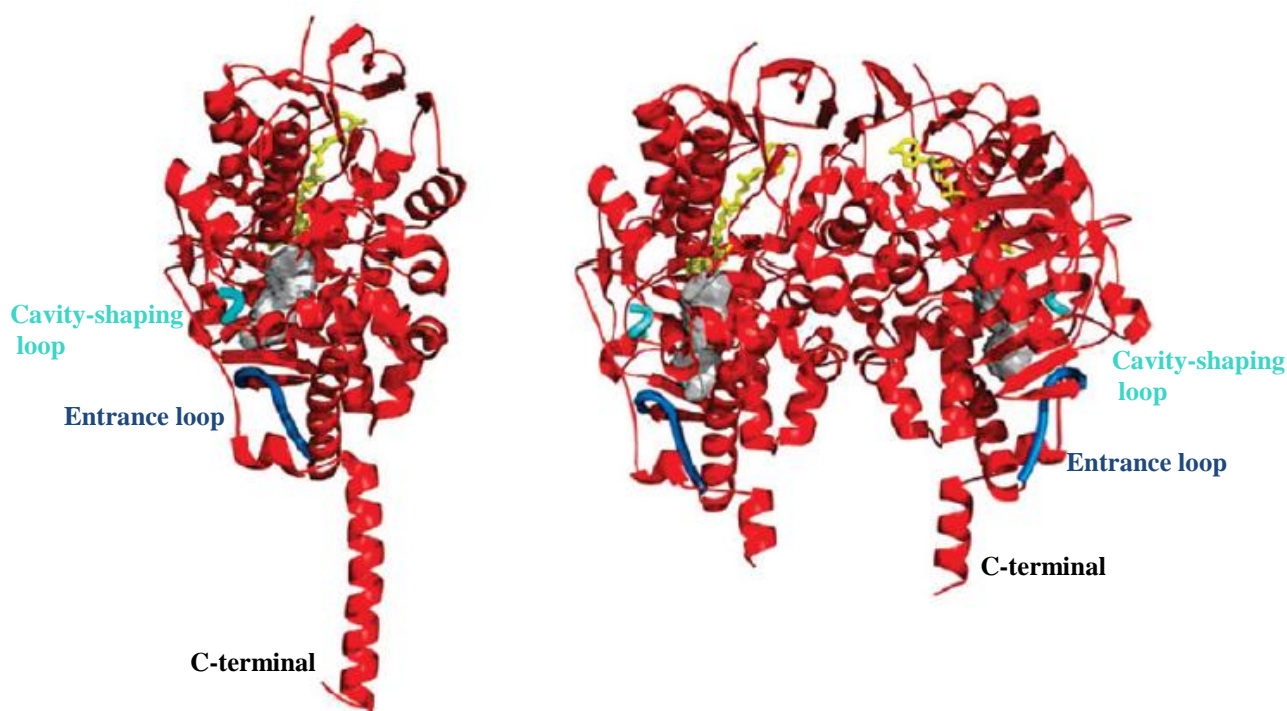
**Figure 1**.**I.** Three-dimensional structures of hMAO-A (left) [3] and hMAO-B (right) [4]. The FAD cofactor is in yellow. The active site cavity in each enzyme molecule is drawn as a gray surface. The cavity-shaping loop (residues 210-216 and 201-207 in hMAO-A and –B respectively) is highlighted in cyan. The entrance loop (residues 108-118 and 99-110 in hMAO-A and –B respectively) is highlighted in blue [2].

The X-ray structure of hMAO-B has been determined in complex with a range of inhibitors to a resolution of 1.60 Å for the best structure (safinamide (**1.I**), 2V5Z.pdb [4], Figure 2.I). Currently, only two X-ray structures of hMAO-A are available in the data bank. Human MAO-A was first co-crystallized with an irreversible inhibitor (clorgyline (**2.I**), 2BXS.pdb [14], Figure 2.I) to a resolution of 3.15 Å. Recently, Son et al have determined the X-ray structure of hMAO-A in complex with a reversible potent inhibitor (harmine (**3.I**), 2Z5X.pdb [3], Figure 2.I) with a better resolution (2.20 Å). The resolution of both structures has provided new insights into the differences that exist between the two human isozymes.

MAO-A and –B have structures with similar folds and with a high degree of identity in their respective $C_\alpha$ coordinates [2]. These structures show that the membrane binding motifs of the enzymes are located in the 35-40 C-terminal residues (Figures 1.I and 3.I). In hMAO-B, this transmembrane region folds into an α-helix protruding perpendicularly from the main globular body of the protein, although the last 20 residues of this motif are too disordered to provide definitive electron density [15] (Figure 1.I, right). The C-terminal part of hMAO-A

displays an electron density sufficiently defined to provide a complete view of the transmembrane α-helix [3] (Figure 1.I, left).
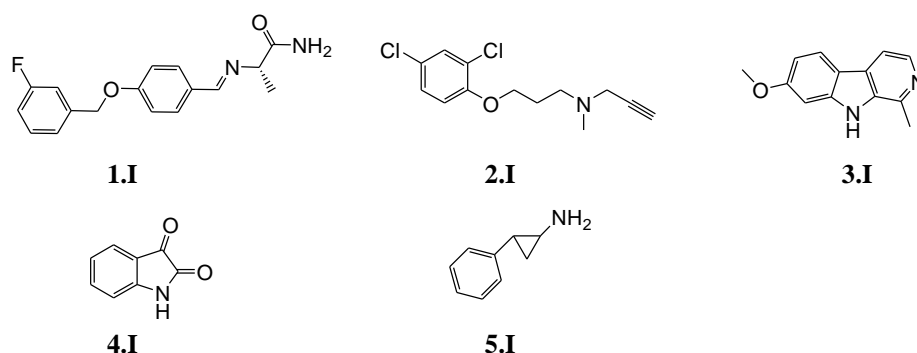


**Figure 2.I.** Chemical structures of safinamide (**1.I**), clorgyline (**2.I**), harmine (**3.I**), isatin (**4.I**) and tranylcypromine (**5.I**).

The protein structures around the active site covalent FAD coenzymes are quite similar among the two isoforms. The position of the FAD cofactor with respect to the overall structure is highly conserved, and the substrate-binding sites consist of elongated cavities (Figure 1.I) whose features will be thoroughly discussed in the next section. In both enzymes, the flavin rings exist in "bent" rather than the more common planar conformations about the N(5)-N(10) axis (Figure 3.I, right), demonstrating strain at the coenzyme binding sites that may have catalytic relevance (*discussed in the section 1.3*).

The largest differences in structures among the two isoforms are the respective natures of their oligomeric states (Figure 1.I) [2]; hMAO-B is a dimer, while hMAO-A is a monomer. A survey of the literature shows membrane proteins are generally oligomeric in the membrane, with dimerization being most common [18]. Recently published data show that hMAO-A and −B enzymes are dimeric in their membrane-bound forms (Figure 3.I, left) [19]. In the detergent-solubilized, purified preparations, hMAO-B is found to remain 100% dimeric, whereas hMAO-A exists only fractionally (50%) in its dimeric form. Dissociation of oligomeric structures of membrane proteins in detergent micelles is found to be the case for MAO-A but not for MAO-B. The hMAO-A monomer species is more likely to crystallize than its dimeric form.
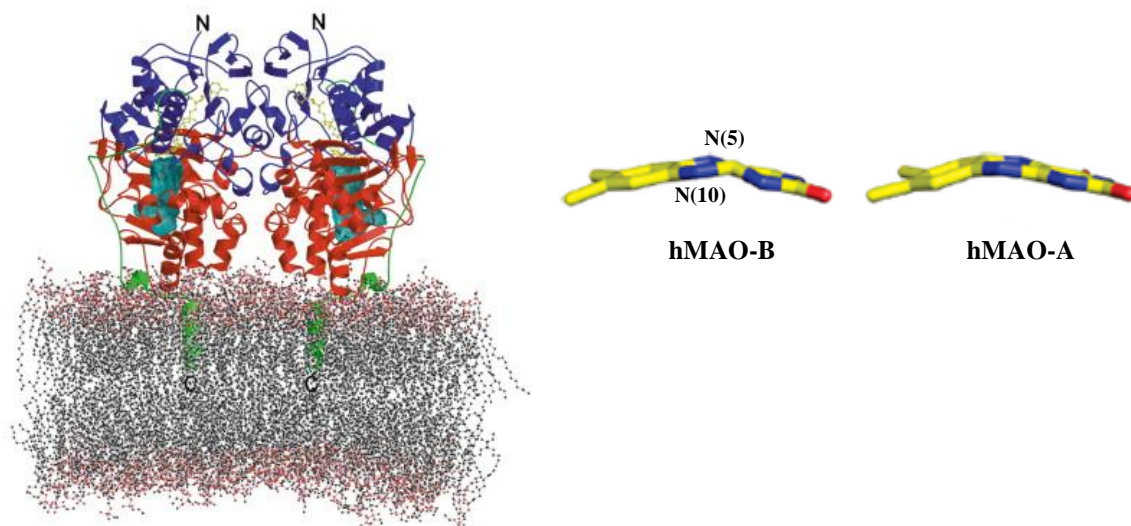
**Figure 3.I.** (Left) Binding mode of hMAO-B (dimeric form) to the outer mitochondrial membrane [16]. (Right) Relative conformations of the isoalloxazine rings in hMAO-B (1OJA.pdb [17]) and hMAO-A (2Z5X.pdb [3]).

## 1.2.4 Structure of active site cavities in hMAO-A and –B [2]

The structural elucidation of hMAO-A and –B revealed that substrate binding and oxidation occurs in elongated cavities extending from the flavin site at the core of the enzyme to the surface of the protein on the opposite side of the FAD adenosine ring (Figures 1.I and 4.I). A comparison of the active sites of hMAO-A and –B is shown in figure 4.I. Although in both enzymes the cavities are generally hydrophobic, details of the active site architectures demonstrate differences in their respective structural properties that account for their distinct substrate and inhibitor specificities. The recently reported 2.20 Å crystal structure of hMAO-A in complex with harmine [3] allows a more detailed comparison of the active sites between the two human enzymes. The volume of the hMAO-A cavity is ~550 Å$^3$ [20], whereas that of the two combined cavities of hMAO-B is ~700 Å$^3$ [21]. The MAO-B cavity is bipartite and is comprised of two separate spaces, the substrate cavity (~400 Å$^3$) and the entrance cavity (~300 Å$^3$). Therefore, MAO-A has a single cavity that exhibits a rounder shape and is larger in volume than the substrate cavity of MAO-B. Analysis of residue side chains in either active site shows the substrate to have less freedom for rotation in the MAO-B site than in MAO-A. Whether the active site of MAO-B is a large single cavity or a bipartite cavity is an example of catalytic site plasticity determined by the conformation of Ile199 (Figure 4.I).

8
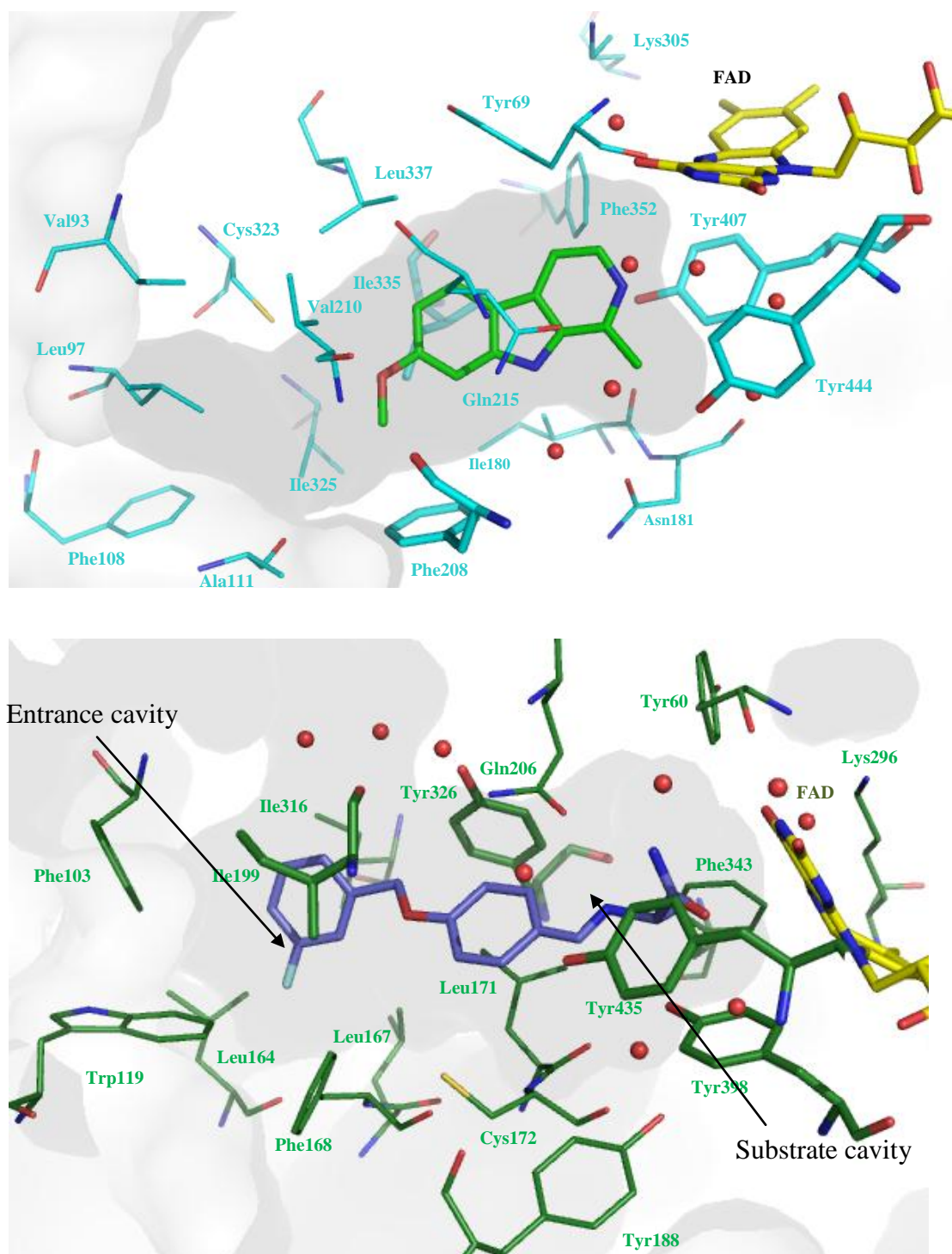
**Figure 4.I.** Active site cavity and inhibitor binding of harmine (**3.I**) in hMAO-A (top, 2Z5X.pdb) and safinamide (**1.I**) in hMAO-B (bottom, 2V5Z.pdb) respectively. The water molecules are displayed as red spheres.

The side chain of this "gating" residue may, depending on the nature of the bound ligand, adopt two different conformations ("closed" and "open") [17]. The cavity can host either small inhibitors (Ile199 into the closed conformation), such as isatin (**4.I**) and

tranylcypromine (**5.I**), or cavity-filling ligands (Ile199 into the open conformation) such as safinamide (**1.I**, Figure 2). In the former case, the active site is restricted to a small cavity separated from an entrance cavity space that opens to the exterior like a funnel, whereas in the latter, the cavity shape is a compact ellipsoid. It is important to note that in all these MAO-B-inhibitor complexes, the position of the active site residues, apart from gating residue Ile199, is highly conserved. From a pharmacological viewpoint, this inhibitory versatility has important implications. Small compounds such as isatin and tranylcypromine, which can be hosted in a limited pocket, show similar binding affinities for both MAO-A and –B, whereas cavity-filling ligands are highly specific MAO-B inhibitors. The corresponding residue in hMAO-A is Phe208, but it does not function as a gating residue (Figure 4.I). Another difference between MAO-A and –B structures also involves the active site cavity structures. The Tyr326 side chain in MAO-B, although not directly involved in the partition of the two cavities, does produce a restriction that is less pronounced in hMAO-A where Ile335 occupies that position. Conserved active site residues in both enzymes include the aromatic cage (formed by Tyr407, Tyr444 and FAD in hMAO-A; Tyr398, Tyr435 and FAD in hMAO-B, Figure 4.I) which is important for recognition and direction of the amine group of the substrate. Positioning of the amine between these residues and the flavin is important for catalysis. Another conserved active site residue includes a Lys residue hydrogen bonded via a water molecule to the N(5) position of the flavin (Lys305 in MAO-A and Lys296 in MAO-B). Other non-conserved residues in the active sites include Ile180 and Asn181 in MAO-A (Leu171 and Cys172 in MAO-B, respectively), which, however, do not significantly affect the shapes of the cavities. Therefore, the MAO-A Phe208-Ile335 and MAO-B Ile199-Tyr326 pairs appear to be major determinants in dictating the differential substrate and inhibitor specificities of the two enzymes.

An intriguing issue in MAO enzymology is to understand where and how the substrates (or inhibitors) are admitted to the active sites. In hMAO-B, the cavity is extended and substrate binding is likely to occur in the proximity of the outer mitochondrial membrane surface region with the entrance loop (residues 99-110) involved in the access (colored blue in figure 1.I). In hMAO-A, the active site cavity is more compact. However, Son et al. [3] have recently demonstrated by site-directed mutagenesis that the conserved Gly110 is important for ensuring flexibility of the entrance loop (residues 108-118) required to provide access for the substrate. Therefore, the structural data suggest that MAO-A and –B ligands follow similar pathways in binding.

Aside from obvious differences in the amino acid residues in the active sites, perhaps the largest difference occurs in the conformation of a 6-residue loop (residues 210–216 in hMAO-A and residues 201-207 in hMAO-B, Figure 1.I) which is referred to as the ''cavity-shaping loop'' [20]. The conformation of this loop has a significant effect on the shape and volume of the substrate binding cavity and probably contributes substantively to the different specificities of the two enzymes.

## 1.3 Mechanistic studies on MAO catalysis [2]

MAO-A and –B catalyze the oxidative deamination of amine neurotransmitters using $O_2$ as the electron acceptor. The catalytic mechanism of MAO catalysis consists of a reductive half reaction where the $C_\alpha$–H bond of the amine is cleaved with the transfer of two reducing equivalents to the flavin to form, respectively the imine and flavin hydroquinone ($E.FAD_{red}$) as shown in the reaction pathway in scheme 2.I [22]. There are two general catalytic reaction pathways (scheme 2.I). For most substrates, both MAO-A and –B follow the lower loop of the pathway in which oxygen reacts with the enzyme product complex ($E.FAD_{red}$ -- Imine) before product has dissociated. There is general consensus that the deprotonated (rather than the protonated) amine moiety on the substrate binds to the active site of the enzymes and is oxidized to the protonated imine (found with both MAO-B and –A) with the FAD cofactor being reduced to its hydroquinone form ($E.FAD_{red}$). To complete the catalytic cycle, the reduced FAD cofactor reacts with $O_2$ to generate oxidized flavin ($E.FAD_{ox}$) and $H_2O_2$. The dissociated protonated imine is released from the enzyme and undergoes a non-catalyzed hydrolysis to form $NH_4^+$ and the corresponding aldehyde.
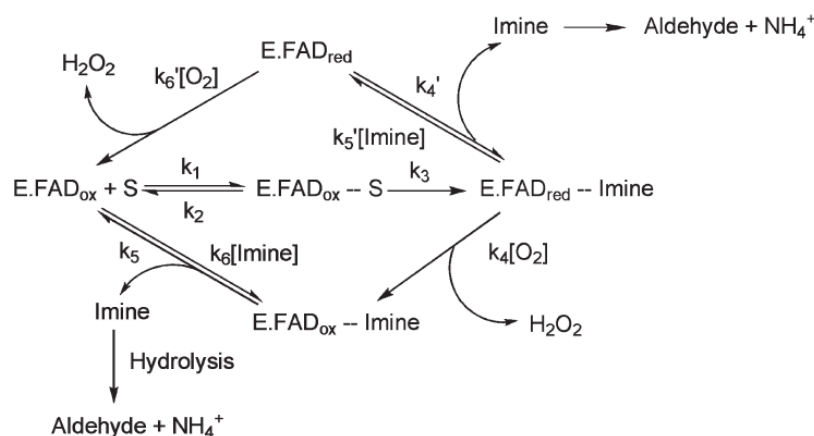


**Scheme 2.I.** General reaction scheme for MAO catalysis [22].

The exact chemical mechanism of this oxidative deamination is, however, still subject to controversy. Currently, two mechanisms are proposed for the reductive half-reaction of MAO catalysis (Scheme 3.I) [22];

- Polar nucleophilic mechanism (Scheme 3.I, top)
- Single electron transfer mechanism (SET) (Scheme 3.I, bottom)

The stereochemistry of the hydrogen transfer step is well-documented to be the pro-*R* H of the substrate for both MAO-A and –B [23]. Furthermore, the *re* face of the covalent FAD forms the amine binding site.

Current mechanistic data do support that both enzymes function by a proton abstraction mechanism with the polar nucleophilic mechanism proposed by Miller and Edmondson for hMAO-A catalysis (Scheme 3.I) [24]. To accomplish this difficult proton abstraction [the $pK_a$ for a benzyl hydrogen is ∼25 [25]], no basic amino acid residues are in the catalytic site, and therefore, the flavin must be activated to become a strong base. This could be accomplished by C(4a) addition of the amine followed by or in conjunction with abstraction of the R-CH group by the resulting basic N(5), which is estimated to exhibit a $pK_a$ of ∼25 from NMR studies of reduced flavin models [26]. The reaction mechanism for this proposed reaction is shown in scheme 3.I (top). Since deprotonated amines do not appear to exhibit the nucleophilicity to readily add to the flavin C(4a) position in model systems and no direct evidence for a stable amine-flavin adduct has been found, one must examine factors in the enzyme that would facilitate this type of reaction. Structural data show the isoalloxazine ring of the flavin to exist in a conformation ∼30° bent from planarity in the oxidized form of the enzyme. This bending has been shown by NMR studies of other flavoenzymes to result in C(4a) being more electrophilic and N(5) being more nucleophilic [27].

A survey of the literature reveals that the SET mechanism for MAO catalysis originally proposed by Lu and co-workers [28] is also favored by a number of investigators (Scheme 3.I, bottom) [22]. This mechanism is based on the rationale that one-electron oxidation of the substrate amine nitrogen results in labilization of the α-CH bond to allow abstraction by a basic residue normally associated with proteins. In spite of considerable experimental effort, no direct evidence has been found for any radical intermediate during substrate oxidation.

Recent theoretical calculations on MAO catalysis have demonstrated the plausibility of the polar nucleophilic mechanism for MAO catalysis [22, 29]. Despite intense research in many

laboratories the mechanism of substrate oxidation in MAO remains to be clarified, with several alternatives having been proposed including a concerted nucleophilic mechanism and a SET mechanism [30].
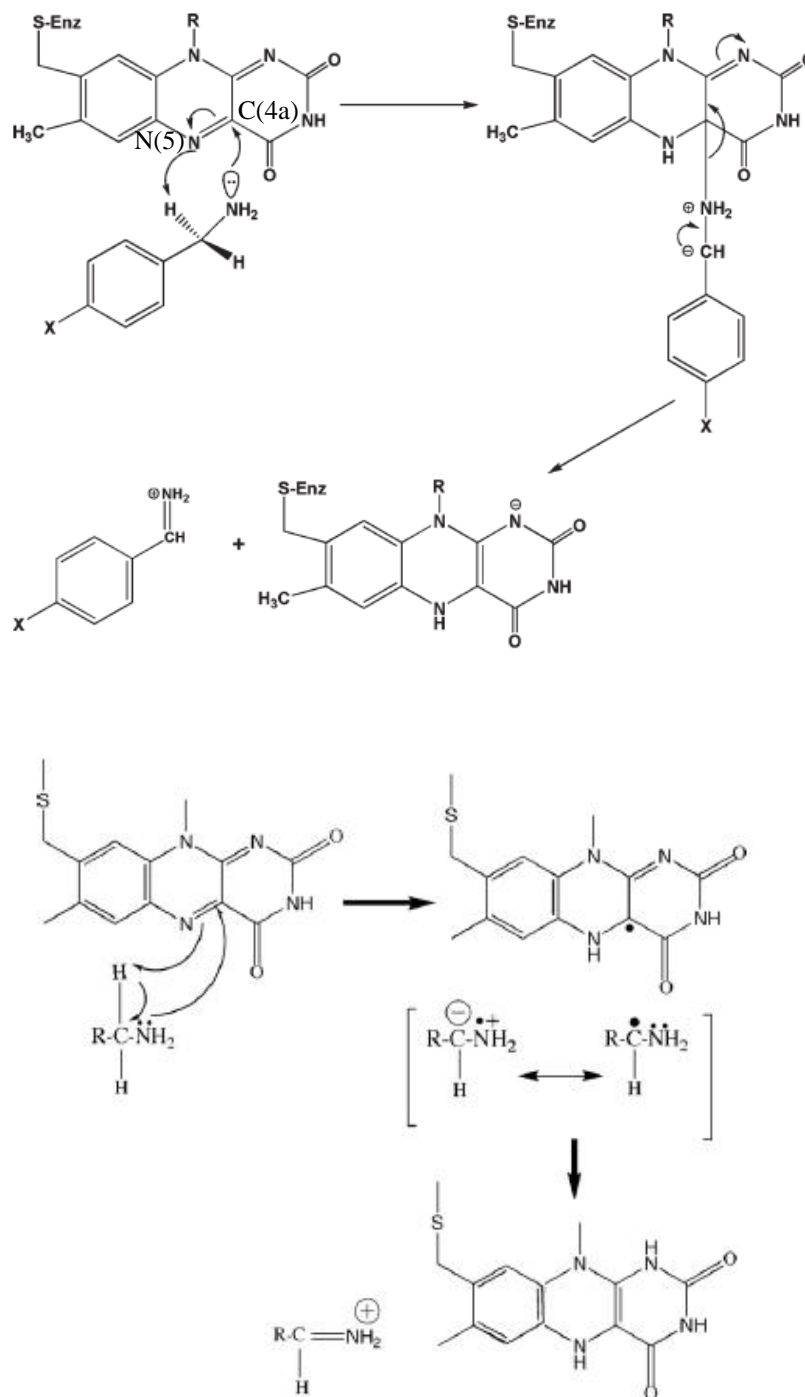


**Scheme 3.I.** Proposed polar nucleophilic (top) and SET (bottom) mechanisms for the reductive half-reaction of MAO catalysis [22].

## 1.4 Therapeutic uses of MAO-A and –B inhibitors

A wide range of MAOIs including reversible and irreversible inhibitors of MAO-A, MAO-B, or both is reported in table 1.I [9-10]. These are proving to have therapeutic value in several diverse conditions, including affective disorders, neurodegenerative diseases, stroke and ageing. The therapeutic use of MAOIs in these conditions is discussed below.

**Table 1.I.** Known MAOIs and their main current or potential therapeutic uses [9-10].

| Group | Class | Compound | MAO selectivity | Inhibition type | Application |
|---|---|---|---|---|---|
| Non-selective | Hydrazines | Isocarboxazid | A and B | Irreversible | Antidepressant |
| | | Phenelzine | A and B | Irreversible | Antidepressant |
| | | Nialamide | A and B | Irreversible | Antidepressant |
| | | Isoniazid | A and B | Irreversible | Antidepressant |
| | | Iproniazid | A and B | Irreversible | Antidepressant |
| | | Iproclozide | A and B | Irreversible | Antidepressant |
| | Amphetamine derivates | Tranylcypromine | A and B | Irreversible | Antidepressant |
| Selective-irreversible | Propargylamines | Clorgyline | A | Irreversible | Antidepressant |
| | | *l*-Deprenyl (Selegiline) | B | Irreversible | Antiparkinson |
| | | Rasagiline | B | Irreversible | Antiparkinson |
| | | 2-HMP (and other aliphatic propargylamines) | B | Irreversible | Antiparkinson |
| | | PF 9601N | B | Irreversible | Antiparkinson |
| Selective-reversible (RIMAS) | Piperidylbenzofurans | Brofaromine | A | Reversible | Antidepressant |
| | Morpholinobenzamides | Moclobemide | A | Reversible | Antidepressant |
| | Oxazolidinones | Toloxatone | A | Reversible | Antidepressant |
| | | Befloxatone | A | Reversible | Antidepressant |
| | | Cimoxatone | A | Reversible | Antidepressant |
| Selective-reversible (MAO-B) | Aminoethylpicolinamide | Lazabemide | B | Reversible | Antiparkinson |
| | Benzylaminopropanamide | Safinamide | B | Reversible | Antiparkinson |
| Mixed MAO-cholinesterase inhibitors | Propylamines | Ladostigil | A and B (brain selective) | Irreversible | Antidepressant, antiparkinson and anti-Alzheimer |
| Other | | M30 | A and B (brain selective) | Irreversible | Antidepressant, antiparkinson and anti-Alzheimer |

2-HMP, N-(2-heptyl)-N-methylpropargylamine

## 1.4.1 Depression and anxiety disorders

MAOIs have been used for decades in the treatment of depression [31-32]. The antidepressant properties of MAOIs result from selective MAO-A inhibition in the CNS, which leads to increased brain levels of dopamine, noradrenaline and serotonin [10]. The development of MAOIs started with the serendipitous finding of antidepressant effects in patients treated with iproniazid (**6.I**), a hydrazine-based antitubercular agent structurally similar to isoniazid (**7.I**) (Figure 5.I, Table 1.I) [9]. Originally proposed as a tuberculostatic agent, iproniazid (**6.I**) was the first modern antidepressant and was introduced into the market under the trade name Marsilid® [33]. This discovery, together with the demonstration that iproniazid (**6.I**) was a potent MAOI, led to the design and production of other MAOIs, such as phenelzine (**8.I**) (Figure 5.I, Table 1.I) [9]. Following the ascertainment that hydrazine-based MAOIs caused liver toxicity, however, novel chemical categories of drugs were established (Table 1.I). Another undesirable side effect of MAO non-selective inhibitors, was the so-called "cheese reaction", consisting in severe, potentially lethal hypertensive crises with cerebral hemorrhages, following the consumption of cheese, wine and other fermented foods, typically rich in tyramine and sympathomimetic amines. Due to the lack of intestinal metabolism by MAO-B, these compounds are absorbed and enter circulation, to induce increased noradrenaline release in the medulla, which in turn activates the sympathetic system and, in the absence of MAO-A-mediated metabolism, causes the sudden increment in blood pressure. The quest for MAOIs devoid of untoward effects prompted research to characterize selective MAO-A and −B inhibitors [9]. Some of the non-selective irreversible inhibitors discussed above, including phenelzine (**8.I**) and tranylcypromine (**5.I**), are still in clinical use along with the reversible MAOIs moclobemide (**9.I**, Moclamine®), befloxatone (**10.I**) and toloxatone (**11.I**, Humoryl®) (Figure 5.I, Table 1.I) [10]. The reversible MAO-A inhibitors (RIMAs) have been reported to be particularly effective in the treatment of depression in elderly patients [34]. MAO-A and non-selective MAOIs seem to be particularly valuable in the treatment of phobic anxiety and atypical depressions, such as those involving hysterical traits, hypersomnia, bulimia, tiredness and impression of rejection, for which they are superior to amine-uptake inhibitors [32].
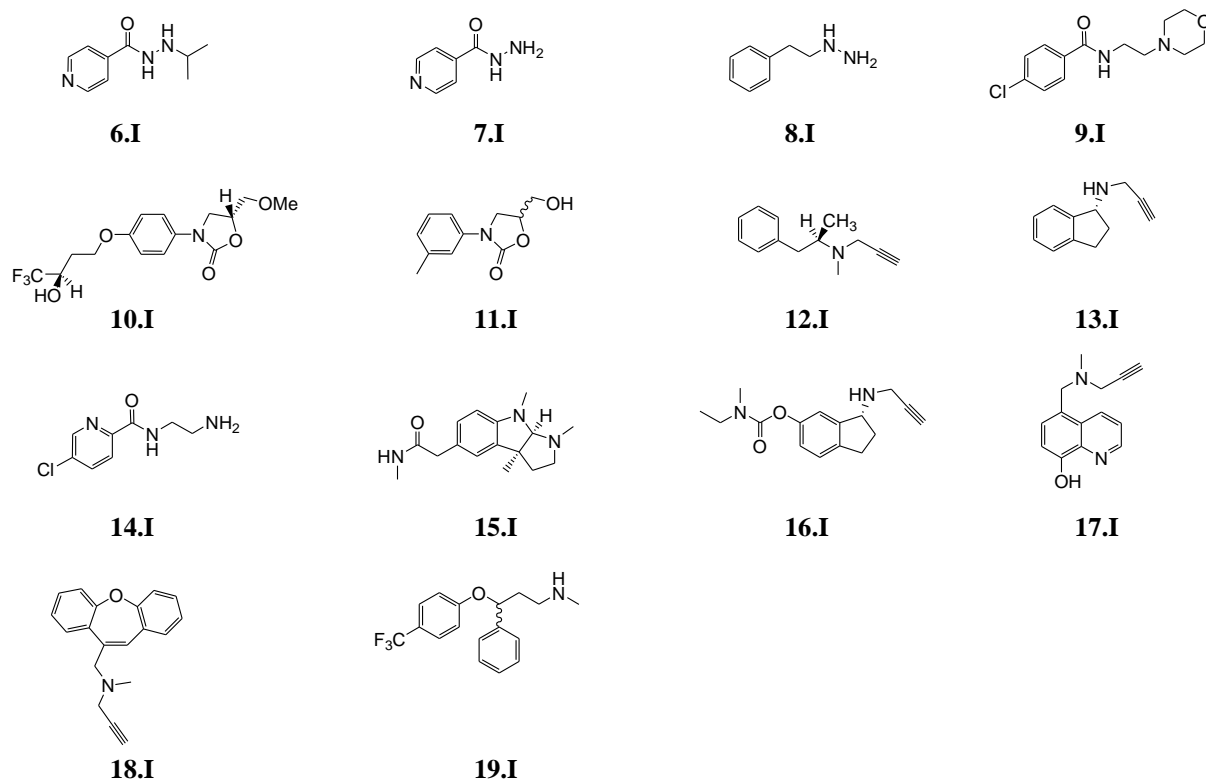
**Figure 5.I.** Chemical structures of iproniazid (**6.I**), isoniazid (**7.I**), phenelzine (**8.I**), moclobemide (**9.I**), befloxatone (**10.I**), toloxatone (**11.I**), *l*-deprenyl (**12.I**), rasagiline (**13.I**), lazabemide (**14.I**), physostigmine (**15.I**), ladostigil (**16.I**), M30 (**17.I**), CGP 3466 (**18.I**) and fluoxetine (**19.I**).

## 1.4.2 Parkinson's disease

The Parkinson's disease (PD) is associated to a neuronal death of the dopaminergic neurons in the substance nigra of the brain [7]. The exact origin of this neuronal death is not yet clearly understood. This neuronal death of the dopaminergic neurons results in a large loss of dopamine (DA) in the brain and throws off the normal dopamine/acetylcholine balance, since the acetylcholine level remains normal. The result of this imbalance is a lack of coordination of the movement that often appears as tremor, stiff muscles and joints, and/or difficulty moving. Currently, there is no way to stop the loss of nerve cells that produce dopamine or to restore those that have already been lost.

The rationale behind the usage of MAO-B inhibitors in PD was originally based on the concept that DA is preferentially deaminated by this isoenzyme in the human nigrostriatal dopaminergic system [9]. The inhibition of this enzyme would result in an increased level of

16

dopamine and therefore conduct to a prolongation of the availability of the dopamine in residual neurons in the substantia nigra [35]. Furthermore, MAO-B is also believed to contribute to the development or progression of the disease [7]. Because the dopamine turnover is elevated in the parkinsonian brain, it follows that the surviving dopaminergic neurons are exposed to an increased flux of hydrogen peroxide ($H_2O_2$) derived as a consequence of MAO-B activity and which contributes to the formation of other ROS (reactive oxygen species) and can trigger mitochondrial damage and neuronal death. Finally, the MAO-B is also responsible of the metabolism of some endogeneous (tetrahydroquinoline) [36] and exogenous compounds (MPTP = 1-methyl-4-phenyl-1,2,3,6-tetrahydropyridine) which are transformed into toxic substances [37]. All such data provide a rationale for the use of MAO-B inhibitors in the treatment of PD.

The use of MAOIs as dopamine-sparing agents or as adjuncts to L-DOPA was considered as a treatment for PD, but such an approach with non-selective inhibitors was abandoned because of the cheese reaction [10]. As levels of MAO-B are increased in the brain of people with PD as a consequence of gliosis, because the human basal ganglia has higher MAO-B than MAO-A activity, and because dopamine is equally well metabolized by both isoenzymes in humans, the selective MAO-B inhibitor *l*-deprenyl (**12.I**, Eldepryl® and Jumex®, Figure 5.I, Table 1.I) was first investigated as an adjuvant to L-DOPA. *l*-Deprenyl (**12.I**) is effective both as an adjuvant to L-DOPA and as monotherapy. Although *l*-deprenyl (**12.I**) seems to slow disease progression during the first year of treatment, no significant effect on the course of the disease was found after that time [10]. Inhibitors that have been demonstrated to be of clinical value include the mechanism based inactivators, *l*-deprenyl (**12.I**) and rasagiline (**13.I**, Figure 5.I, Table 1.I), and reversible inhibitors such as lazabemide (**14.I**) and safinamide (**1.I**, Figure 5.I, Table 1.I) [38]. The efficacy of rasagiline (**13.I**) in early-stage and late-stage PD has previously been demonstrated in phase III clinical trials [39]. Safinamide (**1.I**) is currently in phase III clinical trials for the treatment of PD and displays a novel mode of action as a dopamine modulator (comprising both selective and reversible MAO-B inhibition and also blockade of dopamine reuptake) [4, 40]. From a safety point of view, reversible inhibitors may be therapeutically more desirable than inactivators since MAO-B activity can be regained relatively quickly following withdrawal of the reversible inhibitor. In contrast, return of enzyme activity following treatment with inactivators requires *de novo* synthesis of the MAO-B protein which may require several weeks [38]. For this reason, several studies are currently underway to develop reversible inhibitors of MAO-B.

**1.4.3 Alzheimer's disease**

The origin of the Alzheimer's disease (AD) is not yet clearly understood. It is, however, suggested that the β-amyloid and the tau proteins and genetic factors might play a role in this disease [7, 41]. MAO-B activity has been shown to increase with age and is particularly high around the senile plaques in AD patients [42-43]. The production of the hydroxyl radical from hydrogen peroxide, produced by the MAO-B activity, might also play a role in the development or progression of the disease. It was shown that the hydroxyl radical favor the transformation of the soluble β-amyloid protein into neurotoxic agregated β-amyloid proteins [7].

Age-related increases in MAO-B activity, as well as the neuroprotective effects of its inhibitors, have been considered as rational bases to use selective MAO-B inhibitors in the therapy of AD [9]. Clinical trails with *l*-deprenyl (**12.I**) in patients with AD have not given conclusive results, although MAO-B activity is increased in the brain of such patients and might contribute to oxidative stress in this disorder. Currently, acetylcholinesterase inhibitors are the only drugs approved for the treatment of cognitive dysfunction in AD [10]. Thus, it has been proposed that combined treatment with a MAO-B inhibitor plus one of the approved cholinesterase inhibitors, such as physostigmine (**15.I**, Figure 5.I), could be beneficial for the treatment of AD. A related approach is to combine these two enzyme inhibitory functions in the same molecule. The drug ladostigil (**16.I**, Figure 5.I, Table 1.I) combines the pharmacophore of rasagiline (**13.I**) with a carbamate cholinesterase inhibitory moiety into a single molecule. Its pharmacological activities include neuroprotection, butyrylcholinesterase and acetylcholinesterase inhibition, and brain-selective MAO-A/B inhibition. It appears to be effective in enhancing cognition in old primates, as well as having antidepressant and anxiolytic activity, and is now in clinical trials for AD [10]. M30 (**17.I**, Figure 5.I, Table 1.I) is a brain selective agent characterized by the presence of both propargyl anti-MAO and iron chelating moieties; it might serve as drug for neurodegenerative disorders, such as PD and AD, in which oxidative stress and iron alteration are implicated [44].

**1.4.4 Other neurodegenerative diseases**

Neurodegenerative diseases such as Huntington's disease and amyotrophic lateral sclerosis (ALS) share many of the pathological features of PD and AD, such as oxidative stress, iron accumulation, excitotoxicity, inflammatory processes and the misfolding of toxic proteins that cannot be degraded after ubiquitination [10]. *l*-Deprenyl (**12.I**) treatment has not been successful in the treatment of ALS. However, rasagiline (**13.I**) and CGP 3466 (**18.I**, Figure 5.I) have been reported to be effective in mouse models of ALS [10]. A single-patient study has reported beneficial effects of *l*-deprenyl (**12.I**), in combination with the 5-HT reuptake inhibitor fluoxetine (**19.1**, Prozac®, Figure 5.I), in Huntington's disease [45]. In spite of some promising results in animal models, however, clinical results have not been encouraging so far [9].

**1.4.5 Cerebral ischaemia**

*l*-Deprenyl (**12.I**) decreases the peripheral tissue damage that results from cardiac failure and that arising in the brain from cerebral ischaemia in animal models [10]. This protective effect has been attributed to a decrease in hydrogen peroxide generated by MAO during ischaemia-reperfusion. The results of a Phase II trial with a limited number of participants have confirmed that *l*-deprenyl (**12.I**) can enhance recovery after cerebral infarction [46].

**1.4.6 Ageing**

The process of ageing seems to involve changes in the levels of MAO activity. In human skin fibroblasts cultured from males of between 1 and 60 years of age, the specific activity of MAO-A, assessed during proliferative growth, increased 5 to 10 fold with the age of the donor, whereas the increase in MAO-B activity was less than 3 fold [10].
Increases in human brain MAO-B activity with age have been attributed to glial cell proliferation, whereas for MAO-A activity, both increases and no change have been reported with advancing age [10]. Knoll was first to report that *l*-deprenyl (**12.I**) enhanced the sexual activity and extended the lifespan of rats [47]. This might result from increased antioxidant

capacity and the mobilization of several hormonal factors. The actions of *l*-deprenyl (**12.I**) might increase neuronal survival fitness ('neurofitness') by preventing, or perhaps to some extent reversing, the decline in resistance that is normally associated with cellular ageing. More recent work has shown that *l*-deprenyl (**12.I**) can also enhance the learning ability of aged rats [48].

MAO-A levels have also been found to dramatically increase (~9 fold) in the heart of aged rats, thereby suggesting the probability of age-dependent increases in MAO-A levels in humans [2, 49]. The consequence of this large increase in the level of MAO-A in the heart is suggested to involve increased apoptosis and necrosis of cardiac cells due to increased levels of reactive oxygen species from the $H_2O_2$ produced. As suggested from the work of Parini and co-workers [50], the identification of the involvement of MAO-A in cardiac cellular degeneration thus presents a potential drug target for the development of cardioprotective agents for an aging population. Initial attempts have been published [51]; however, this area of MAO research is still in its infancy.

### 1.4.7 Smoking cessation

MAO-B inhibitors are devoid of antidepressant activity and do not promote the cheese reaction unless administered at concentrations high enough to inhibit MAO-A [10]. However, *l*-deprenyl (**12.I**) and lazabemide (**14.I**) have both been reported to aid smoking cessation and continued abstinence [52-53]. The MAO-A inhibitor moclobemide has been shown to have similar effects, and this might relate to increased levels of 5-HT in the brain [54]. Because MAO-A and −B are inhibited in cigarette smokers [55], this effect might simply be related to the continuation of a level of MAO inhibition to which smokers have become habituated [10].

## 1.5 Concluding remarks

So, the development of MAOIs is important not only from the standpoint of symptomatic treatment (e.g., by increasing the biological half-life of monoamine neurotransmitters), but also with regard to the neuroprotective effects (e.g., prevention or delay of neurodegeneration itself) [56]. All of these aspects have led to an intensive search for novel MAOIs and this

20

effort has increased considerably in recent years. Due to their selective and reversible inhibition of MAO, this new generation of MAOIs displays a safer profile compared to the former irreversible MAOIs, particularly with regard to the cheese-effect, and drug interactions. The next point discusses about diverse series which have also been extensively used as scaffolds in medicinal chemistry programs searching for novel MAO-A and –B inhibitors.

## 1.6 MAO-A and –B inhibitors

### 1.6.1 Indole derivatives

Studies have shown that the indole derivatives may be used for the design of potent anti-MAO agents [57-62]. Previous studies on indolylmethylamine derivatives bearing substituents in the 1 and 5-positions of the indole ring acted as irreversible and selective MAOIs in rat liver mitochondrial [60]. For example, the irreversible MAO-B inhibitor PF9601N (**20a.I**, $K_i$ rMAO-B = 0.75 nM with a selectivity index (SI) **>**1000 toward rMAO-B, Figure **6.I**) shows antioxidant/neuroprotective properties in an experimental model of PD [61] whereas **20b.I** is a potent MAO-A inhibitor ($K_i$ rMAO-A = 0.8 nM with a SI of 5 toward rMAO-A, Figure **6.I**).
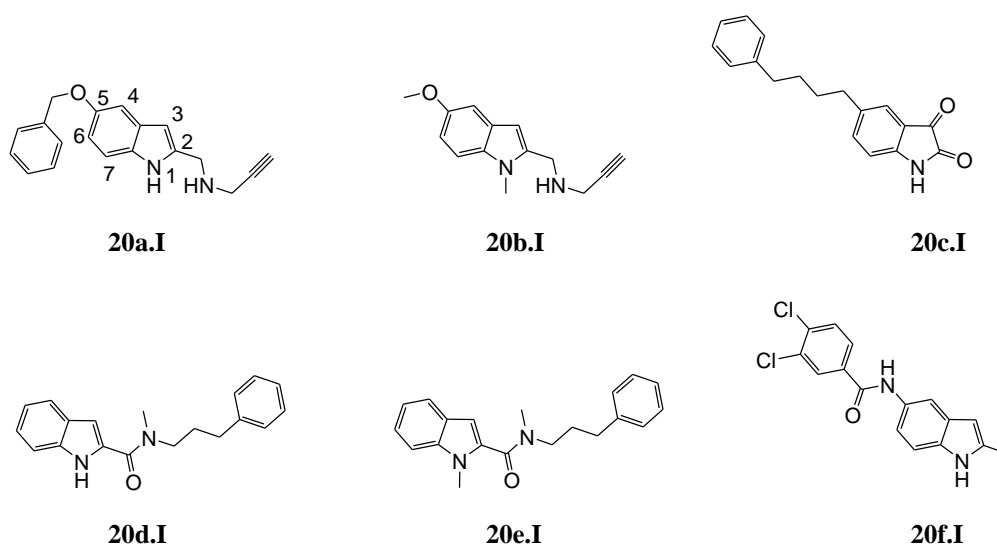


**Figure 6.I.** Chemical structures of indole derivatives (**20a-f.I**).

The small molecule isatin (**4.I**, Figure 2.I) is a natural reversible inhibitor of both hMAO-A and −B ($K_i$ = 15 and 3 µM respectively) [63]. The crystal structure of hMAO-B in complex with isatin has been solved (1OJA.pdb) [17]. The isatin binds within the substrate cavity leaving the entrance cavity of MAO-B unoccupied and so explains the weak affinity of isatin on hMAO-B. In an attempt to identify inhibitors with enhanced potencies and specificities for MAO-B, investigations of additional C5- and C6-substituted isatin analogues with hydrophobic groups toward hMAO-A and −B have revealed that the C5-substituted isatins exhibited higher binding affinities to MAO-B than the corresponding C6-substituted analogues [64]. The most potent and selective MAO-B inhibitor, 5-(4-phenylbutyl)isatin (**20c.I**, Figure 6.I), exhibited a $K_i$ value of 0.28 nM and a SI of 2030 toward hMAO-B, approximately 18500-fold more potent than isatin. Molecular docking studies with MAO-B indicate that the increased binding affinity exhibited by **20c.I** analogue, in comparison to isatin, is best explained by the ability of the lateral chain to bridge both the entrance and substrate cavities of the enzyme.

Recently, La Regina et al have identified new reversible MAOIs with indole scaffold [61]. Several compounds were potent MAO-A or −B inhibitors, and displayed $K_i$ values in the nanomolar concentration range. In particular, **20d.I** ($K_i$ bovine MAO-A ($K_i$ boMAO-A) = 0.92 nM, SI of 68478 toward MAO-A, Figure 6.I) was exceptionally potent and selective as MAO-A inhibitor. Introduction of a methyl group in the 1-position of the indole provided a compound endowed with higher MAO-B inhibitory activity but low selectivity ($K_i$ boMAO-B = 1.5 nM, SI of 29 toward MAO-B, **20e.I**, Figure 6.I).

From the observation that bulky C5 substituents generally increase potency and selectivity for the MAO-B isoform by increasing the molecular lipophilicity, Prins et al have studied a series of indole derivatives with bulky C5 susbtituents on hMAO-A and −B [62]. The most potent reversible MAO-B inhibitor, **20f.I** (Figure 6.I), exhibited a $K_i$ value of 30 nM and was also the most selective MAO-B inhibitor with a SI of 99 toward hMAO-B. An important observation was that chlorine substitution at the C5 phenyl side chain of the indoles enhances both MAO-A and −B inhibition potencies.

## 1.6.2 β-Carbolines

β-Carbolines (pyrido[3,4-*b*]indoles), naturally occurrent in South American plants as harmala alkaloids, contain an indole ring structure within their molecules. β-Carboline alkaloids are psychopharmacologically active compounds that may occur in foods and endogenously in human tissues, including the brain and are reported to be potent inhibitors of MAO-A [65-66]. In the human organism they may be formed from the condensation of the biogenic amines tryptamine and serotonin with aldehydes or α-keto acids, respectively [67].

First experiments have shown that the β-carboline derivatives were more effective inhibitors of MAO than their the 1,2,3,4-tetrahydro and 3,4-dihydro analogues [66, 68-69]. β-carbolines reported in figure 7.I display a reversible competitive inhibition and are selective of MAO-A. Norharman (**21a.I**) is a weak inhibitor of purified MAO-A and −B ($K_i$ hMAO-A = 3.34 μM [69], $K_i$ hMAO-B = 1.12 μM [55]). Methylation in the 1-position of norharman to give harman (**21b.I**, $K_i$ hMAO-A = 0.26 μM [69]) results in a 13-fold decrease in the $K_i$ value. Furthermore, the introduction of a 7-methoxy group (harmine, **3.I**, $K_i$ hMAO-A = 5 nM [69]) decreases the $K_i$ further by 50-fold compared to harman (**21b.I**). The ring reduction of harmine to give harmaline (**21c.I**, $K_i$ hMAO-A = 48 nM [69]) results in a 10-fold increase in the $K_i$ value whereas the 6-methoxy substitution of harmalan (**21d.I**, $K_i$ hMAO-A = 0.39 μM [69]) is less effective (8-fold) compared to 7-methoxy derivative (harmaline, **21c.I**).



**21a.I**  **21b.I**  **3.I**  **21c.I**  **21d.I**
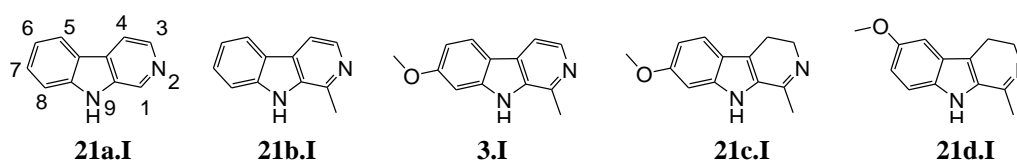
**Figure 7.I.** Chemical structures of β-carbolines (**21a-d.I** and **3.I**).

Recently, the crystal structure of hMAO-A in complex with harmine has been solved (2Z5X.pdb) [3]. Furthermore, Herraiz et al have identified two β-carboline alkaloids, norharman (**21a.I**) and harman (**21b.I**) in tobacco smoke [55] and coffee [70] which inhibited MAO-A (norharman and harman) and −B (norharman) isozymes with a competitive inhibition. The presence of MAOIs like β-carbolines in smoke and coffee might play a role in the neuroactive actions including a purported neuroprotection (i.e., a lower risk for developing PD) associated with coffee consumption and smoke. Indeed, norharman (**21a.I**) might act as a

potential neuroprotective agent by its MAO-B inhibition ability (resulting in a higher dopamine and lower hydrogen peroxide, a ROS). Further research is needed to clarify this topic.

### 1.6.3 5*H*-Indeno[1,2-*c*]pyridazin-5-ones

First studies on 5*H*-indeno[1,2-*c*]pyridazin-5-one scaffold (Table 2.I) as MAOIs performed by the Testa's team have shown that 5*H*-indeno[1,2-*c*]pyridazin-5-one (**22a.I**) is a moderate selective inhibitor of MAO-B (IC$_{50}$ rMAO-B = 27.5 µM, SI of 4 toward rMAO-B) [71]. The substitution in the 3-position with a phenyl group (**22b.I**, IC$_{50}$ rMAO-B = 21.0 µM) increases slightly the inhibition on MAO-B compared to **22a.I** and methylated derivative (**22c.I**, IC$_{50}$ rMAO-B = 74.4 µM) which abolishes the inhibition. Reduction of the carbonyl group to a methylene group (**22d.I**, IC$_{50}$ rMAO-B = 23.4 µM) shows a MAO-B inhibition comparable to corresponding carbonyl derivative (**22b.I**) [71]. This suggests that the presence of carbonyl group is not a critical requisite for MAO-B inhibition. Interestingly, the loss of carbonyl group produces a measurable MAO-A inhibition (compared to **22b.I**).

**Table 2.I.** Chemical structures of 5*H*-indeno[1,2-*c*]pyridazin-5-one derivatives (**22a-m.I**).
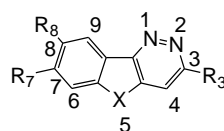


**22a-m.I**

| Compound | X | R$_3$ | R$_7$ | R$_8$ | IC$_{50}$ (µM) |
|----------|-----|-----------|--------------------|-------------------------------------|----------------------------------|
| **22a.I** | CO | H | H | H | 27.5 (rMAO-B) |
| **22b.I** | CO | Ph | H | H | 21.0 (rMAO-B) |
| **22c.I** | CO | Me | H | H | 74.4 (rMAO-B) |
| **22d.I** | CH$_2$ | Ph | H | H | 23.4 (rMAO-B) |
| **22e.I** | CO | 4'-CF$_3$-Ph | H | H | 0.090 (rMAO-B) |
| **22f.I** | CO | 3'-CF$_3$-Ph | H | H | 0.280 (rMAO-B); 0.0085 (hMAO-B) |
| **22g.I** | CO | 4'-NO$_2$-Ph | H | H | 0.500 (rMAO-B) |
| **22h.I** | CO | 4'-OMe-Ph | H | H | 3.22 (rMAO-B) |
| **22i.I** | CO | Me | H | OCH$_2$Ph | 0.170 (rMAO-B) |
| **22j.I** | CO | Me | H | OCH$_2$CH$_2$CH$_2$CF$_3$ | 0.014 (baMAO-B) |
| **22k.I** | CO | Me | H | OCH$_3$ | >1 (rMAO-B) |
| **22l.I** | CO | 3'-CF$_3$-Ph | OCH$_3$ | H | 0.038 (baMAO-B) |
| **22m.I** | CO | 3'-CF$_3$-Ph | H | OCH$_3$ | 0.0001 (baMAO-B) |

24

Derivative **22b.I** was thus taken as a lead compound and its activity optimized by variously substituting the 3-phenyl ring in the 2', 3', and/or 4'-positions [72]. Results show that a given substituent was more favorable in the meta or para than in the ortho position. Para-substituted derivatives (e.g., **22e.I**, $IC_{50}$ rMAO-B = 90 nM) generally appeared as slightly more active than the meta-substituted analogues (e.g., **22f.I**, $IC_{50}$ rMAO-B = 280 nM). Moreover, the introduction of an electron-withdrawing group like nitro (**22g.I**, $IC_{50}$ rMAO-B = 500 nM) or trifluoromethyl (**22e.I**, $IC_{50}$ rMAO-B = 90 nM) is more favorable for activity on MAO-B compared to an electron-donating methoxy group (**22h.I**, $IC_{50}$ rMAO-B = 3.22 μM) on the phenyl ring.

More recently, Novaroli et al have evidenced important species-dependent differences in MAO-B inhibitor specificity between human and rat for 5*H*-indeno[1,2-*c*]-pyridazin-5-one derivatives [73]. Indeed, these derivatives show a greater inhibitory potency toward hMAO-B than toward rMAO-B (e.g., **22f.I**, $IC_{50}$ rMAO-B = 280 nM and $IC_{50}$ hMAO-B = 8.5 nM). Molecular docking simulations of **22f.I** into the active site of hMAO-B show that the 3-phenyl moiety points to the substrate cavity [73].

Other studies performed by our group on 5*H*-indeno[1,2-*c*]pyridazin-5-one scaffold bearing lipophilic and bulky side chains in the 8-position show that groups like benzyloxy (**22i.I**, $IC_{50}$ rMAO-B = 170 nM) and trifluorobutyloxy (**22j.I**, $IC_{50}$ baboon MAO-B ($IC_{50}$ baMAO-B) = 14 nM) increase the selectivity and inhibitory potency on MAO-B compared to methoxy derivative (**22k.I**, $IC_{50}$ rMAO-B **>**1 μM), and **22a.I** [74-75]. Furthermore, both benzyloxy and trifluorobutyloxy derivatives do not inhibit MAO-A. Investigation of the regioisomeric structures established that substitution of the 5*H*-indeno[1,2-*c*]pyridazin-5-one core in the 7 vs 8-positions dramatically influences the MAO-inhibiting properties of these compounds (e.g., **22l.I**, $IC_{50}$ baMAO-B = 38.0 nM and **22m.I**, $IC_{50}$ baMAO-B = 0.10 nM) [74]. Moreover, neither compounds inhibited MAO-A confirming their very good selectivity profile. These data show thus differences in MAO-B inhibitory potency of these indeno[1,2-*c*]pyridazin-5-one regioisomers. Molecular docking simulations for **22j.I** in hMAO-B revealed that compound positions in the vicinity of the FAD cofactor with the trifluorobutoxy side chain settling within the entrance cavity lined with hydrophobic amino acid residues [75].

## 1.6.4 Other inhibitors

### 1.6.4.1 Azines

Carotti et al have recently extended the study of condensed azines on the MAO effects to the families of indeno-fused, pyrimidines (**23a.I**, Figure 8.I) and 1,2,4-triazines (**23b-c.I**, Figure 8.I) [76]. The preference toward the MAO isoenzymes proved to be dependent on the type of azine-containing tricyclic scaffold. Indeed, **23b.I** (21% of rMAO-A inhibition at 10 μM and $IC_{50}$ rMAO-B = 6.31 μM) is a selective MAO-B inhibitor more potent than the 5*H*-indeno[1,2-*c*]pyridazin-5-one analogue (**22b.I**, $IC_{50}$ rMAO-B = 21.0 μM, Table 2.I) whereas the indeno-pyrimidinone fusion isomer (**23a.I**, $IC_{50}$ rMAO-A = 2.37 μM with a SI of 5 toward MAO-A) moderately inhibits both MAO isoenzymes with a preference toward MAO-A. A major outcome of this study was the identification of **23c.I** as a new promising MAO-B selective inhibitor ($IC_{50}$ rMAO-B = 80 nM).
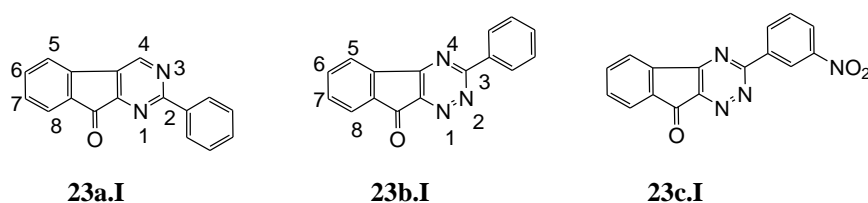


**Figure 8.I.** Chemical structures of azine derivatives (**23a-c.I**).

### 1.6.4.2 Benzopyran and benzofuran derivatives

#### a) Coumarins

Coumarins are benzopyrones which have been intensively studied for their MAO inhibitory activity [4-5, 73, 77-84]. Variations mainly in the 3, 4, and 7-positions of the coumarin core revealed that most of the compounds acted preferentially on MAO-B with $IC_{50}$ and $K_i$ values in the micromolar to low-nanomolar range. 7-Benzyloxy-3,4-dimethylcoumarin (**24a.I**, Figure 9.I, $IC_{50}$ hMAO-B = 1.1 nM) is a potent reversible and selective inhibitor toward hMAO-B [73] whereas high inhibitory activities toward rMAO-A were also measured for sulfonic acid esters as **24b.I** (Figure 9.I, $IC_{50}$ rMAO-A = 10.7 nM with a SI of 1349 toward rMAO-A) [77, 79]. These results demonstrate a key role of the 7-substituent, the ether derivatives being MAO-B selective but the sulfonic acid esters displaying MAO-A selectivity [77]. The study

26

of coumarin-3-carboxamides reported potent and selective inhibitors of hMAO-B with $IC_{50}$ values in the nanomolar range (e.g., **24c.I**, Figure 9.I, $IC_{50}$ = 1.4 nM with a SI of 6664 toward hMAO-B) [5]. Recently, structures of hMAO-B in complex with two coumarin derivatives (**24d.I** and **24e.I**, Figure 9.I) were determined by X-ray crystallography at high resolution (1.7 and 2.0 Å respectively) [4]. These compounds competitively inhibit hMAO-B with $K_i$ values of 0.10 and 0.40 μM respectively with a SI of 27 and 157 toward hMAO-B. Furthermore, **24d.I** is an *in vivo* potent and selective MAO-B inhibitor. In *ex vivo* experiments, it showed a rapid blood-brain barrier penetration, short-acting and reversible inhibitory activity, and low *in vitro* toxicity [83]. On the basis of this preliminary preclinical profile, this inhibitor could be viewed as a promising clinical candidate for the treatment of neurodegenerative diseases. Santana et al have recently discovered that the introduction of bulky groups in the 7-acetonyl substituent of coumarin scaffold increases MAO-A selectivity [81]. **24f.I** (Figure 9.I) is a potent MAO-A inhibitor ($IC_{50}$ hMAO-A = 7.2 nM) and displays a high MAO-A specificity (1000-fold higher compared to MAO-B). The introduction of bulky groups such as cyclohexyl or phenyl in the 3,4-positions of the 7-acetonyl derivatives increases both MAO-A and –B inhibitory activities with concomitant loss of selectivity, whereas the replacement of the acetonyl substituent in the 7-position by the bromoallyloxy group (**24g.I**, Figure 9.I, $IC_{50}$ hMAO-B = 1.5 nM) shows a high activity and selectivity for MAO-B (1600-fold higher compared to hMAO-A) [81]. More recently, **24h.I** (Figure 9.I) was found to be a potent inhibitor of hMAO-B ($IC_{50}$ hMAO-B = 0.80 nM) and inactive at 100 μM on hMAO-A [82].



**24a.I**          **24b.I**          **24c.I**          **24d.I**

**24e.I**          **24f.I**          **24g.I**          **24h.I**
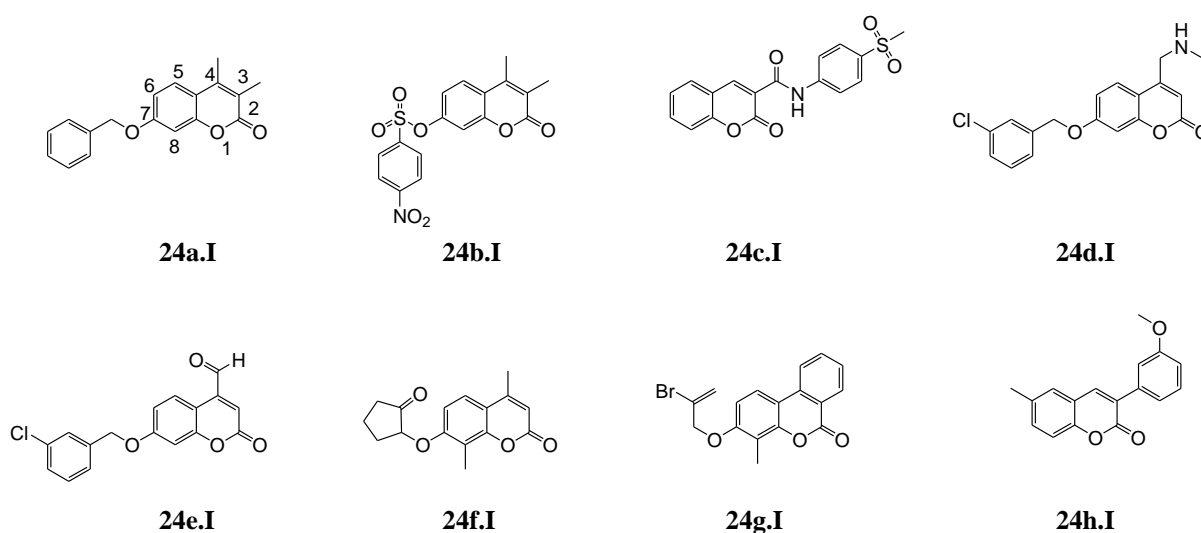
**Figure 9.I.** Chemical structures of coumarin derivatives (**24a-h.I**).

## b) Chromone, flavanone and xanthone derivatives

Chromone-3-carboxylic acid (**25a.I**, Figure 10.I) was identified as a potent hMAO-B inhibitor ($IC_{50}$ hMAO-B = 48 nM) with a high degree of selectivity for hMAO-B compared to hMAO-A (SI >2083 toward hMAO-B) [56]. A recent study on flavone, thioflavone and flavanone derivatives as potential MAOIs has shown that the most active series was the flavanone one with higher selective inhibitory activity for hMAO-B [85]. **25b.I** (Figure 10.I) was identified as the most potent and selective hMAO-B inhibitor within this series ($IC_{50}$ hMAO-B = 0.13 µM with a SI >769 toward hMAO-B). The introduction of a double bond in the flavones and of the sulfur in the thioflavones leads to a relevant decrease in the inhibitory activity although keeping a hMAO-B selectivity. The xanthone derivatives are known for their ability to reversibly inhibit MAO [86]. **25c.I** (Figure 10.I, $IC_{50}$ hMAO-A = 40 nM with a SI of 825 toward hMAO-A) emerged as a potent and selective inhibitor.
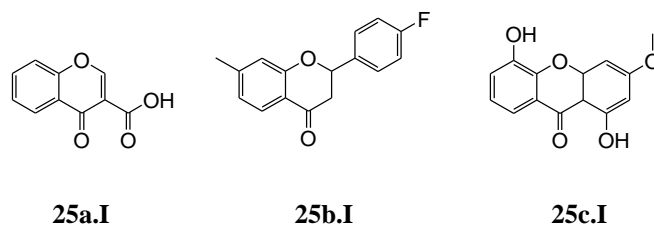


**Figure 10.I.** Chemical structures of chromone (**25a.I**), flavanone (**25b.I**) and xanthone (**25c.I**) derivatives.

## c) Benzofuran derivatives

From the observation that bulky C5 substituents in indole scaffold generally increase potency and selectivity for the MAO-B isoform by increasing the molecular lipophilicity, Prins et al have studied a series of benzofuran derivatives with bulky C5 susbtituents on hMAO-A and –B [62]. **26.I** (Figure 11.I) was the most potent reversible MAO-B inhibitor in this series with a $K_i$ value of 0.19 µM but is less selective (SI of 5 toward hMAO-B).
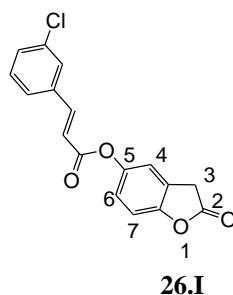


**Figure 11.I.** Chemical structure of benzofuran derivative (**26.I**).

An important observation is that chlorine substitution at the C5 phenyl side chain of the benzofuran enhances both MAO-A and –B inhibition potencies.

1.6.4.3 Chalcone derivatives

A large series of substituted chalcones have been tested *in vitro* for their ability to inhibit hMAO-A and –B [87]. While all the compounds show hMAO-B selective activity in the micro- and nanomolar ranges, the most active compound (**27.I**, Figure 12.I, $IC_{50}$ hMAO-B = 4.4 nM) also shows the highest MAO-B selectivity (SI >11364 toward hMAO-B).
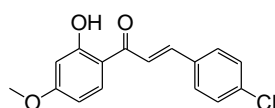


**27.I**

**Figure 12.I.** Chemical structure of chalcone derivative (**27.I**).

1.6.4.4 Caffeine and benzimidazole derivatives

While the caffeine is only a weak inhibitor of MAO-B ($K_i$ = 3.6 mM), several studies have evidenced that substitution in the 8-position by a styryl group enhances affinity of caffeine analogues acting as moderate to very potent competitive inhibitors of MAO-B [38, 88-90]. (*E*)-8-(3-Chlorostyryl) caffeine (CSC, **28a.I**, Figure 13.I) and **28b.I** (Figure 13.I) with $K_i$ baMAO-B values of 128 nM and 36 nM respectively were the most potent members of the series [38, 91]. By analogy to CSC (**28a.I**), **28c.I** (Figure 13.I) displayed promising baMAO-B inhibition with a $K_i$ value of 181 nM [92]. Based on results of (*E*)-8-styrylcaffeinyl analogues, a series of 8-benzyloxycaffeinyl analogues were evaluated as MAOIs [93]. They inhibited reversibly both MAO isoforms. The most potent MAO-A inhibitor was 8-(3-methylbenzyloxy)caffeine (**28d.I**, Figure 13.I, $K_i$ hMAO-A = 140 nM with a SI of 1.3 toward hMAO-A) while 8-(3-bromobenzyloxy)caffeine (**28e.I**, Figure 13.I, $K_i$ hMAO-B = 23 nM with a SI of 14.5 toward hMAO-B) was the most potent MAO-B inhibitor. Furthermore, these results confirm that the styryl and benzyloxy side chains have similar properties with respect to binding to MAO-B and probably exhibit similar binding modes within the active site of MAO-B. Modeling studies have also evidenced that the benzyloxy side chains of the

inhibitors are rotated in hMAO-A to avoid unfavourable interactions with the side chain of Phe208 [93].
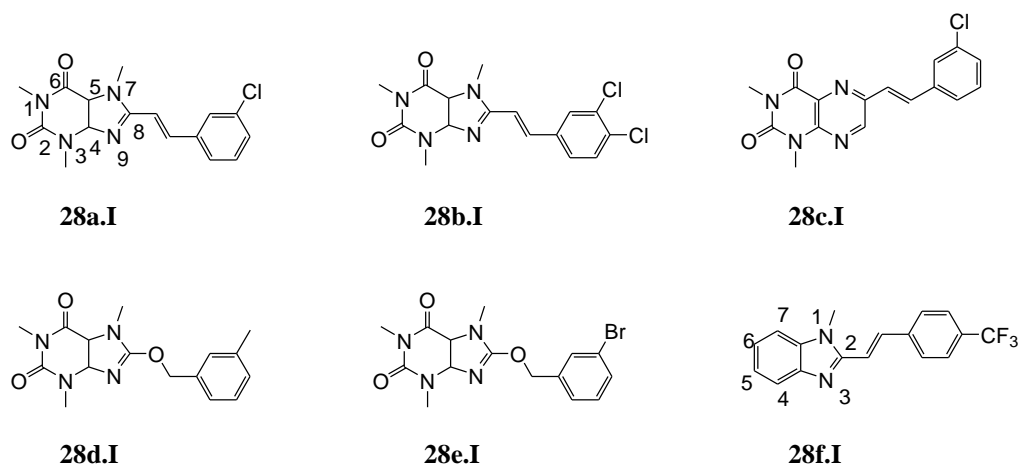


**Figure 13.I.** Chemical structures of caffeine (**28a-e.I**) and benzimidazole (**28f.I**) derivatives.

A study on (*E*)-2-styryl-1-methylbenzimidazole analogues identified **28f.I** (Figure 13.I) as the most potent inhibitor with a $K_i$ value of 430 nM [38]. The potency of MAO-B inhibition by (*E*)-8-styrylcaffeines and (*E*)-2-styrylbenzimidazoles may possibly also be explained by a similar mode of binding that involves traversing both the entrance and substrate cavities [38, 94]. These inhibitors possibly bind to MAO-B with the benzimidazole or caffeine ring located in the substrate cavity of the active site while the styryl substituent extends into the entrance cavity.

1.6.4.5 Pyrole and pyrazole derivatives

Among the most potent pyrole derivatives, **29a.I** (Figure 14.I, $K_i$ boMAO-A = 24 nM with a SI of 12500 toward boMAO-A) shows high selectivity for MAO-A while **29b.I** (Figure 14.I, $K_i$ boMAO-B = 20 nM with a SI of 175 toward boMAO-B) was highly selective for the B isoenzyme [95-96].

The pyrazole derivatives have been widely studied for their ability to inhibit reversibly MAO-A and –B [97-106]. Among them, N1-acetyl pyrazoline derivatives display higher activity on MAO-A compared to MAO-B [97-98]. For example, **29c.I** (Figure 14.I) is a potent and selective MAO-A inhibitor (IC$_{50}$ boMAO-A = 8.6 nM with a SI of 12500 toward boMAO-A) [98]. N1-Thiocarbamoyl pyrazole derivatives show high activity on both isoforms. For example, **29d.I** (Figure 14.I) is a potent and selective MAO-B inhibitor ($K_i$ boMAO-B = 1.5

nM with a SI of 21 toward boMAO-B) while **29e.I** (Figure 14.I) inhibits selectively MAO-A ($K_i$ boMAO-A = 6.0 nM with a SI of 166 toward boMAO-A) [99]. 2-Thiocarbamoyl indazole derivatives show high activity on both rMAO-A (e.g., **29f.I**, $K_i$ rMAO-A = 4.2 nM with a SI of 294 toward rMAO-A) and rMAO-B (e.g., **29g.I**, $K_i$ rMAO-B = 0.90 nM with a SI >3322 toward rMAO-B) isoforms [103].



**29a.I**          **29b.I**          **29c.I**          **29d.I**



**29e.I**          **29f.I**          **29g.I**
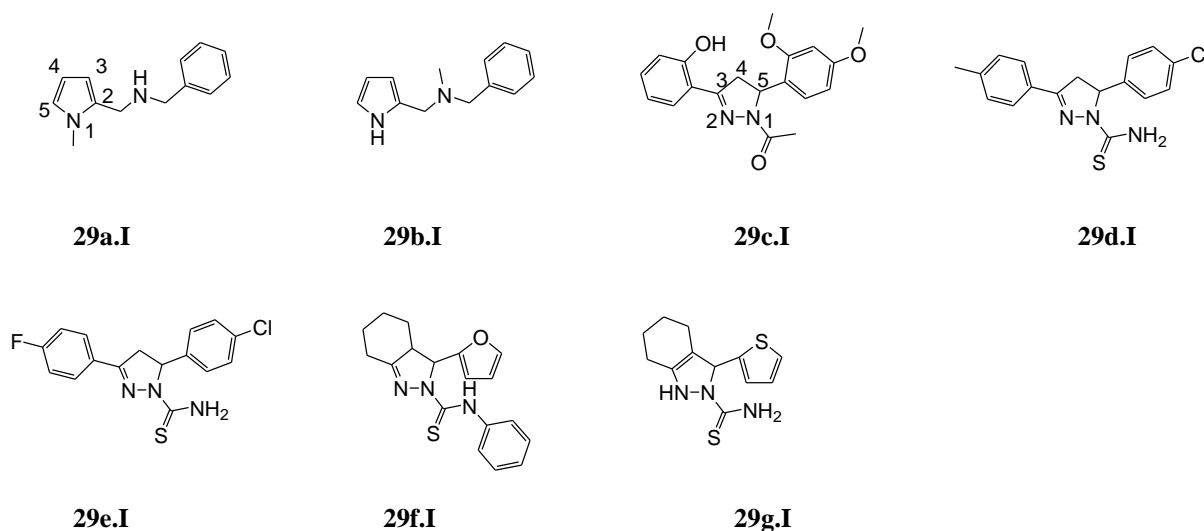
**Figure 14.I.** Chemical structures of pyrole (**29a-b.I**) and pyrazole (**29c-g.I**) derivatives.

1.6.4.6 Thiazolylhydrazone derivatives

2-Thiazolylhydrazone derivatives have been investigated for their ability to inhibit selectively the *in vitro* activity of hMAO-A and −B [107-109]. Among the most active and selective derivatives toward hMAO-B, **30a.I** (Figure 15.I, assessed as mixture of *E* and *Z* conformers), displays an $IC_{50}$ value of 3.8 nM with a SI of 119 toward hMAO-B [108]. It was evident that the anti-MAO activity and selectivity were strongly associated with the presence of a heterocyclic or a bicyclic moiety on the hydrazonic nitrogen. For example, **30b.I** (Figure 15.I) (assessed as mixture of *E* and *Z* conformers), displays both low inhibitory activity and the best selectivity toward hMAO-A ($IC_{50}$ hMAO-A = 874.7 nM with a SI >115 toward hMAO-A) [108].



**30a.I**          **30b.I**
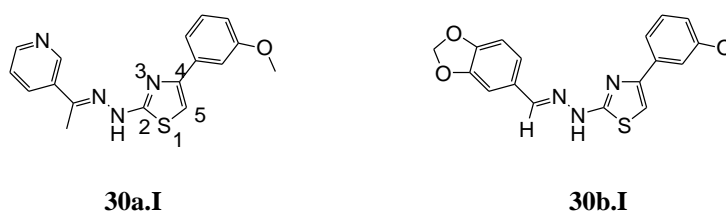
**Figure 15.I.** Chemical structures of thiazolylhydrazone derivatives (**30a-b.I**).

1.6.4.7 Thiazolidinedione derivatives

Recently, it was shown that the anti-diabetic drug pioglitazone (**31a.I**, Figure 16.I, $IC_{50}$ hMAO-B = 298 nM) was protective in the 1-methyl-4-phenyl-1,2,3,6-tetrahydropyridine (MPTP) parkinsonian mouse model [110-112]. The neuroprotective mechanism of pioglitazone was shown to be, at least in part, through its inhibition of MAO-B which prevents the conversion of MPTP to its toxic metabolite MPP+ [110]. Further study has identified the thiazolidinedione scaffold as a novel scaffold which can be used for the inhibition of the hMAO-B enzyme [112]. From this study, inhibition assays identified two thiazolidinedione derivatives (A6355 (**31b.I**) and L136662 (**31c.I**)) which inhibit hMAO-B with $IC_{50}$ values of 82 and 195 nM, respectively (Figure 16.I).



|  | **31a.I** |  | **31b.I** |  | **31c.I** |
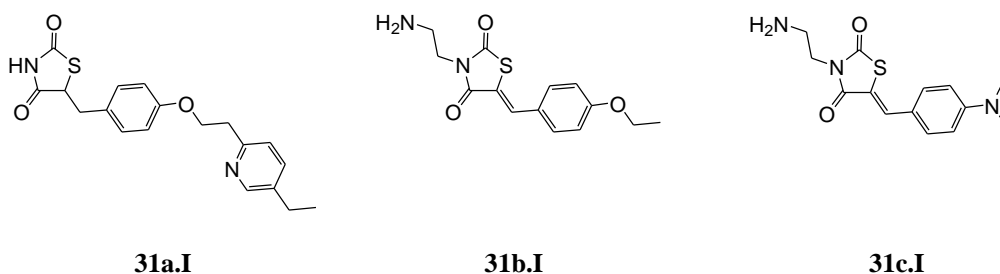
**Figure 16.I.** Chemical structures of pioglitazone (**31a.I**), A6355 (**31b.I**) and L136662 (**31c.I**).

1.6.4.8 Quinoxaline derivatives

Recently, a series of 3-benzylquinoxaline derivatives was investigated for their MAO inhibitory property [1, 113]. The results revealed that all 3-benzylquinoxaline derivatives studied display a MAO-A selectivity. **32.I** was the most potent and selective inhibitor (Figure 17.I, $IC_{50}$ boMAO-A = 2.8 nM with a SI of 3.0 x $10^{6}$ toward boMAO-A).



**32.I**
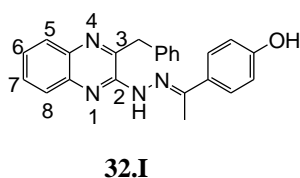
**Figure 17.I.** Chemical structure of quinoxaline derivative **32.I**.

1.6.4.9 Nicotinamide derivatives

Iproniazid (**6.I**, Figure 5.I) was the prototype of potent MAOI introduced in therapy of depression in 1957 [114]. However, due to its side interactions with other drugs and certain food, the therapeutic applications of iproniazid (**6.I**) have been diminished. Moclobemide (**9.I**, Figure 5.I) was the first nonhydrazine, reversible MAO-A selective inhibitor approved for use as an antidepressant drug. Although it is a potent MAO-A inhibitor *in vivo*, it is only a weak inhibitor *in vitro*. For pursuing more potent and less toxic MAO-A inhibitors as antidepressant agents, a series of nicotinamide derivatives which merges both picolinate and morpholine moieties of two antidepressant drugs iproniazid and moclobemide respectively were designed and have been tested on rMAO-A and –B [114]. Most of these compounds proved to be potent, and selective inhibitors of rMAO-A rather than of rMAO-B. **33a.I** (Figure 18.I) displays the highest rMAO-A inhibitory potency ($IC_{50}$ rMAO-A = 45 nM) and a good selectivity (SI of 578 toward rMAO-A), whereas **33b.I** (Figure 18.I) is the most potent rMAO-B inhibitor with an $IC_{50}$ value of 0.32 μM, but it was not selective (SI of 26 toward MAO-B).



**33a.I**          **33b.I**
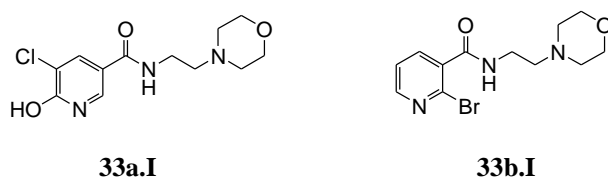
**Figure 18.I.** Chemical structures of nicotinamide derivatives (**33a-b.I**).

1.6.4.10 Phenylethylamine derivatives

Several phenylethylamine derivatives, particularly α-methylphenylethylamines with a single alkoxy or alkylthio substituent in the para position, have proved to be potent and selective MAO-A inhibitors with negligible activity on MAO-B (e.g., **34a.I**, Figure 19.I, $K_i$ hMAO-A = 22 nM with a SI of 208 toward hMAO-A) [115]). Recently, the study of rigid phenylethylamine analogues (2-(4'alkoxyphenyl)thiomorpholine derivatives) has shown that fixing the amine chain in an extended six-membered ring conformation might lead to increased potency as MAO-B inhibitors [116]. Indeed, **34b.I** (Figure 19.I) was the most

potent and selective inhibitor of hMAO-B ($K_i$ hMAO-B = 38 nM with a SI >2600 toward hMAO-B).



**34a.I**          **34b.I**
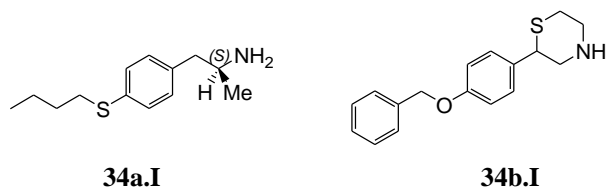
**Figure 19.I.** Chemical structures of phenylethylamine derivatives (**34a-b.I**).

1.6.4.11 Safinamide derivatives

Leonetti et al have studied safinamide analogues for their MAO inhibitory activity and selectivity [117]. All the compounds bound MAO-B isoform with higher affinity than MAO-A. **35a.I** (Figure 20.I) proved to be a more potent MAO-B inhibitor than safinamide (**1.I**, Figure 20.I) ($IC_{50}$ rMAO-B = 33 nM vs 98 nM) but with a lower MAO-B selectivity (SI of 3455 vs 5918). The highest MAO-B inhibitory potency ($IC_{50}$ rMAO-B = 17 nM) and a good selectivity (SI of 2941) were displayed by **35b.I** (Figure 20.I), a tetrahydroisoquinoline analogue of safinamide.



**1.I**          **35a.I**          **35b.I**
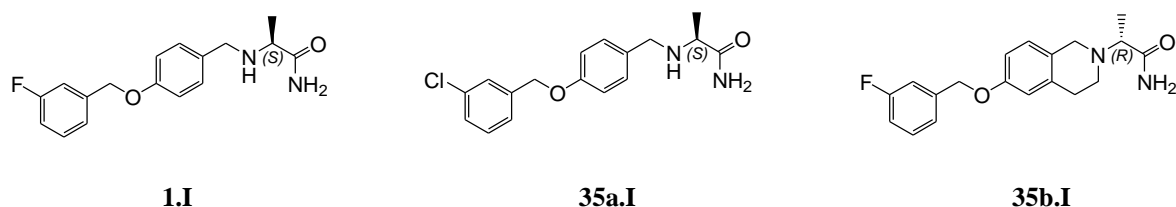
**Figure 20.I.** Chemical structures of safinamide (**1.I**) and derivatives (**35a-b.I**).

1.6.4.12 Tranylcypromine derivatives

Tranylcypromine (**5.I**, Figure 2.I) is a very potent antidepressant that has been in clinical use since the 1960s. However, side effects associated with this compound preclude its use as a first-line drug and it is prescribed in cases where other therapies do not work, for example, for the treatment of resistant depressions [118-119]. So, new studies have been performed to develop highly active and more selective inhibitors of MAO-A and –B using tranylcypromine as a lead compound which would have fewer side effects [119]. Recently, Binda et al have

evidenced that two tranylcypromine enantiomers inhibited differently hMAO-B (**36a.I**, Figure 21.I, $K_i$ hMAO-B = 4.4 μM and **36b.I**, Figure 21.I, $K_i$ hMAO-B = 89 μM) [120]. Moreover, **36c.I** (Figure 21.I) displays a good inhibition on hMAO-B ($K_i$ hMAO-B = 0.4 μM) and **36d.I** (Figure 21.I) displays a good inhibition and selectivity toward hMAO-A ($K_i$ hMAO-A = 1.2 μM and no inhibition at 133 μM on hMAO-B).
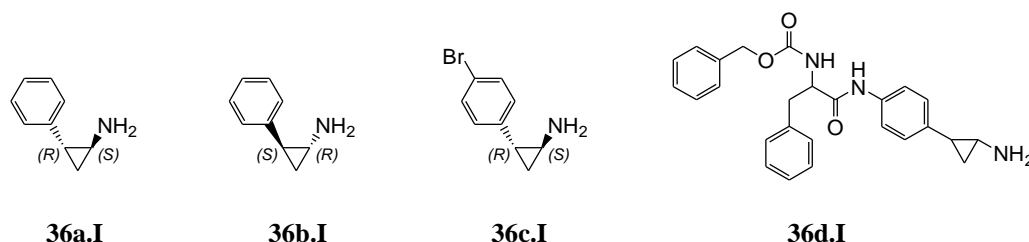


**Figure 21.I.** Chemical structures of tranylcypromine derivatives (**36a-d.I**).

# 2. INDOLEAMINE 2,3-DIOXYGENASE (IDO)

## 2.1 Biological actions of IDO

Indoleamine 2,3-dioxygenase (IDO) is an extrahepatic cytosolic heme-containing dioxygenase that catalyzes the conversion of tryptophan (Trp) to *N*-formylkynurenine (NFK), by the addition of oxygen across the C-2/C-3 double bond of the indole ring of tryptophan (Scheme 4.I) [121-122].
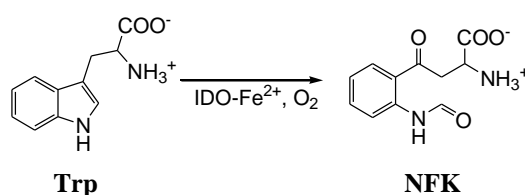


**Scheme 4.I.** Reaction catalyzed of Trp by IDO [124].

In the active form of IDO, the heme iron is in its ferrous state ($Fe^{2+}$), while in its inactive form, the heme iron is in the ferric state ($Fe^{3+}$). The catalytic cycle of IDO does not alter the oxidation state of the iron. However, IDO is prone to autoxidation, and therefore, a reductant is necessary in the enzymatic assay to maintain enzyme activity. Cytochrome $b_5$ has been suggested to be responsible for IDO reduction *in vivo* [123]. Besides Trp, IDO displays a wide

specificity of substrates. IDO degrades indoleamines such as L-Trp, D-Trp, serotonin (a MAO-A substrate) and tryptamine [125-126].

## 2.2 Kynurenine pathway

IDO is implicated in the metabolism of Trp (Scheme 5.I). Of the dietary Trp that is not used in protein synthesis, most is metabolized by IDO through the kynurenine pathway, and a small amount of it is used to synthesize the neurotransmitter serotonin (serotonergic pathway) [127]. IDO catalyzes the initial and rate-limiting step in the catabolism of the essential amino acid Trp along the kynurenine pathway, which leads to biologically active metabolites such as quinolinic acid and nicotinamide.
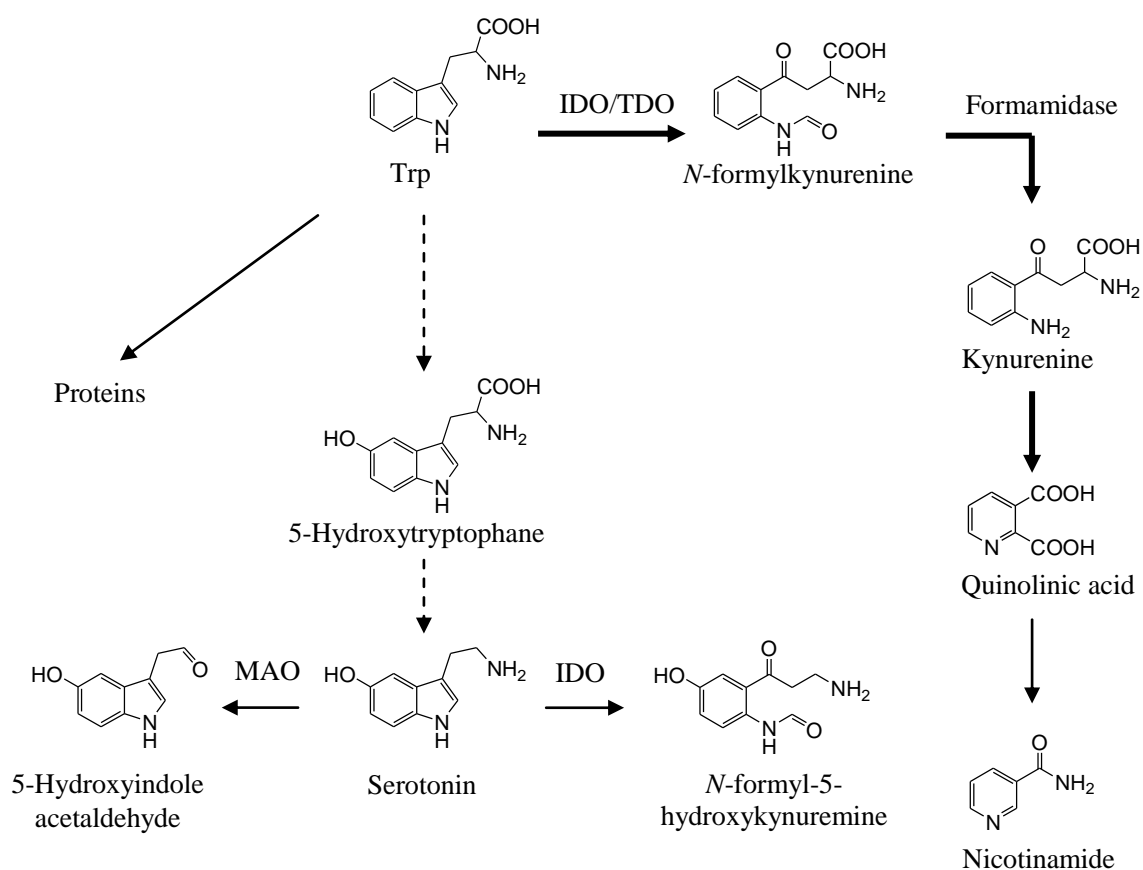


**Scheme 5.I.** Pathways of Trp metabolism. Of the dietary Trp that is not used in protein synthesis, 99% is metabolized along the kynurenine pathway (bold arrow). Alternative pathway is the conversion of Trp to serotonin (serotonergic pathway, dotted arrow) [127].

A second heme-containing dioxygenase, tryptophan 2,3-dioxygenase (TDO) catalyses the same reaction than IDO (Scheme 5.I). However, TDO and IDO enzymes are tissue specific,

36

with the former being confined almost exclusively to the liver, whereas IDO is found in most other tissues, including the CNS [127]. As the major dietary tryptophan not used in protein synthesis is metabolized by IDO/TDO through the kynurenine pathway, consequently, IDO and TDO play a critical role in determining the relative Trp flux in the serotonergic and kynurenine pathways [122]. Previous studies have shown the interest to use TDO inhibitors as serotonergic antidepressants [128]. Furthermore, MAO and IDO share a same substrate (serotonin). So, this similarity in substrate between IDO and MAO, and the implication of IDO/TDO and MAO in the serotonergic and kynurenine pathways lead us to study the selectivity of our compounds against the three enzymes and especially in our study between IDO and MAO.

## 2.3 Physiological and pathological roles of IDO

IDO is expressed ubiquitously but predominately in cells within the immune system where it is specifically induced in dendritic cells and macrophages at the sites of inflammation by cytokines, most importantly by interferon-γ (IFNγ) [129]. The expression of IDO can be inductible [130] or constitutive [131], according to the type of cell.

Roles of IDO;

- Its first role consists in the immune defense. It was shown that IDO was overexpressed in presence of infectious agents. Indeed, certain microorganisms are dependent on exogenous Trp. So, the growth of these microorganisms will be restricted by the lack in Trp generated by the action of IDO [130, 132].
- The second role of IDO— the most studied —is its implication in the regulation of the immune system. Various studies showed that IDO regulated the activity of T lymphocytes [133]. By depleting Trp, resulting from the action of IDO, this last one blocks the proliferation of T lymphocytes. This inhibition of T lymphocytes will allow a tolerance of IDO-expressing cells against the immune system (Figure 22.I). Furthermore, it was shown that kynurenine, the metabolite of IDO, was able to lead to the apoptosis of some lymphocytes; this has an influence on the immune response (Figure 22.I) [134]. In addition, IDO has also been involved as an immunosuppressive agent, contributing to maternal tolerance toward the allogeneic fetus [135]. Indeed, the

37

survival of the fetus is described as resulting from the capacity of this one to be able of protecting itself from T lymphocytes of the mother, by expressing IDO.
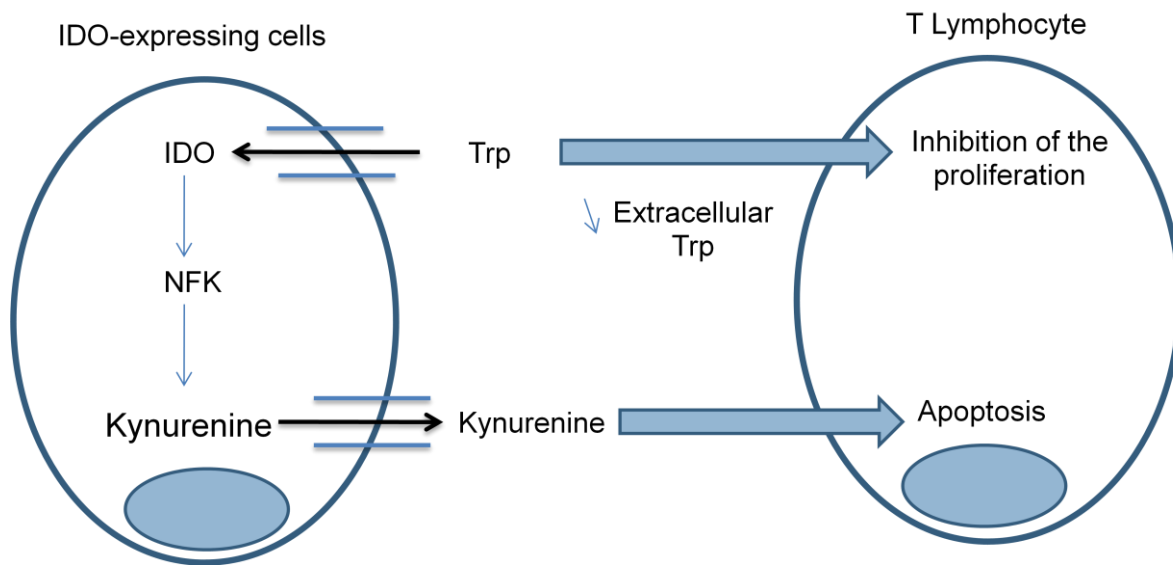


**Figure 22.I.** Depiction of the involvement of IDO in the regulation of the immune system [136].

Uyttenhove et al have previously shown that human tumor cells of various origins also constitutively expressed active IDO [137]. Table 3.I reports the relationship between the samples of tumors containing IDO (IDO-positive) and all the tested samples of tumors, for several types of tumors.

**Table 3.I.** Expression of IDO in human tumors [137].

| Tumor type | IDO-positive tumor samples/Tested samples |
|---|---|
| Prostatic carcinomas | 11/11 |
| Pancreatic carcinomas | 10/10 |
| Cervical carcinomas | 10/10 |
| Colorectal carcinomas | 10/10 |
| Non-small-cell lung carcinomas | 9/11 |
| Breast carcinomas | 3/10 |

The highest proportions were observed in prostatic, colorectal, pancreatic and cervical carcinomas [137]. By expressing IDO, tumor cells suppress immune responses by blocking T

38

lymphocyte proliferation locally. So, it is important to identify inhibitors of this protein. Indeed, by promoting antitumor immune responses in combination with immunotherapy or chemotherapy, IDO inhibitors may offer a drug-based strategy to more effectively attack systemic cancer. Until now, the tests of therapeutic vaccines failed because they focused only on the stimulation of the immune systems of the patients against the tumor cells [136]. So, use of IDO inhibitors would allow working also on the mechanism by which tumors can resist immune rejection. Other studies also suggest that immune modulation via IDO inhibition can significantly increase the efficacy of a variety of traditional chemotherapeutic drugs [138]. In several preclinical models of cancer, single-agent therapy with an IDO inhibitor is only marginally efficacious, at best slowing tumor growth [137, 139]. In contrast, regression of established tumors can be achieved by combining an IDO inhibitor with a cytotoxic chemotherapeutic drug [139].

It is also known that IDO is overexpressed in a variety of diseases, including neurodegenerative disorders (e.g., Alzheimer's disease [140] and Huntington's disease [141]), or still in psychiatric diseases such as the depression [142]. Furthermore, infection by HIV increases the activity of IDO in the brain. It is then suggested that compound neurotoxins (quinolinic acid) resulting from the kynurenine pathway would contribute to the neuropathology associated with the HIV [143].

## 2.4 Three-dimensional structure and active site

Previously, the crystal structures of human IDO (hIDO) in complex with 4-phenylimidazole (PIM, **37.I**, Figure 26.I, right) (2D0T.pdb), a non-competitive IDO inhibitor or with the cyanide ion (2D0U.pdb) have been solved with resolutions of 2.3 Å and 3.4 Å respectively [144]. The two cocrystals also show two molecules of crystallization buffer, 2-(*N*-cyclohexylamino)ethane sulfonic acid (CHES). Crystal structures of hIDO, obtained as dimers, unveil the presence of two folding domains containing mainly alpha-helices (Figure 23.I);

- The large domain (green) is an all-helical domain and is comprised of 13 $\alpha$-helices and two $3_{10}$ helices. Four long helices (A, B, C, and D) in the large domain run parallel to the heme plane and interact with the neighboring helix by hydrophobic interactions.

The heme-binding pocket is created mainly by these four helices and three other helices (F, G and H, cyan). The side chains of helices F, G and H also contribute to heme–protein interactions and connect the two domains.

- The small domain (blue) and a long loop (red) connecting the two domains above the sixth coordination site of the heme (distal side) cover the top of the heme pocket. The small domain consists of six $\alpha$-helices, two short $\beta$-sheets, and three $3_{10}$ helices.

Contact between these two domains is very extensive with a buried surface area of 3.100 $\text{Å}^2$. The interface is formed by a combination of hydrophobic interactions, salt bridges, or hydrogen bonds mediated by the side chains of amino acid residues [144].
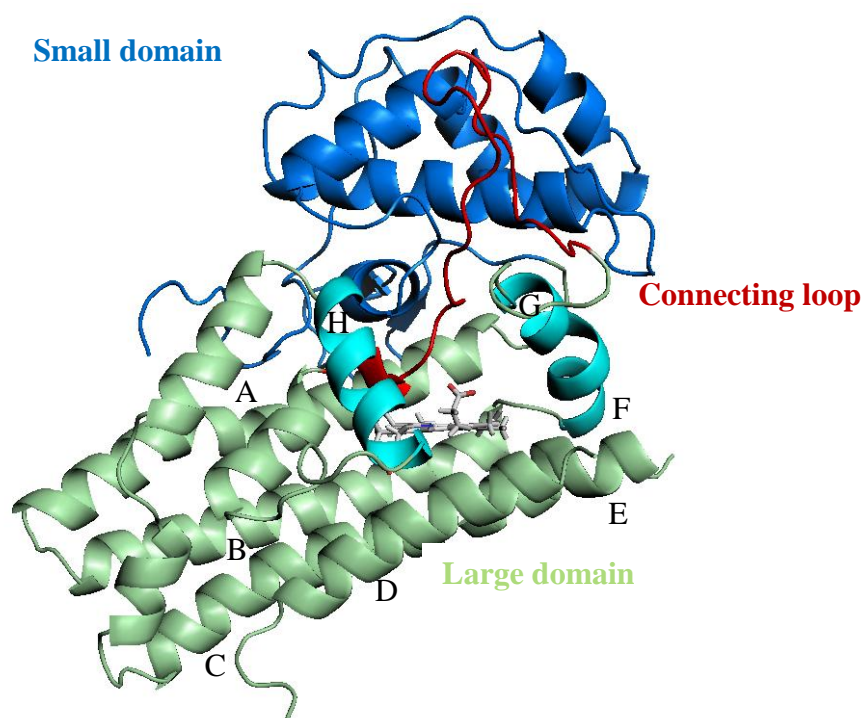


**Figure 23.I**. Three-dimensional structure of hIDO [144].

A loop is also present on the outside of the heme pocket, between two $\alpha$-helices (D and E) of the large domain (residues 360-380) [144]. This loop being flexible, the electron density is poorly defined and it does not allow the observation of this loop. However, it was suggested by theoretical calculations that this flexible loop allows the closing and the opening of the active site of the enzyme [145]. This allows to regulate the access of the substrate to the catalytic site and to regulate the release of product. The theoretical studies of various types of complexes (enzyme-$O_2$; enzyme-substrate and enzyme-$O_2$-substrate) showed that Arg231 was

also subject to a conformational shift allowing an interaction with the 7-propionate of the heme, according to the type of complexe [145]. These two aspects (flexible loop and conformational shift of Arg231) are reported in figure 24.I. So, the conformational states of both the electrostatic gate, constituted by Arg231 and the 7-propionate moiety of the heme, and the flexible loop (residues 360–380) are key elements that control the conformational shift of the enzymes from the inactive to the active form. Figure 24a.I shows an unbound inactive form of the enzyme, endowed by both an open electrostatic gate and region 360–380. This form would be adopted by the complexes enzyme-$O_2$ and enzyme-substrate. Figure 24b.I shows an active state, as that observed by the complex enzyme-substrate-$O_2$ where the electrostatic gate is closed onto the substrate and region 360–380 is packed over the catalytic site [145].
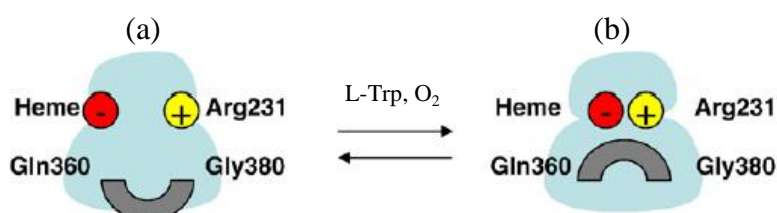


**Figure 24.I.** Proposed model of substrate recognition by IDO. (a) Unbound inactive form of the enzyme: both the electrostatic gate and region 360–380 are open. (b) Substrate bound active state of the enzyme: the electrostatic gate is closed onto the substrate and region 360–380 is packed over the catalytic site [145].

As regards the environment of the heme pocket, this one consists of two sides: the proximal and the distal heme pockets (Figure 25.I, left) [144].

- The proximal side of the heme is occupied by only side chains from the large domain. The heme iron is connected with the protein by His346. The heme is also stabilized by residues of the protein such as Arg343 which interacts by coulomb interactions with the 6-propionate of the heme.

- The distal side of the heme, which is a coordination site of the heme iron for the sixth external ligand, consists of a combination of the small domain, the large domain and the loop connecting the two domains. The distal side mainly consists of residues: Tyr126, Cys129, Phe163, Phe164, Ser167, Phe226, Phe227, Arg231 and Ser263 (Figure 25.I, right). These residues mainly apolar, favor the hydrophobic interactions between the ligand and the enzyme. Furthermore, the active site contains no water molecule.
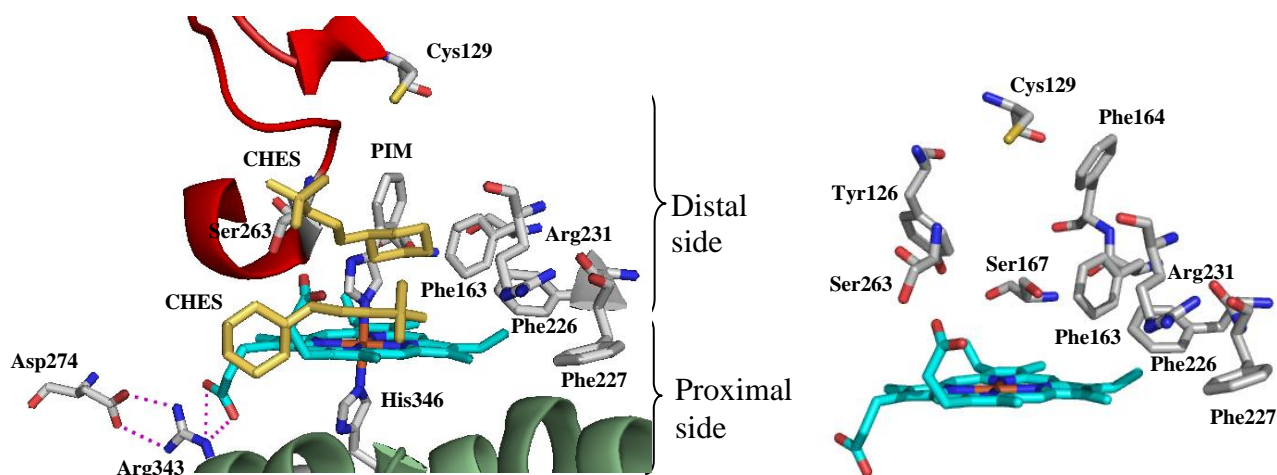
**Figure 25.I.** Environment of the heme pocket (left) and the active site of hIDO (right) (2D0T.pdb).

In a structural comparison between the PIM (**37.I**) and the cyanide-bound forms (Figure 26.I, left), the connecting loop exhibits a large conformational change in the main chain with a 1.3 Å displacement. So, it was suggested that the ligand and/or substrate binding induces a conformational change in the main chain of the connecting loop [144].
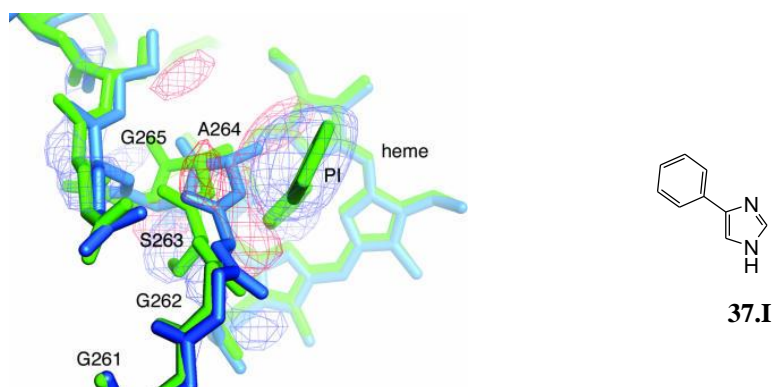


**Figure 26.I.** (Left) Comparison of the PIM (PI) and CN⁻-bound hIDO viewed from the distal side [144]. The PIM and CN⁻-bound structures are shown as stick models in green and blue, respectively. (Right) Chemical structure of PIM (**37.I**).

## 2.5 IDO inhibitors

Several IDO inhibitors have been reported to date (Figure 27.I). Most of the IDO inhibitors are directly derived from Trp. It is the case of the competitive 1-methyltryptophan (1MT, **38.I**) inhibitor, the most frequently used inhibitor which displays a weak $K_i$ of 35 μM [146]. A clinical trial is currently investigating the efficacy of 1MT in the treatment of advanced

42

malignancies [126, 147]. 1MT has long been known to be a competitive IDO inhibitor [148] but there remains a discussion concerning the efficacy of the two stereoisomers. L-1MT inhibits IDO in a cell-free assay with a $K_i$ of 19 μM, while D-1MT is inactive [126, 146]. However, *in vivo* the D-isomer has been reported to be more efficacious as an anticancer agent in chemo-immunotherapy regimens [146]. The reason for this discrepancy is still being vigorously debated [126, 149-152]. The oxygen (**39.I**, $K_i = 25$ μM) and sulfur (**40.I**, $K_i = 70$ μM) analogues of Trp display similar inhibitory potency compared to 1MT (**38.I**) and are always competitive [148]. Brassinin (**41.I**, $K_i = 97.7$ μM) is a moderately active competitive inhibitor and studies on brassinin dithiocarbamate analogues evidenced **42.I** ($K_i = 11.6$ μM) as a competitive IDO inhibitor [153]. Methyl-thiohydantoin-tryptophan (**43.I**, MTH-trp, $K_i = 11.6$ μM) also displays a good inhibition on IDO [139]. Recently, with the aim of discovering novel IDO inhibitors, a virtual screen was undertaken by our group and led to the discovery of the keto-indole derivative **44.I** endowed with an *in vitro* inhibitory potency in the micromolar range (IC$_{50}$ = 65 μM) [154]. Detailed kinetics were performed and revealed an uncompetitive inhibition profile. Pharmacomodulations around the indol-2-yl ethanone scaffold show that a fivefold improvement in potency (IC$_{50}$ = 13 μM) could be achieved by introducing a trifluoromethoxy group in the 5-position of the indole nucleus (**45.I**) [155]. Moreover, **45.I** and **44.I** are both endowed with 12-13% IDO inhibition at a 20 μM concentration in the cellular assay, which indicates reasonable cell penetration. β-carbolines are also reported as IDO inhibitors. To date, 3-butyl-β-carboline (**46.I**, $K_i = 3.3$ μM) is the most potent known non-competitive β-carboline inhibitor of IDO [156].

Various other scaffolds have also shown an interest for inhibition of IDO.

A structure-based study of PIM (**37.I**)-derived compounds led to the discovery of inhibitors with low micromolar activities (e.g., **47.I**, $K_i = 4.8$ μM), a 10-fold decrease compared to that of the parent compound [157]. Kumar et al. also worked on the naphthoquinone core of annulin B and designed new derivatives, partly based on structural modeling, with IC$_{50}$ values of up to 60 nM (e.g., **48.I**, IC$_{50}$ = 55 nM) [158]. Exiguamine A (**49.I**), a natural molecule, revealed a potent IDO inhibitor ($K_i = 41$ nM) [159]. Carr et al. identified tryptamine quinone as the core pharmacophore of exiguamine A and described a series of derivatives, the best displaying a $K_i$ of 200 nM (**50.I**) [159]. More recently, new potent competitive inhibitors including a hydroxyamidine motif (e.g., **51.I**, IC$_{50}$ = 67 nM) have also been described [160]. In 2010, three new series of IDO inhibitors have been reported: benzothiazoles (e.g., **52.I**,

IC$_{50}$ = 50 μM), phenylthiazoles (e.g., **53.I**, IC$_{50}$ = 50 μM) and triazoles (e.g., **54.I**, IC$_{50}$ = 60 μM) [126]. These compounds display good results *in vitro* as well as in cellular tests with low cytotoxicity. Furthermore, in cellular assays, 4-alkylamino-1-naphthol derivatives such as **55.I** (IC$_{50}$ = 2.5 μM) exhibit good activity on IDO and low cytotoxicity. The dimerized form (**56.I**) showed an IC$_{50}$ of 450 nM *in vitro*. In cellular assays, however, this compound shows slightly worse result than reduced **55.I** [126].
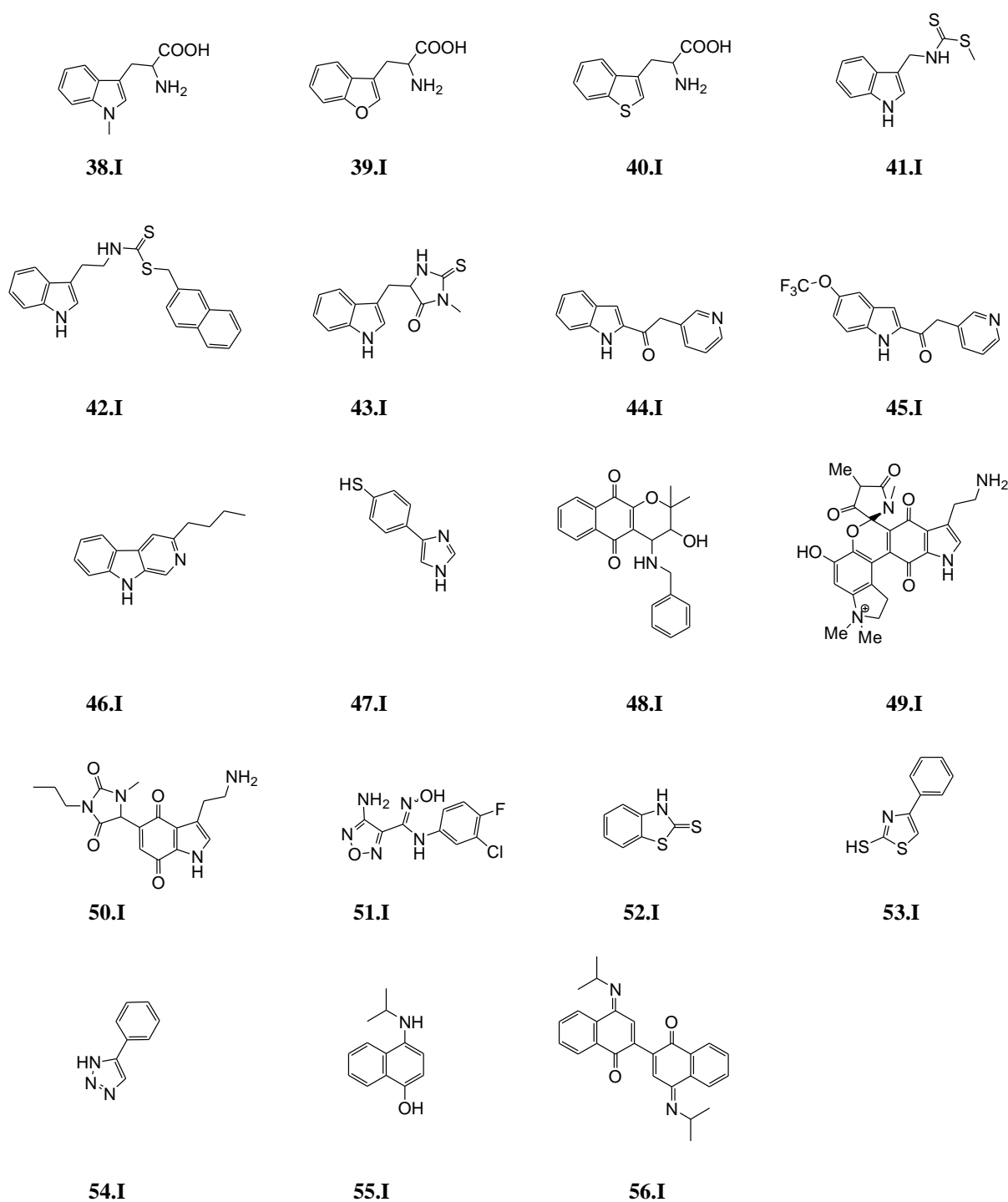


**Figure 27.I.** Chemical structures of selected IDO inhibitors.

44

# 3. LYSINE SPECIFIC DEMETHYLASE 1 (LSD1)

Eukaryotic DNA is packaged within a nucleic acid–protein complex termed chromatin. The basic structural unit of chromatin is the nucleosome, which consists of 146 base pairs of DNA wrapped around a histone octamer (reported in Cat.# 53200 (histone demethylase assay), Active Motif, Inc). The histone octamer consists of two copies each of the core histones H2a-H2b dimers and a tetramer of H3-H4. A linker histone, histone H1, binds chromatin outside the nucleosome unit to regulate chromatin structure. Histone modifications such as phosphorylation, acetylation and methylation at specific amino acid residues on the histone tails that extend beyond the core nucleosome have been found to influence and regulate transcription, chromosome packaging and DNA damage repair. While histone acetylation occurs only on lysine residues, histone methylation occurs at both lysine and arginine residues on the N-terminal histone tails. Histone lysine methylation is of particular interest given its association with transcriptional activation and repression, DNA damage response and X chromosome inactivation [161-163]. Histone methyltransferases (HMTs) and histone demethylases (HDMs) regulate histone methylation. There are currently two classes of HDMs: the lysine specific demethylase (LSD1 and 2) class and the jumonji (JmjC)-domain-containing class. Each class of HDM uses a different reaction mechanism, which leads to different substrate specificity and requires the use of different cofactors for enzymatic activity.

## 3.1 Biological actions of LSD1

Mammals contain two lysine specific demethylases: LSD1 and LSD2. LSD1, also known as KDM1 for lysine demethylase 1, is a nuclear enzyme which uses a flavin adenine dinucleotide (FAD)-dependent amine oxidase domain for its demethylase activity. It catalyzes the specific removal of methyl groups from mono and dimethylated Lys4 of histone H3 (H3K4), although an androgen receptor-controlled activity on H3K9 has also been reported [164]. LSD1 catalyzes oxidative cleavage of the C–N bond by a two-electron reduction of the FAD coenzyme, which produces an imine intermediate that is then non-enzymatically hydrolyzed to release a formaldehyde molecule (Scheme 6.I) [165]. Reduced FAD can be reoxidized by molecular oxygen, which generates hydrogen peroxide and makes the enzyme available for a

new catalytic cycle. If a dimethyl H3K4 substrate is used, the demethylation reaction will produce a monomethyl H3K4 substrate that is then able of undergoing a subsequent reaction to become unmethylated. A formaldehyde molecule will be released at each step [164]. LSD1 is not active on trimethylated Lys4, which is consistent with the flavin-catalyzed amine oxidation reaction that requires a lone pair of electrons on the lysine amino group [165]. LSD2, like LSD1, displays a strict specificity for mono- and dimethylated Lys4 of H3. However, the biology of LSD2 is proposed to differ from that of LSD1 since LSD2 does not bind CoREST. LSD1 and LSD2 share a similar catalytic domain (45% sequence identity) [120].
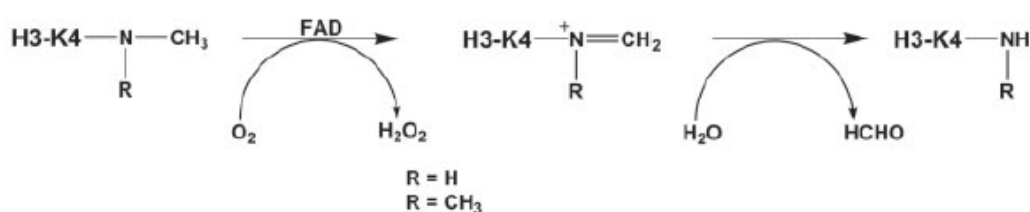


**Scheme 6.I.** Reaction catalyzed by LSD1 [164].

## 3.2 Physiological and pathological roles of LSD1

Genes coding for LSD1 proteins exist only in eukaryotes and have undergone distinct evolutionary development in plants and animals [166]. LSD1 plays a key role in the regulation of the expression of the active gene working as a corepressor or a coactivator of the transcription [167]. In non-neural cells, LSD1 in complex with the CoREST removes the transcriptionally activate mark of H3K4 methyl groups, thereby repressing neuron-specific genes [168]. LSD1 can also act as a transcriptional activator. Androgen receptor and LSD1 form a complex in a ligand-dependent manner and remove the transcriptionally repressive H3K9 methyl groups, thereby de-repressing androgen-receptor-target genes [168]. Consequently, LSD1 can target various lysine residues and regulate transcription positively or negatively depending on its partners of binding. The enzyme is an interesting target for epigenetic medicines as suggested by its implication in the regulation of many cancer cells, such as breast, colon, prostate and neural cancer cells [169-174]. LSD1 is also implicated in viral gene activation [175] and its association to the histone deacetylase 1, a medicine target validated and thus is regarded as a promising drug target protein.

46

## 3.3 Three-dimensional structure and active site

Currently, several X-ray structures of human LSD1 (hLSD1) alone or in complex are reported in the data bank with resolutions in the range of 2.25-3.30 Å. X-ray structures of hLSD1 were solved in complex with the C-terminal domain of CoREST [168, 176-178], bound to a histone H3 peptide (residues 1–16 of the N-terminal tail) [179] or a peptide of the transcription factor SNAIL1, mimicking the H3 tail [180]. Furthermore, X-ray structures of hLSD1 were also solved in complex with suicide inhibitors such as tranylcypromine derivatives [120, 168, 181-182] or with a suicide inhibitor consisting of a 21-residue histone H3 peptide in which K4 is modified by an *N*-methylpropargyl group [183].

LSD1 forms an elongated structure with three major parts (Figure 28.I) [184]:
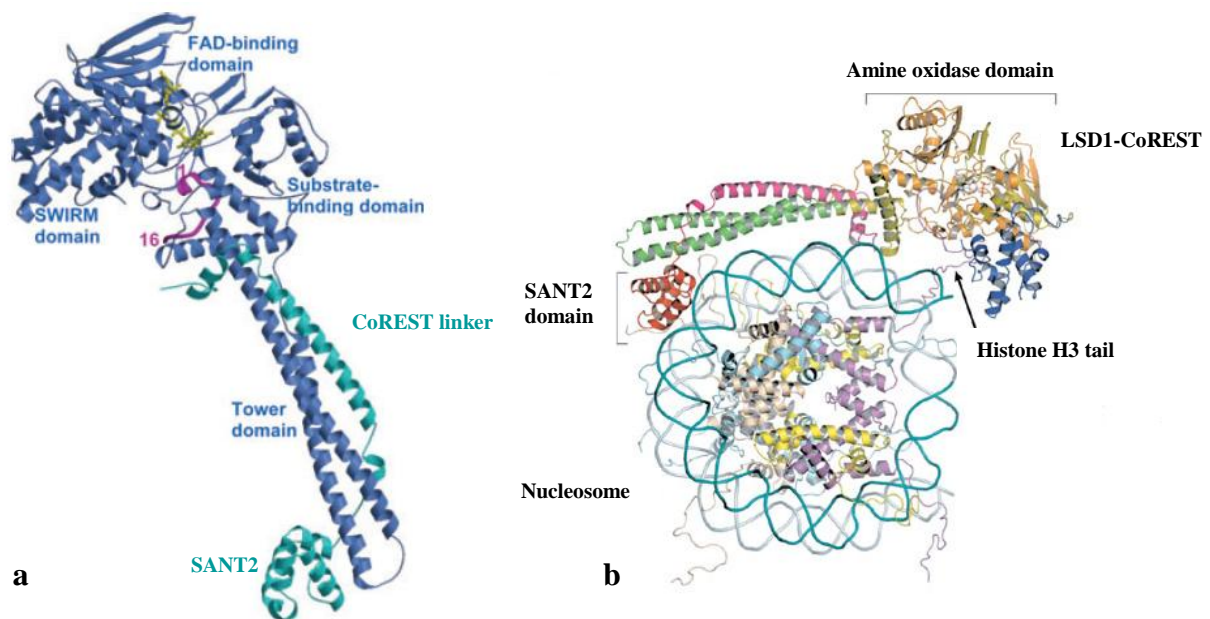


**Figure 28.I.** (a) Depiction of the LSD1-CoREST crystal structure in complex with a histone H3 peptide (2V1D.pdb) [165] [179]. LSD1, CoREST, FAD and histone H3 peptide (residues 1–16 of the N-terminal tail) are in blue, cyan, yellow and magenta respectively. (b) Depiction of the potential association of LSD1–CoREST with nucleosomal DNA [186]. The figure shows a nucleosome with the core histone octamer in the center and the associated DNA double helix in blue.

- The N-terminal SWIRM domain. The SWIRM domain is a motif commonly found in chromatin enzymes and is responsible for protein–protein and DNA–protein interactions [165].

- The amine oxidase domain (AOD) consists of two subdomains (the substrate-binding and FAD-binding domains) [165]. The SWIRM and AOD domains pack against each other to form a globular structural core [184]. So far, LSD1 is unique among the AOD proteins in catalyzing an amine oxidation reaction in the chromatin environment. As expected, the AOD of LSD1 has a fold highly similar to conventional FAD-dependent amine oxidases. The AOD of LSD1 is homologous to equivalent domains found in MAO-A and –B (17.6% identity) [185]. Despite the similar overall folding topology in the AOD enzymes, there is significant variability in the size and shape of their substrate-binding sites [165]. The active site of LSD1 lies at the interface of the two domains and forms a large cavity. The isoalloxazine ring of FAD is located at the base of this cavity. The volumes of the cavities are 637 and 1736 $Å^3$ for MAO-B and LSD1, respectively. In LSD1, the substrate-binding site is represented by a large funnel that originates from the flavin and opens wide towards the outside to accommodate the histone substrate (Figure 29a.I). In contrast to other histone-modifying enzymes, the mechanism of histone tail recognition by LSD1 is complex and highly specific. The structure of the enzyme in complex with a histone peptide revealed that the histone tail adopts a folded conformation when bound to the enzyme and creeps deep into the funnel cavity, establishing a network of interactions with the active site residues [165]. These specific interactions act together to fix the histone tail in the correct register, which positions Lys4 (the site of the demethylation reaction) in front of the flavin cofactor.
- The Tower domain, formed by the two antiparallel helices belonging to the insert between the two AOD domains, provides the binding platform for CoREST [184]. The CoREST linker folds into a long helix and stimulates the binding and activity of LSD1 toward nucleosomes by binding to nucleosomal DNA. The SANT2 domain of CoREST which is crucial for nucleosome demethylation is located at the tip of the stalk and far away from the active site of LSD1. Interestingly, the Tower domain originates on the surface of the AOD structure that corresponds (with respect to the position of the FAD coenzyme) to the area where the transmembrane helix branches off in MAO-A and –B (Figure 29a.I) [165].

Despite differences in the shape of the substrate-binding site, the details of the active sites of flavin amine oxidases are strikingly conserved (Figure 29b.I) [165]. MAO and LSD1 show a

lysine residue on top of the flavin, bridged to the N5 atom of the coenzyme via a water molecule, which is proposed to have a role in the enzymatic activity. Another conserved feature in the structure of the AOD active site is the so-called 'aromatic cage'. The substrate binds in front of the FAD cofactor, which has alongside one or two aromatic amino acids that form a sort of cage together with the flavin ring. In MAO-A and –B, the cage is composed of a Tyr–Tyr couple. In LSD1 one of these aromatic residues is conserved, with the other being replaced by a Thr residue (Figure 29b.I). Although the role of Tyr761 in the histone demethylation reaction has not been clarified, it could be involved in recognition of the methylated Lys4 amino group.

LSD1 is a multidomain protein and its involvement in many diverse gene-expression programs [187] is strictly related to its domain organization [165]. In addition to the SWIRM domain, whose role in the interaction with chromatin proteins is well known, the N-terminal part of LSD1 is of interest. This 200-residue segment is predicted to be disordered and, some studies suggest that this N-terminal putative disordered domain may have a role in providing the enzyme with the necessary flexibility to target different chromatin proteins and to adapt LSD1 enzymatic activity to distinct gene transcription events [165].
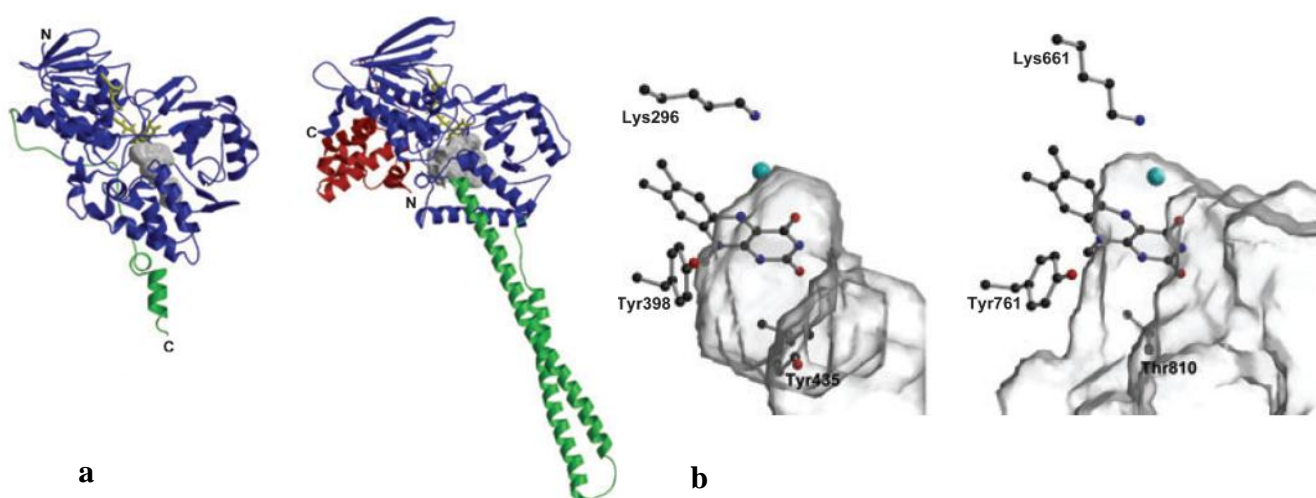


**Figure 29.I.** a) Comparative structural analysis of hMAO-B (left, 1GOS.pdb) and hLSD1 (right, 2V1D.pdb) [165]. The AOD and FAD are in blue and yellow respectively. In each structure, the cavity representing the substrate-binding site is drawn as a gray surface. The MAO-B C-terminal segment responsible for anchoring the protein to the outer mitochondrial membrane is depicted in green. In LSD1, the Tower domain and SWIRM domain are in green and red respectively. b) Overview of the active site surrounding the flavin cofactor in hMAO-B (left) and hLSD1 (right). The conserved water molecule H-bonded with the flavin N5 atom is represented as a cyan sphere. The substrate-binding site cavity is drawn as gray surface [165].

The architecture of the substrate-binding site in hLSD1 is characterized by the presence of various niches that accommodate the side chains of the histone peptide (Figure 30.I) [187]. In particular, the polar residues Arg2, Thr6, Arg8, Lys9 and Thr11, in addition to the N-terminal amino group of Ala1 (N-term pocket), lie in well defined pockets, thereby establishing specific interactions with the surrounding protein residues. Biochemical evidence indicates that substrate recognition by LSD1 requires a peptide comprising at least the first 20 N-terminal amino acids of H3 – that is, peptides of shorter length bind poorly to the enzyme and are not demethylated. Moreover, the side chain of Arg2 is crucial for stabilization of the folded conformation of the LSD1-bound H3 peptide, being at the heart of a network of intrapeptide hydrogen bonds (shown as dashed lines in figure 30.I). These interactions underlie the LSD1 specificity for H3K4 and position the methylated Lys4 side chain in proximity to the flavin for oxidative demethylation. The addition of epigenetic markers introduces steric and electrostatic perturbations which alter this network of interactions predictably, thus explaining the negative effect that nearly all epigenetic modifications have on LSD1–H3 binding.
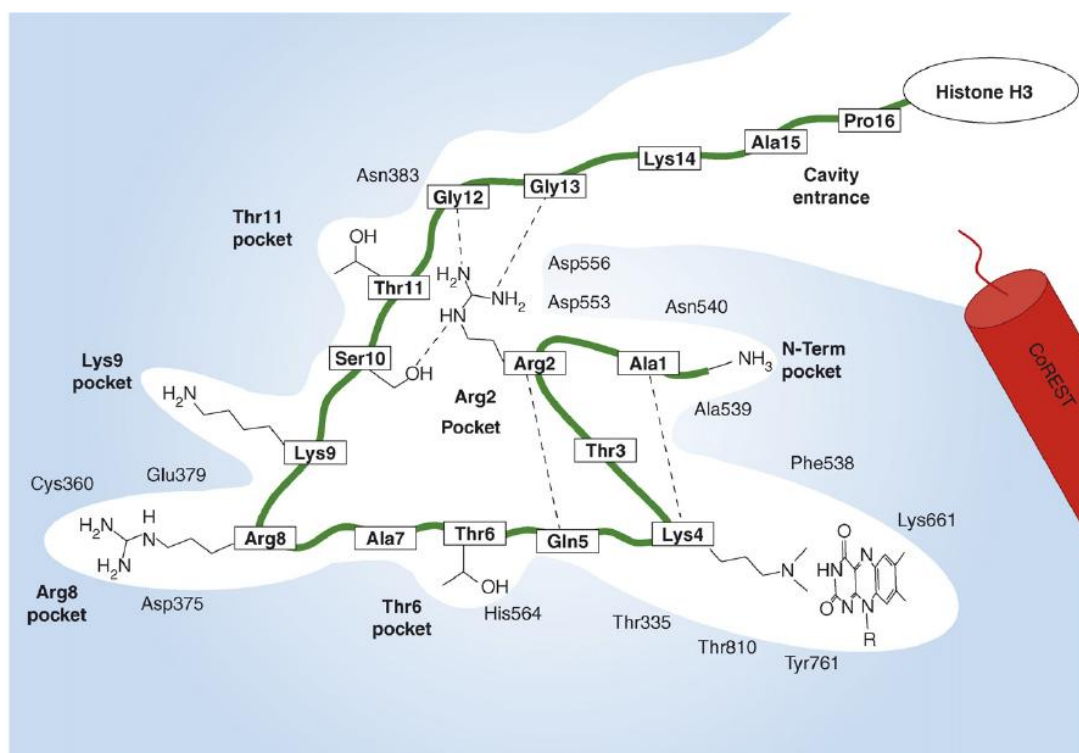


**Figure 30.I.** Defining features of the histone peptide-binding site in LSD1. LSD1 side chains involved in substrate binding are indicated. Histone H3 peptide (residues 1–16 of the N-terminal tail) and CoREST are in green and red respectively [187].

## 3.4 LSD1 inhibitors

To date, only a few types of LSD1 inhibitors were identified (Figure 31.I). Because of the AOD of LSD1 shares moderate sequence similarity with MAO, MAOIs such as phenelzine (**8.I**, Figure 5.I), tranylcypromine (**5.I**, Figure 2.I) and pargyline (**57.I**), were reported as inhibitors of LSD1, although their inhibitory potency and selectivity for LSD1 are very weak [169, 188]. Modifications of these three MAOIs have led to the development of potent LSD1 inactivators. *N*-Propargyl lysine-containing H3 peptides have been reported to be LSD1-selective inhibitors [183, 189]. Recently, Yang et al. cocrystallized the enzyme with a suicide inhibitor consisting of a 21-residue histone H3 peptide in which K4 is modified by an *N*-methylpropargyl group (**58.I**, $K_i$ = 107 nM [190]) [183]. The hydrazine containing H3 peptide (**59.I**, structurally derived from phenelzine) was found as a potent suicide inactivator of LSD1 ($K_i$ = 4.35 nM [190]).
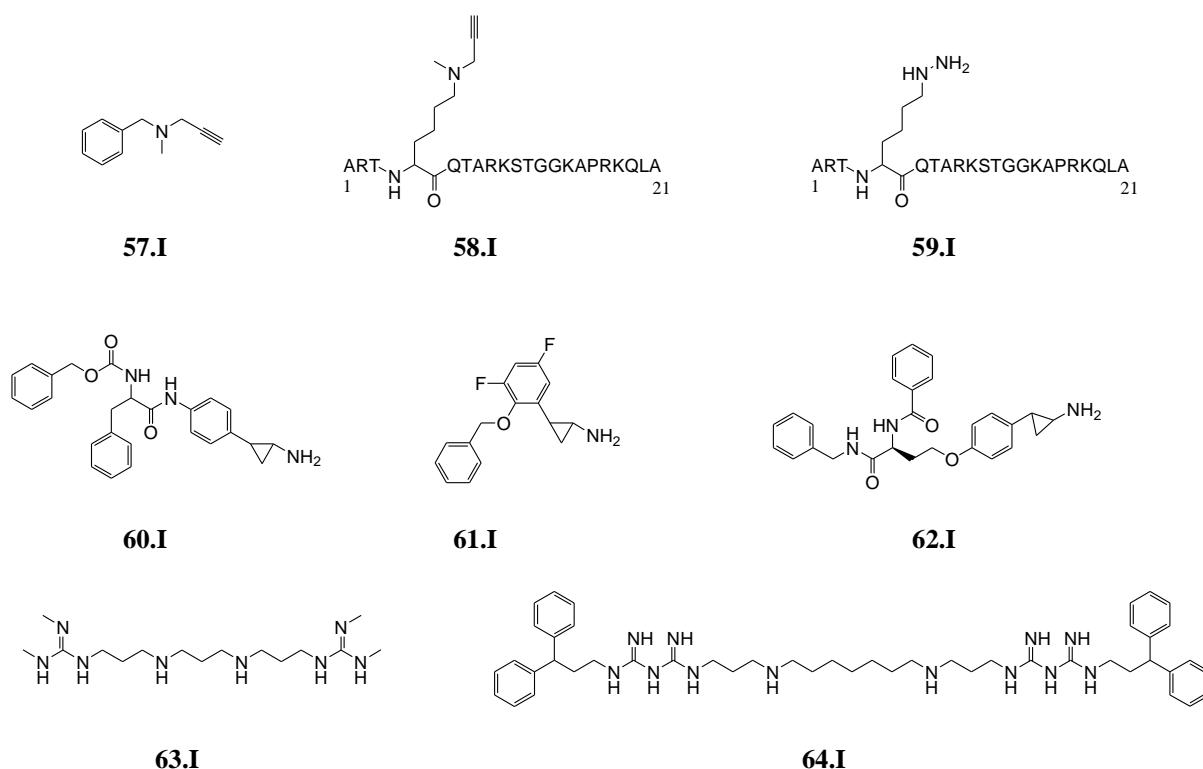


**Figure 31.I.** Chemical structures of selected LSD1 inhibitors.

Chemical substitutions on the phenyl ring of tranylcypromine (**5.I**, Figure 2.I) have greatly improved the potency and selectivity of this class of LSD1 inhibitors [120, 182, 190-191]. For

example, **60.I** displays a $K_i$ value of 1.3 µM on LSD1 and is selective of LSD1 compared to MAO-B (no inhibition at 133 µM) but displays a weak selectivity compared to MAO-A ($K_i$ = 1.2 µM) [120]. Compound **61.I** is selective of LSD1 ($K_i$ = 0.61 µM) compared to MAO-A ($K_i$ = 110 µM) and –B ($K_i$ = 17 µM) [182] and **62.I** ($IC_{50}$ = 1.9 µM with a SI of 150 and **>**520 toward LSD1 compared to MAO-A and –B respectively) is more potent and selective than tranylcypromine (**5.I**, $IC_{50}$ = 32 µM with a SI of 0.23 and 0.13 toward LSD1 compared to MAO-A and –B respectively) on LSD1 compared to MAO-A and –B [191].

Recently, a series of bisguanidine and biguanide polyamine analogues were tested for inhibitory activity on LSD1 [173]. The *in vitro* analysis of the two most potent inhibitors (**63.I** and **64.I**) exhibits non-competitive inhibition kinetics at concentrations < 2.5 µM, suggesting that, although the polyamine compounds could be considered analogues of the natural methyl lysine substrate of LSD1, they do not appear to compete with H3K4me2 at the active site. Interestingly, these compounds proved successful in reactivating the expression of silenced genes associated with tumor suppression, hinting at the therapeutic potential of LSD1 inhibition in the treatment of cancer.

# OBJECTIVES AND STRATEGY

As previously mentioned, monoamine oxidases are attractive targets for a broad range of treatments against pathologies including depression, anxiety disorders, Parkinson's and Alzheimer's diseases. Most current monoamine oxidase inhibitors lead to side effects by a lack of affinity and selectivity towards one of the isoforms. So, it remains fundamental to design new more potent, reversible and selective inhibitors of MAO-A and –B.

With this aim in view, the main objective of this work was the design, synthesis and evaluation of potential inhibitors of MAO. Therefore, we designed new MAO-A and –B inhibitors derived from β-carbolines, indoles and 5*H*-indeno[1,2-*c*]pyridazin-5-ones following a classical strategy including experimental (synthesis and biological evaluation) and theoretical (molecular modeling) approaches (Scheme 1.II).
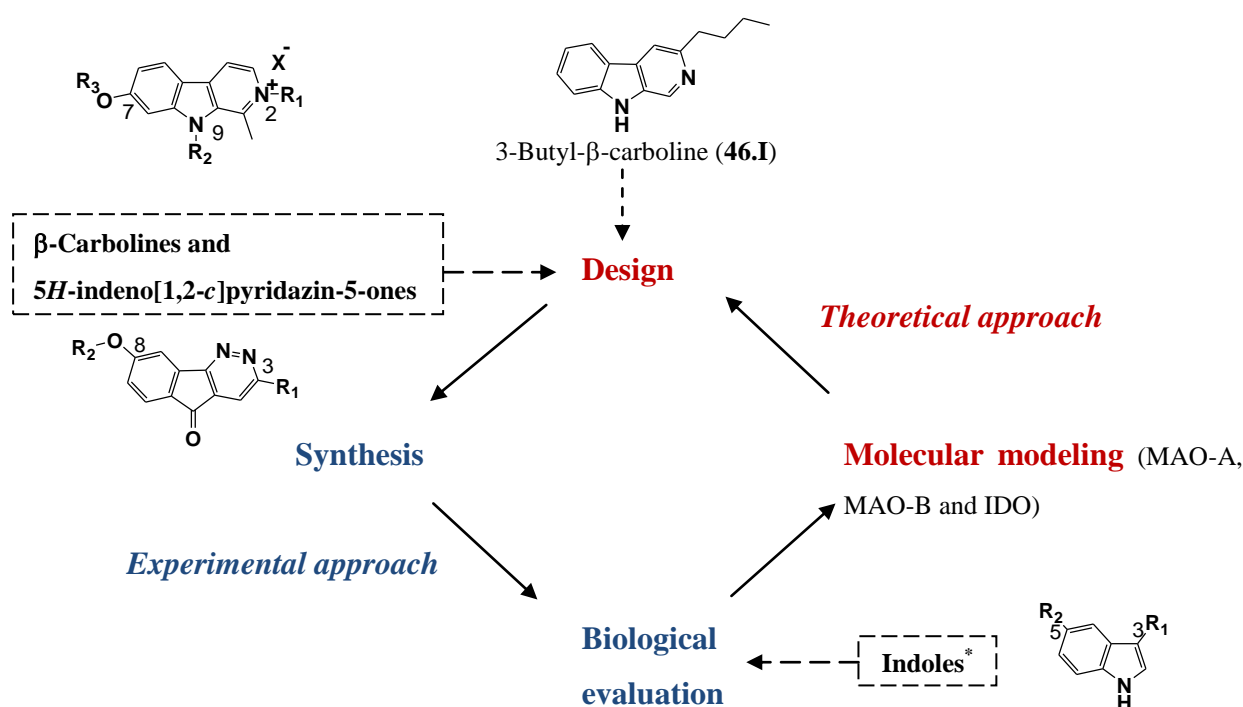


**Scheme 1.II.** Schematic depiction of the strategy used for this work.
* Available in the department of pharmacy

The β-carboline template displays a reversible competitive inhibition and is selective of MAO-A. Currently, harmine (**3.I**, $K_i$ hMAO-A = 5 nM, Figure 1.II) is described as the most potent inhibitor of this series on MAO-A [69]. Moreover, the crystal structure of hMAO-A in complex with harmine has been recently solved [3] and shows that nearby the methoxy group of harmine, a lipophilic pocket is left vacant. So, the objective was to optimize the β-carboline template for hMAO-A inhibition in order to study this lipophilic pocket. Thus, a series of β-carboline derivatives (**2a-5.III**) mainly substituted in the 7-position with lipophilic and bulky groups was synthesized.

The 5*H*-indeno[1,2-*c*]pyridazin-5-one template displays a reversible competitive inhibition and is selective of MAO-B. Currently, analogues **22f.I** (IC$_{50}$ hMAO-B = 8.5 nM [73]) and **22j.I** (IC$_{50}$ baMAO-B = 14.0 nM [74]) reported in figure 1.II, are described among the most potent inhibitors of this series on MAO-B. Moreover, the docking studies of **22f.I** and **22j.I** with hMAO-B reported from the literature [73, 75] suggest that these two 5*H*-indeno[1,2-*c*]pyridazin-5-one analogues could be the starting point for the design of novel and potentially more potent MAO-B inhibitors. Thus, in order to design new, selective and more potent MAO-B inhibitors, a series of 5*H*-indeno[1,2-*c*]pyridazin-5-one derivatives substituted both in the 3 and 8-positions by lipophilic groups has been synthesized (**22m.I**, **28a-b.III** and **30a-b.III**).

Previous studies have shown that indole derivatives may be used for the design of potent anti-MAO agents [57-62]. So, in order to identify new potential MAO-A and –B inhibitors including an indole core, a series of indole analogues including bulky and/or lipophilic groups in the 3 or 5-positions from the department of Pharmacy (Prof. Masereel, FUNDP, Belgium) was evaluated.
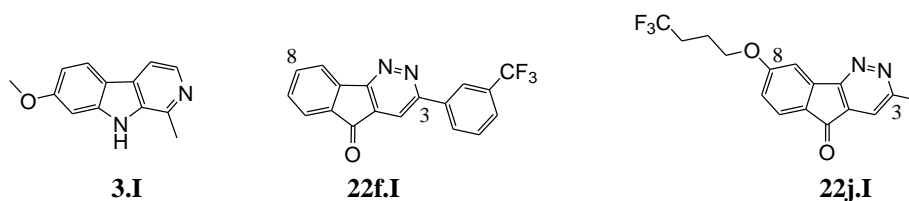


**Figure 1.II.** Chemical structures of harmine (**3.I**), **22f.I** and **22j.I**.

The involvement through a same metabolic pathway for MAO-A and IDO as well as their similarity for serotonin like substrate and the similarity in the structural properties of MAO and LSD1 led us to evaluate the inhibitory potency and selectivity of the β-carboline and 5*H*-indeno[1,2-*c*]pyridazine-5-one inhibitors of MAO against IDO and LSD1 (Scheme 2.II).

Furthermore, the β-carboline scaffold is also present in IDO inhibitor 3-butyl-β-carboline (**46.I**, $K_i$ = 3.3 μM, Scheme 1.II). So, starting from a same strategy than the one used on MAO (Scheme 1.II), we are also interested in design of new 3-substituted-β-carboline analogues directly derived from 3-butyl-β-carboline (**46.I**) and potentially more active on IDO. These derivatives display an amino group in the 3-position which should allow to establish supplementary interactions (coulomb interactions) with 7-propionate of the heme in the pocket B of IDO which are missing with 3-butyl-β-carboline.
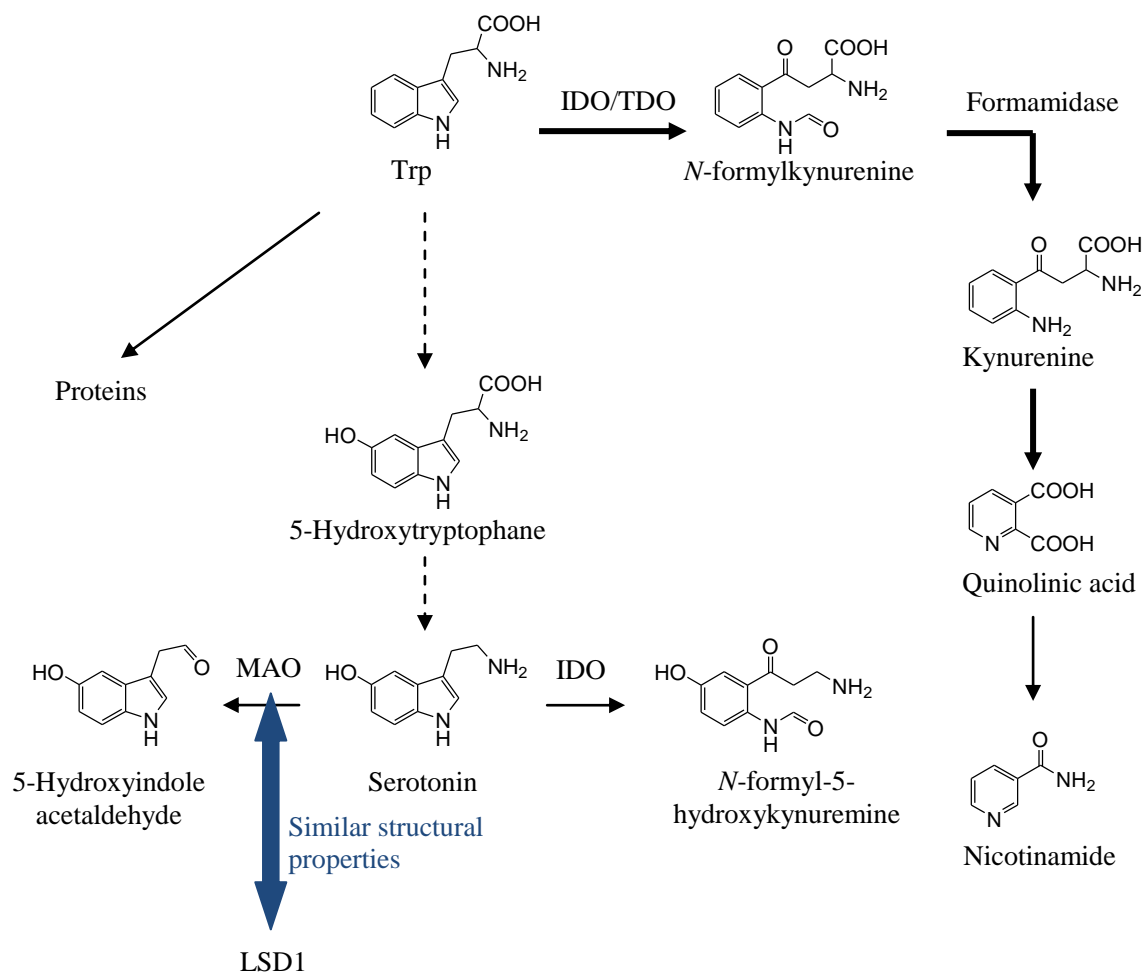
**Scheme 2.II.** Pathways of Trp metabolism. Of the dietary Trp that is not used in protein synthesis, 99% is metabolized along the kynurenine pathway (bold arrow). Alternative pathway is the conversion of Trp to serotonin (serotonergic pathway, dotted arrow) [127].

# RESULTS

# β-CARBOLINES

# 1. MAO

As mentioned in the introduction, the β-carboline template displays a reversible competitive inhibition and is selective of MAO-A. Currently, harmine (**3.I**, Table 1.III) with a $K_i$ value of 5 nM on hMAO-A is described as the most potent inhibitor of this series on MAO-A [69]. Moreover, the crystal structure of hMAO-A in complex with harmine has been recently solved [3]. So, we considered harmine as the starting point for the design of novel and more potent MAO-A inhibitors.

## 1.1 Structure-based rational design

In the cocrystal structure (2Z5X.pdb), harmine is located in the active center cavity of MAO-A. It interacts with Tyr69, Asn181, Phe208, Val210, Gln215, Cys323, Ile325, Ile335, Leu337, Phe352, Tyr407, Tyr444, and FAD (Figure 1.III) [3].



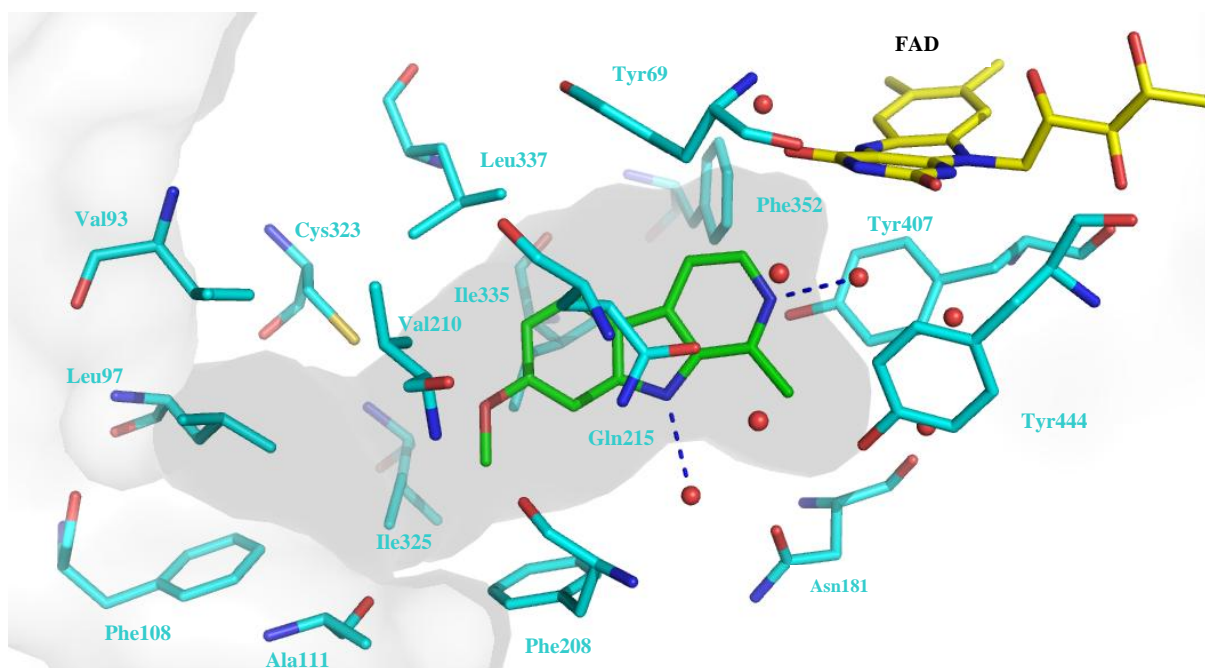**Figure 1.III.** Binding mode of harmine in the cocrystal structure (2Z5X.pdb). Only amino acids directly implicated in the active site are displayed and labeled in cyan. Harmine is in green. FAD is in yellow. The water molecules are displayed as red spheres. The hydrogen bonds discussed in the text are depicted as dashed blue lines.

Seven water molecules occupy the space between the inhibitor and these groups. Both nitrogen atoms of harmine establish also hydrogen bonds (depicted as dashed blue lines in figure 1.III) with two water molecules. Furthermore, the pyridine moiety is stabilized by the aromatic cage (Tyr407, Tyr444 and FAD) by $\pi$-$\pi$ interaction. The amide group of the Gln215 side chain interacts tightly with harmine by a $\pi$-$\pi$ interaction. Moreover, nearby the methoxy group of harmine, a lipophilic pocket formed by Val93, Leu97, Phe108, Ala111, Phe208, Cys323 and Ile325 is left vacant.

So, the objective was to optimize the $\beta$-carboline template for hMAO-A inhibition in order to study this lipophilic pocket. Thus, a series of $\beta$-carboline derivatives (**2a-5.III**) was synthesized and is reported in table 1.III. Previous works by our group carried out on 5*H*-indeno[1,2-*c*]pyridazin-5-ones (Figure 2.III) as MAO-B inhibitors have shown it is possible to increase the inhibitory potency in this series by substituting the heterocycle core in the 8-position by lipophilic and bulky side chains like benzyloxy (**22i.I**, $IC_{50}$ rMAO-B = 170 nM) and trifluorobutyloxy (**22j.I**, $IC_{50}$ baMAO-B = 14 nM) compared to a methoxy side chain (**22k.I**, $IC_{50}$ rMAO-B >1 $\mu$M) which are stabilized in the lipophilic entrance cavity of MAO-B [74-75]. Therefore, by structural analogy with 5*H*-indeno[1,2-*c*]pyridazin-5-ones, a series of $\beta$-carboline derivatives (**2a-l.III**) substituted in the 7-position with lipophilic and bulky groups including benzyloxy (**2g.III**) and trifluorobutyloxy (**2e.III**) groups, was synthesized. Three compounds including more hydrophilic groups such as dimethylaminoethyl, dimethylaminopropyl and ethylmorpholine (**2m-o.III**) were also synthesized to increase the solubility of compounds by keeping the ability to establish hydrophobic interactions into the active site. Compounds **3-5.III** were synthesized to study the impact of benzyl group in the 2, 7 and 9-positions on inhibition compared to mono-benzylated **2g.III**. Their human monoamine oxidase A and B inhibitory potency was investigated. The $IC_{50}$ values of the most potent compounds were evaluated and $K_i$ values were estimated using Cheng-Prusoff equation [192].



**22i.I**          **22j.I**          **22k.I**
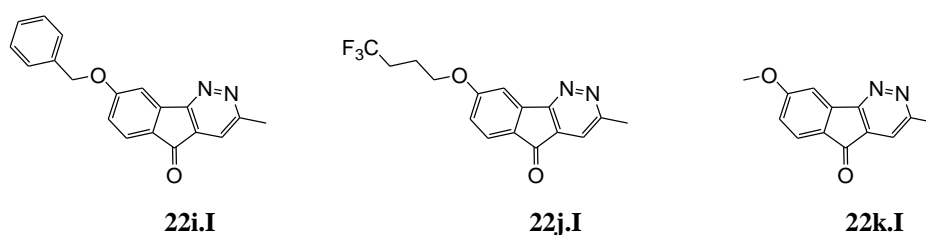
**Figure 2.III.** Chemical structures of 5*H*-indeno[1,2-*c*]pyridazin-5-one derivatives (**22i-k.I**).

**Table 1.III.** Envisioned pharmacomodulations around β-carboline scaffold. Chemical structures of harmine (**3.I**) and synthesized β-carboline analogues (**2a-5.III**) tested on hMAO-A and –B.

introduction of various substituents ← $R_3-O$ — [β-carboline scaffold] $N^{\oplus}-R_1$ → influence of substitution

[with $R_2$ on indole nitrogen]

influence of substitution
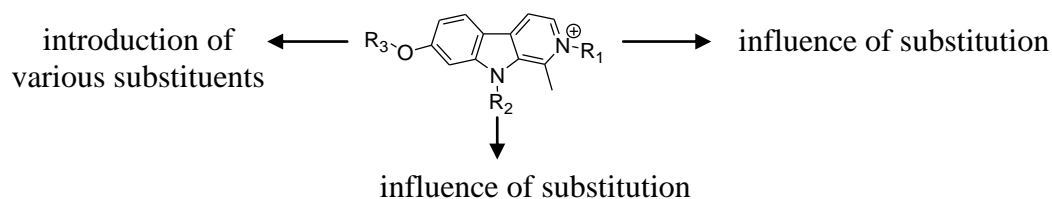
| Compound | $R_1$ | $R_2$ | $R_3$ | Yield (%) | XRD | Solubility in phosphate buffer, pH 7.4 at RT (μM) | Mp (°C) |
|---|---|---|---|---|---|---|---|
| harmine | / | H | $CH_3$ | / | / | 328 | 262.0 |
| 2a.III | / | H | $CH_2CH=CH_2$ | 75 | * | / | 173.9 |
| 2b.III | / | H | $CH_2CH(CH_3)_2$ | 87 | / | 150 | 202.9 |
| 2c.III | / | H | $(CH_2)_2OCH_3$ | 70 | / | / | 175.8 |
| 2d.III | / | H | $(CH_2)_2OH$ | 58 | * | / | 264.4 |
| 2e.III | / | H | $(CH_2)_3CF_3$ | 72 | * | < 3 | 284.3 |
| 2f.III | / | H | $CH_2C_6H_{11}$ | 85 | * | < 3 | 231.8 |
| 2g.III | / | H | $CH_2C_6H_5$ | 70 | * | 5 | 212.3 |
| 2h.III | / | H | $(CH_2)_2C_6H_5$ | 72 | / | 21 | 139.7 |
| 2i.III | / | H | $CH_2$-2'-pyridyl | 90 | / | / | 187.5 |
| 2j.III | / | H | $CH_2$-3'-pyridyl | 91 | * | 37 | 226.6 |
| 2k.III | / | H | $CH_2$-4'-pyridyl | 62 | / | 71 | 232.5 |
| 2l.III | / | H | $CH_2$-2'-naphthyl | 82 | * | / | 238.6 |
| 2m.III | / | H | $(CH_2)_2N(CH_3)_2$ | 44 | * | / | 218.3 |
| 2n.III | / | H | $(CH_2)_3N(CH_3)_2$ | 52 | / | / | 179.5 |
| 2o.III | / | H | $(CH_2)_2$-morpholine | 38 | * | >500 | 174.3 |
| 3.III | $CH_2C_6H_5$ | H | $CH_2C_6H_5$ | 31 | * | / | 257.3 |
| 4.III | / | $CH_2C_6H_5$ | $CH_2C_6H_5$ | 84 | * | / | 155.7 |
| 5.III | $CH_2C_6H_5$ | $CH_2C_6H_5$ | $CH_2C_6H_5$ | 36 | * | / | 261.8 |

## 1.2 Synthesis of β-carboline analogues

Compounds **2a-o.III** were synthesized following an original two steps procedure including the demethylation of harmine (**3.I**) to the corresponding harmol (**1.III**) followed by a re-alkylation of harmol (**1.III**) to the corresponding β-carboline derivative (Scheme 1.III). The key intermediate, harmol (**1.III**), was generated by cleavage of the methyl ether present in harmine (**3.I**) with hydrobromic acid in quantitative (100%) yield. Finally, compounds **2a-o.III** were obtained by *O*-alkylation of harmol (**1.III**) in the presence of cesium carbonate with the corresponding alkyl halide in 38-92% yield [193]. Compound **3.III** was synthesized by *N*-benzylation of **2g.III** with benzyl bromide in 31% yield (Scheme 1.III). Compound **4.III** was prepared by *O,N*-benzylation of harmol (**1.III**) in the presence of potassium hydroxide with benzyl bromide in 84% yield (Scheme 1.III). Compound **4.III** was then *N*-benzylated with benzyl bromide to afford compound **5.III** in 36% yield (Scheme 1.III). X-ray diffraction was used to unambiguously establish the position of the benzyl groups in the β-carboline template. ORTEP views of the conformations of **2g.III** and **3-5.III**, with their atomic numbering scheme are depicted in figure 3.III.

The structure of the synthesized compounds was determined by $^1$H NMR, $^{13}$C NMR, mass spectrometry (MS) and their purity was assessed by elemental analyses and HPLC. The data are reported in the chapter Materials and Methods.
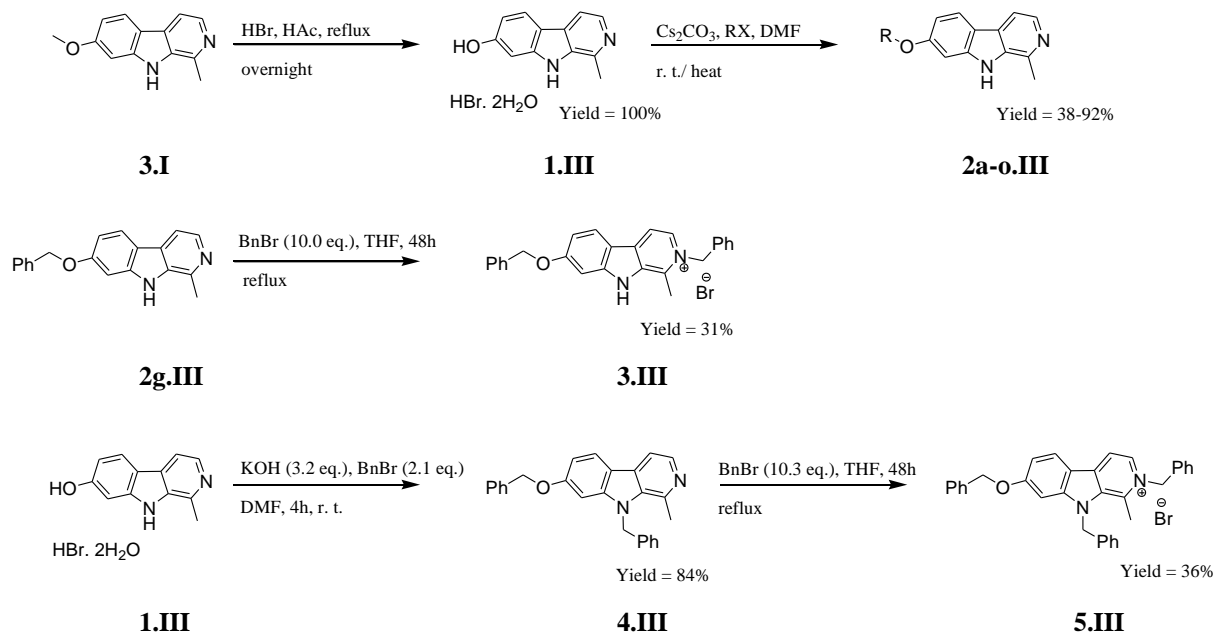


**Scheme 1.III.** Synthetic pathway to analogues **2a-5.III**.
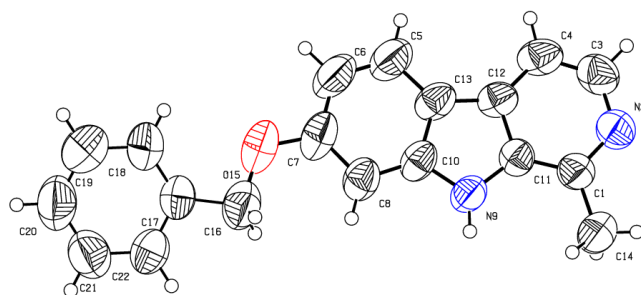
**Figure 3.III.** ORTEP diagram (50% probability) of compounds **2g.III** and **3-5.III**.

## 1.3 Biological evaluation

Now that compounds are synthesized, our objective is to evaluate the human monoamine oxidase A and B inhibitory potency of β-carboline derivatives to establish structure-activity relationships for both activity and selectivit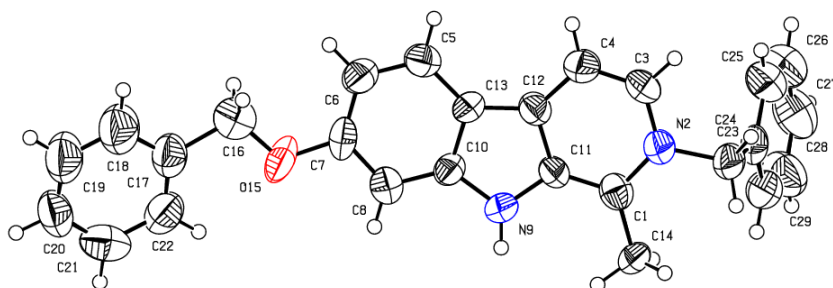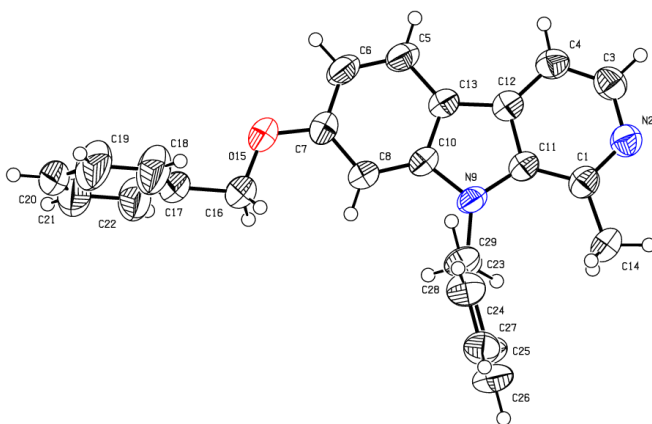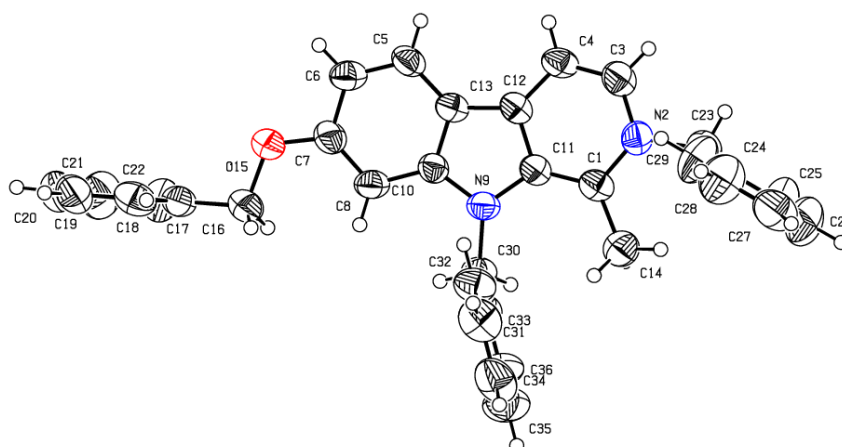y of compounds on the two isoforms of MAO. Hence, the ability to measure MAO activity and the effects of test compounds on that activity is critical for selecting specific MAOIs. Current methods for assaying MAO activity have several disadvantages [194]. Direct methods that use HPLC and/or radiochemical detection are common but are generally expensive and time-consuming. Methods that monitor changes in absorbance can be rapid and simple but are not very sensitive. Fluorescent assays, although both simple and sensitive, often are confounded by the spectroscopic interference of test compounds [194]. In addition, any indirect methods that monitor the formation of $H_2O_2$ [195-196] are not specific for MAO and can be misleading because a variety of enzymes and cellular processes can change the concentration of $H_2O_2$. To overcome these limitations, we have adapted a high-throughput screening assay (MAO-Glo™ assay) from Promega Corporation that couples the activity of MAO to the production of light by luciferase in a convenient two-step format (Figure 4.III) [194]. This bioluminescent assay is a simple, homogeneous, and robust method for the sensitive and rapid measurement of MAO activity and the effects of test compounds on that activity. The MAO-A and –B enzymes used in this study were purchased from Sigma-Aldrich (Cat.# M7316 and M7441 respectively) in the form of microsomal protein prepared from insect cells infected with recombinant baculovirus containing cDNA inserts for the human MAO genes. The recombinant MAO enzymes were provided under microsomes at a protein concentration of 5 mg.mL$^{-1}$.

To evaluate our test compounds, the first step was the optimization of the MAO-Glo™ assay parameters in our conditions. After the optimization of parameters, we have validated the activity test on hMAO-A and –B using competitive inhibitors, harmine (**3.I**, Table 1.III, $K_i = 5$ nM [69]) and isatin (**4.I**, Figure 2.I, $K_i = 3$ μM [17]) respectively which are commercially available from Sigma-Aldrich.

### 1.3.1 Inhibition study of MAO-A and –B

a) Description of MAO-Glo™ assay (Promega) [194]

The MAO-Glo™ assay is performed in two steps (Figure 4.III):

**Step 1. The MAO reaction**: the MAO enzyme is incubated with a luminogenic MAO substrate. The substrate of the MAO-Glo™ assay is a derivative of beetle luciferin (($4S$)-4,5-dihydro-2-(6-hydroxybenzothiazolyl)-4-thiazolecarboxylic acid). The MAO enzyme oxidizes the amine to an imine (reaction **1**), which is subsequently hydrolyzed by water to the corresponding aldehyde (reaction **2**). The aldehyde then spontaneously undergoes a β-elimination reaction to generate methyl ester luciferin (reaction **3**). Since the latter two reactions are not rate limiting, the amount of methyl ester luciferin produced is proportional to the activity of MAO.

**Step 2. The luciferin detection**: after the MAO reaction has been performed, the reconstituted luciferin detection reagent (LDR) inactivates MAO and provides both the enzymes and cosubstrates necessary to convert the product of step 1 into a luminescent signal. As shown in figure 4.III (reactions **4–5**), an esterase converts the methyl ester luciferin into luciferin, which is subsequently consumed by luciferase to yield oxyluciferin and light. This addition initiates a stable glow-type luminescent signal with a half-life greater than 5 h. The amount of light produced is directly proportional to the activity of MAO.
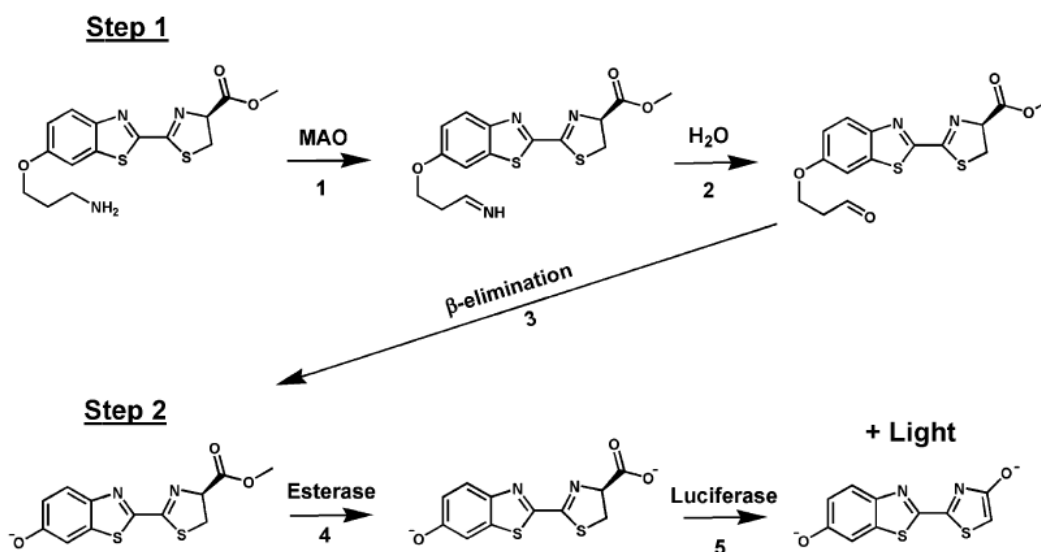


**Figure 4.III.** Description of MAO-Glo™ assay [194].

The activity on the MAO-A and –B isoforms can be estimated using this test. However, MAO-A and –B are affected differently by environmental conditions (Promega). So, while the DMSO in a final concentration from 0.5 to 25% decreases the activity of MAO-A, it increases that of MAO-B (Figure 5.III) (Promega).
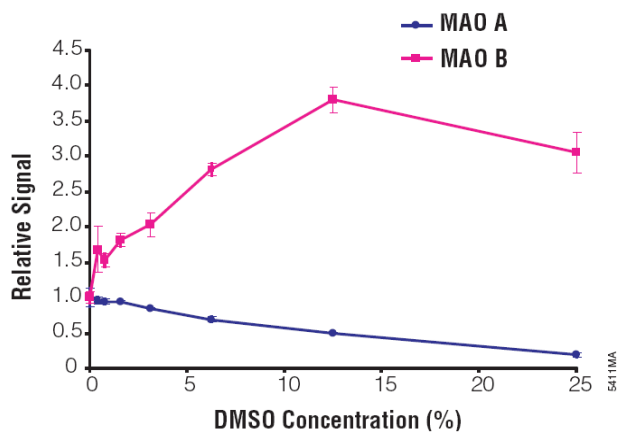


**Figure 5.III.** The effect of DMSO concentration on MAO activity (Promega).

The temperature also has a much greater effect on the MAO-B reaction compared to the MAO-A reaction (Figure 6.III) (Promega). A decrease of the temperature from 35°C to 25°C decreases in a more important way the activity of MAO-B than that of MAO-A (Promega).
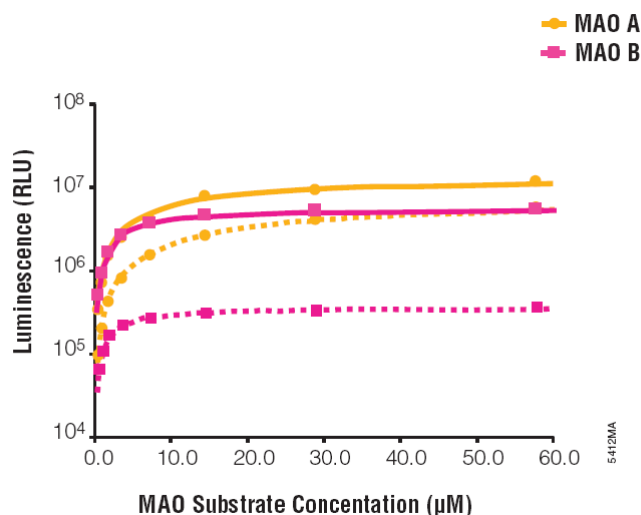


**Figure 6.III.** The effect of temperature on MAO activity; dashed line: T = 25°C and continuous line: T = 35°C (Promega).

b) Optimization of MAO-Glo™ assay

*Parameters to be optimized*

**- Inhibitor concentration and percentage of DMSO**: as the most of our test compounds display a relatively weak solubility, the addition of DMSO was required to solubilize them in the enzymatic test. An arbitrary concentration of 50 µM was fixed for a first screening of compounds on both isoforms of MAO. So, the DMSO concentration was optimized to use only a minimum of DMSO in the enzymatic tests.

**- Contact time between the enzyme and the inhibitor**: we have fixed a contact time between the enzyme and the inhibitor of 2.5 min. As a result of the fact that our test compounds have to act more probably by a competitive binding assay compared to harmine (**3.I**, Table 1.III), this contact time displays no impact on their inhibitory potency.

**- Reaction time**: the reaction time for the first step of MAO-Glo™ assay (Figure 4.III: reactions **1**-**3**) was fixed at 1 h ($t_1$ = 1h) in agreement with the available data in the technical bulletin of the MAO-Glo™ assay (Promega). The optimal reaction time for the second step (Figure 4.III: reactions **4**-**5**) was determined by a kinetic measure of the luminescent signal appearance. This reaction time corresponds to the necessary time to have a stable luminescent signal.

**- Reaction temperature**: we have fixed a temperature of 37°C to maximize the luminescent signal.

**- Intensity of the luminescent signal**: to quantify the inhibitory potency of our test compounds on MAO-A and –B, it is required to measure a luminescent signal of sufficient intensity for the enzymatic reaction without test compound (100% initial activity). Thus, an intensity of 10 RLU (relative luminescence unit) was fixed like minimun intensity to be reached without test compound.

**- Enzyme concentration**: to study the selectivity of our test compounds, we have decided to work with the same "quantity" of MAO-A and –B expressed in specific activity (activity unit

by mg of proteins) such as specified by the supplier. 1 enzymatic unit is defined as the quantity of enzyme which deaminates 1 nanomol of kynuramine per minute in pH 7.4 at 37 °C. Human MAO-A (M7316) and –B (M7441) display a specific enzymatic activity of 75 U.mg$^{-1}$ and 34 U.mg$^{-1}$, respectively.

**- Substrate concentration**: we have decided to work with a substrate concentration equal to the Michaelis constant ($K_m$) for both isoforms of MAO to be in experimental conditions where the Michaelis-Menten kinetics are respected. So, the evaluation of $K_m$ was performed for both isoforms of MAO.

*Evaluation of the minimun DMSO concentration*

An arbitrary concentration of 50 µM was fixed for a first screening of test compounds on both isoforms of MAO. Thus, a solubility test was performed on β-carboline and 5*H*-indeno[1,2-*c*]pyridazine-5-one derivatives displaying a high hydrophobicity. This solubility test was performed in the same proportions that the enzymatic assay (*discussed in the section "Optimized parameters and protocol"*): 12.5 µL of test compound (200 µM) in a final volume of 50 µL (12.5 µl of test compound + 25.0 µl of enzyme + 12.5 µL of substrate). In solubility test, the enzyme and substrate were substituted by the buffer of reaction (100 mM Hepes pH 7.5 and 5% glycerol). To solubilize all test compounds, a stock solution of test compound (200µM) in a mixture buffer/DMSO (1:1) was required. Thus, a final DMSO percentage of 12.5% is brought in the enzymatic assay by the test compound. This percentage of DMSO introduced by the test compound was fixed for all the enzymatic assays. It is also to note that the substrate is also dissolved in DMSO and so, introduces an additional percentage of DMSO in the enzymatic assay dependent on the substrate concentration.

*Evaluation of the optimal MAO-A and –B concentration*

To quantify the inhibitory potency of our test compounds, an evaluation of the optimal MAO-A and –B concentration was required to measure a luminescent signal of sufficient intensity for the enzymatic reaction without test compound (100% initial activity). So, we have varied the MAO-A and –B concentration from 0.3 to 0.7 U.mg$^{-1}$ and fixed a substrate concentration of 100 µM for MAO-A and 20 µM for MAO-B. These substrate concentrations were selected

to be in large excess compared to the enzyme (non-limiting substrate concentrations; enzyme working at $V_{max}$) on the basis of the Michaelis-Menten curves supplied in the technical bulletin of the MAO-Glo™ assay (Promega).

First, the kinetic evolution of the luminescent signal at various enzyme concentrations depicted in figure 7.III (MAO-A; top, MAO-B; bottom), allows to optimize the reaction time of the second step (Figure 4.III, reactions **4**-**5**). Indeed, we observe that a time of 20 min is required to have a stable luminescent signal. Thus, the reaction time of the second step was fixed at 20 min ($t_2$ = 20 min) for all assays. It is to note that the luminescent signal has been systematically checked before the addition of LDR required to the second step of the enzymatic assay (Figure 4.III). This one was nearly zero excluding a luminescent side effect of the step 1 (Figure 4.III).
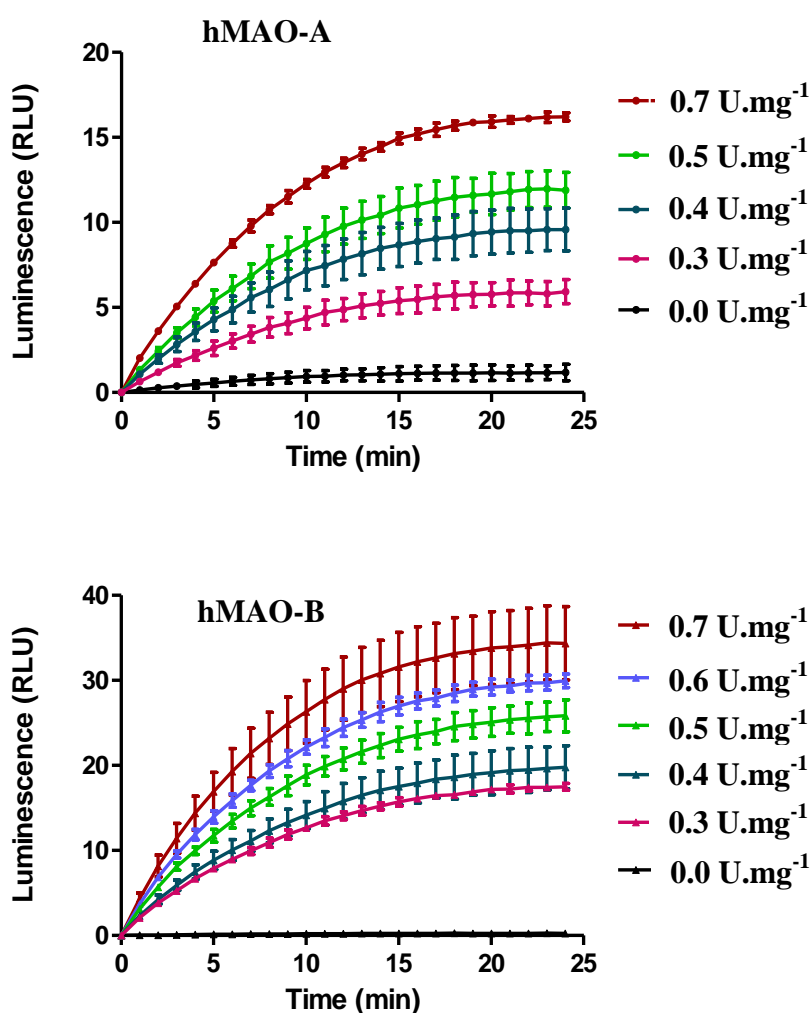


**Figure 7.III.** Kinetic evolution of the luminescent signal at various hMAO-A (top) and –B (bottom) concentrations. Results are expressed as mean ± SD (n = 2).

We also note that the luminescent signal varies linearly with the enzyme concentration (Figure 8.III, MAO-A; blue, MAO-B; red). Furthermore, for an unchanged enzyme concentration, the signal obtained is the same for both isoforms. In conclusion, to quantify the inhibitory potency of our test compounds and to have an unchanged specific activity for both enzymes, we have decided to work with a specific activity fixed at 0.5 U.mg$^{-1}$ for inhibition assays (559 nM/U, determined from the specific activity and the molecular weight of the protein sequences (59682 g.mol$^{-1}$ for MAO-A (expasy: P21397) and 58763 g.mol$^{-1}$ for MAO-B (expasy: P27338))).
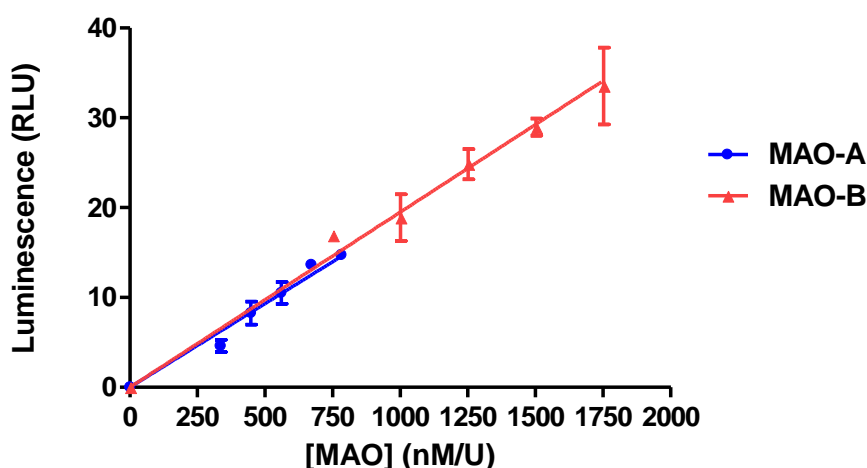


**Figure 8.III.** Effect of enzyme concentration on the luminescent signal ($t_2 = 20$ min). Results are expressed as mean $\pm$ SD (n = 2).

*Evaluation of the optimal substrate concentration*

As mentioned above, we have decided to work with a substrate concentration equal to the Michaelis constant ($K_m$) for both isoforms of hMAO. So, the evaluation of $K_m$ was performed for the two isoforms of MAO (Figure 9.III). We have fixed the enzyme concentration at 0.5 U.mg$^{-1}$ (evaluated previously) for the two isoforms and we have varied the substrate concentration from 0 to 250 µM for MAO-A and from 0 to 60 µM for MAO-B by keeping an unchanged percentage of DMSO (6.25% for the substrate and 12.5% for the test compound).
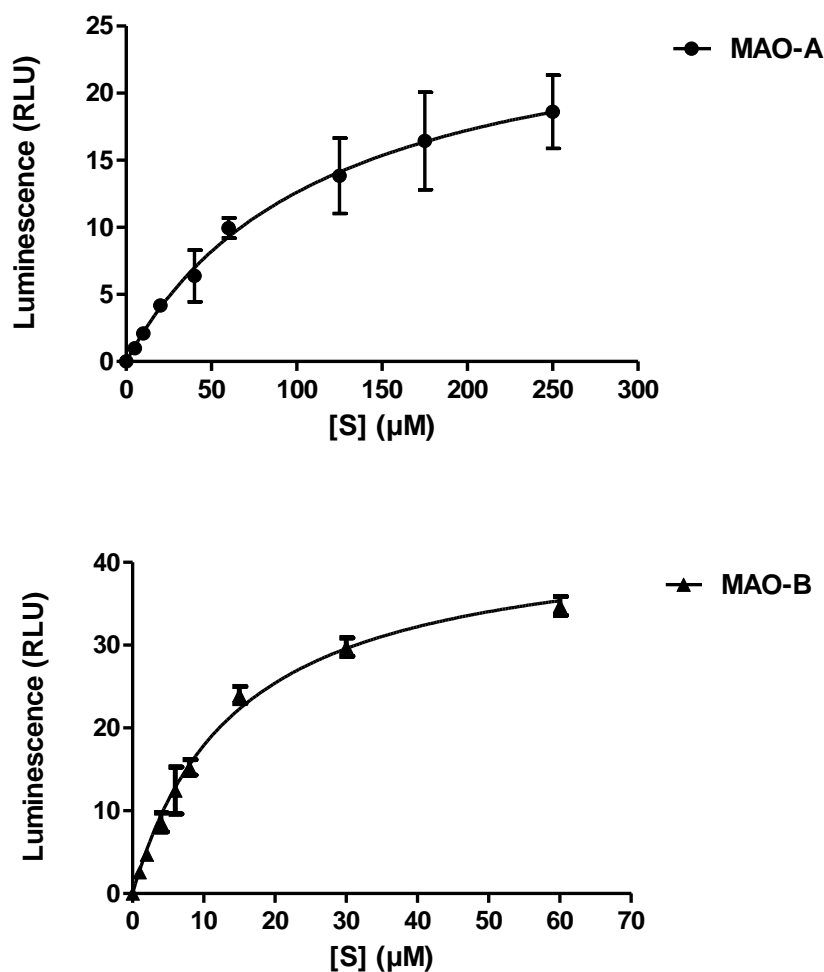
**Figure 9.III.** Michaelis-Menten curves of hMAO-A (top) and -B (bottom). Results are expressed as mean ± SD (n = 2).

The table 2.III reports the kinetic parameters measured for the two enzymes. $K_m$ values of 116.1 µM and 14.6 µM were measured for hMAO-A and –B, respectively. Thus, we observe that the substrate displays a better affinity for MAO-B than for MAO-A (8-fold). By comparison, the $K_m$ values evaluated in the technical bulletin of the MAO-Glo™ assay (Promega) for MAO-A and –B were 40 and 4 µM (10-fold), respectively. These close data tend to validate our experimental approach. In conclusion, for inhibition assays, we have fixed the substrate concentration at 120 and 15 µM for hMAO-A and –B, respectively.

**Table 2.III.** Kinetic parameters of hMAO-A and −B.

| Kinetic parameters[a] | hMAO-A | hMAO-B |
|:---:|:---:|:---:|
| $V_{max}$ **(RLU)** | **27.2** (20.8 − 33.6) | **44.0** (40.9 − 47.1) |
| $K_m$ **(µM)** | **116.1** (56.8 − 175.3) | **14.6** (12.1 − 17.1) |
| $R^2$ | 0.9568 | 0.9905 |

[a] Results are expressed as mean with 95% confidence intervals in brackets (n=3).

*Optimized parameters and protocol*

The MAO-Glo™ assay is performed in 96-wells plates at 37°C (Table 3.III).

1) Recombinant MAO enzyme (25.0 µL, final concentration of 0.5 U.mg$^{-1}$) is first incubated with the test compound (12.5 µL, final concentration of 50 µM (12.5% of DMSO)) or with a mixture buffer (100 mM Hepes pH 7.5 and 5% glycerol)/DMSO (1:1) (12.5 µL, final DMSO percentage of 12.5%) for 2.5 min.
2) Then, the substrate (12.5 µL, final concentration of 120 µM (final DMSO percentage of 3.0%) and 15 µM (final DMSO percentage of 0.4%) for MAO-A and −B, respectively) is added to the mixture.
3) Finally, after 1 h of reaction, 50.0 µL of LDR is added to the wells.
4) The luminescent signal is measured 20 min after the addition of the LDR with a 96-wells luminometer Fluoroskan FL (Thermo Fisher Scientific).

Now that the parameters of MAO-Glo™ assay are optimized for our assays, the next step is the validation of the inhibition assay on hMAO-A and −B using known competitive inhibitors, harmine ($K_i$ = 5 nM [69]) and isatin ($K_i$ = 3 µM [17]), respectively.

**Table 3.III.** Optimized MAO-Glo™ assay protocol.

| Components (µL) | 100% Initial activity | Inhibition assay |
|---|---|---|
| Buffer/DMSO (1: 1) | 12.5 | / |
| Test compound | / | 12.5 |
| Enzyme (hMAO-A or –B) (1.0 U.mg$^{-1}$) | 25.0 | 25.0 |
| Substrate (480 µM (hMAO-A); 60 µM (hMAO-B)) | 12.5 | 12.5 |
| LDR | 50.0 | 50.0 |
| Final volume | 100.0 | 100.0 |

## 1.3.2 Inhibition constant ($K_i$) evaluation of harmine on MAO-A and –B

The $K_i$ evaluation of harmine (**3.I**, Table 1.III) is required to validate the inhibition assay on hMAO-A but also to position our test compounds structurally derived from harmine compared to the latter. Furthermore, to date, no data concerning the hMAO-B inhibitory potency of harmine is available. First, IC$_{50}$ values of harmine on hMAO-A and –B were evaluated using the optimized MAO-Glo™ assay and we have varied harmine concentration from $10^{-3}$ to $10^{-9}$ M. Inhibition percentages at each concentration were calculated as follows: I (%) = 100 x {1 – (luminescent signal with harmine/luminescent signal without harmine)}. The inhibition percentages were plotted against the logarithms of harmine molar concentrations. The IC$_{50}$ values were calculated from normalized sigmoidal dose-response non-linear regression curves using the GraphPad Prism 5.01 software. Then, $K_i$ values were estimated from the IC$_{50}$ values using the Cheng–Prusoff equation depicted below [192].

$$K_i = IC_{50}/(1 + [S]/K_m)$$

Dose-response curves and the inhibition parameters of harmine (**3.I**) on hMAO-A and –B are depicted in figure 10.III and table 4.III.

**Figure 10.III.** Dose-response curves of harmine (**3.I**) on hMAO-A (●) and –B (▲). Results are expressed as mean ± SD (n = 3).

**Table 4.III.** Inhibition parameters of harmine (**3.I**) on hMAO-A and –B.

| Inhibition parameters[a] | hMAO-A | hMAO-B |
|---|---|---|
| $IC_{50}$ | **34.4** (27.8 – 42.7) **nM** | **244.9** (192.3 – 312.0) **μM** |
| $K_i$ | **16.9** (13.7 – 21.0) **nM** | **120.8** (94.9 – 153.9) **μM** |
| $R^2$ | 0.9882 | 0.9886 |

[a] Results are expressed as mean with 95% confidence intervals in brackets (n=3).

As expected, harmine (**3.I**) is a strong and selective hMAO-A inhibitor ($K_i$ = 16.9 nM) whereas it poorly inhibits hMAO-B ($K_i$ = 120.8 μM). This selectivity of harmine for the MAO-A isoenzyme can be explained with the superimposition of the crystal structures of hMAO-A in complex with harmine (2Z5X.pdb [3]) and hMAO-B (2V5Z.pdb [4]) (Figure 11.III). The relative geometry of the harmine molecule in hMAO-A could not be accommodated into hMAO-B because of steric overlap with Tyr326 of hMAO-B [3]. Indeed, the Tyr326 side chain in hMAO-B produces a restriction that is less pronounced in hMAO-A where Ile335 occupies that position. Thus, Ile335 in hMAO-A and Tyr326 in hMAO-B play a crucial role in inhibitor selectivity in agreement with previous results [2]. Furthermore, the evaluated $K_i$ value of harmine (**3.I**) on hMAO-A is in agreement with the literature [69] which allows to validate our inhibition assay on hMAO-A.

78
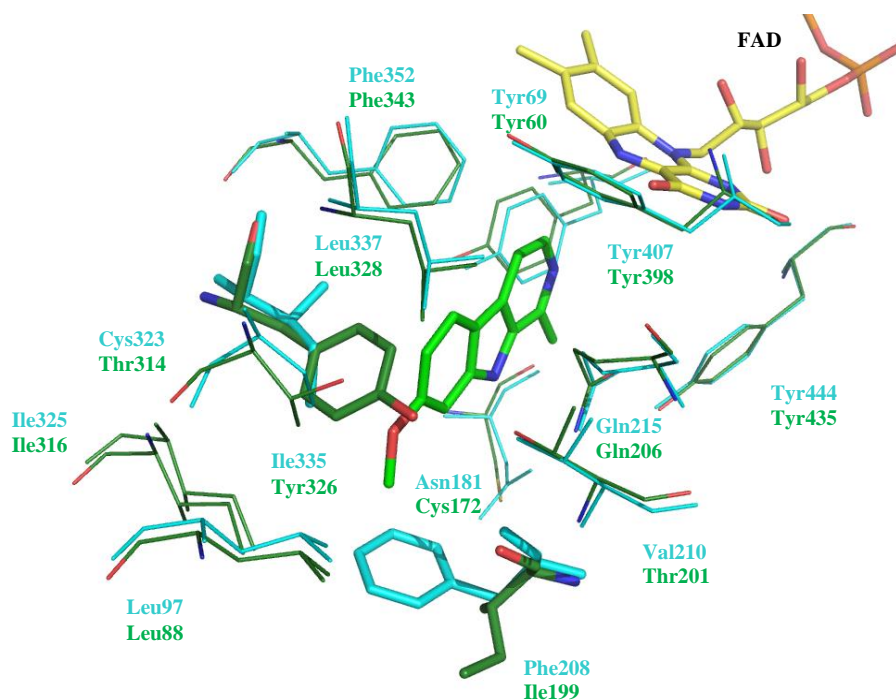
**Figure 11.III.** Superimposition of the crystal structures of hMAO-A (cyan, 2Z5X.pdb [3]) in complex with harmine and hMAO-B (green, 2V5Z.pdb [4]). Harmine and FAD are in green and yellow, respectively. Only amino acids directly implicated in the active site are displayed and labeled in cyan (MAO-A) and in green (MAO-B).

### 1.3.3 $K_i$ evaluation of isatin on MAO-B

Isatin (**4.I**) was used to validate the inhibition assay on hMAO-B. $IC_{50}$ and $K_i$ values of isatin on hMAO-B were evaluated using the same approach than for harmine (**3.I**). Dose-response curve and the inhibition parameters of isatin on hMAO-B are depicted in figure 12.III and table 5.III. Isatin displays a $K_i$ value of 32.6 µM on hMAO-B, which confirms its weak affinity for MAO-B. Although the evaluated $K_i$ is 10-fold higher than the literature value ($K_i$ = 3 µM [17]) and potentially underestimates the inhibitory potency on MAO-B, we have decided to validate the inhibition assay on hMAO-B. Consequently, the inhibitory potency of new β-carboline analogues can be assessed on hMAO-A and –B.
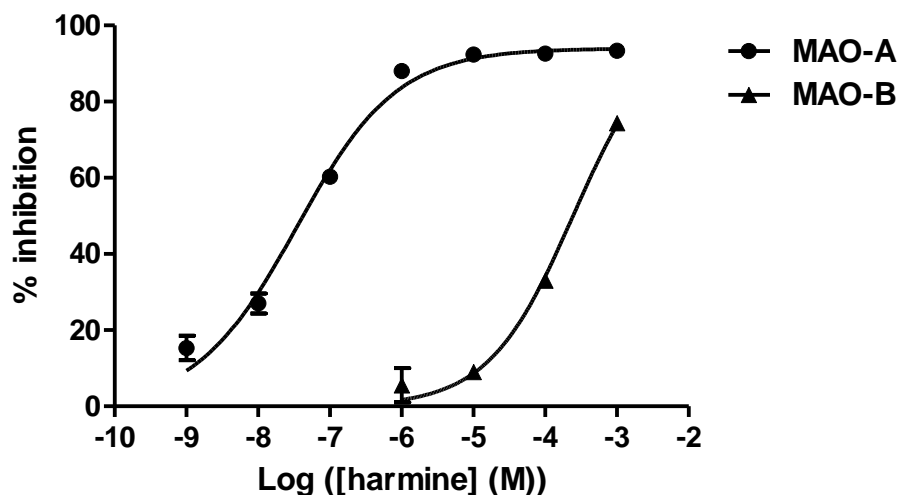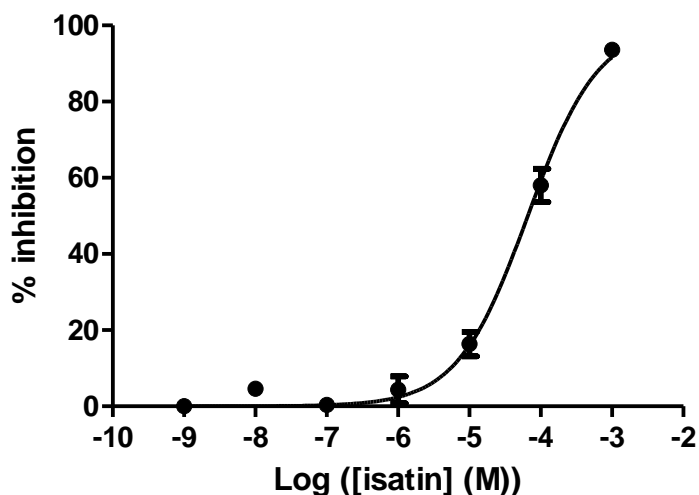
**Figure 12.III.** Dose-response curve of isatin (**4.I**) on hMAO-B. Results are expressed as mean $\pm$ SD (n = 3).

**Table 5.III.** Inhibition parameters of isatin (**4.I**) on hMAO-B.

| Inhibition parameters[a] | hMAO-B |
|---|---|
| IC$_{50}$ | **66.0** (57.0 – 76.4) **µM** |
| $K_i$ | **32.6** (28.1 – 37.7) **µM** |
| R$^2$ | 0.9925 |

[a] Results are expressed as mean with 95% confidence intervals in brackets (n = 3).

### 1.3.4 Inhibitory potency of β-carboline analogues

The inhibitory potency of the newly synthesized β-carbolines was assessed *in vitro* using the inhibition assay previously validated on hMAO-A and –B. First, the IC$_{50}$ values of the most potent were evaluated on hMAO-A and –B. Then, the $K_i$ values were estimated from the IC$_{50}$ values using the Cheng–Prusoff equation [192]. The inhibitory potency of harmine (**3.I**) and the synthesized related β-carbolines (**2a-5.III**) on hMAO-A and –B are reported in table 6.III. All the tested compounds (**2a-3.III**) except the derivatives **4.III** and **5.III**, present a higher inhibitory potency on MAO-A than MAO-B. *O*-Alkylation of the compounds by lipophilic groups like aliphatic chains (**2a.III, 2b.III, 2e.III**), cyclohexyl (**2f.III**) and phenyl (**2g.III,**

80

**2h.III**) allows to significantly increase inhibition of MAO-A compared to harmine (**3.I**). *N*-Benzylations (**3-5.III**) of compound **2g.III** abolish inhibition of MAO-A compared to **2g.III**. Extension of the methoxy group by a methoxyethoxy group (**2c.III**) decreases the inhibition. The substitution of methoxy group of compound **2c.III** by a hydroxyl group (**2d.III**) does not improve the inhibition. Substitution by a pyridyl group (**2i-k.III**) decreases the inhibition compared to harmine (**3.I**) and compound **2g.III**. The substitution of a phenyl group (**2g.III**) by a naphthyl group (**2l.III**) decreases the inhibition. Introduction of more hydrophilic groups like dimethylaminoethyl, dimethylaminopropyl and ethylmorpholine (**2m-o.III**) highly decreases the inhibition. Compound **2e.III**, with the trifluorobutyloxy group, is the most active and selective within this series, with a $K_i$ on MAO-A of 3.6 nM (Figure 13.III). The solubility of some β-carbolines in phosphate buffer (pH 7.4) at room temperature reported in table 1.III, was evaluated following a protocol developed by our group [197]. We observe that the introduction of more lipophilic groups decreases the solubility compared to harmine. Interestingly, although the compound **2o.III** ($K_i$ = 255.7 nM) containing an ethylmorpholine group is less active compared to **2e.III**, it is a potent and selective inhibitor of MAO-A, and displays also a higher solubility compared to **2e.III**. Compound **2o.III** is totally soluble for concentrations higher than 500 μM compared to **2e.III** (<3 μM). Moreover, several compounds (**2b.III**, **2e.III**, **2g.III**, **2h.III**, **3-5.III**) show a better inhibition of MAO-B ($K_i$ >500 nM) compared to harmine (**3.I**, $K_i$ = 120.8 μM). Interestingly, compound **2f.III** displayed the best inhibitory activity on MAO-B with a $K_i$ value of 221.6 nM (Figure 13.III). This cyclohexyl bearing analogue is also a potent MAO-A inhibitor with a $K_i$ value of 4.3 nM.
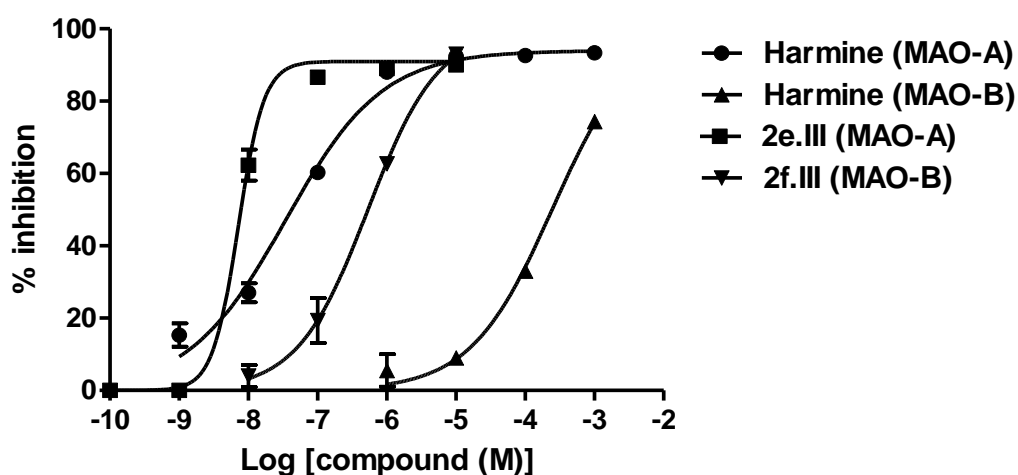


**Figure 13.III.** Dose-response curve of harmine (**3.I**) on hMAO-A (●) and –B (▲), of compound **2e.III** on hMAO-A (■) and of compound **2f.III** on hMAO-B (▼). Inhibition percentages are shown as mean ± SD with n = 3.

**Table 6.III.** Structure and inhibitory potency of harmine (**3.I**) and the synthesized related β-carbolines (**2a-5.III**) on hMAO-A and −B.



| Compound | $R_1$ | $R_2$ | $R_3$ | $K_i$ (nM)[a] | |
|---|---|---|---|---|---|
| | | | | **hMAO-A** | **hMAO-B** |
| **harmine** | / | **H** | $CH_3$ | **16.9** (13.7 – 21.0) | **120800** (94900 – 153900) |
| **2a.III** | / | **H** | $CH_2CH=CH_2$ | **5.0** (4.5 – 5.6) | **NI**[b] |
| **2b.III** | / | **H** | $CH_2CH(CH_3)_2$ | **3.9** (2.0 – 7.7) | **>500**[c] |
| **2c.III** | / | **H** | $(CH_2)_2OCH_3$ | **29.5** (24.0 – 36.3) | **NI** |
| **2d.III** | / | **H** | $(CH_2)_2OH$ | **28.4** (20.0 – 40.3) | **NI** |
| **2e.III** | / | **H** | $(CH_2)_3CF_3$ | **3.6** (2.6 – 5.0) | **>500** |
| **2f.III** | / | **H** | $CH_2C_6H_{11}$ | **4.3** (3.2 – 5.6) | **221.6** (145.1 – 338.3) |
| **2g.III** | / | **H** | $CH_2C_6H_5$ | **12.6** (11.6 – 13.7) | **>500** |
| **2h.III** | / | **H** | $(CH_2)_2C_6H_5$ | **5.0** (4.0 – 6.2) | **>500** |
| **2i.III** | / | **H** | $CH_2$-2'-**pyridyl** | **≈ 500** | **NI** |
| **2j.III** | / | **H** | $CH_2$-3'-**pyridyl** | **24.9** (20.1 – 30.7) | **NI** |
| **2k.III** | / | **H** | $CH_2$-4'-**pyridyl** | **35.4** (18.9 – 66.5) | **NI** |
| **2l.III** | / | **H** | $CH_2$-2'-**naphthyl** | **100 < $K_i$ < 500** | **NI** |
| **2m.III** | / | **H** | $(CH_2)_2N(CH_3)_2$ | **1023.8** (920.0 – 1139.4) | **NI** |
| **2n.III** | / | **H** | $(CH_2)_3N(CH_3)_2$ | **684.0** (558.6 – 836.9) | **NI** |
| **2o.III** | / | **H** | $(CH_2)_2$-**morpholine** | **255.7** (196.7 – 324.5) | **NI** |
| **3.III** | $CH_2C_6H_5$ | **H** | $CH_2C_6H_5$ | **≈ 500** | **>500** |
| **4.III** | / | $CH_2C_6H_5$ | $CH_2C_6H_5$ | **NI** | **>500** |
| **5.III** | $CH_2C_6H_5$ | $CH_2C_6H_5$ | $CH_2C_6H_5$ | **NI** | **>500** |

[a] Results are expressed as mean with 95% confidence intervals in brackets (n = 3).
[b] NI : no inhibition at 1 µM.
[c] >500: Inhibition percentage at 1 µM are shown as mean with ± SD in brackets (n = 3), **2b.III** = 14% (±6%), **2e.III** = 24% (±4%), **2g.III** = 42% (±2%), **2h.III** = 39% (±2%), **3.III** = 34% (±3%), **4.III** = 46% (±2%), **5.III** = 29% (±5%).

With the aim of rationalizing the inhibitory potencies obtained for β-carbolines on hMAO-A and –B, molecular docking studies of compounds **2e.III** and **2f.III** were performed and are discussed in the next section.

## 1.4 Structural approach

### 1.4.1 X-ray crystal analysis

With the aim of trying to understand the types of interactions that the compounds **2e.III** and **2f.III** can establish within the binding site of MAO-A and –B, the molecular structure of these compounds was determined by X-ray crystallographic analysis. ORTEP diagram and crystalline cohesion pattern of compounds **2e.III** and **2f.III** are depicted in figure 14.III.
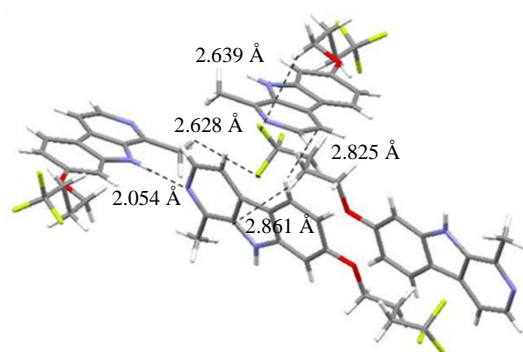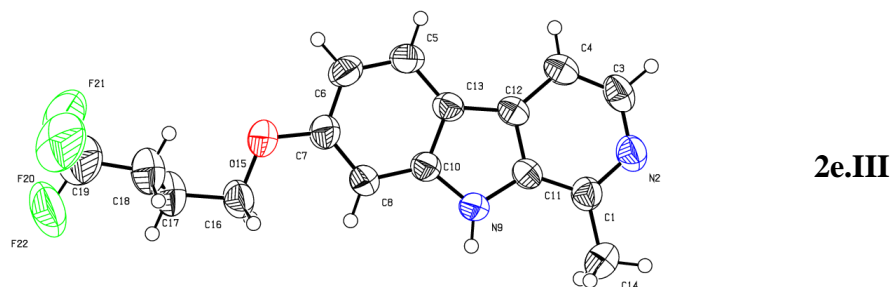
a) Compound **2e.III**

Single crystals of compound **2e.III** were obtained by slow evaporation at room temperature of a solution in dichloromethane/ethanol. The compound crystallizes in the trigonal,        space group ($R_1$ = 0.0617). The planar aromatic β-carboline ring is prolonged by the lateral trifluorobutyloxy chain that adopts a *anti, anti, gauche, anti* conformation [torsion angles are C6-C7-O15-C16 = -176.6(2)°, C7-O15-C16-C17 = 176.6(2)°, O15-C16-C17-C18 = 66.5(3)°, C16-C17-C18-C19 = -174.2(3)°]. The C7-O15-C16 bond angle 117.3(2)° is indicative of a $sp^2$ character of the oxygen underlining electronic delocalization from the β-carboline ring to the alkoxy chain. Crystal packing results from antiparallel arrangement of molecules. The crystalline cohesion is further maintained by hydrogen bonds formed between N9-H…N2 (2.054 Å), weak CH-π(C($sp^2$)) hydrogen bonds (in the range of 2.8 Å) and weak C-H…F hydrogen bonds (in the range of 2.6 Å).

b) Compound **2f.III**

Single crystals of compound **2f.III** were obtained by slow evaporation at room temperature of a solution in dichloromethane/ethanol. The compound crystallizes in the trigonal,        space group ($R_1$ = 0.0642). The C7-O15-C16 bond angle 118.6(6)° is indicative of a $sp^2$ character of the oxygen underlining electronic delocalization from the β-carboline ring to the cyclohexyl chain. Crystal packing results from antiparallel arrangement of molecules. The crystalline

cohesion is further maintained by hydrogen bonds formed between N9-H…N2 (2.076 Å), weak CH-π(C(sp$^2$)) hydrogen bonds (in the range of 2.8 Å) and weak hydrogen bonds between the methylene groups of cyclohexyl chains (in the range of 2.3 Å).



**(a)**
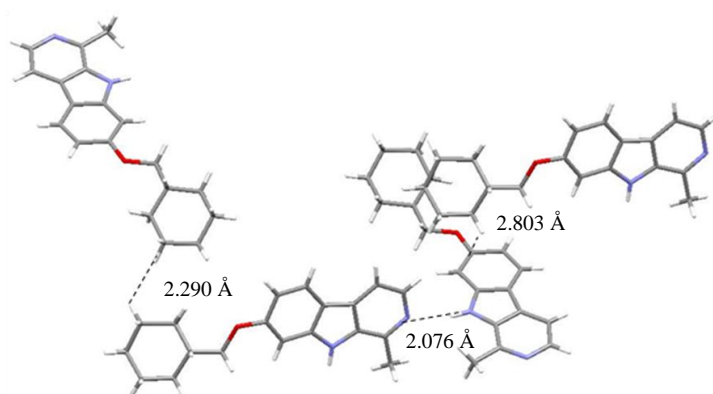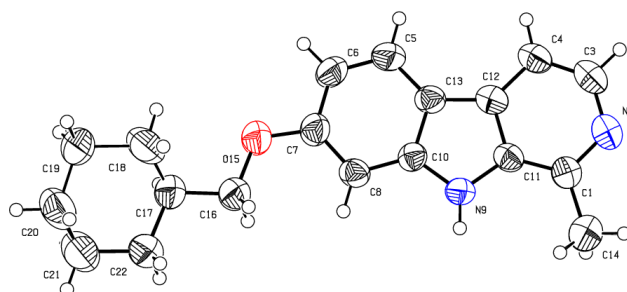


**(b)**

**Figure 14.III.** ORTEP diagram (50% probability) and crystalline cohesion pattern of compounds **2e.III** (a) and **2f.III** (b).

84

## 1.4.2 Validation of docking studies on MAO-A and –B

Before to study the binding mode of β-carboline derivatives on hMAO-A and –B, it is required to validate the docking procedures. Thus, X-ray crystallography structures of hMAO-A and –B in complex with harmine (**3.I**, 2Z5X.pdb [3]) and safinamide (**1.I**, 2V5Z.pdb [4]) respectively, were used as case studies. The selection of these structures was guided by the quality of the crystallographic data and the fact that safinamide (**1.I**) in 2V5Z X-ray crystallography is a non-covalent ligand crossing the entire binding site of MAO-B. As a consequence, the side chain of key residue Ile199 is oriented such as the entrance and substrate cavities are merged. This structural prerogative is essential to model the binding of β-carboline derivatives that must be accommodated by both cavities. Seven water molecules which occupy the space between harmine and FAD were conserved from X-ray crystallography (2Z5X.pdb) into the MAO-A model (Figure 15.III, left). In the MAO-B model, three conserved water molecules are buried in the vicinity of FAD and proved to be important for docking simulation of MAO-B selective ligand [73]. So these water molecules are kept inside the binding site as an integral part of the protein structure during the whole computational procedure (Figure 15.III, right).



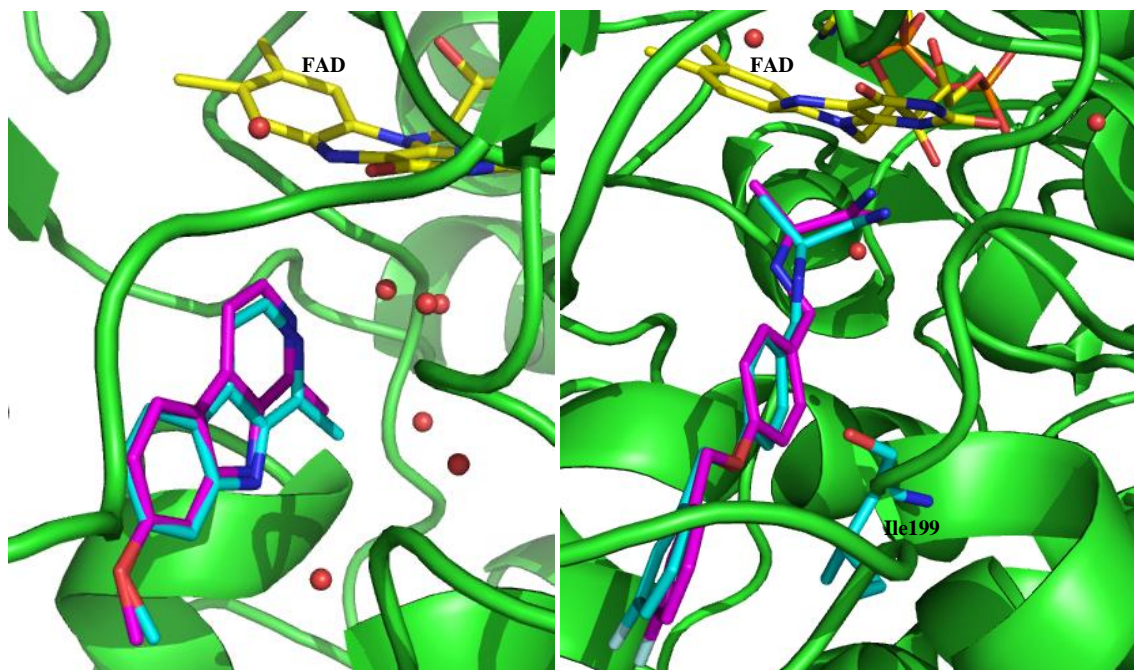**Figure 15.III.** Superimposition of, (left) the crystal structure of hMAO-A (2Z5X.pdb) in complex with harmine (**3.I**, cyan) and the top docking solution of harmine in hMAO-A model (magenta), and (right) the crystal structure of hMAO-B (2V5Z.pdb) in complex with safinamide (**1.I**, cyan) and the top docking solution of safinamide in hMAO-B model (magenta). The water molecules are displayed as red spheres.

The structures of ligands are built and geometry optimised at physiological pH within Discovery studio® 2.5 software (Accelrys Software Inc., San Diego, USA). The interaction sphere in the docking was centered on the N5 atom of the flavin (FAD) in the catalytic site of the protein (MAO-A and –B) and delimited by a 20 Å radius. A total of twenty-five docking solutions were generated using GOLD (version 3.2) software and the scoring function used to rank the docking was Goldscore. All docking solutions obtained for harmine (**3.I**) and safinamide (**1.I**) displayed a similar binding mode compared to the crystal structures of complexes with hMAO-A and –B (2Z5X.pdb and 2V5Z.pdb) respectively (Figure 15.III). The RMSD calculated between the crystal structure and the top solution coordinates for ligand heavy atoms is 0.39 Å and 0.46 Å for harmine (**3.I**) and safinamide (**1.I**) on hMAO-A and –B respectively.

### 1.4.3 Molecular docking studies of compound 2e.III on MAO-A

Analysis of the optimal binding mode for compound **2e.III** (Figure 16.III)—identified from the docking study— revealed that this compound is located in the vicinity of the FAD cofactor. The β-carboline derivative incorporates in the active site with harmine-like interactions. In comparison with the harmine interactions, the hydrogen bonds with two water molecules are conserved. The $\pi$-$\pi$ interaction between the amide group of the Gln215 side chain and harmine is also conserved. The binding mode adopted by compound **2e.III** allows the trifluorobutyloxy side chain to settle within a cavity lined with hydrophobic amino acid residues. This hydrophobic pocket includes Val93, Leu97, Phe108, Ala111, Phe208, Val210, Cys323 and Ile325. All docking solutions show a similar binding mode but the trifluorobutyl chain is flexible and adopts several conformations. Among these conformations, we selected the *anti, anti, gauche, anti* conformation which also corresponds to the geometry observed in the crystal structure. These data may explain the increase of MAO-A inhibitory potency of compound **2e.III** ($K_i$ = 3.6 nM) compared to harmine (**3.I**, $K_i$ = 16.9 nM). Furthermore, the hydrophobic aspect of the cavity around the lateral chain may also explain the increase of inhibition for the compounds with lateral chains displaying lipophilic groups like cyclohexyl (**2f.III**) or aliphatic chains (**2a.III**, **2b.III**, **2e.III**). The presence of aromatic amino acids in this cavity also allows to favour $\pi$-$\pi$ interactions with phenyl groups (**2g.III**, **2h.III**). The fact that the cavity is highly hydrophobic may be one plausible explanation for the decrease in

inhibition seen with hydrophilic groups (**2m-o.III**) compared to harmine (**3.I**). Finally, the inhibition decrease of compounds (**3-5.III**) substituted in the 2 and 9-positions by benzyl groups compared to **2g.III** is probably due to the loss of hydrogen bonds with water molecules and the lack of space available for the substituents.
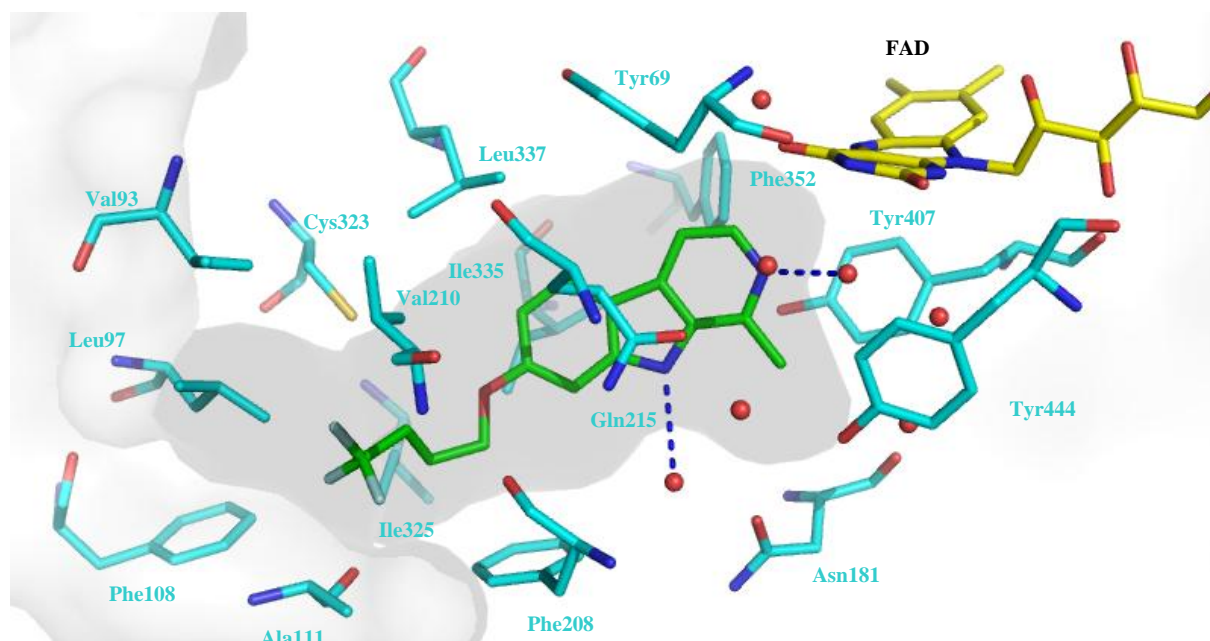


**Figure 16.III.** Binding mode of compound **2e.III** in the active site of hMAO-A (2Z5X.pdb). Only amino acids directly implicated in the active site are displayed and labeled in cyan. Compound **2e.III** and FAD are in green and yellow respectively. The water molecules are displayed as red spheres. The hydrogen bonds discussed in the text are depicted as dashed blue lines.

### 1.4.4 Molecular docking studies of compound 2f.III on MAO-A and –B

The interesting result obtained for compound **2f.III** on hMAO-B led us to study the potential binding mode of this β-carboline derivative with hMAO-A and –B. The results of docking simulations are represented in figure 17.III.

Compound **2f.III** in MAO-A adopts a similar binding mode compared to derivative **2e.III** with the cyclohexyl chain pointing to the hydrophobic cavity and stabilization of the β-carboline moiety through two hydrogen bonds and π-π interaction.

Docking simulations for compound **2f.III** performed on hMAO-B show that the β-carboline core incorporates into the substrate cavity with a shift of the β-carboline orientation compared to docking solution on MAO-A because of steric clash caused by Tyr326. Compared to

hMAO-A, the β-carboline core is stabilized by only one hydrogen bond between one of the nitrogen atoms of β-carboline and one water molecule. The pyridine moiety is also stabilized with the aromatic cage (Tyr407, Tyr444 and FAD) by $\pi$-$\pi$ interaction but the interaction of the β-carboline with the lateral chain of Gln206 is less favorable. This may explain the better inhibitory activity of our compounds on hMAO-A.
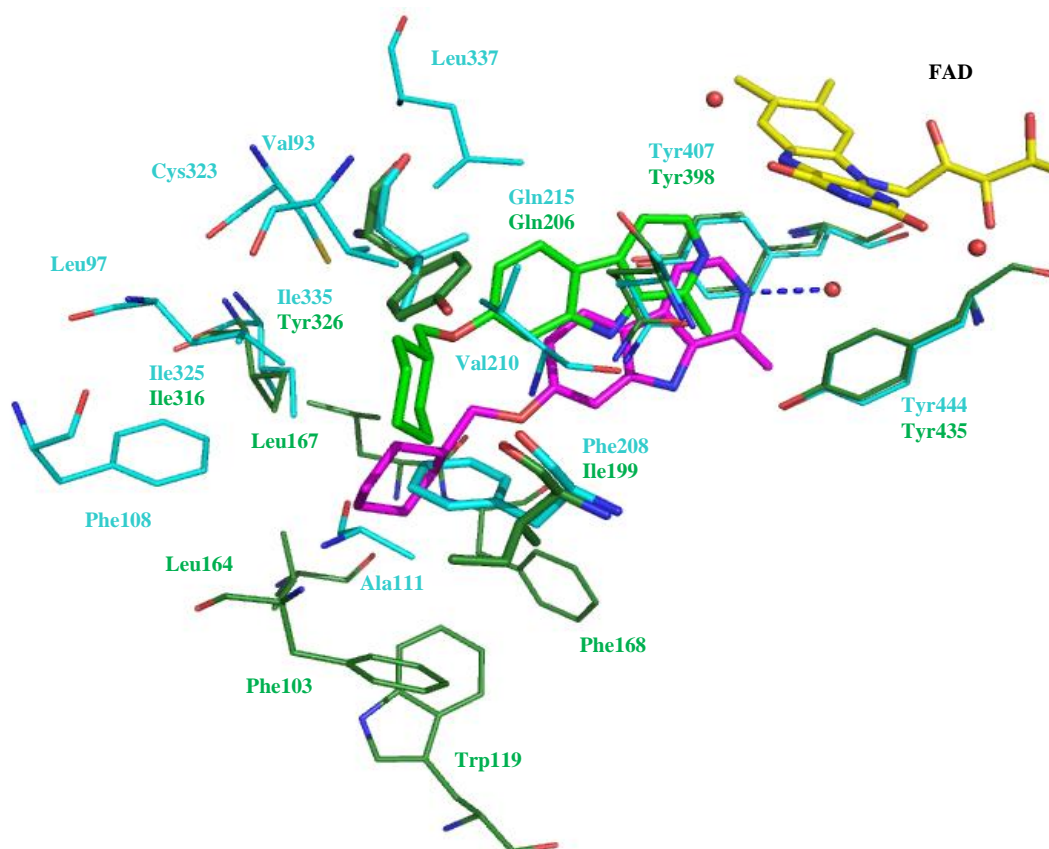


**Figure 17.III.** Binding mode of compound **2f.III** in the active site of hMAO-A and –B. Only amino acids directly implicated in the active site are displayed and labeled in cyan (MAO-A) and in green (MAO-B). Compound **2f.III** is in green (MAO-A) and magenta (MAO-B). FAD is in yellow. The water molecules involved in MAO-B are displayed as red spheres. The hydrogen bond discussed in the text is depicted as a dashed blue line.

In the case of β-carboline derivative **2f.III**, the lateral chain occupies a hydrophobic pocket of the entrance cavity coated by Phe103, Trp119, Leu164, Leu167, Phe168, and Ile316 where it is stabilized in agreement with an enhanced inhibitory potency towards hMAO-B compared to harmine (**3.I**). So, docking simulations allow to explain the stabilization of the cyclohexyl chain in the hydrophobic pocket but also of the aliphatic groups like trifluorobutyl (**2e.III**) or isobutyl (**2b.III**). The presence of aromatic amino acids in the hydrophobic pocket allows to understand the inhibition increase for compounds including phenyl groups (**2g.III** and **2h.III**)

compared to harmine (**3.I**). As well as with MAO-A, the fact that the cavity where the lateral chain incorporates is hydrophobic may be related to the absence of inhibition with hydrophilic groups (**2m-o.III**).

**1.4.5 β-Carboline analogues binding sites on MAO-A and –B**

Figure 18.III shows the schematic diagram of the β-carboline analogues binding sites in hMAO-A and –B respectively.



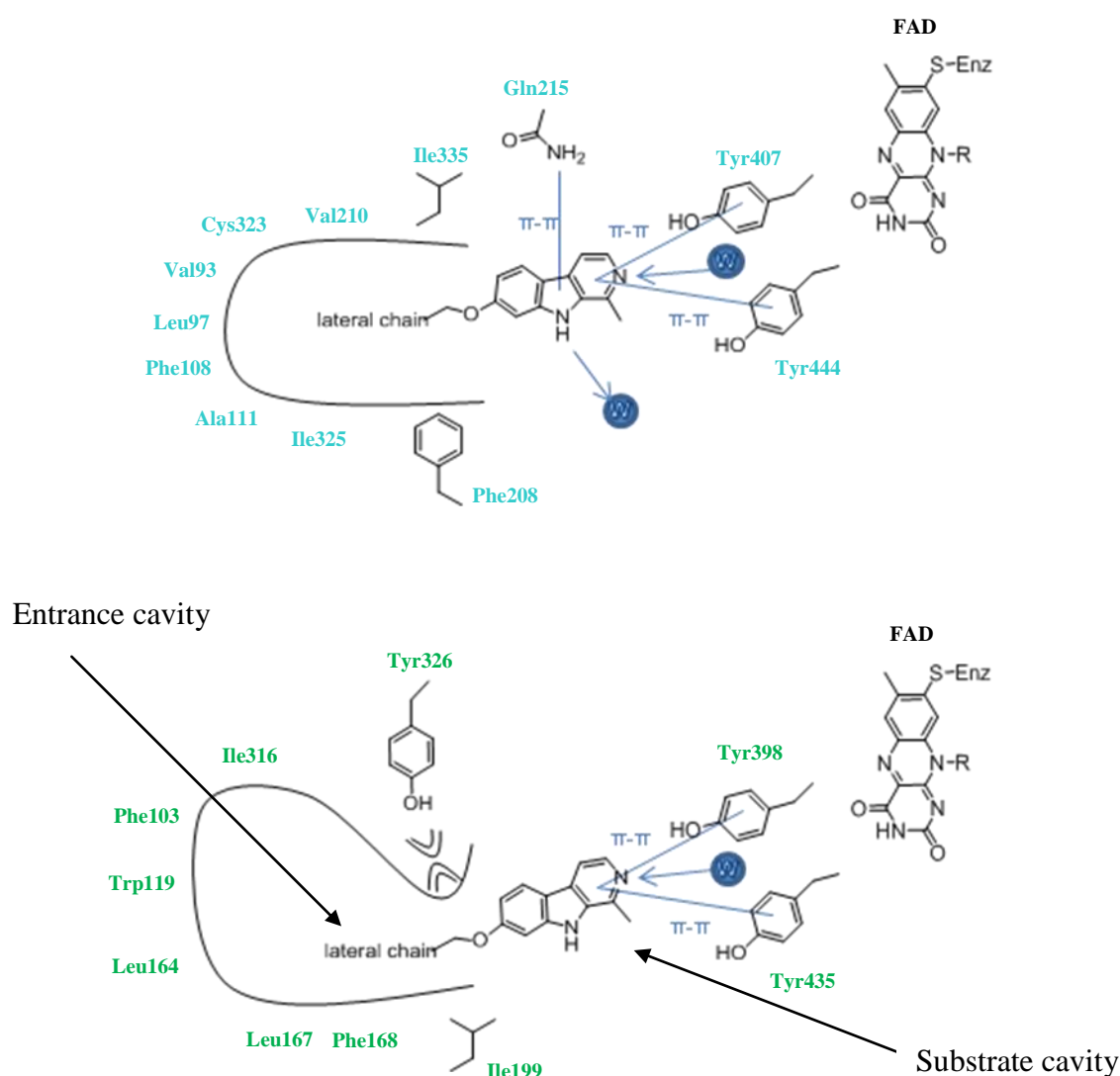**Figure 18.III.** Schematic diagram of the β-carboline derivatives binding sites on hMAO-A (top) and hMAO–B (bottom). The strongest interactions stabilizing the β-carboline core are represented in blue. The amino acids forming the pocket available for the lateral chain are labeled in cyan (MAO-A) and in green (MAO-B). Hydrogen-bond interactions are represented by a blue line with an arrow head directed towards the electron donor.

The docking studies on MAO-A and –B have revealed that β-carboline derivatives are located in the vicinity of the FAD cofactor. In both enzymes, the β-carboline core is stabilized by $\pi$-$\pi$ interactions with the aromatic cage (Tyr407-Tyr444 in MAO-A, Tyr398-Tyr435 in MAO-B and FAD). In contrast to Gln215 in MAO-A, $\pi$-$\pi$ interaction of the β-carboline core with the equivalent amide group of Gln206 in MAO-B is less favorable. Furthermore, the β-carboline core is stabilized by two hydrogen bonds with water molecules in MAO-A compared to only one hydrogen bond in MAO-B. So, the stabilization of the β-carboline core by the $\pi$-$\pi$ interaction with the amide group of the Gln215 and the two hydrogen bonds may explain the selectivity of the β-carboline derivatives towards MAO-A compared to MAO-B. In hMAO-A, the lateral chain occupies a hydrophobic pocket including Val93, Leu97, Phe108, Ala111, Phe208, Val210, Cys323 and Ile325. As previously mentioned, the active site of hMAO-A differs from hMAO-B in that it has a monopartite cavity with a total volume of ~550 $\text{Å}^3$ [20]. The substrate cavity in hMAO-B has a volume of ~400 $\text{Å}^3$ and that of the entrance cavity is ~300 $\text{Å}^3$. The combined volume of the two cavities when the gating Ile199 is in its open conformation is ~700 $\text{Å}^3$. The Tyr326 side chain in MAO-B, although not directly involved in the partition of the two cavities, does produce a restriction that is less pronounced in hMAO-A where Ile335 occupies that position [2]. Therefore, the MAO-A Phe208-Ile335 and MAO-B Ile199-Tyr326 pairs appear to be major determinants in dictating the differential substrate and inhibitor specificities of the two enzymes. In hMAO-B, the lateral chains of studied β-carboline derivatives point to a hydrophobic pocket coated by Phe103, Trp119, Leu164, Leu167, Phe168, and Ile316.

# 2. IDO

## 2.1 Biological evaluation

Now that the activity of β-carbolines on both isoforms of MAO was evaluated, some being very potent and selective MAO-A inhibitors, our objective is to evaluate the inhibitory potency and selectivity of these derivatives on hIDO. Indeed, as mentioned in the introduction, some β-carbolines are known as IDO inhibitors (e.g., 3-butyl-β-carboline **46.I**, $K_i = 3.3$ μM). Furthermore, the similarity in substrate (serotonin) between IDO and MAO, and the implication of IDO and MAO in the serotonergic and kynurenine pathways lead us to

study the selectivity of our β-carboline derivatives on IDO. Plasmid coding for human IDO was obtained from Van Den Eynde's team of the UCL university (Woluwe-Saint-Lambert, Belgium). The recombinant plasmid, phIDO, encodes a histidine tag at the N-terminus of IDO. *Escherichia coli* strain BL21 (DE3) (Invitrogen) was used for overexpression of IDO and transformed with the phIDO plasmid. The enzyme was purified by IMAC using $Ni^{2+}$ and an IMAC Hitrap column (GE Healthcare). The overexpression and purification of IDO were performed by Jenny Pouyez and Céline Meinguet (Biological Structural Chemistry Laboratory, FUNDP, Belgium).

The IDO inhibition assay was performed by a colorimetric method as described by Takikawa et al [198] with some modifications and was adapted by Céline Meinguet within the framework of her final report. 1-Methyl-L-tryptophan (L-1MT, **6.III**, commercially available from Sigma-Aldrich, Figure 19.III), a competitive IDO inhibitor ($K_i$ = 19 μM [146]) was used as reference and validation drug in IDO inhibition assay.

### 2.1.1 Inhibition study of IDO

a) Description of IDO assay

As mentioned above, the IDO inhibition assay was performed by a colorimetric method as described by Takikawa et al [198] with some modifications. It is based on the conversion of L-Trp to *N*-formylkynurenine (NFK), followed by hydrolysis to produce kynurenine (Scheme 2.III).
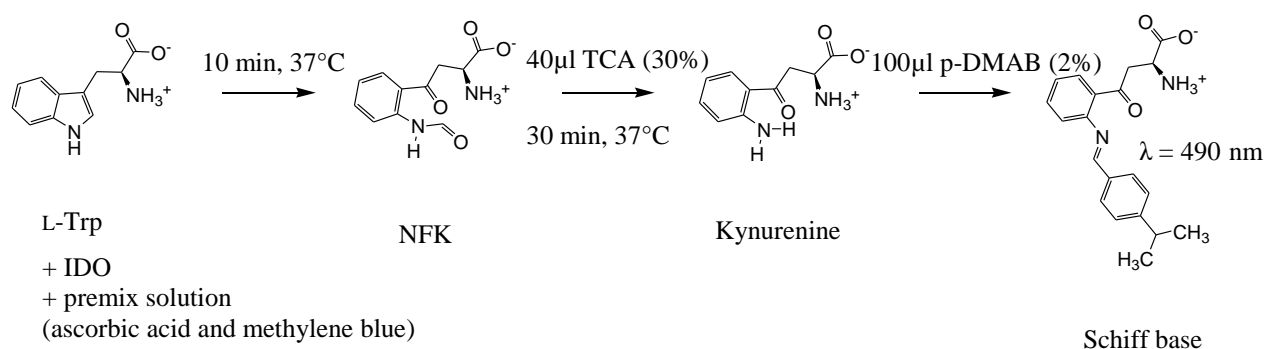


**Scheme 2.III.** Description of IDO assay. pDMAB = *para*-dimethylaminobenzaldehyde.

The IDO heme is first reduced from its ferric state to ferrous state (active form of IDO) by adding a premix solution (ascorbic acid and methylene blue). The conversion of L-Trp to NFK is then initiated by the addition of substrate (L-Trp) on the enzyme. NFK is then hydrolysed to kynurenine by adding a solution of trichloroacetic acid (TCA). The measurement of IDO activity in this method relies on quantifying the amount of kynurenine produced in the assay through an indirect mean. It relies on absorption at $\lambda = 490$ nm of the imine (Schiff base) produced by the reaction of the aromatic amino group of kynurenine with *para*-dimethylaminobenzaldehyde (p-DMAB).

b) Optimized parameters and protocol of IDO assay

The IDO inhibition assay adapted by Céline Meinguet within the framework of her final report, was performed in 96-wells plates at 37°C (Table 7.III).

1) Human IDO (20.0 µL, 50 µg.mL$^{-1}$) is first incubated with the reaction mixture containing, a premix solution (100.0 µL of a solution containing ascorbic acid (20 mM) and methylene blue (17 µM) in potassium phosphate buffer (50 mM, pH 6.5)), potassium phosphate buffer (60.0 µL, 50 mM, pH 6.5), and the test compound diluted in DMSO (10.0 µL, final DMSO percentage of 5%) or a DMSO solution (10.0 µL, final DMSO percentage of 5%) for 2.5 min.

2) Then, L-Trp (10.0 µL, 2 mM) is added to the mixture.

3) After 10 min of incubation at 37°C, the reaction is stopped by addition of 30% (w/v) TCA (40.0 µL).

4) Finally, after 30 min of reaction at 37°C, 100.0 µL of reaction mixture are transferred to 100.0 µL of a solution of p-DMAB 2% in a 96-wells plate to form a yellow schiff base. So, the absorption of the Schiff base is detected at $\lambda = 490$ nm with a 96-wells microplate absorbance reader (Model 680 BIO-RAD).

For each test compound, an enzyme control (substitution of L-Trp by potassium phosphate buffer (50 mM, pH 6.5)) is performed and subtracted from the measured absorbance.

**Table 7.III** Optimized IDO inhibition assay protocol.

| Components (µL) | 100% Initial activity | Inhibition assay | Enzyme control |
|---|---|---|---|
| Premix solution | 100.0 | 100.0 | 100.0 |
| buffer | 60.0 | 60.0 | 70.0 |
| L-Trp (2 mM) | 10.0 | 10.0 | / |
| DMSO | 10.0 | / | / |
| Test compound | / | 10.0 | 10.0 |
| IDO (50 µg.mL$^{-1}$) | 20.0 | 20.0 | 20.0 |
| Final volume | 200.0 | 200.0 | 200.0 |

Validation of the inhibition assay on hIDO was performed using L-1MT (**6.III**, $K_i$ = 19 µM [146]).

## 2.1.2 IC$_{50}$ evaluation of L-1MT on IDO

The IC$_{50}$ evaluation of L-1MT (**6.III**) was required to validate the inhibition assay on hIDO but also to position our compounds compared to a reference inhibitor. IC$_{50}$ value of L-1MT on hIDO was evaluated using the optimized IDO inhibition assay. The inhibition percentages at each concentration were calculated as follows: I (%) = 100 x {1 − (absorbance signal with L-1MT/absorbance signal without L-1MT)}. The inhibition percentages were plotted against the logarithm of L-1MT molar concentrations. The IC$_{50}$ value was calculated from normalized sigmoidal dose-response non-linear regression curves using the GraphPad Prism 5.01 software.

Dose-response curve and the inhibition parameters of L-1MT on hIDO are depicted in figure 19.III and table 8.III.
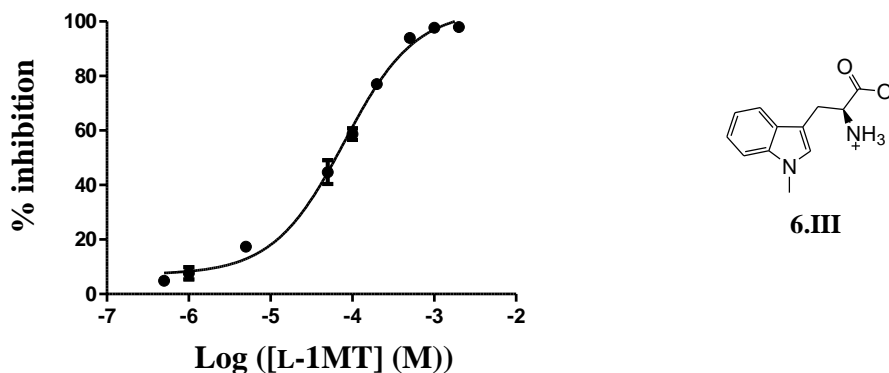
**Figure 19.III.** Dose-response curve of L-1MT (**6.III**) on hIDO. Results are expressed as mean ± SD (n = 3).

**Table 8.III.** Inhibition parameters of L-1MT (**6.III**) on hIDO.

| Inhibition parameters[a] | hIDO |
|---|---|
| $IC_{50}$ | **79.3** (68.8 – 91.4) **µM** |
| $R^2$ | 0.9940 |

[a] Result is expressed as mean with 95% confidence intervals in brackets (n = 3).

As expected, L-1MT is a weak hIDO inhibitor ($IC_{50}$ = 79.3 µM) in agreement with the literature ($K_i$ = 19 µM [146]) which allows to validate the IDO inhibition assay.

### 2.1.3 Inhibitory potency of β-carboline analogues

The inhibitory potency of harmine (**3.I**) and the synthesized β-carbolines (**2a-5.III**) was assessed *in vitro* at 25 µM in triplicate using the inhibition assay previously validated on hIDO. L-1MT was used as reference inhibitor (58% of inhibition at 100 µM). Results revealed that test compounds display no inhibition on hIDO at this concentration. The data of β-carboline derivatives both on hIDO, hMAO-A and −B are reported in table 9.III and show unambiguous that synthesized β-carbolines (**2a-5.III**) are selective of MAO and especially of MAO-A.

**Table 9.III.** Structure and inhibitory potency of harmine (**3.I**) and the synthesized related β-carbolines (**2a-5.III**) on hMAO-A, hMAO-B and hIDO.



| Compound | R₁ | R₂ | R₃ | $K_i$ (nM)[a] hMAO-A | $K_i$ (nM)[a] hMAO-B | Inhibition percentage hIDO at 25 μM |
|---|---|---|---|---|---|---|
| harmine | / | H | CH$_3$ | **16.9** (13.7 – 21.0) | **120800** (94900 – 153900) | NI[d] |
| 2a.III | / | H | CH$_2$CH=CH$_2$ | **5.0** (4.5 – 5.6) | NI[b] | NI |
| 2b.III | / | H | CH$_2$CH(CH$_3$)$_2$ | **3.9** (2.0 – 7.7) | >500[c] | NI |
| 2c.III | / | H | (CH$_2$)$_2$OCH$_3$ | **29.5** (24.0 – 36.3) | NI | NI |
| 2d.III | / | H | (CH$_2$)$_2$OH | **28.4** (20.0 – 40.3) | NI | NI |
| 2e.III | / | H | (CH$_2$)$_3$CF$_3$ | **3.6** (2.6 – 5.0) | >500 | NI |
| 2f.III | / | H | CH$_2$C$_6$H$_{11}$ | **4.3** (3.2 – 5.6) | **221.6** (145.1 – 338.3) | NI |
| 2g.III | / | H | CH$_2$C$_6$H$_5$ | **12.6** (11.6 – 13.7) | >500 | NI |
| 2h.III | / | H | (CH$_2$)$_2$C$_6$H$_5$ | **5.0** (4.0 – 6.2) | >500 | NI |
| 2i.III | / | H | CH$_2$-2'-pyridyl | ≈ **500** | NI | NI |
| 2j.III | / | H | CH$_2$-3'-pyridyl | **24.9** (20.1 – 30.7) | NI | NI |
| 2k.III | / | H | CH$_2$-4'-pyridyl | **35.4** (18.9 – 66.5) | NI | NI |
| 2l.III | / | H | CH$_2$-2'-naphthyl | **100 < $K_i$ < 500** | NI | NI |
| 2m.III | / | H | (CH$_2$)$_2$N(CH$_3$)$_2$ | **1023.8** (920.0 – 1139.4) | NI | NI |
| 2n.III | / | H | (CH$_2$)$_3$N(CH$_3$)$_2$ | **684.0** (558.6 – 836.9) | NI | NI |
| 2o.III | / | H | (CH$_2$)$_2$-morpholine | **255.7** (196.7 – 324.5) | NI | NI |
| 3.III | CH$_2$C$_6$H$_5$ | H | CH$_2$C$_6$H$_5$ | ≈ **500** | >500 | NI |
| 4.III | / | CH$_2$C$_6$H$_5$ | CH$_2$C$_6$H$_5$ | NI | >500 | NI |
| 5.III | CH$_2$C$_6$H$_5$ | CH$_2$C$_6$H$_5$ | CH$_2$C$_6$H$_5$ | NI | >500 | NI |

[a] Results are expressed as mean with 95% confidence intervals in brackets (n = 3).
[b] NI: no inhibition at 1 μM.
[c] >500: Inhibition percentage at 1μM are shown as mean with ± SD in brackets (n = 3), **2b.III** = 14% (±6%), **2e.III** = 24% (±4%), **2g.III** = 42% (±2%), **2h.III** = 39% (±2%), **3.III** = 34% (±3%), **4.III** = 46% (±2%), **5.III** = 29% (±5%).
[d] NI: no inhibition at 25 μM.

With the aim of rationalizing the results obtained with the β-carboline derivatives (**3.I** and **2a-5.III**) evaluated on hIDO, we are interested in binding mode described of two known IDO inhibitors, belonging to β-carboline series (norharman (**7.III**) and 3-butyl-β-carboline (**46.I**), Figure 20.III) which is discussed in the next section [126].
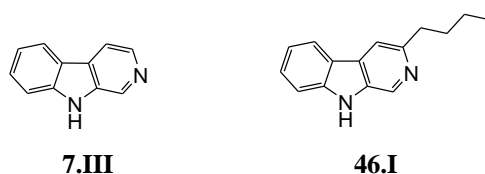


**7.III**                    **46.I**

**Figure 20.III.** Chemical structures of norharman (**7.III**) and 3-butyl-β-carboline (**46.I**).


## 2.2 Molecular modeling

### 2.2.1 Validation of docking studies on IDO

Before to study the binding mode of norharman (**7.III**) and 3-butyl-β-carboline (**46.I**) on hIDO, it is required to validate the docking procedure. Thus, 4-phenylimidazole (PIM)-bound X-ray structure (2D0T.pdb, chain A) was used as a scaffold, because it has a higher resolution and provides a larger binding site than the cyanide-bound structure (2D0U.pdb) [144]. In addition to PIM (**37.I**), there are two molecules of CHES bound at the entrance of the binding site. Since they are likely to interfere with the binding modes of ligands other than PIM, they were removed for docking studies [126]. The structure of ligand is built and geometry optimised at physiological pH within Discovery studio® 2.5 software (Accelrys Software Inc., San Diego, USA). The interaction sphere in the docking was centered on the heme in the catalytic site of IDO and delimited by a 7 Å radius. A total of twenty-five docking solutions were generated using GOLD (version 3.2) software and the scoring function used to rank the docking was Goldscore. All docking solutions obtained for PIM displayed a similar binding mode compared to the crystal structure of hIDO in complex with the PIM (2D0T.pdb). Figure 21.III depicts the superimposition of the crystal structure of hIDO (2D0T.pdb [144]) in complex with the PIM and docking solution of PIM in hIDO model. The RMSD calculated between the crystal structure and the top solution coordinates for ligand heavy atoms is 0.48 Å for PIM on hIDO. In conclusion, the docking procedure is validated.
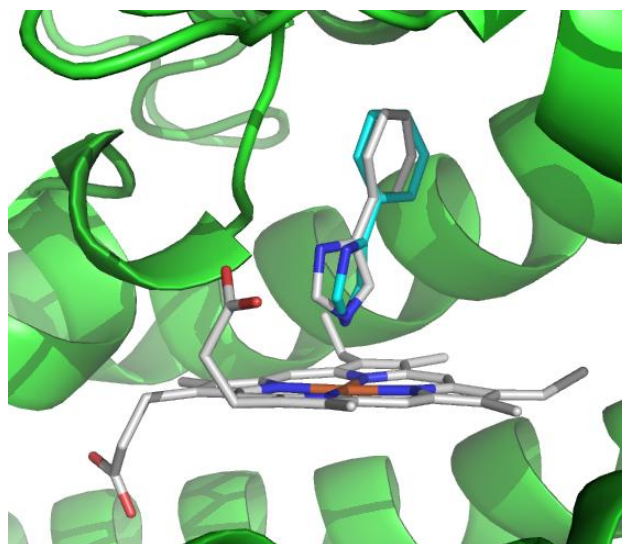
**Figure 21.III.** Superimposition of the crystal structure of hIDO (2D0T.pdb [144]) in complex with the PIM (**37.I**, gray) and the top docking solution of PIM in hIDO model (cyan).

**2.2.2 Molecular docking studies of β-carboline analogues on IDO**

Molecular docking studies of norharman (**7.III**) and 3-butyl-β-carboline (**46.I**) revealed a same binding mode for both compounds within hIDO (2D0T.pdb). Analysis of the binding mode for 3-butyl-β-carboline (**46.I**) within IDO reported in figure 22.III suggests that the β-carboline scaffold incorporates into the active site. Figure 22.III reveals two pockets (A and B) constituting the active site of IDO. Pocket A is located into the center of the active site whereas pocket B is located into the entrance of the active site in proximity of the protein surface. Pocket A which includes the β-carboline core displays mainly a hydrophobic character because of aromatic amino acids coating the active site (Tyr126, Cys129, Val130, Phe163, Phe164, Ser167, Leu234 and Ala264). Pocket B displays both a hydrophobic (Phe226, side chain of Arg231 and Ile354) and hydrophilic (Ser263 and 7-propionate of the heme) character. The β-carboline core is stabilized in pocket A by various interactions; the heme iron is complexed by pyridin nitrogen of β-carboline scaffold in the range of 2 Å as previously described in Cambridge structural database (CSD) between N-terminal pyrrolidine and porphyrin iron [199]. The indole NH of β-carboline core is also stabilized by a hydrogen bond with Ser167. Pocket A consisting mainly of hydrophobic residues, the β-carboline core is mainly stabilized by Van der Waals interactions (Tyr126, Cys129, Val130, Phe163, Phe164, Leu234 and Ala264).
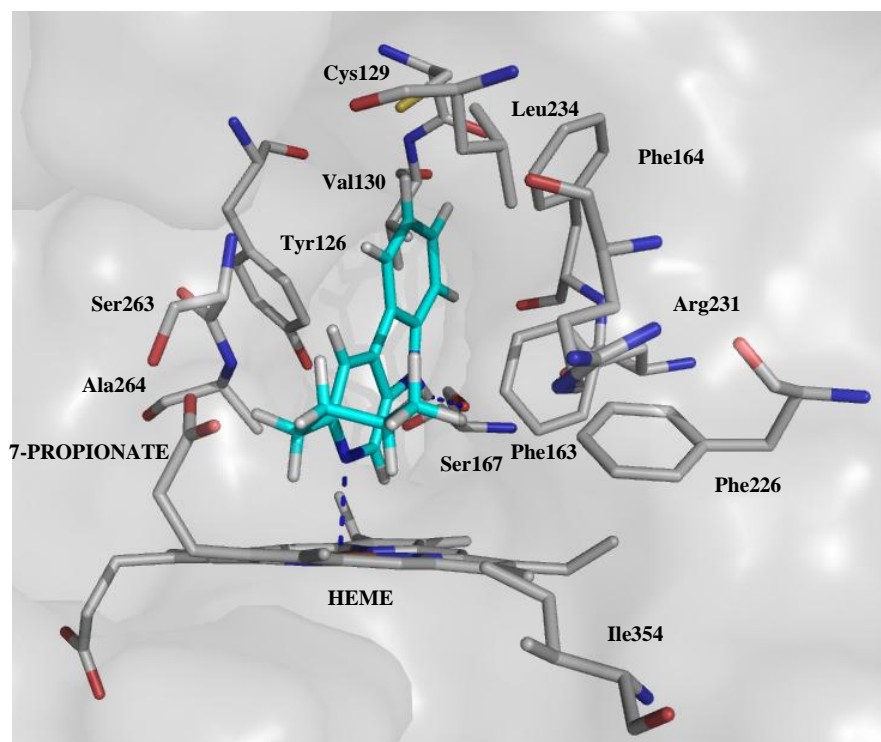
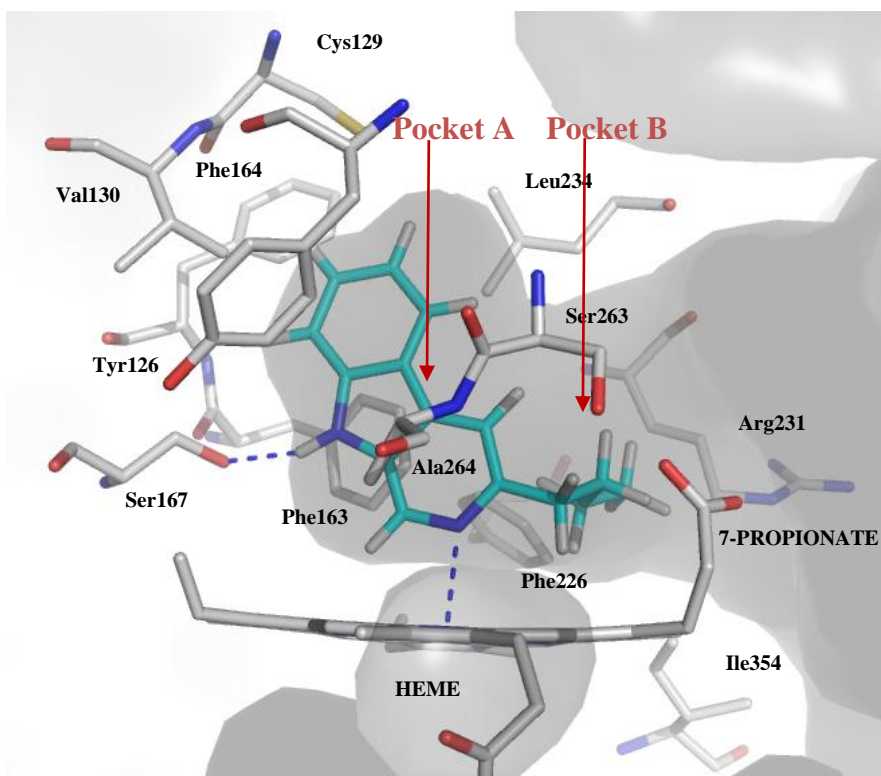**Figure 22.III.** Simulated binding mode of 3-butyl-β-carboline (**46.I**) in the active site of hIDO (2D0T.pdb). Only amino acids directly implicated in the active site are displayed and labeled. Two perpendicular views are presented.

Figure 22.III shows also that the substitution in the 3-position of β-carboline scaffold by a butyl side chain allows to fit pocket B [126] lined with hydrophobic amino acid residues which is in agreement with literature data which display a higher inhibition on IDO with 3-butyl-β-carboline (**46.I**, $K_i$ = 3.3 μM) compared to norharman (**7.III**, $K_i$ = 178 μM) [156]. Indeed, butyl side chain establishes Van der Waals interactions with Phe226, side chain of Arg231 and Ile354.

These observations evidence that the substitution in the 7-position (**2a-o.III**), 2 and/or 9-positions (**3-5.III**) are not tolerated. Indeed, from the conformation of 3-butyl-β-carboline (**46.I**), steric clashes can be observed between substituents in the 2, 7 and 9-positions and the amino acid residues of the active site. So, these substitutions lead to a new binding mode of β-carboline scaffold which is not stabilized into the active site in agreement with weak obtained inhibition percentages. Furthermore, we observe that the presence of a methyl group in the 1-position of synthesized β-carbolines prevents the complexation between the pyridin nitrogen and the heme iron.

Figure 23.III shows the lipophilic potential of pocket B calculated by Sybyl 8.1 software (Tripos International, Missouri, USA). The hydrophilic moiety comes mainly from 7-propionate of the heme (**1**) whereas the hydrophobic moiety comes from apolar residues (Phe226, side chain of Arg231 and Ile354) (**2**).
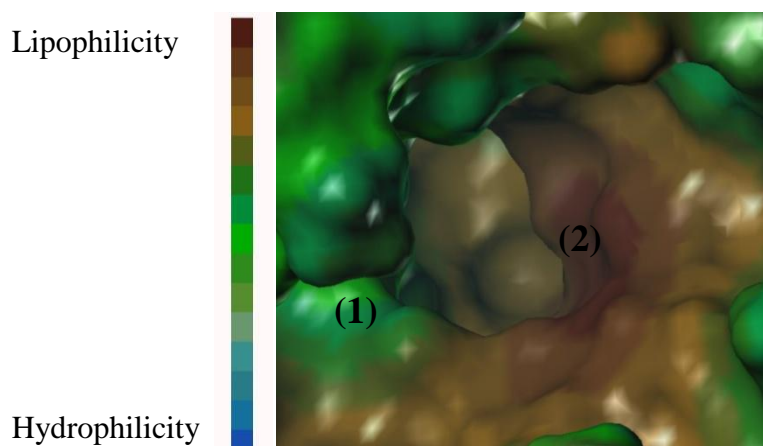


**Figure 23.III.** Hydrophobic and lipophilic potential of pocket B. Colour scale is provided on the left.

## 2.3 Structure-based rational design of 3-substituted-β-carboline analogues

Recently, Rohrig et al investigated the modes of binding of all known IDO inhibitors. On the basis of the observed docked conformations, they developed a pharmacophore model which concluded that a good ligand should contain some or all of the following features [126];

- An aromatic fragment, at least bicyclic, to fill pocket A in the binding site
- An atom with a free electron pair that can coordinate to the heme iron, such as oxygen, nitrogen, or sulfur
- A group that can form van der Waals interactions with pocket B
- Groups that can hydrogen bond to Ser167, Gly262, Ala264, and Arg231 (possibly a negatively charged group that can form a salt bridge) or to the heme 7-propionate (possibly a positively charged group that can form a salt bridge)

From results of synthesized β-carbolines (**2a-5.III**), docking studies of 3-butyl-β-carboline (**46.I**) and the pharmacophore model on IDO, we are interested in the synthesis of new 3-substituted-β-carbolines potentially more potent compared to 3-butyl-β-carboline (**46.I**) (Scheme 3.III). Indeed, it can be interesting to add an amino group and/or a carboxylate group in the 3-position which should allow to establish supplementary interactions with 7-propionate of the heme and Arg231 in the pocket B respectively which are missing with 3-butyl-β-carboline. In this study, we are focused on the synthesis of two new compounds containing an amino group; *N*-ethyl-3-methylamino-β-carboline (**8.III**) and 3-methylamino-β-carboline (**9.III**).



n = 0,1,2
X = $NH_3^+$, H
Y = alkyl, $COO^-$

**8.III**                                **9.III**
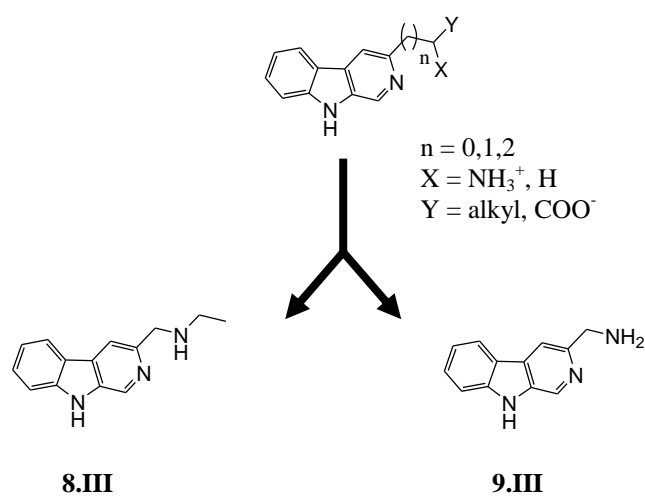
**Scheme 3.III.** Chemical structures of 3-substituted-β-carbolines proposed; *N*-ethyl-3-methylamino-β-carboline (**8.III**) and 3-methylamino-β-carboline (**9.III**).

100

These two derivatives should incorporate in the active site with 3-butyl-β-carboline-like interactions but display also a positive charge at physiological pH which should allow to establish a coulomb interaction with 7-propionate of the heme in agreement with molecular docking studies reported in figure 24.III. Furthermore, besides adding a coulomb interaction between 7-propionate of the heme and amino group, compound **8.III** should allow to establish Van der Waals interactions with the hydrophobic residues coating the pocket B.
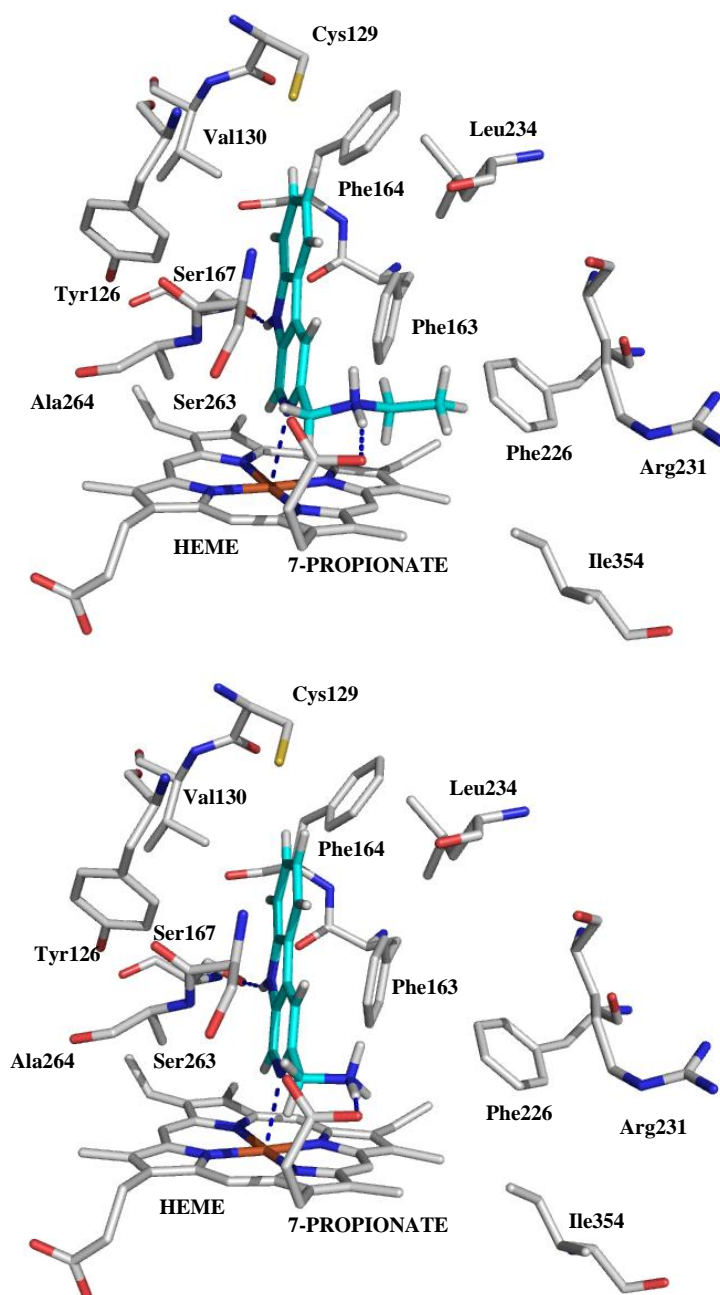


**Figure 24.III.** Simulated binding mode of *N*-ethyl-3-methylamino-β-carboline (**8.III**, top) and 3-methylamino-β-carboline (**9.III**, bottom) in the active site of hIDO (2D0T.pdb). Only amino acids directly implicated in the active site are displayed and labeled.

The next section reports the synthesis of compounds **8.III** and **9.III** as well as the first steps leading to 3-butyl-β-carboline (reference inhibitor, **46.I**). This synthesis was performed in the frame of a graduate thesis (Sylvain Arcidiacono, Paul Lambin institute, Belgium).

## 2.4 Synthesis of 3-substituted-β-carboline analogues

The strategy used to synthesize the 3-substituted-β-carboline derivatives (**8-9.III** and **46.I**) is depicted in scheme 4.III. The synthetic pathway of three compounds follows two-four steps procedures from the common ethyl β-carboline-3-carboxylate (**10.III**) intermediate (commercially available from Sigma-Aldrich).
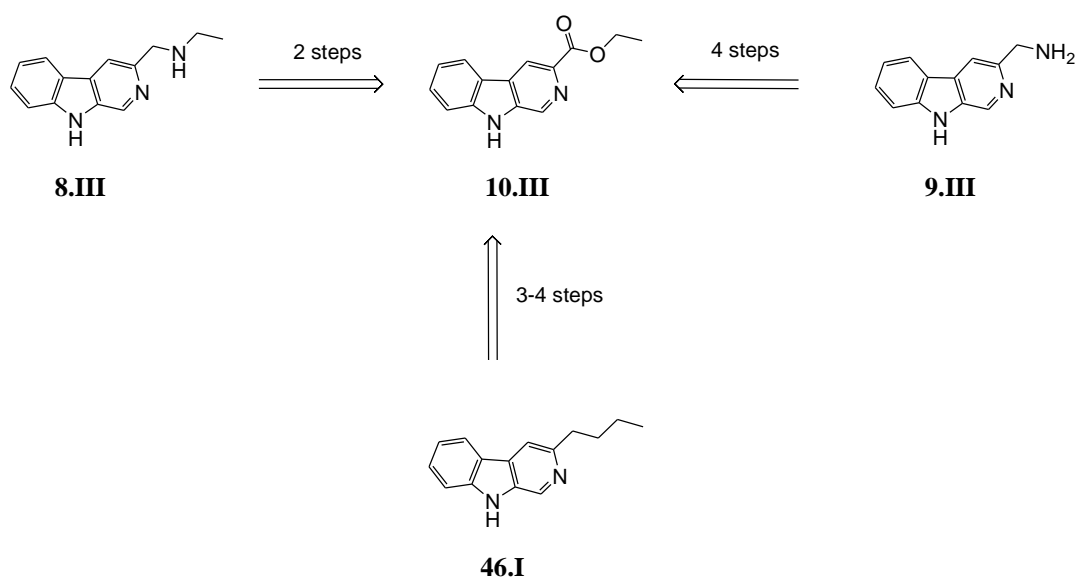


**Scheme 4.III.** Synthetic pathway to 3-substituted-β-carboline analogues **8-9.III** and **46.I**.

### 2.4.1 Synthesis of *N*-ethyl-3-methylamino-β-carboline (8.III)

The synthetic pathway to amino derivative **8.III** follows a two steps procedure from the ethyl β-carboline-3-carboxylate (**10.III**) intermediate (Scheme 5.III). This intermediate **10.III** is successively transformed in *N*-ethyl-3-carboxamide-β-carboline (**11.III**) intermediate and finally in the corresponding secondary amine **8.III**.
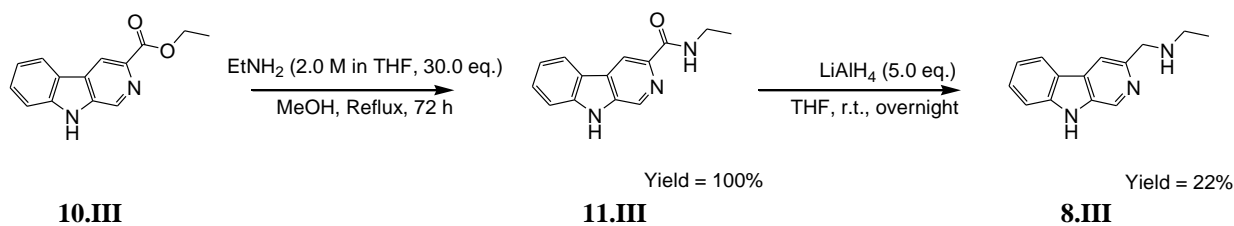
**Scheme 5.III.** Synthetic pathway to *N*-ethyl-3-methylamino-β-carboline (**8.III**).

The synthesis of amide **11.III** was previously reported in the literature in one step from the methyl β-carboline-3-carboxylate (**12.III**) intermediate [200] (Scheme 6.III). The intermediate **12.III** was reacted with ethylamine (used as solvent and reagent) to produce the amide **11.III** in 45% yield.
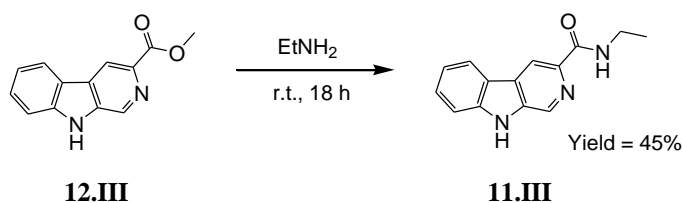


**Scheme 6.III.** Synthesis of *N*-ethyl-3-carboxamide-β-carboline (**11.III**) reported from the literature [200].

So, the synthesis of amide **11.III** was performed following scheme 6.III with some modifications (temperature and time of reaction). After optimization, ethyl β-carboline-3-carboxylate (**10.III**) was reacted with ethylamine in methanol for 72 h at reflux to give quantitatively the *N*-ethyl-3-carboxamide-β-carboline (**11.III**) (Scheme 5.III). The secondary amine **8.III** was then obtained by reduction of amide **11.III** with LiAlH$_4$ in THF overnight at room temperature [201]. After purification by semi-preparative HPLC, *N*-ethyl-3-methylamino-β-carboline (**8.III**) was obtained in modest 22% yield.

### 2.4.2 Synthesis of 3-methylamino-β-carboline (9.III)

The synthetic pathway to amino derivative **9.III** follows a four steps procedure from the ethyl β-carboline-3-carboxylate (**10.III**) intermediate (Scheme 7.III). This carboxylate intermediate **10.III** is first reduced in alcohol **13.III**. Alcohol group is then transformed in a good leaving group such a chloride or a triflate group (**14.III** and **15.III**, respectively) which are substituted

103

by SN$_2$ to form the azide derivative **16.III**. Finally, compound **16.III** is reduced by a Staudinger reaction in the corresponding primary amine **9.III**.
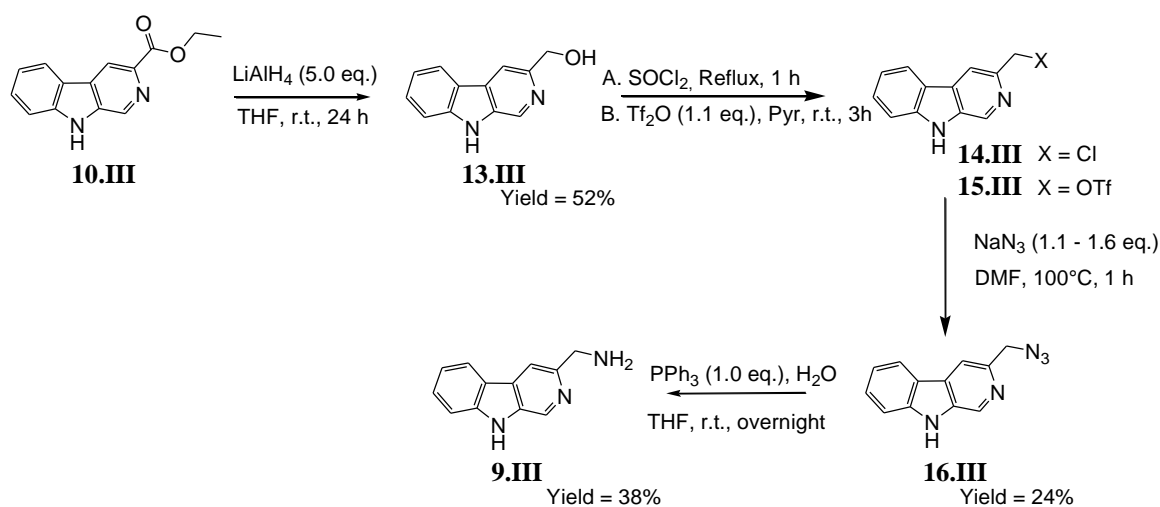


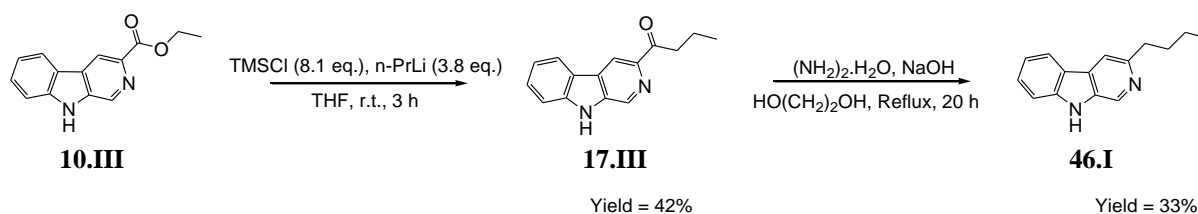**Scheme 7.III.** Synthetic pathway to 3-methylamino-β-carboline (**9.III**).

The reduction of carboxylate derivative **10.III** in alcohol **13.III** was already described in the literature [202]. This reduction is described in using NaBH$_4$ as reducing agent for 12 h in 81% yield. However, we observe that the conversion in corresponding alcohol is very low. So, we have substituted the NaBH$_4$ for LiAlH$_4$ which is a classical reducing agent for reduction of ester in corresponding alcohol. Ethyl β-carboline-3-carboxylate (**10.III**) was then reacted with LiAlH$_4$ in THF for 24 h at room temperature to give the 3-hydroxymethyl-β-carboline (**13.III**) in 52% yield. The transformation of alcohol in azide group was performed in two steps. The first step is the formation of a good leaving group. Primary alcohol **13.III** was first transformed in primary chloride (**14.III**) using thionyl chloride (used as solvent and reagent). This reaction is described for 1 h at reflux [202]. However, we observe the formation of a second product containing a same retention factor (R$_f$) compared to derivative **14.III**. The second product was not identified but might come from indole NH group which is known to react with thionyl chloride. Furthermore, the reaction of solution containing the derivative **14.III** with sodium azide in DMF at 100°C for 1 h gave the compound **16.III** and a by-product containing a same retention factor compared to derivative **16.III**. Finally, Staudinger reaction gave also two products with a same retention factor including compound **9.III** which could be purified by HPLC.

Consequently, an alternative approach was the substitution of thionyl chloride by trifluoromethanesulfonic anhydride. So, alcohol derivative **13.III** was reacted with

104

trifluoromethanesulfonic anhydride in pyridine for 3 h at room temperature to give the 3-(trifluoromethanesulfonate)methyl-β-carboline (**15.III**). Only product **15.III** is formed and directly reacted with sodium azide in DMF at 100°C for 1 h to obtain the azide product **16.III** in 24% yield. Furthermore, no by-product is formed and the product can be used without further purification for the last step. Finally, the primary amino derivative **9.III** is formed from azide derivative **16.III** by a Staudinger reaction. This reaction is performed using triphenylphosphine and water in THF at room temperature overnight. After an acid-base extraction, 3-methylamino-β-carboline (**9.III**) was obtained in 38% yield.
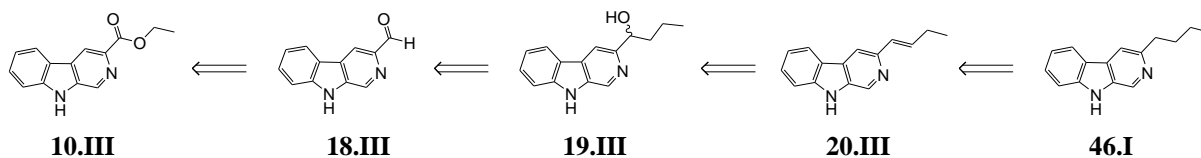
### 2.4.3 Synthesis of 3-butyl-β-carboline (46.I)

The synthesis of 3-butyl-β-carboline (**46.I**) was previously reported in the literature in two steps from the intermediate **10.III** (Scheme 8.III) [203]. First, carboxylate derivative **10.III** is transformed using n-propyllithium (Grignard reaction) in corresponding propyl ketone **17.III**. Finally, compound **46.I** is synthesized by Wolff-Kishner reduction of propyl ketone **17.III**. However, this synthetic pathway was not retained because of the difficulty to synthesize n-propyllithium.



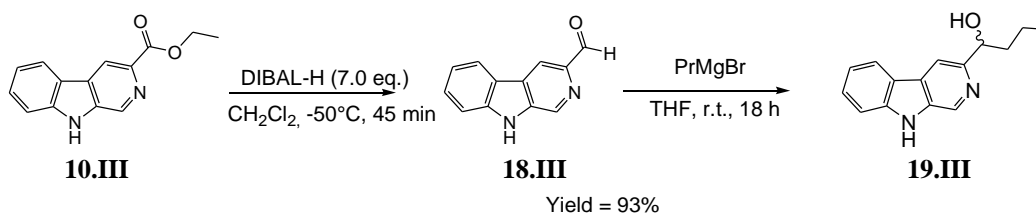**Scheme 8.III.** Synthetic pathway to 3-butyl-β-carboline (**46.I**) reported from the literature [203].

So, the synthetic pathway depicted in scheme 9.III was adopted. This synthetic pathway follows a four steps procedure from the ethyl β-carboline-3-carboxylate (**10.III**) [204]. First, carboxylate derivative **10.III** is reduced using DIBAL-H in corresponding aldehyde **18.III**. Grignard reaction is then performed using n-propylmagnesium bromide to obtain 3-(butan-1-ol)-β-carboline (**19.III**). This one can be transformed in 3-(but-1-enyl)-β-carboline (**20.III**) by elimination of alcohol group. Finally, the reduction of **20.III** by hydrogenation gives the compound **46.I**. Furthermore, this synthetic pathway leads to the formation of 3-(butan-1-ol)-β-carboline (**19.III**) intermediate which could be a potential IDO inhibitor. Indeed, this

intermediate displays both an alcohol group and a propyl side chain which might interact with pocket B establishing interactions with 7-propionate of the heme and hydrophobic residues, respectively.



**Scheme 9.III.** Modified synthetic pathway to 3-butyl-β-carboline (**46.I**).

Here, we show the first results of this synthetic pathway (Scheme 10.III). Carboxylate derivative **10.III** was reduced with DIBAL-H in dichloromethane for 45 min at -50°C to give the 3-carbaldehyde-β-carboline (**18.III**) in almost quantitative (93%) yield. A first assay of Grignard reaction using n-propylmagnesium bromide and aldehyde **18.III** evidenced the formation of 3-(butan-1-ol)-β-carboline (**19.III**). However, this result was not reproduced because of the stability and availability of Grignard reagent.



**Scheme 10.III.** Synthetic pathway to 3-(butan-1-ol)-β-carboline (**19.III**).

So, an optimization of Grignard reaction was required (Scheme 11.III). n-Propylmagnesium bromide was first synthesized *in situ* from 1-bromopropane and magnesium for 30 min at room temperature. Then, Grignard reaction using n-propylmagnesium bromide and benzaldehyde (**21.III**) as model reagent was performed. The addition of n-propylmagnesium bromide to a solution of benzaldehyde (**21.III**) for 3 h at room temperature gave the 1-phenylbutan-1-ol (**22.III**) in 65% yield. Consequently, the Grignard reaction will be adapted for the synthesis of 3-(butan-1-ol)-β-carboline (**19.III**).

106
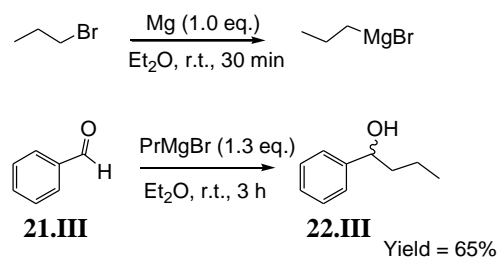
**Scheme 11.III.** Synthesis of n-propylmagnesium bromide and 1-phenylbutan-1-ol (**22.III**).

The structure of the synthesized compounds (**8-9.III**) was determined by ^{1}H NMR, ^{13}C NMR and mass spectrometry (MS). The purity of compound **9.III** must be yet confirmed by elemental analyses. The data are reported in the chapter Materials and Methods.

### 2.4.4 Perspectives

Several synthetic pathways are possible to synthesize the 3-butyl-β-carboline (**46.I**) (Scheme 12.III). Among these pathways, we propose;

- Elimination of alcohol group from 3-(butan-1-ol)-β-carboline (**19.III**) using trifluoromethanesulfonic anhydride and a base such pyridine should give 3-(but-1-enyl)-β-carboline (**20.III**) [205]. This one could be reduced by hydrogenation using palladium on activated charcoal as catalyst to form 3-butyl-β-carboline (**46.I**) (Scheme 12a.III) [206].
- An alternative method is the Barton-McCombie reaction (Scheme 12b.III) [207]. The alcohol derivative **19.III** is first converted to the thiocarbonyl derivative **23.III**, and is then treated with Bu₃SnH which reacts following a radicalar reaction to give 3-butyl-β-carboline derivative (**46.I**).
- Wittig olefination of 3-carbaldehyde-β-carboline (**18.III**) could also be performed to give 3-(but-1-enyl)-β-carboline (**20.III**) which reduces by hydrogenation to give 3-butyl-β-carboline derivatve (**46.I**) (Scheme 12c.III) [204].
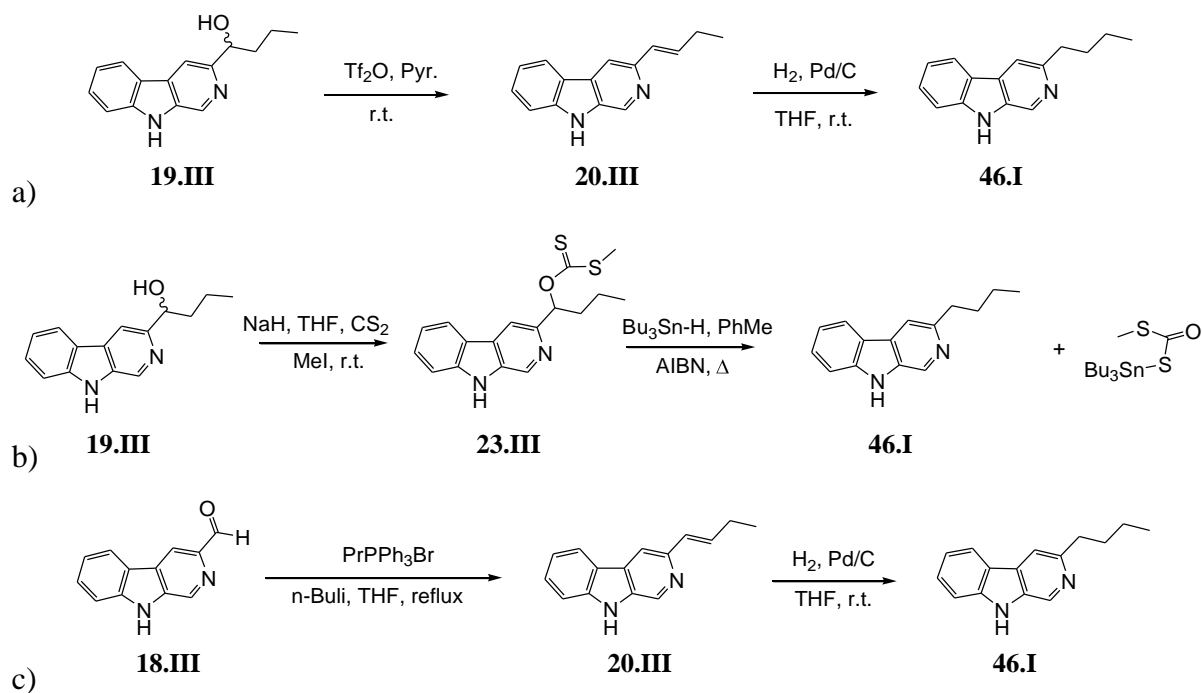
**Scheme 12.III.** Synthetic pathway (a-c) to 3-butyl-β-carboline (**46.I**).

## 2.5 Preliminary biological evaluation

The IDO inhibitory potency of the norharman (**7.III**) and *N*-ethyl-3-methylamino-β-carboline (**8.III**) was assessed *in vitro* in triplicate at 100 μM by Céline Meinguet using the colorimetric test previously validated on hIDO. The inhibition percentage obtained for norharman (**7.III,** 43% (±4%)) is in agreement with literature data which display a weak inhibition on IDO ($K_i =$ 178 μM) [156]. Surprisingly, the results also reveal that the *N*-ethyl-3-methylamino-β-carboline (**8.III**) displays no inhibition on IDO at this concentration. Although it was impossible to test the compound **9.III** due to a lack of availability of this latter, the absence of inhibition observed for **8.III** tends to show that the introduction of a positive charge is not tolerated. The result of compound **8.III** must be yet confirmed again but this inactivity may be explained by a more hydrophobic character of the pocket B (Figure 23.III). So, from the result of compound **8.III** and the pharmacophore model developed on IDO by Rohrig et al [126], it can be interesting to explore the possibility to synthesize of new 3-substituted-β-carbolines with a negatively charged group such as a carboxylate that can form a salt bridge with Arg231 (Scheme 3.III).

# 3. LSD1

## 3.1 Biological evaluation

Besides the selectivity study of β-carbolines (**2a-5.III**) on hIDO compared to MAO-A and – B, we are also interested in the inhibitory potency of these compounds on hLSD1. Indeed, as mentioned in the introduction, the similarity in the catalytic and structural properties of MAO and LSD1 leads us to study the selectivity of β-carbolines, inhibitors of monoamine oxydases as potential LSD1 inhibitors. Then, to evaluate the affinity of synthesized β-carboline derivatives on LSD1, we have adapted a fluorometric screening assay (LSD1 inhibitor screening assay, Cat.# 700120) from Cayman Corporation with some modifications. Tranylcypromine (**5.I**, Figure 2.I, Cat.# 10010494, Cayman), an irreversible inhibitor of LSD1 which displays an $IC_{50}$ value of 22 μM (Cayman), was used like reference and validation drug of LSD1 inhibition assay.

### 3.1.1 Inhibition study of LSD1

a) Description of LSD1 inhibitor screening assay (Cayman)

The LSD1 inhibitor screening assay kit (Cayman) provides a convenient fluorescence-based method for screening LSD1-specific inhibitors. The assay is based on the multistep enzymatic reaction in which LSD1 first produces $H_2O_2$ during the demethylation of lysine 4 on a peptide corresponding to the first 21 amino acids of the N-terminal tail of histone H3 (Figure 25.III). In the presence of horseradish peroxidase (HRP), $H_2O_2$ reacts with ADHP (10-acetyl-3,7-dihydroxyphenoxazine) to produce the highly fluorescent compound resorufin. Resorufin fluorescence can be analyzed with an excitation wavelength of 530-540 nm and an emission wavelength of 585-595 nm. A LSD1 inhibitor screening assay kit provides just the quantities required for a 96-wells plate. Thus, we are mainly interested in the activity study of our β-carboline derivatives (**2a-5.III**) on LSD1 compared to tranylcypromine (**5.I**). Before to evaluate the inhibitory potency of β-carbolines, the study of some parameters was required such as the emission spectrum of β-carbolines, the fluorescent signal of background and the intensity of the fluorescent signal (100% initial activity).
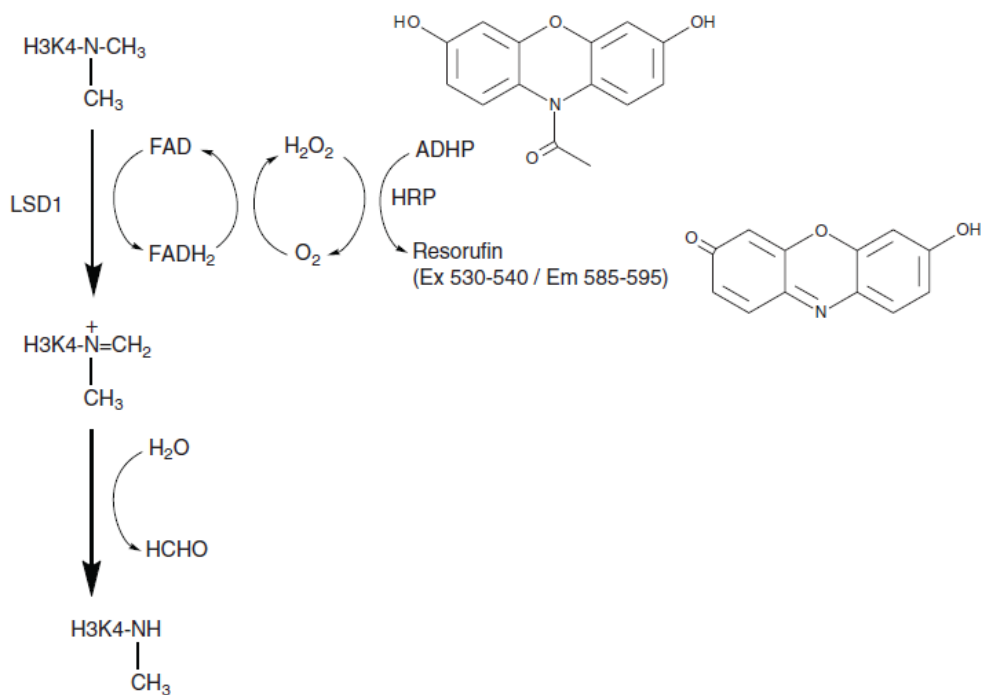
**Figure 25.III.** Description of LSD1 inhibitor screening assay (Cayman). HRP = horseradish peroxidase and ADHP = 10-acetyl-3,7-dihydroxyphenoxazine.

b) Protocol of LSD1 inhibitor screening assay (Cayman)

*Analyzed parameters*

- **The emission spectrum of β-carbolines**: to quantify the inhibitory potency of β-carbolines, it is required to know if these compounds emit a fluorescent signal at an excitation wavelength of 535 nm. So, harmine (**3.I**, Table 1.III) was used as reference of this series.

- **The fluorescent signal of background**: to study the fluorescent signal induced by the substrate and the enzyme on the 100% initial activity. The highest signal will be subtracted from 100% initial activity.

- **Intensity of the fluorescent signal**: to quantify the inhibitory potency of our test compounds on LSD1, it is required to measure a fluorescent signal of sufficient intensity for the enzymatic reaction without test compound (100% initial activity). Thus, tranylcypromine (**5.I**) was used as reference inhibitor. It has been shown that this compound displays an $IC_{50}$ of 22 μM in the conditions of the LSD1 inhibitor screening assay.

110

*Emission spectrum of harmine*

In the LSD1 inhibitor screening assay, the measurement of LSD1 activity is quantified by the amount of resorufin produced which is detected by fluorescence ($\lambda_{ex}$ 535 nm; $\lambda_{em}$ 595 nm). Before to quantify the inhibitory potency of the β-carbolines, it is required to know if these compounds emit a fluorescent signal ($\lambda_{ex}$ 535 nm) around 595 nm. Thus, the emission spectrum of harmine (**3.I**) in the range 500–700 nm ($\lambda_{ex}$ 535 nm, Figure 26.III) was performed.
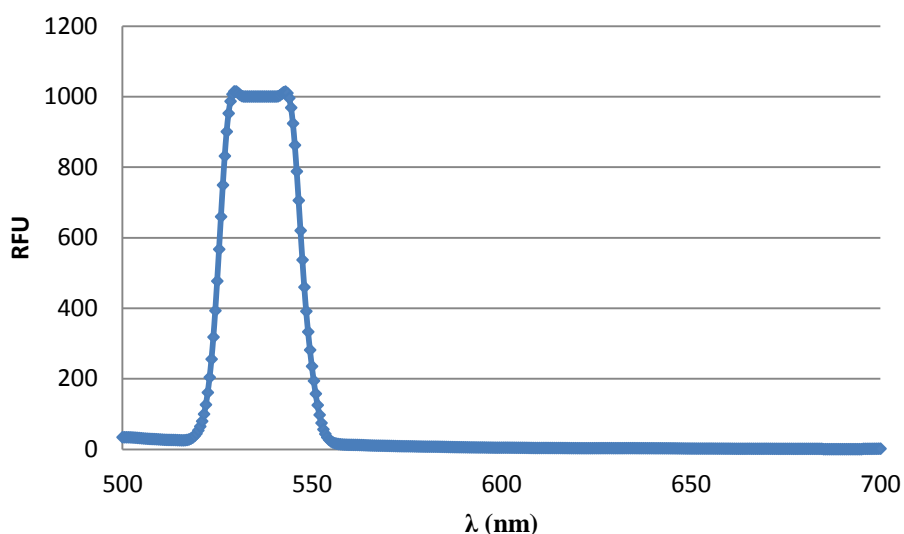


**Figure 26.III.** Emission spectrum of harmine (**3.I**; $\lambda_{ex}$ 535 nm).

Emission spectrum of harmine (**3.I**) depicted in figure 26.III shows that harmine does not emit fluorescent signal at 595 nm.

*Fluorescent signal of background (substrate and enzyme controls)*

In the LSD1 inhibitor screening assay, a final percentage of 12.5% in DMSO introduced by the inhibitor was conserved compared to MAO-Glo™ assay. We have studied the fluorescent signal induced by the substrate and the enzyme on the 100% initial activity (Figure 27.III). The highest signal was the enzyme control and thus, will be subtracted from 100% initial activity for all experiments.
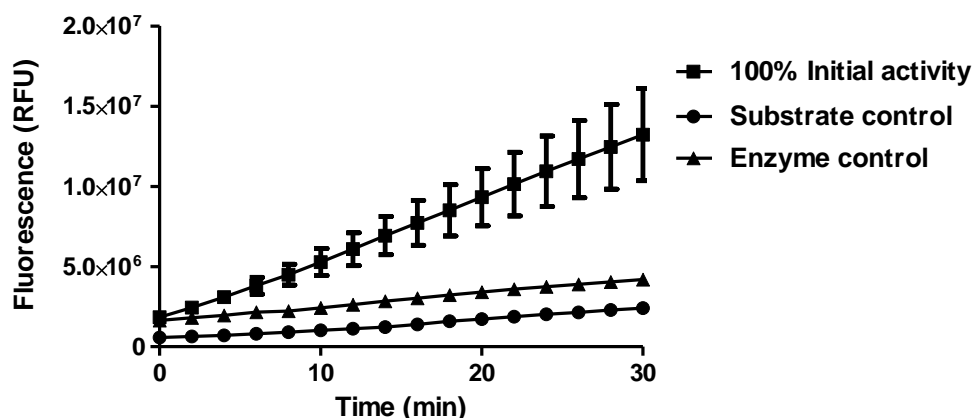
**Figure 27.III.** Kinetic evolution of the fluorescent signal, from 100% initial activity (■) and background (substrate (●) and enzyme (▲) controls) in LSD1 inhibitor screening assay. Results are expressed as mean ± SD (n = 2).

*Intensity of the fluorescent signal*

Our objective is to quantify the inhibitory potency of our test compounds on hLSD1. So, it is required to measure a fluorescent signal of sufficient intensity for the enzymatic reaction without test compound (100% initial activity). Tranylcypromine (**5.I**) was then used as reference inhibitor and was reported with an $IC_{50}$ of 22 μM in the conditions of LSD1 inhibitor screening assay kit (Cayman). The inhibition percentage of tranylcypromine was evaluated on LSD1 at 25 μM (47% (±7%), Figure 28.III) and is in agreement with $IC_{50}$ value reported in the LSD1 inhibitor screening assay. In conclusion, the intensity of fluorescent signal is sufficient to quantify the inhibition of our compounds on LSD1, and we thus validate the LSD1 inhibitor screening assay for the study of β-carbolines.
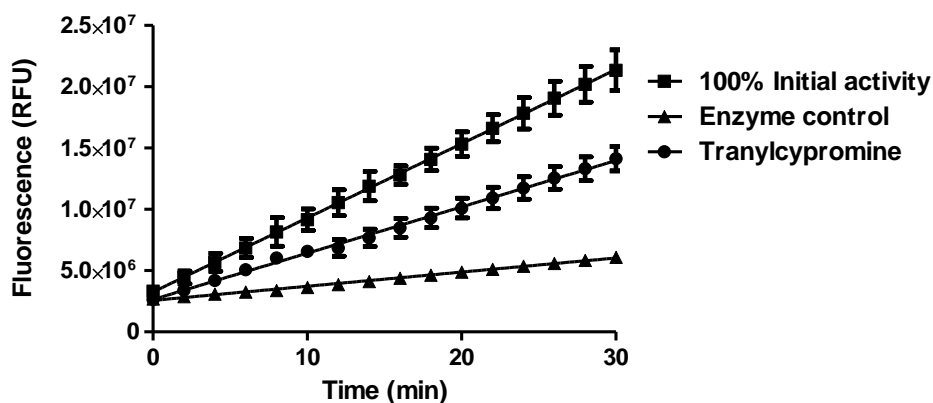


**Figure 28.III.** Evolution of the fluorescent signal in presence of tranylcypromine inhibitor (**5.I**, 25 μM) in hLSD1 inhibitor screening assay. Results are expressed as mean ± SD (n = 2).

112

The LSD1 inhibition assay from Cayman Corporation was performed in 96-wells plates at 37°C (Table 10.III).

1) Human LSD1 (20.0 µL) was first incubated with the reaction mixture containing a buffer solution (105.0 µL; 50 mM Hepes, pH 7.5), a solution of HRP (20.0 µL), a solution of ADHP (10.0 µL) and the test compound dissolved in DMSO (25.0 µL, final DMSO percentage of 12.5%) or a DMSO solution (25.0 µL, final DMSO percentage of 12.5%) for 2.5 min.
2) Then, the substrate (peptide; 20.0 µL, 1mM) was added to the mixture.
3) The fluorescent signal of resorufin was measured during 30 min at 37°C with a 96-wells Beckman Coulter DTX 880 Multimode Detector ($\lambda_{ex}$ 535 nm; $\lambda_{em}$ 595 nm).

Moreover, for each experiment, an enzyme control (substitution of substrate (peptide) by a buffer solution (50 mM Hepes, pH 7.5)) is performed and subtracted from the measured fluorescence of 100% initial activity.

**Table 10.III.** LSD1 inhibitor screening assay protocol.

| Components (µL) | 100% Initial activity | Inhibition assay | Enzyme control |
|---|---|---|---|
| Buffer | 105.0 | 105.0 | 125.0 |
| HRP | 20.0 | 20.0 | 20.0 |
| ADHP | 10.0 | 10.0 | 10.0 |
| DMSO | 25.0 | / | 25.0 |
| Test compound | / | 25.0 | / |
| hLSD1 | 20.0 | 20.0 | 20.0 |
| Substrate (peptide) (1 mM) | 20.0 | 20.0 | / |
| Final volume | 200.0 | 200.0 | 200.0 |

The next step is the evaluation of inhibitory potency of β-carboline analogues on hLSD1.

### 3.1.2 Inhibitory potency of β-carboline analogues

The inhibitory potency of harmine (**3.I**) and the synthesized β-carbolines (**2a-5.III**) was assessed *in vitro* at 25 μM except compounds **3-5.III** (at 50 μM) using the LSD1 inhibitor screening assay kit (Cayman). Tranylcypromine (**5.I**) was used as reference inhibitor (47% of inhibition at 25 μM). The data of β-carbolines both on hLSD1, hMAO-A and –B, and hIDO are reported in table 11.III. Results reveal that synthesized β-carbolines (**2a-5.III**) are weak inhibitors of LSD1. They are selective of MAO and especially of MAO-A. Inhibition percentages show high standard deviations on hLSD1. Nevertheless, interesting trends can be observed from these results. First, harmine (**3.I**) displays no inhibition at 25 μM and 50 μM on LSD1. The introduction of lipophilic and bulky groups like aliphatic (**2c.III**), cyclohexyl (**2f.III**), phenyl (**2g.III**, **2h.III** and **3.III**) and naphthyl (**2l.III**) groups allows to increase the inhibitory potency of β-carboline scaffold on hLSD1 compared to harmine (**3.I**). Furthermore, these compounds display an inhibitory potency in the same range as tranylcypromine under the same test conditions. The introduction of more hydrophilic groups like dimethylaminoethyl and ethylmorpholine (**2m.III** and **2o.III**) abolishes the inhibition. Finally, the *N*-benzylation of compound **2g.III** in the 2-position (**3.III**) displays an inhibitory potency in the same range as **2g.III** whereas the *N*-benzylation of **2g.III** and **3.III** in the 9-position (**4.III** and **5.III**, respectively) decreases their inhibitory potency.

**Table 11.III.** Structure and inhibitory potency of harmine (**3.I**) and the synthesized related β-carbolines (**2a-5.III**) on hMAO-A, hMAO-B, hIDO and hLSD1.



| Compound | $R_1$ | $R_2$ | $R_3$ | $K_i$ (nM)[a] hMAO-A | hMAO-B | Inhibition percentage[d] hIDO | hLSD1 |
|---|---|---|---|---|---|---|---|
| harmine | / | H | $CH_3$ | **16.9** (13.7 – 21.0) | **120800** (94900 – 153900) | NI[b] | NI[b] |
| 2a.III | / | H | $CH_2CH=CH_2$ | **5.0** (4.5 – 5.6) | NI[b] | NI | ND[e] |
| 2b.III | / | H | $CH_2CH(CH_3)_2$ | **3.9** (2.0 – 7.7) | >500[c] | NI | 37% (±10%) |
| 2c.III | / | H | $(CH_2)_2OCH_3$ | **29.5** (24.0 – 36.3) | NI | NI | 60% (±2%) |
| 2d.III | / | H | $(CH_2)_2OH$ | **28.4** (20.0 – 40.3) | NI | NI | 42% (±21%) |
| 2e.III | / | H | $(CH_2)_3CF_3$ | **3.6** (2.6 – 5.0) | >500 | NI | 35% (±17%) |
| 2f.III | / | H | $CH_2C_6H_{11}$ | **4.3** (3.2 – 5.6) | **221.6** (145.1 – 338.3) | NI | 74% (±18%) |
| 2g.III | / | H | $CH_2C_6H_5$ | **12.6** (11.6 – 13.7) | >500 | NI | 58% (±45%) |
| 2h.III | / | H | $(CH_2)_2C_6H_5$ | **5.0** (4.0 – 6.2) | >500 | NI | 61% (±19%) |
| 2i.III | / | H | $CH_2$-2'-pyridyl | **≈ 500** | NI | NI | 39% (±16%) |
| 2j.III | / | H | $CH_2$-3'-pyridyl | **24.9** (20.1 – 30.7) | NI | NI | 19% (±27%) |
| 2k.III | / | H | $CH_2$-4'-pyridyl | **35.4** (18.9 – 66.5) | NI | NI | 22% (±11%) |
| 2l.III | / | H | $CH_2$-2'-naphthyl | **100 < $K_i$ < 500** | NI | NI | 73% (±4%) |
| 2m.III | / | H | $(CH_2)_2N(CH_3)_2$ | **1023.8** (920.0 – 1139.4) | NI | NI | 6% (±11%) |
| 2n.III | / | H | $(CH_2)_3N(CH_3)_2$ | **684.0** (558.6 – 836.9) | NI | NI | ND |
| 2o.III | / | H | $(CH_2)_2$-morpholine | **255.7** (196.7 – 324.5) | NI | NI | NI |
| 3.III | $CH_2C_6H_5$ | H | $CH_2C_6H_5$ | **≈ 500** | >500 | NI | 79% (±10%)[f] |
| 4.III | / | $CH_2C_6H_5$ | $CH_2C_6H_5$ | NI | >500 | NI | 44% (±2%)[f] |
| 5.III | $CH_2C_6H_5$ | $CH_2C_6H_5$ | $CH_2C_6H_5$ | NI | >500 | NI | 19% (±8%)[f] |

[a] Results are expressed as mean with 95% confidence intervals in brackets (n = 3).
[b] NI: no inhibition at 1 μM and 25 μM on MAO-A/MAO-B and IDO/LSD1, respectively.
[c] >500: Inhibition percentage at 1μM are shown as mean with ± SD in brackets (n = 3). **2b.III** = 14% (±6%), **2e.III** = 24% (±4%), **2g.III** = 42% (±2%), **2h.III** = 39% (±2%), **3.III** = 34% (±3%), **4.III** = 46% (±2%), **5.III** = 29% (±5%).
[d] Inhibition percentages at 25 μM are expressed as mean with ± SD in brackets (n = 3).
[e] ND: not determined.
[f] Inhibition percentages at 50 μM are expressed as mean with ± SD in brackets (n = 3).

The $IC_{50}$ value of compound **3.III** on hLSD1 was evaluated. The dose-response curve is represented in figure 29.III. The result ($IC_{50}$ = 31.5 μM (13.2 μM − 75.1 μM)) shows that compound **3.III** presents a similar $IC_{50}$ value on LSD1 compared to tranylcypromine (**5.I**, $IC_{50}$ = 22 μM) and could be an interesting scaffold for the design of new more potent and selective inhibitors of LSD1.
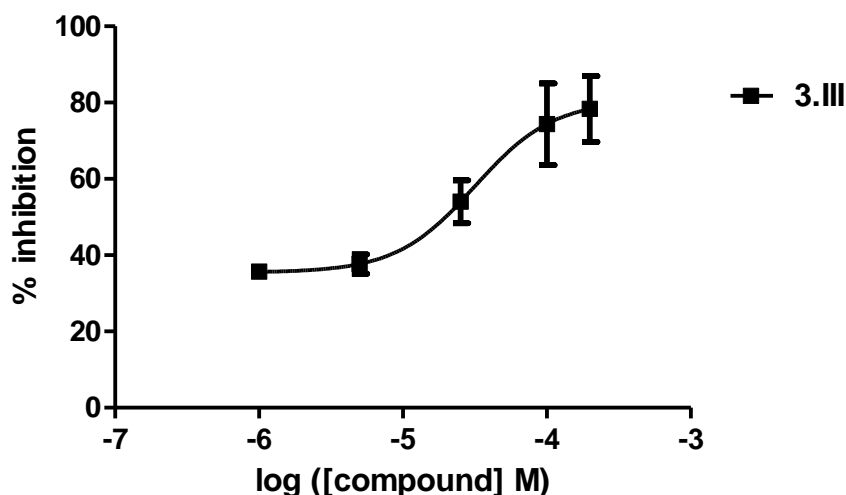


**Figure 29.III.** Dose-response curve of compound **3.III** (■) on hLSD1. Inhibition percentages are shown as mean ± SD with n = 3.

The LSD1 inhibitor screening assay presents a major disadvantage. Indeed, the activity of LSD1 is unknown. Furthermore, to assay the inhibitory potency of β-carbolines ($IC_{50}$ values) and 5*H*-indeno[1,2-*c*]pyridazin-5-ones (discussed in the second part), a new batch of Cayman's LSD1 inhibitor screening assay kit was used. However, the activity of the enzyme and so, the $IC_{50}$ value of tranylcypromine have changed. Thus, this $IC_{50}$ value has to be re-evaluated which was not performed by Cayman Corporation. Consequently, we have decided to stop the LSD1 inhibitor screening assay at the moment.

### 3.1.3 Perspectives

To monitor the activity of the enzyme in the LSD1 inhibitor screening assay, it would be interesting to overexpress directly the enzyme in the laboratory. Furthermore, to date, no small, potent and non-irreversible inhibitor of LSD1 is known. Although the β-carboline analogues displayed moderate activities on LSD1, compound **3.III** ($IC_{50}$ = 31.5 μM (13.2 μM − 75.1 μM)) could be an interesting scaffold for the design of new more potent inhibitors of
116

LSD1. Then, the purification of the enzyme and efforts in trying to obtain a crystal structure of LSD1 in complex with analogues of compound **3.III** could be performed.

# 4. CONCLUSION

In order to design new and more potent MAO-A inhibitors related to harmine (**3.I**), a series of β-carboline analogues (**2a-5.III**) has been synthesized. Their inhibitory potency has been evaluated by a luminescent assay on hMAO-A and –B enzymes. The results show that the replacement of the methyl moiety in the 7-position of harmine by a lipophilic group like a cyclohexyl, a phenyl or an aliphatic chain increases the inhibition for MAO-A. Compound **2e.III**, with the trifluorobutyloxy group, is the most active of this series, with a $K_i$ on MAO-A of 3.6 nM. Docking simulations into the active site of hMAO-A show that compound **2e.III** incorporates into the active site with harmine-like interactions. The lateral chain points to the lipophilic pocket where it is stabilized in agreement with an enhanced inhibitory potency towards MAO-A. Interestingly, compound **2o.III** ($K_i$ = 255.7 nM) containing an ethylmorpholine group, although less active compared to **2e.III**, is a potent and selective inhibitor of MAO-A, and displays a higher solubility in buffer (pH 7.4) (totally soluble at >500 μM) compared to **2e.III** (<3 μM). Therefore, efforts in trying to obtain a crystal structure of hMAO-A in complex with **2o.III** could be pursued. All the synthesized compounds are selective of MAO-A but some of them show also a moderate MAO-B inhibition (e.g., **2f.III**, $K_i$ = 221.6 nM) when compared to harmine (**3.I**). Docking simulations for compound **2f.III** performed in hMAO-B show that the β-carboline core incorporates into the substrate cavity. A shift is observed for the β-carboline core orientation in MAO-B compared to MAO-A induced by the Tyr326 side chain in MAO-B which produces a restriction that is less pronounced in hMAO-A where Ile335 occupies that position. In contrast to Gln215 in MAO-A, $\pi$-$\pi$ interaction of the β-carboline core with the equivalent amide group of Gln206 in MAO-B is less favorable. In addition, the β-carboline core is stabilized by two hydrogen bonds with water molecules in MAO-A compared to only one hydrogen bond in MAO-B which may explain the selectivity of the β-carboline derivatives towards MAO-A compared to MAO-B. Interestingly, the cyclohexyl chain of compound **2f.III** points to a lipophilic pocket in the entrance cavity where it is stabilized in agreement with an enhanced inhibitory potency towards MAO-B compared to harmine (**3.I**).

Secondly, the selectivity of β-carbolines was also established on hIDO, an enzyme involved in the serotonergic and kynurenine pathways and inhibited by 3-butyl-β-carboline (**46.I**) ($K_i$ = 3.3 µM). IDO inhibitory potency of our original β-carbolines was determined by a colorimetric method. The results show that, at 25 µM, the synthesized β-carbolines display no inhibition of IDO. Thus, they are selective of MAO and especially of MAO-A. Molecular docking studies of 3-butyl-β-carboline (**46.I**) suggest that the β-carboline core is stabilized in pocket A by Van der Waals interactions, complexation with the heme iron and a hydrogen bond while the butyl side chain points to pocket B lined with hydrophobic residues. This binding mode evidences that the substitutions in the 1, 2, 7 and 9-positions are not tolerated because of steric clashes within the active site of the enzyme. So, these substitutions lead to a new binding mode of β-carboline scaffold which is not stabilized into the active site in agreement with weak inhibition percentages obtained. From results of synthesized β-carbolines, molecular docking studies of 3-butyl-β-carboline and the pharmacophore model developed on IDO by Rohrig et al, we are interested in the synthesis of two new 3-substituted-β-carbolines (*N*-ethyl-3-methylamino-β-carboline (**8.III**) and 3-methylamino-β-carboline (**9.III**)) potentially more potent compared to 3-butyl-β-carboline (**46.I**). These new derivatives should incorporate in the active site with 3-butyl-β-carboline-like interactions but the side chain would display also a positive charge at physiological pH which might establish a coulomb interaction with the 7-propionate of the heme present in pocket B, as suggested by our docking studies. Compounds **8.III** and **9.III** were synthesized in two and four steps, respectively from the ethyl β-carboline-3-carboxylate (**10.III**) intermediate. Surprisingly, the results reveal that the *N*-ethyl-3-methylamino-β-carboline (**8.III**) displays no inhibition on IDO at 100 µM. Although it was impossible to test the compound **9.III** due to a lack of availability of this latter, the absence of inhibition observed for **8.III** tends to show that the introduction of a positive charge is not tolerated. The result of compound **8.III** must be yet confirmed again but this inactivity maybe explained by a more hydrophobic character of the pocket B. So, from the result of compound **8.III** and the pharmacophore model developed on IDO by Rohrig et al, it can be interesting to explore the possibility to synthesize of new 3-substituted-β-carbolines with a negatively charged group such as a carboxylate that can form a salt bridge with Arg231.

Finally, the selectivity of our β-carbolines was also established on hLSD1, an enzyme displaying a similarity in the catalytic and structural properties with MAO. LSD1 inhibitory potency of β-carbolines was determined by a fluorometric method. The results show that, at

25 µM, the synthesized β-carbolines are weak inhibitors of LSD1. The introduction of lipophilic and bulky groups like aliphatic (**2c.III**), cyclohexyl (**2f.III**), phenyl (**2g.III**, **2h.III** and **3.III**) and naphthyl (**2h.III**) groups allows to increase the inhibitory potency of β-carboline scaffold on LSD1 compared to harmine (**3.I**, inactive at 50 µM). Thus, the synthesized β-carboline derivatives are selective of MAO-A. However, although the β-carboline analogues display moderate activities on LSD1, compound **3.III** ($IC_{50}$ = 31.5 µM) could be an interesting scaffold for the design of new more potent and selective inhibitors of LSD1.

120

# 5*H*-INDENO[1,2-*C*]PYRIDAZIN-5-ONES

# 1. MAO

As mentioned in the introduction, the 5*H*-indeno[1,2-*c*]pyridazin-5-one template displays a reversible competitive inhibition and is selective of MAO-B. Currently, analogues **22f.I** ($IC_{50}$ hMAO-B = 8.5 nM [73]) and **22j.I** ($IC_{50}$ baMAO-B = 14.0 nM [74]) reported in scheme 13.III, are described among the most potent inhibitors of this series on MAO-B. Moreover, the docking studies of **22f.I** and **22j.I** with hMAO-B (Figure 30.III) reported from the literature [73, 75] suggest that these two 5*H*-indeno[1,2-*c*]pyridazin-5-one analogues could be the starting point for the design of novel and potentially more potent MAO-B inhibitors.
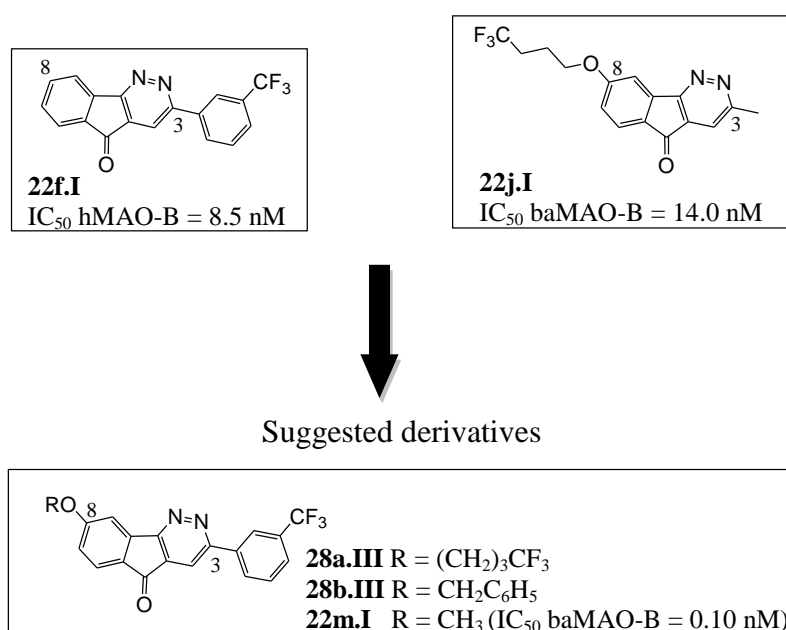


**Scheme 13.III.** Rational design of 5*H*-indeno[1,2-*c*]pyridazin-5-one analogues (**28a-b.III** and **22m.I**).

## 1.1 Structure-based rational design

Previous studies on 5*H*-indeno[1,2-*c*]pyridazin-5-one derivatives as MAO-B inhibitors revealed that the substitution of 5*H*-indeno[1,2-*c*]pyridazin-5-one scaffold in the 3-position with lipophilic and bulky groups such as *meta*-CF$_3$-phenyl (**22f.I**, $IC_{50}$ hMAO-B = 8.5 nM [73], scheme 13.III) increases the MAO-B inhibitory potency of this series [73, 76]. Molecular docking studies suggest that the *meta*-CF$_3$-phenyl occupies the substrate cavity to

reach the hydrophobic pocket (Tyr60, Phe343, Tyr398), finding a favorable environment [73] (Figure 30.III).
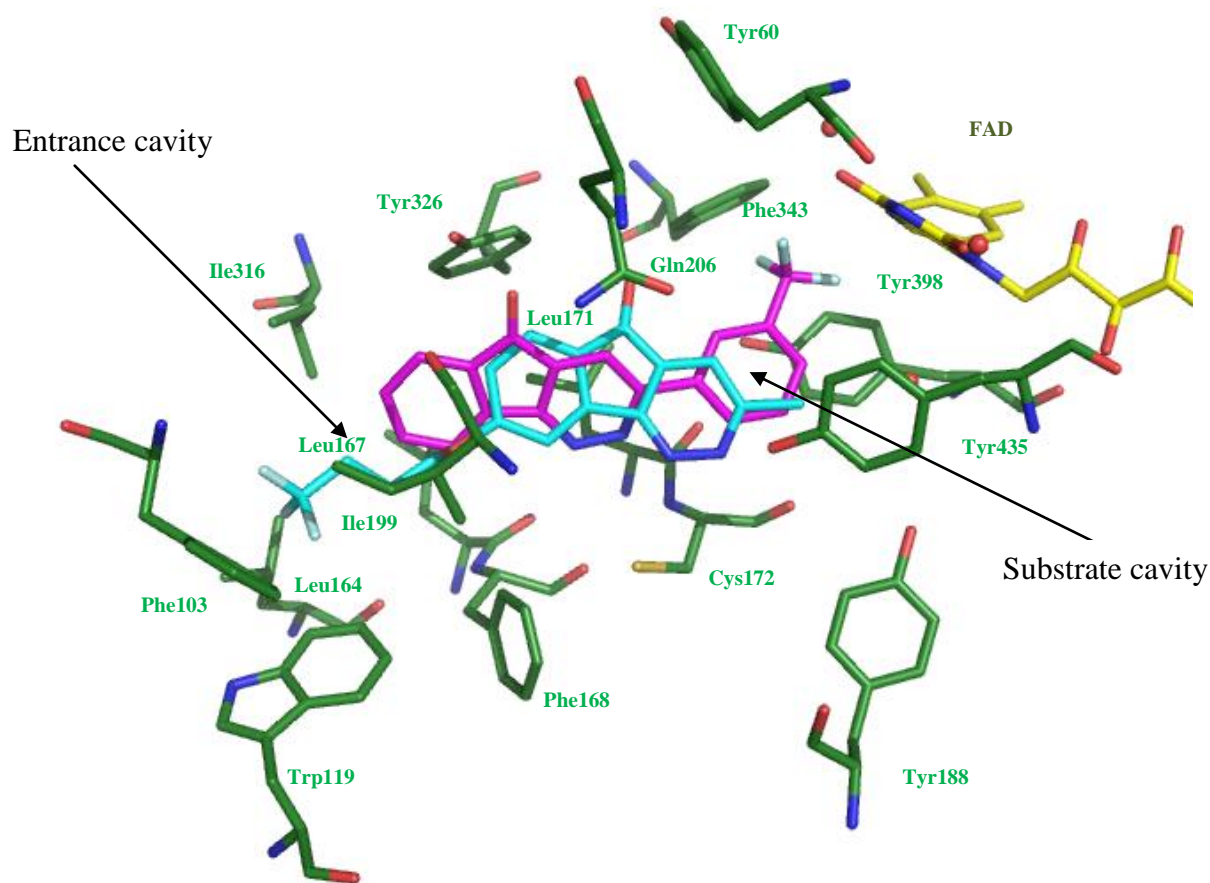


**Figure 30.III.** Docking solutions of compounds **22f.I** (magenta [73]) and **22j.I** (cyan [75]) in the active site of hMAO-B (2V5Z.pdb). Only amino acids directly implicated in the active site are displayed and labeled in green. FAD is in yellow and the water molecules are displayed as red spheres.

Further studies performed by our group revealed that the substitution in the 8-position of the central heterocycle with lipophilic and bulky groups such as trifluorobutyloxy (**22j.I**, $IC_{50}$ baMAO-B = 14.0 nM [74], scheme 13.III) increases the MAO-B inhibitory potency of this series [74-75]. Docking studies suggest that this trifluorobutyloxy side chain occupies the entrance cavity (Figure 30.III) [75]. Interestingly, the inhibitory activity reported by our group on derivative **22m.I** ($IC_{50}$ baMAO-B = 0.10 nM, Scheme 13.III) bearing *meta*-CF$_3$-phenyl and methoxy groups in the 3 and 8-positions, respectively [74] leads us to synthesize new 5*H*-indeno[1,2-*c*]pyridazin-5-one derivatives containing lipophilic and bulky groups at both positions (**28a-b.III**, Scheme 13.III) including **22m.I** as a reference drug. Their human monoamine oxidase A and B inhibitory potency was investigated. In addition, compounds

124

**30a.III** and **30b.III** (Scheme 15.III), previously synthesized in the framework of a master's thesis (Fabrice Camus, Biological Structural Chemistry Laboratory, FUNDP, Belgium) and structurally related to compound **22j.I**, were also evaluated for their human monoamine oxidase A and B inhibitory potency. The $IC_{50}$ values of the most potent compounds were evaluated and $K_i$ values were estimated using the Cheng-Prusoff equation [192]. A competitive-type inhibition for the most potent inhibitor was confirmed from the Lineweaver–Burk plots. The $K_i$ value was in good agreement with the value deduced from the $IC_{50}$.


## 1.2 Synthesis of 5*H*-indeno[1,2-*c*]pyridazin-5-one analogues

The strategy used to synthesize 8-(alkoxy)-3-(3'-(trifluoromethyl)phenyl)-5*H*-indeno[1,2-*c*]pyridazin-5-one derivatives (**28a-b.III** and **22m.I**) is depicted in scheme 14.III. This synthetic pathway follows a four steps procedure reported by our group from the common 5-hydroxy-1-indanone (**24.III**) intermediate [74-75].

5-Hydroxy-1-indanone (**24.III**) reacted with 1-tosyl-4,4,4-trifluorobutane in the presence of $K_2CO_3$ in acetonitrile for 4 h at 90°C to give the 5-(4,4,4-trifluoromethylbutyloxy)-1-indanone (**25a.III**) in almost quantitative (96%) yield. 5-Benzyloxy-1-indanone (**25b.III**) was obtained by reaction between the indanone (**24.III**), $K_2CO_3$, benzyl bromide in DMF for 5 h at room temperature in almost quantitative (90%) yield. 5-(Methoxy)-1-indanone (**25c.III**) is commercially available. The alkoxyninhydrins (**26a-c.III**) were synthesized by selenium dioxide oxidation of 5-alkoxy-1-indanones (**25a-c.III**). A dioxane solution of 5-alkoxy-1-indanone was mixed with selenium dioxide and refluxed for 3 h. This gave the 5-alkoxyninhydrins **26a-c.III** in 73-81% yield. A solution of 5-alkoxyninhydrin (**26a-c.III**) and 3'-(trifluoromethyl)acetophenone in acetic acid was refluxed for 3 h to give the intermediate aldol adduct (**27a-c.III**). After cooling to room temperature, the mixture reacted with hydrazine overnight. After purification on a silica gel column, the 8-(alkoxy)-3-(3'-(trifluoromethyl)phenyl)-5*H*-indeno[1,2-*c*]pyridazin-5-one (**28a-b.III** and **22m.I**) regioisomer was obtained in 39-46% yield. X-ray diffraction was used to unambiguously establish the position of the alkoxy group in the 8-position of the 5*H*-indeno[1,2-*c*]pyridazin-5-one moiety. ORTEP views of the conformations of **28a.III** and **28b.III**, with their atomic numbering scheme are depicted in figure 31.III.
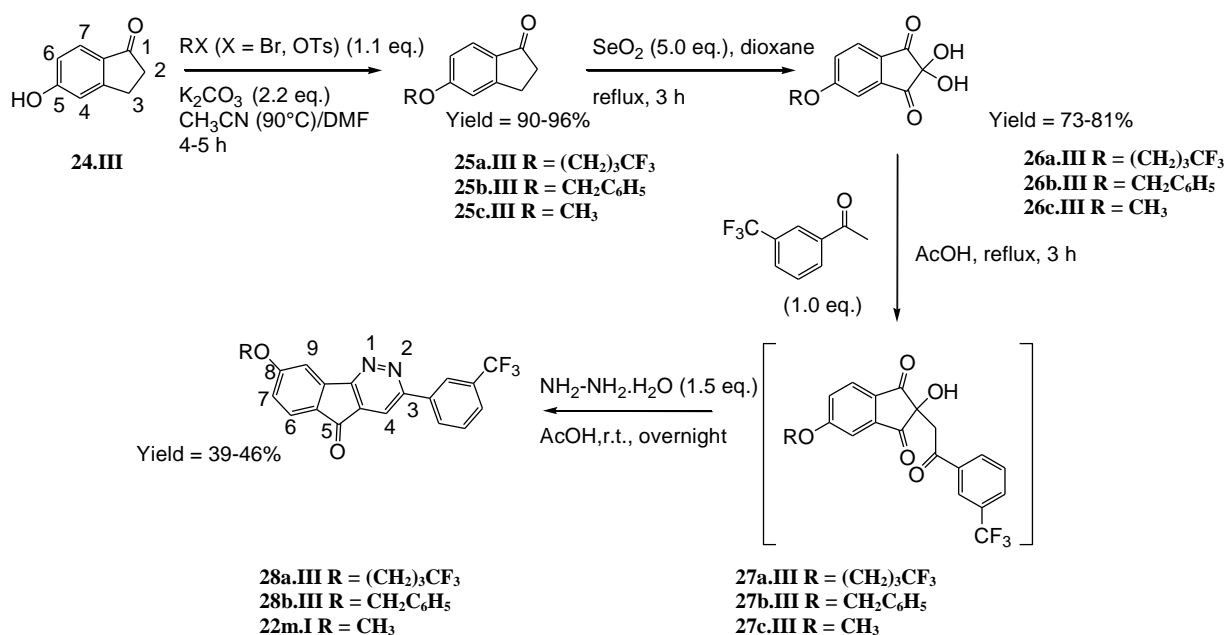
**Scheme 14.III.** Synthetic pathway to 5*H*-indeno[1,2-*c*]pyridazin-5-one analogues **28a-b.III** and **22m.I**.

As mentioned previously, the synthesis of compounds **30a-b.III** was reported in the master's thesis of Fabrice Camus (Biological Structural Chemistry Laboratory, FUNDP, Belgium) and started from the phenol **29.III** [74] (Scheme 15.III). Benzylation of **29.III** was achieved upon reaction with 1-(bromomethyl)-3-chlorobenzene or 1-(bromomethyl)-3-methylbenzene in the presence of silver oxide in DMF at room temperature for 4 h. This provided **30a-b.III** in modest yields (6-15% yield). In this thesis, the two compounds were fully characterized and again, X-ray diffraction was used to confirm the structure of **30a.III** (Figure 31.III).

The structure of the synthesized compounds was confirmed by $^1$H NMR, $^{13}$C NMR, mass spectrometry (MS) and their purity was assessed by elemental analyses. The data are reported in the chapter Materials and Methods.
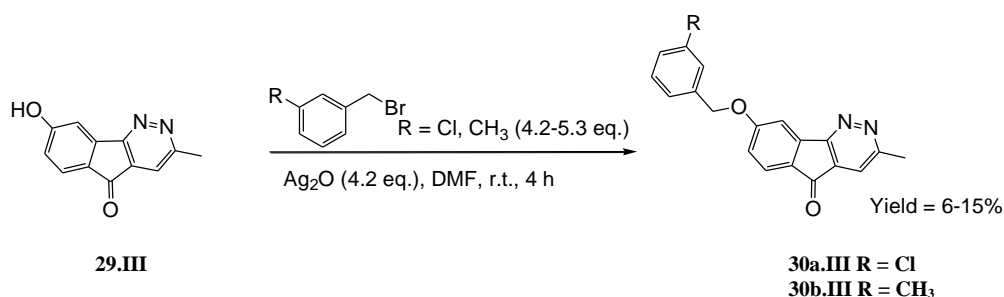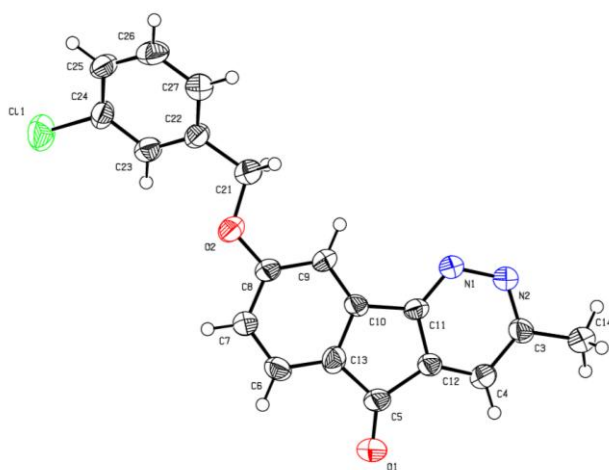


**Scheme 15.III.** Synthetic pathway to 5*H*-indeno[1,2-*c*]pyridazin-5-one analogues **30a-b.III** (Master's thesis of Fabrice Camus, Biological Structural Chemistry Laboratory, FUNDP, Belgium).

126
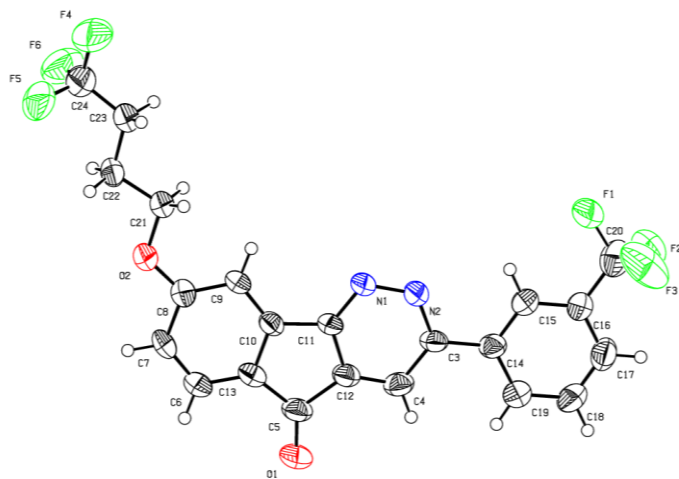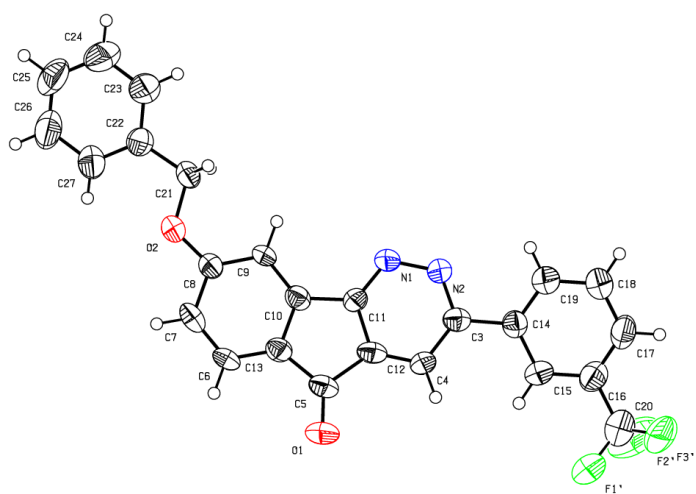
**Figure 31.III.** ORTEP diagram (50% probability) of compounds **28a.III**, **28b.III** and **30a.III**.

## 1.3 Biological evaluation

The inhibitory potency of the 5*H*-indeno[1,2-*c*]pyridazin-5-ones was assessed *in vitro* in triplicate at 10 µM using the inhibition assays previously validated on hMAO-A and –B. First, the $IC_{50}$ values of the most potent were evaluated on hMAO-B. The $K_i$ values of the most potent compounds were then estimated from the $IC_{50}$ values using the Cheng-Prusoff equation [192]. The results of MAO inhibition studies are reported in tables 12.III and 13.III.

Compounds **22m.I** and **22j.I** are known as inhibitors of MAO-B [72, 74] and were used as references. All the 5*H*-indeno[1,2-*c*]pyridazin-5-one analogues except **28b.III** present a higher inhibitory potency on MAO-B than MAO-A. The MAO inhibitory potency of these compounds proved to be highly dependent on the alkyl/aryl-substituent in the 3-position. Analogues with a *meta*-CF<sub>3</sub>-phenyl group and a lipophilic group (methoxy, benzyloxy or trifluorobutyloxy) in the 3 and 8-positions respectively (**28a-b.III** and **22m.I**) show moderate or no inhibition of MAO-B at 10 µM. Thus, the inhibitory activity of **22m.I** is not in agreement with the data reported by our group on baboon enzyme [74]. However, it was evidenced in the literature that MAO affinity depends on species studied. In particular, Novaroli et al have evidenced important species-dependent differences in MAO-B inhibitor specificity between human and rat for 5*H*-indeno[1,2-*c*]-pyridazin-5-one derivatives [73]. Indeed, these derivatives show a greater inhibitory potency toward hMAO-B than toward rMAO-B (e.g., **22f.I**, $IC_{50}$ rMAO-B = 280 nM and $IC_{50}$ hMAO-B = 8.5 nM) [73]. So, a difference of affinity between baboon and human enzymes can be conceivable.

In contrast, the substitution of *meta*-CF<sub>3</sub>-phenyl group in the 3-position with a methyl group (**30a.III**, **30b.III** and **22j.I**) leads to better inhibition (in the submicromolar range) of hMAO-B (Tables 12-13.III and figure 32.III). Compound **30a.III**, with a chlorine *meta*-substituted benzyloxy group, is the most active and selective within this series, with a $K_i$ on MAO-B of 0.16 µM (Table 13.III and figure 32.III).

**Table 12.III.** Structure and inhibitory potency of synthesized 5*H*-indeno[1,2-*c*]pyridazin-5-one derivatives on hMAO-A and −B.

| Compound | Structure | Inhibition percentage[a] | |
| --- | --- | --- | --- |
| | | hMAO-A | hMAO-B |
| 28a.III |  | NI[b] | 57% (±10%) |
| 28b.III |  | 10% (±10%) | 7% (±3%) |
| 22m.I |  | NI | 36% (±2%) |
| 30a.III |  | 15% (±5%) | 93% (±4%) |
| 30b.III |  | 17% (±1%) | 90% (±0%) |
| 22j.I |  | NI | 92% (±0%) |

[a] Inhibition percentages at 10 µM are expressed as mean with ± SD in brackets (n = 3).
[b] NI: no inhibition at 10 µM.

**Table 13.III.** $K_i$ values deduced from IC$_{50}$/measured on hMAO-B for compounds **30a.III**, **30b.III** and **22j.I**.

| | $K_i$ (µM) | |
| --- | --- | --- |
| Compound | Deduced from IC$_{50}$[a] | Measured[b] |
| 30a.III | **0.16** (0.14 − 0.19) | **0.11** ± 0.01 |
| 30b.III | **0.48** (0.42 − 0.55) | |
| 22j.I | **0.28** (0.26 − 0.30) | |

[a] $K_i$ values are estimated from the experimentally measured IC$_{50}$ values using the Cheng-Prusoff equation and are expressed as mean within brackets 95% confidence intervals (n = 3).
[b] $K_i$ value is measured from the Lineweaver-Burk representation and is expressed as the mean ± SD (n = 3).
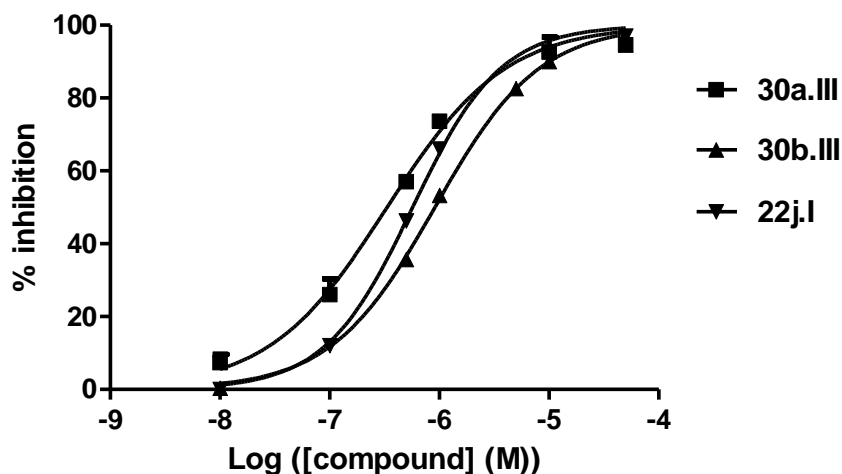
**Figure 32.III.** Dose-response curve of compounds **30a.III** (■), **30b.III** (▲) and **22j.I** (▼) on hMAO-B. Inhibition percentages are shown as mean ± SD with n = 3.

To confirm the inhibition mode of MAO-B by **30a.III**, the Lineweaver–Burk plots were obtained from incubations at four different substrate concentrations with and without three different inhibitor concentrations. Lineweaver-Burk representation for **30a.III** on MAO-B demonstrates that its mechanism of inhibition is competitive (Figure 33.III). The $K_i$ value for the inhibition of MAO-B by **30a.III** was determined to be 0.11 μM which is in agreement with the $K_i$ value estimated from the $IC_{50}$ value using the Cheng-Prusoff equation (Table 13.III) [192]. These results show that the substitution at both positions by lipophilic and bulky groups (**28a-b.III** and **22m.I**) is not tolerated compared to analogues **30a.III**, **30b.III** and **22j.I**.
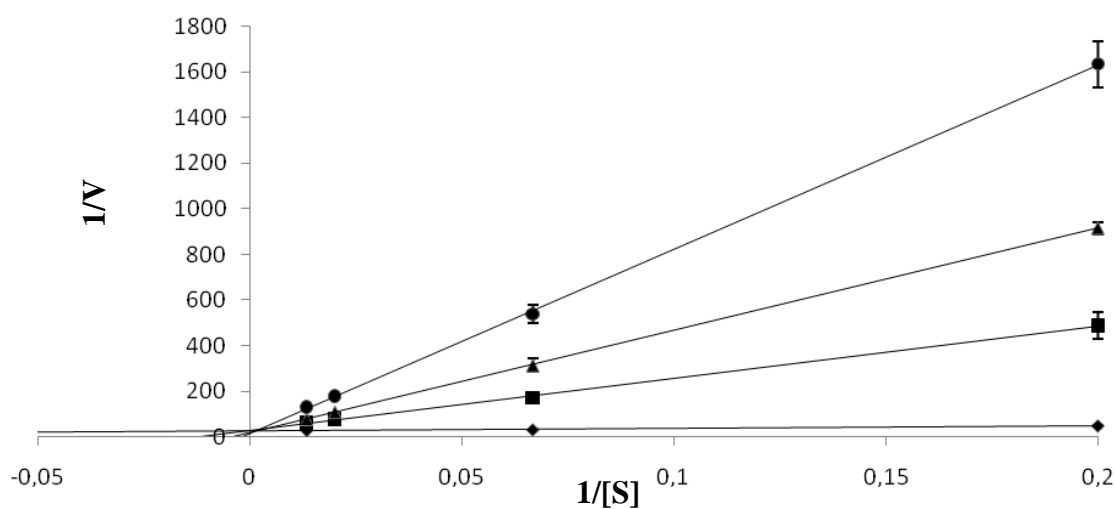


**Figure 33.III.** Lineweaver-Burk plots of the inhibition of recombinant human MAO-B by **30a.III**. The lines were constructed in the absence (♦) and presence of 2 μM (■), 5 μM (▲) and 15 μM (●) of **30a.III** with n = 3.

130

With the aim of understanding the role of an aryl group in the 3-position, molecular docking studies of compounds **30a.III** were performed and discussed in the next section.

## 1.4 Molecular modeling

Analysis of the binding mode for compound **30a.III** (Figure 34.III, top)—selected from the docking study as a plausible solution in agreement with docking solution of **22j.I** ([75]) in the active site of hMAO-B (Figure 30.III)— revealed that 5*H*-indeno[1,2-*c*]pyridazin-5-one core is located in the vicinity of the FAD cofactor with the C-8 side chain projecting towards the entrance cavity of MAO-B. The substrate cavity is mainly hydrophobic, the only hydrophilic region being located between Tyr398, Tyr435 and the flavin which form an aromatic cage. The examination of the molecular electrostatic potential (MEP) distribution for compound **30a.III** shows the presence of two large attractive zones around the 5*H*-indeno[1,2-*c*]pyridazin-5-one ring (Figure 34.III, bottom). The first one is centered on the carbonyl and the second one is centered on the endocyclic hydrazine. So, it is not surprising to observe that both regions are located within the hydrophilic region of the MAO-B substrate cavity. The 5*H*-indeno[1,2-*c*]pyridazin-5-one ring is stabilized by $\pi$-$\pi$ interactions with Tyr398 and Tyr435. The binding mode adopted by compound **30a.III** allows the *meta*-chlorobenzyloxy side chain to settle within the entrance cavity lined with hydrophobic amino acid residues. This hydrophobic pocket is coated by Phe103, Trp119, Leu164, Leu167, Phe168, and Ile316. Interestingly, the introduction of a chlorine atom on the benzyl ring (**30a.III**, $K_i$ = 0.16 μM) increases the inhibitory potency on MAO-B compared to the derivative bearing a methyl group (**30b.III**, $K_i$ = 0.48 μM). Previous studies have shown that addition of a chlorine substituent on the phenyl group side chain enhances the lipophilicity of the inhibitor, and therefore its affinity and its selectivity on MAO-B establishing Van der Waals interactions in the hydrophobic entrance cavity [62]. Compound **22j.I** ($K_i$ = 0.28 μM) with the trifluorobutyloxy group displays a similar inhibition compared to **30a.III**. The methyl group in the 3-position is stabilized within the hydrophobic cage formed by Tyr398, Tyr435 and FAD. The substrate cavity being more sterically constrained than the entrance cavity, the *meta*-CF$_3$-phenyl group of compounds **28a-b.III** and **22m.I** cannot accommodate into the substrate cavity without modifying the binding mode of 5*H*-indeno[1,2-*c*]pyridazin-5-one

ring. So, these observations may explain the reduced inhibition of compounds **28a-b.III** and **22m.I** compared to **30a.III**, **30b.III** and **22j.I**.
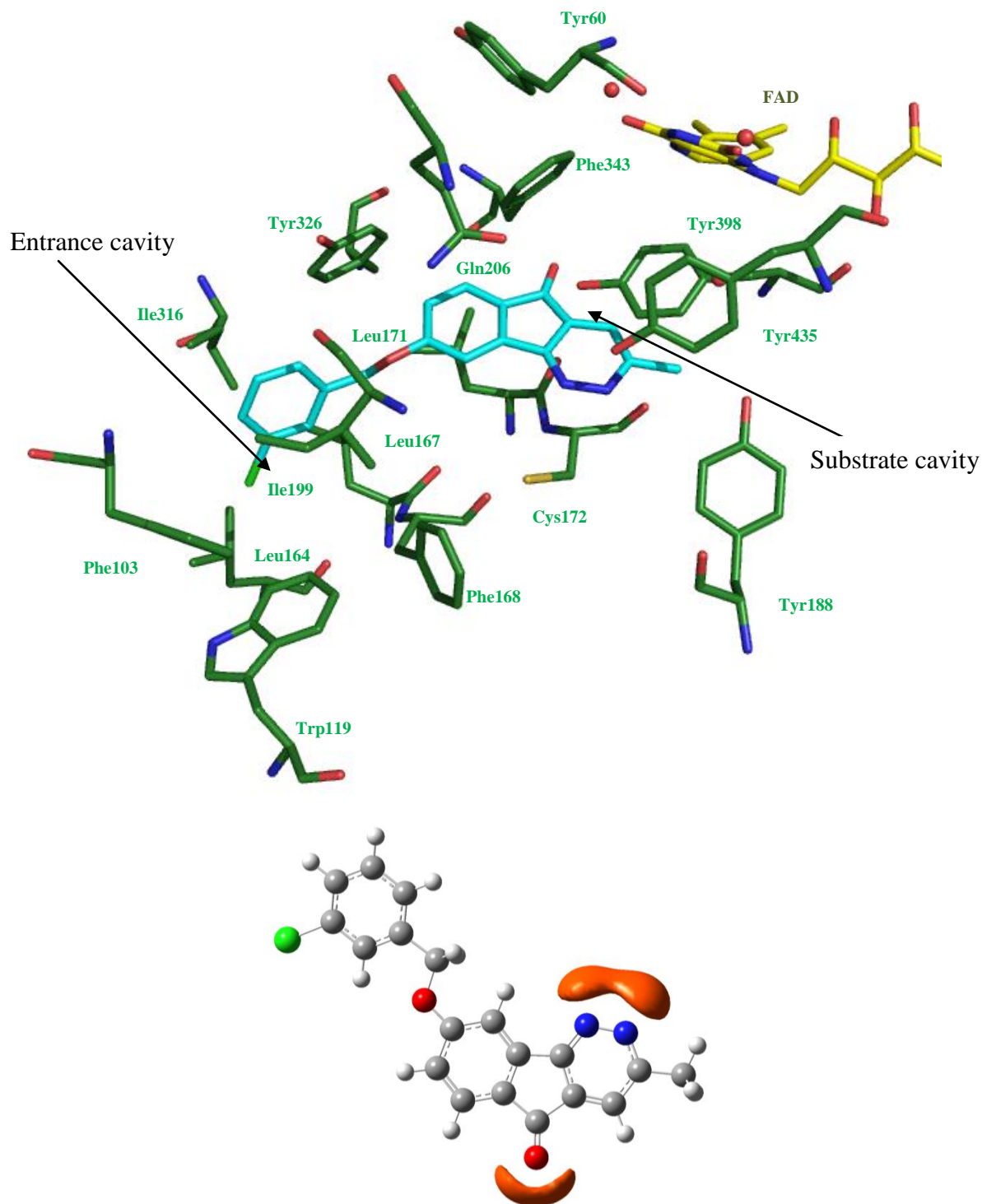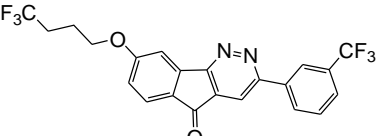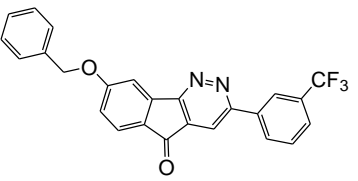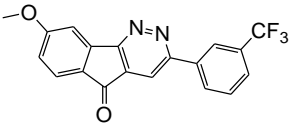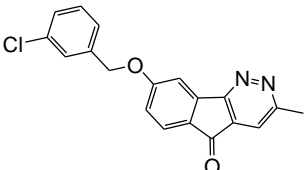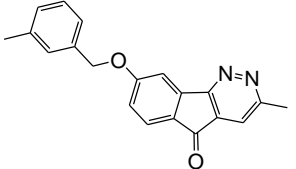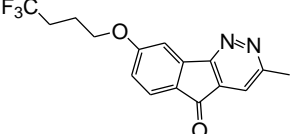


**Figure 34.III.** (top) Simulated binding mode of compound **30a.III** in the active site of hMAO-B (2V5Z.pdb). Only amino acids directly implicated in the active site are displayed and labeled (in green). Compound **30a.III** and FAD are in cyan and yellow respectively. The water molecules in the active site are displayed as red spheres. (Bottom) Attractive molecular electrostatic potential (isovalue for surfaces = 10 kcal/mol) calculated around compound **30a.III**. (PBE1PBE, 6-311G**)

# 2. IDO

## 2.1 Biological evaluation

In this study, we also appraised the selectivity of our 5*H*-indeno[1,2-*c*]pyridazin-5-one series on hIDO. The IDO inhibitory potency of these analogues was assessed *in vitro* in triplicate at 25 µM using the colorimetric test previously validated on hIDO. The results of MAO and IDO inhibition studies are reported in table 14.III.

**Table 14.III.** Structure and inhibitory potency of synthesized 5*H*-indeno[1,2-*c*]pyridazin-5-one derivatives on hMAO-A, hMAO-B and hIDO.

| | | Inhibition percentage[a] | | |
| Compound | Structure | hMAO-A | hMAO-B | hIDO |
|---|---|---|---|---|
| 28a.III |  | NI[b] | 57% (±10%) | NI[b] |
| 28b.III |  | 10% (±10%) | 7% (±3%) | 17% (±1%) |
| 22m.I |  | NI | 36% (±2%) | NI |
| 30a.III |  | 15% (±5%) | 93% (±4%) | 25% (±3%) |
| 30b.III |  | 17% (±1%) | 90% (±0%) | 14% (±2%) |
| 22j.I |  | NI | 92% (±0%) | 19% (±2%) |

[a] Inhibition percentages at 10 µM and 25 µM on MAO-A/MAO-B and IDO respectively, are expressed as mean with ± SD in brackets (n = 3).
[b] NI: no inhibition at 10 µM and 25 µM on MAO-A/MAO-B and IDO, respectively.

The results reveal that the synthesized 5*H*-indeno[1,2-*c*]pyridazin-5-one analogues display no significant inhibition on IDO. So, 5*H*-indeno[1,2-*c*]pyridazin-5-one derivatives display a higher activity and selectivity on hMAO-B.

## 3. CONCLUSION

In order to design new, selective, and more potent MAO-B inhibitors, a series of 5*H*-indeno[1,2-*c*]pyridazin-5-one derivatives substituted both in the 3 and 8-positions by lipophilic groups has been synthesized. X-ray diffraction technique was used to unambiguously establish the position of the alkoxy group on the phenyl ring of the 5*H*-indeno[1,2-*c*]pyridazin-5-one moiety. Inhibitory potency of the compounds has been evaluated by a luminescent test on hMAO-A and –B. In this study, the selectivity of our series was also established on hIDO by a colorimetric method. The results show that, at 25 μM, the synthesized 5*H*-indeno[1,2-*c*]pyridazin-5-ones display no significant inhibition on IDO. All compounds, except **28b.III**, display a higher activity and selectivity on MAO-B. 3-Methyl-8-*meta*-chlorobenzyloxy-5*H*-indeno[1,2-*c*]pyridazin-5-one (**30a.III**), is the most active and selective within this series, with a $K_i$ on MAO-B of 0.11 μM. Replacement of the methyl moiety in the 3-position by a lipophilic group like a *meta*-CF$_3$-phenyl group (**28a-b.III** and **22m.I**) abolishes the inhibitory potency on MAO-B. So, the substitution of the 5*H*-indeno[1,2-*c*]pyridazin-5-one core in the 3-position dramatically influences the MAO-inhibiting properties of these compounds. Docking simulations of compound **30a.III** in hMAO-B suggest that the 5*H*-indeno[1,2-*c*]pyridazin-5-one core incorporates into the substrate cavity with the *meta*-chlorobenzyloxy side chain extending towards a hydrophobic pocket of the entrance cavity space. Finally, it would be interesting to investigate the 5*H*-indeno[1,2-*c*]pyridazine-5-one inhibitors of MAO as potential LSD1 inhibitors once the problem of the control of enzyme activity solved.

# INDOLE DERIVATIVES

# 1. MAO

## 1.1 Selection of compounds

As mentioned in the introduction, previous studies have shown that indole derivatives may be used for the design of potent anti-MAO agents [57-62]. For example, the irreversible MAO-B inhibitor PF9601N (**20a.I**, Figure 35.III; $K_i$ rMAO-B = 0.75 nM [60]) shows antioxidant/neuroprotective properties in an experimental model of PD [61].



**20a.I**          **48.III**          **3.I**

**4.I**          **2f.III**
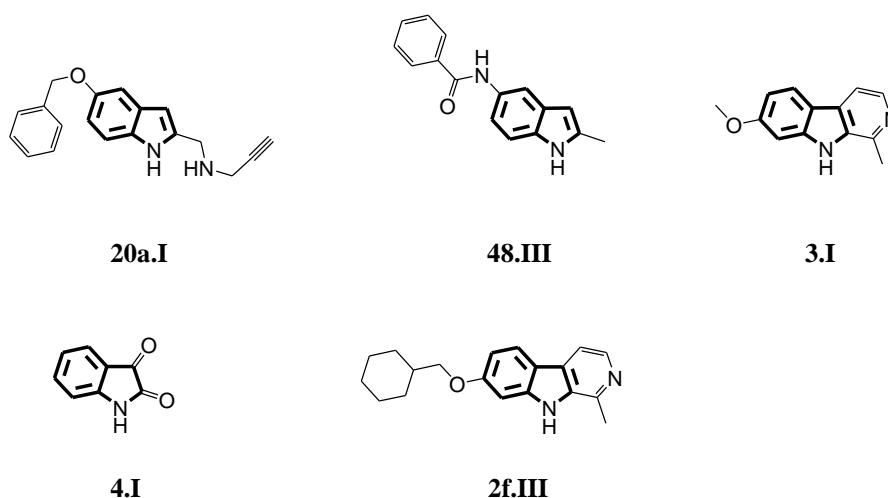
**Figure 35.III.** Chemical structures of PF9601N (**20a.I**), *N*-(2-methyl-1*H*-indol-5-yl)benzamide (**48.III**), harmine (**3.I**), isatin (**4.I**) and 7-(cyclohexylmethoxy)-1-methyl-*β*-carboline (**2f.III**).

In this study, we are interested in two series including bulky and/or lipophilic groups in the 3-(**31-43.III**, Figure 36.III) or 5-positions (**44-47.III**, Figure 36.III) and available at the department of Pharmacy (Prof. Masereel, FUNDP, Belgium). Though the compounds (**31-47.III**) are already known, their potential inhibitory activity on MAO isoforms has never been described except for 680C91 (**40.III**). 680C91 is a potent ($K_i$ = 51 nM) and selective TDO inhibitor with no inhibitory activity on MAO-A and −B [208].
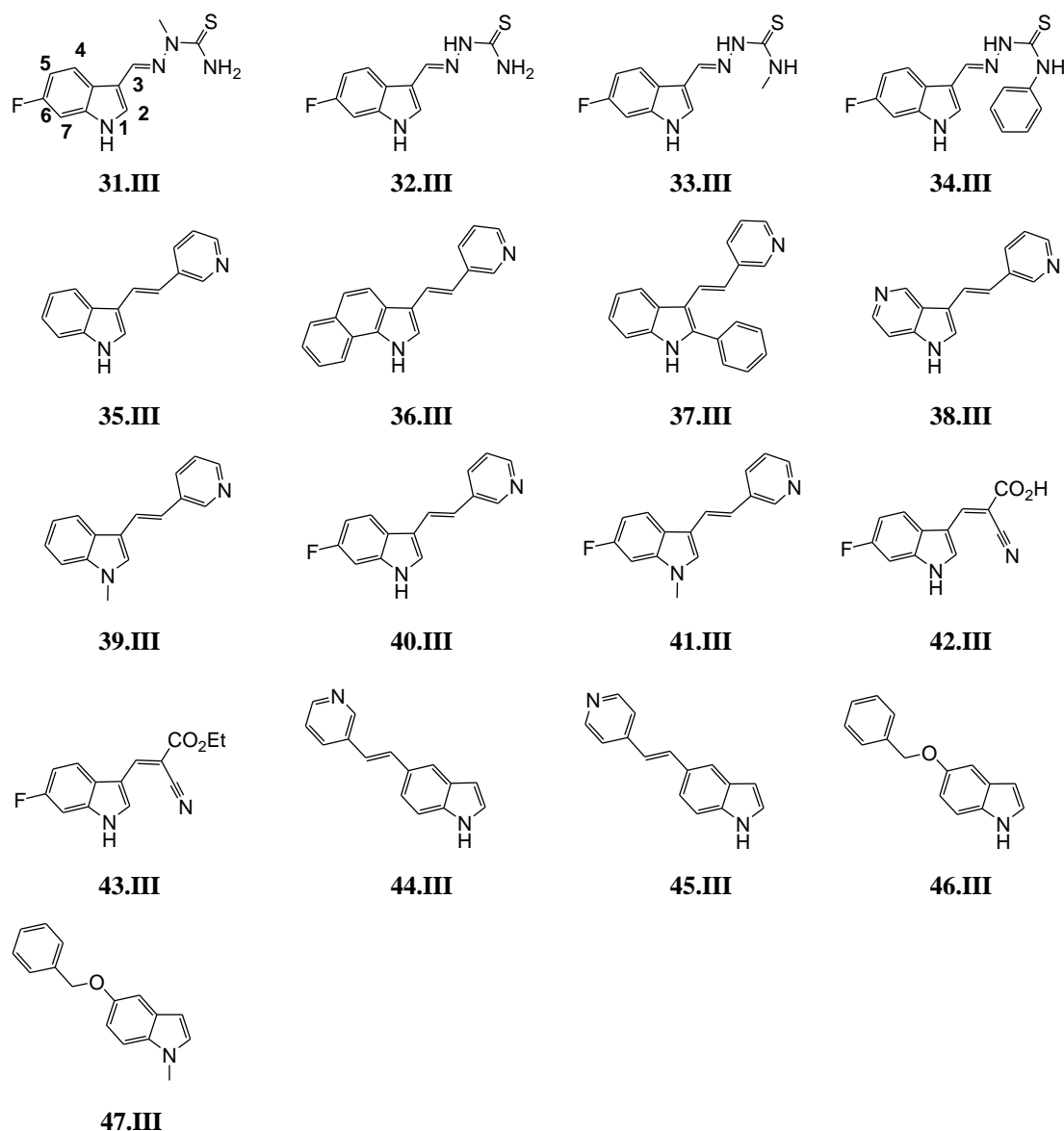
**Figure 36.III.** Chemical structures of selected indole derivatives tested on hMAO-A and −B.

The first series consists of 680C91 (**40.III**) analogues. Compounds **31**-**34.III** include a thiosemicarbazone group instead of a pyridinyl vinyl group. We have also studied a series of 3-(2-(pyridin-3-yl)vinyl)-1*H*-indol differently substituted (**35**-**41.III**) which are directly derived from 680C91 (**40.III**). Compounds **42.III** and **43.III** correspond to acrylic acid and ester derivatives. Finally, we have evaluated the inhibition of four indole derivatives (**44-47.III**) substituted in the 5-position by a lipophilic group. Previous studies have indicated that bulky C-5 substituents (e.g., **20a.I** [60] and **48.III** ($K_i$ hMAO-B = 1.65 μM [62]), Figure 35.III) like the benzyloxy or phenyl moiety on the indole core generally increase potency and selectivity on MAO-B.

## 1.2 Biological evaluation

The inhibitory potency of the indole derivatives was assessed *in vitro* in triplicate at 10 µM using the inhibition assays previously validated on hMAO-A and –B. The $IC_{50}$ values of the most potent were evaluated on hMAO-A and –B. Then, the $K_i$ values were estimated from the $IC_{50}$ values using the Cheng–Prusoff equation [192]. The results of MAO inhibition studies are reported in table 15.III. The indole references used on MAO-A and –B were harmine (**3.I,** $K_i$ = 16.9 nM) and isatin (**4.I,** $K_i$ = 32.6 µM), respectively (Figure 35.III). The thiosemicarbazone compounds **31-34.III** show weak inhibition of MAO-A and no inhibition at 10 µM of MAO-B except for compound **34.III** which shows 50% of inhibition. Among the other indole derivatives, compound **41.III**, a 3-(2-(pyridin-3-yl)vinyl)-1*H*-indol, substituted both in the N-1 position with a methyl group and at C-6 with a fluorine atom, is the most active inhibitor on MAO-A, with a $K_i$ of 1.15 µM (Figure 37.III (top) and table 15.III). Interestingly, the unsubstituted 3-(2-(pyridin-3-yl)vinyl)-1*H*-indol (**35.III**) does not inhibit MAO-A at 10 µM. The introduction of a phenyl group in the 2-position (**37.III**) does not improve the inhibition on MAO-A. The extension to three cycles of the central aromatic ring (**36.III**) as well as the introduction of a nitrogen on the indole (**38.III**), a methyl group in the N-1 position (**39.III**) or a fluorine in the 6-position (**40.III**) does not significantly increase the inhibition of MAO-A compared to compound **35.III**. Interestingly, the substitution of the 3-(2-(pyridin-3-yl)vinyl)-1*H*-indol scaffold with both a methyl group at N-1 and a fluorine atom at C-6 significantly enhances the inhibitory potency of compound **41.III** compared to unsubstituted analogue **35.III** and the corresponding N-methyl and fluorine substituted compounds **39.III** and **40.III**.

Concerning MAO-B, the ethyl ester derivative **43.III** significantly inhibits MAO-B compared to its acid analogue **42.III**. The 3-(2-(pyridin-3-yl)vinyl)-1*H*-indol compounds (**35-41.III**) do not inhibit MAO-B and so display a selectivity on MAO-A. Interestingly, the substitution in the 5-position of the indole core with a vinyl pyridin group (**44-45.III**) leads to relatively weak inhibitors of the two isoforms of MAO. The introduction of a benzyloxy group (**46.III**) instead of vinyl pyridin group increases both the inhibitory potency and the selectivity on MAO-B. This result is in agreement with previous studies which indicate that bulky C-5 substituents including the benzyloxy moiety generally increase potency and selectivity on MAO-B [62, 209].

**Table 15.III.** Inhibitory potency of indole derivatives on hMAO-A and –B.

| Compound | Inhibition percentage[a] | | $K_i$ (µM)[b] | |
| | hMAO-A | hMAO-B | hMAO-A | hMAO-B |
|---|---|---|---|---|
| harmine | | | **0.017** (0.014 – 0.021) | **120.80** (94.90 – 153.90) |
| Isatin | | | | **32.55** (28.11 – 37.68) |
| **31.III** | **4%** (±4%) | **NI[c]** | | |
| **32.III** | **11%** (±1%) | **NI** | | |
| **33.III** | **20%** (±3%) | **NI** | | |
| **34.III** | **12%** (±3%) | **50%** (±8%) | | |
| **35.III** | **5%** (±6%) | **9%** (±6%) | | |
| **36.III** | **20%** (±3%) | **7%** (±1%) | | |
| **37.III** | **NI** | **NI** | | |
| **38.III** | **9%** (±5%) | **6%** (±7%) | | |
| **39.III** | **22%** (±1%) | **NI** | | |
| **40.III** | **14%** (±5%) | **17%** (±1%) | | |
| **41.III** | **73**% (±2%) | **27%** (±3%) | **1.15** (0.92 – 1.44) | |
| **42.III** | **4%** (±4%) | **NI** | | |
| **43.III** | **9%** (±1%) | **51%** (±6%) | | |
| **44.III** | **15%** (±2%) | **42%** (±2%) | | |
| **45.III** | **22%** (±1%) | **34%** (±0%) | | |
| **46.III** | **6%** (±2%) | **66**% (±1%) | | **2.91** (2.75 – 3.08) |
| **47.III** | **7%** (±5%) | **96**% (±0%) | | **0.12** (0.11 – 0.14) |

[a] Inhibition percentages at 10 µM are expressed as mean with ± SD in brackets (n = 3).
[b] Results are expressed as mean within brackets 95% confidence intervals (n = 3).
[c] NI: no inhibition at 10 µM.

Surprisingly, the introduction of a methyl group in the N-1 position (**47.III**) significantly increases the selectivity and the inhibitory potency on MAO-B compared to derivative **46.III**. So, compound **47.III** was found to be the most selective and moderately potent MAO-B inhibitor within this series with a $K_i$ value of 0.12 µM compared to analogue **46.III** which

displays a $K_i$ value of 2.91 μM (Figure 37.III (bottom) and table 15.III). These $K_i$ values show the crucial role played by the methyl group in the N-1 position on activity and selectivity of MAO-B compared to MAO-A. With the aim of trying to understand the role of this methyl group, a comparative study of packing from crystallography structures of compounds **46.III** and **47.III**, and molecular docking studies were performed and will be discussed in the next sections.
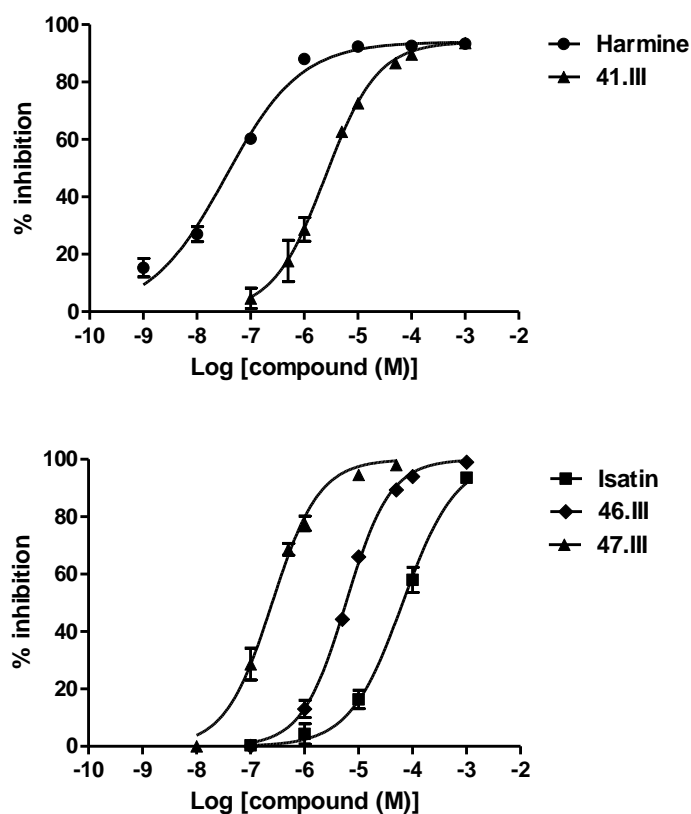


**Figure 37.III.** (Top) Dose-response curve of harmine (**3.I**, ●) and compound **41.III** (▲) on hMAO-A. (Bottom) Dose-response curve of isatin (**4.I**, ■), compounds **46.III** (♦) and **47.III** (▲) on hMAO-B. Inhibition percentages are shown as mean ± SD with n = 3.

## 1.3 X-ray crystallographic analysis

The molecular structures of compounds **46.III** and **47.III**, were determined by X-ray crystallographic analysis. Compounds **46.III** and **47.III** crystallize in the trigonal ($R_1$ = 0.0972) and the monoclinic $P2_1$ ($R_1$ = 0.0354) space groups respectively. ORTEP diagram and crystalline cohesion pattern of compounds **46.III** and **47.III** are depicted in figure 38.III. The C5-O10-C11 bond angles 117.2(3)° and 116.6(9)° for **46.III** and **47.III** respectively are

indicative of a sp$^2$ character of the oxygen underling electronic delocalization from the indole ring to the benzyloxy chain. The benzyloxy chains adopt a similar conformation with torsion angles C5–O10–C11–C12 and O10-C11-C12-C13 of 168.0(3)° and 114.9(5)° for compound **46.III** and of 174.3(1)° and 110.3(3)° for **47.III**. Crystal packing of **46.III** is mainly maintained by hydrogen bonds formed between N1-H…O10 (2.085 Å) and π-π interactions. For *N*-methyl analogue (**47.III**), the crystalline cohesion is mainly maintained by π-π interactions, weak CH-π(C(sp$^2$)) hydrogen bonds (in the range of 2.8 Å) and weak C-H…O interactions (formed between C3-H…O10 (2.669 Å)). While hydrogen bonds such as CH-π and C-H…O interactions can be regarded as weak interactions compared to an ordinary hydrogen bond observed in the molecular structures of compound **46.III**, these can play an important role because many CH groups can participate simultaneously.
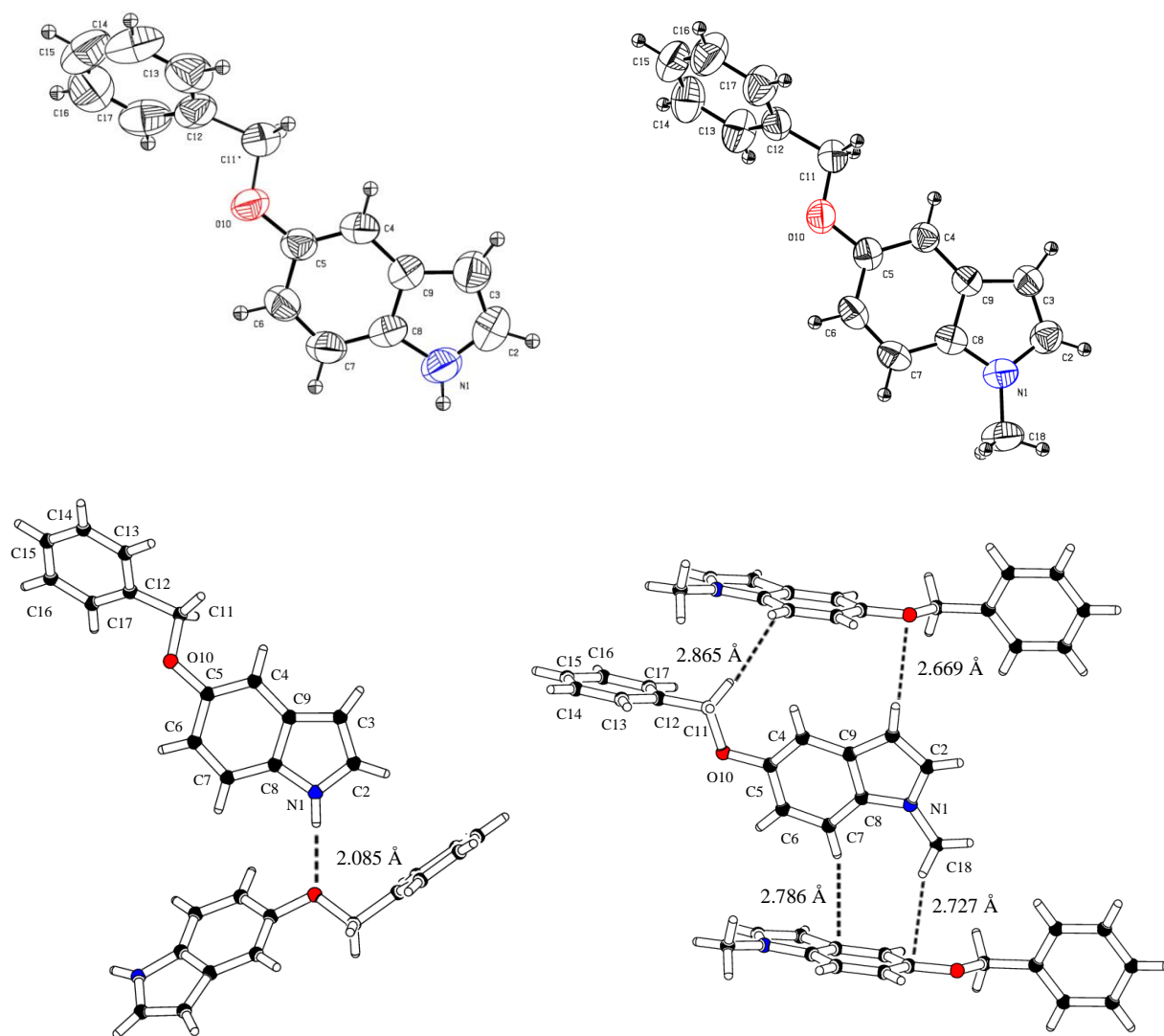


**Figure 38.III.** ORTEP diagram (50% probability) and crystalline cohesion pattern of compounds **46.III** (left) and **47.III** (right).

## 1.4 Molecular modeling

From this study on a series of indole analogues differently substituted, 5-benzyloxyindole (**46.III**) and *N*-methyl-5-benzyloxyindole (**47.III**) were found to be the most potent and selective MAO-B inhibitors. The encouraging result obtained for compounds **46.III** and **47.III** as moderate inhibitors of MAO-B lead us to study the potential binding mode of these compounds with MAO-B and to try to explain the structure-activity relationships.

Previously, in the *β*-carboline series, we have shown that 7-(cyclohexylmethoxy)-1-methyl-*β*-carboline (**2f.III**, Figure 35.III) displayed the best inhibitory activity on MAO-B with a $K_i$ value of 0.22 μM. Docking simulations of **2f.III** within hMAO-B show that the β-carboline core incorporates into the substrate cavity (Figure 39.III, top). In addition, the β-carboline core is stabilized by a hydrogen bond between nitrogen atom N2 (H bond acceptor) and a conserved water molecule (H bond donor). The pyridine ring is also stabilized within an aromatic cage (Tyr398-Tyr435 and FAD) by π-π interaction. The amide group of the Gln206 side chain also interacts with the β-carboline core by π-π interaction but this interaction is less favorable compared to harmine (**3.I**) in hMAO-A. The cyclohexyl chain points to a hydrophobic pocket of the entrance cavity coated by Phe103, Trp119, Leu164, Leu167, Phe168, and Ile316 where it is stabilized in agreement with an enhanced inhibitory potency towards MAO-B compared to harmine.

The result of docking simulations for 5-benzyloxyindole (**46.III**) is represented in figure 39.III (bottom). Docking studies suggest that the indole core incorporates into the substrate cavity of MAO-B with the C-5 side chain extending towards the entrance cavity space. The indole ring is stabilized by a hydrogen bond between NH group (H bond donor) and a conserved water molecule (H bond acceptor). This hydrogen bond corresponds to the one observed with the β-carboline derivative. The indole ring is stabilized by π-π interactions with the aromatic cage (Tyr398-Tyr435 and FAD). Compared to the β-carboline derivative, the reduction to two cycles of the central aromatic ring leads to loss of the π-π interaction with the amide group of the Gln206 side chain. Moreover, the reduction of the size of the central aromatic linker prevents the benzyloxy group to extend into the entrance cavity compared to the β-carboline derivative. So, the comparison of binding modes may explain the better inhibition of MAO-B by the β-carboline derivative **2f.III** compared to 5-benzyloxyindole (**46.III**).
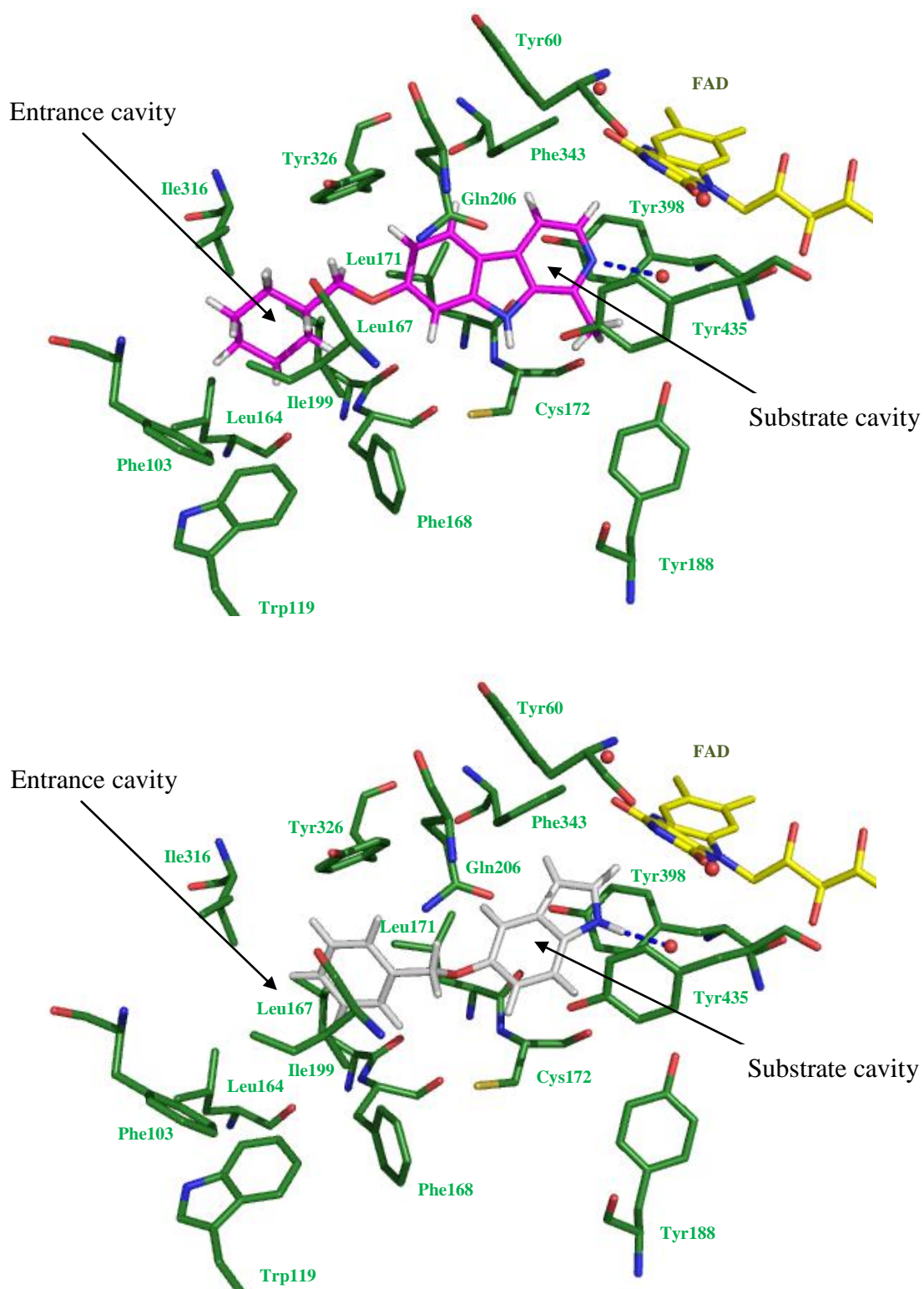
**Figure 39.III.** Simulated binding mode of **2f.III** (top) and **46.III** (bottom) in the active site of hMAO-B (2V5Z.pdb). Only amino acids directly implicated in the active site are displayed and labeled (in green). Compounds **2f.III** and **46.III** are in magenta and gray, respectively. FAD is in yellow. The water molecules involved in MAO-B are displayed as red spheres. The hydrogen bonds discussed in the text are depicted as dashed blue lines.

144

Interestingly, the introduction of a methyl group in the N-1 position (**47.III**, $K_i$ = 0.12 μM) significantly increases the inhibitory potency on MAO-B compared to 5-benzyloxyindole (**46.III**, $K_i$ = 2.91 μM). These $K_i$ values thus show the crucial role played by the methyl group in the N-1 position on activity of MAO-B. Based on the docking simulation of **46.III** with MAO-B, the effect of the methyl group is difficult to rationalize since the NH group of corresponding analogue **46.III** is supposed to be implicated in a hydrogen bond with a conserved water molecule. The X-ray structures of compounds **46.III** and **47.III** show that the NH of compound **46.III** establishes a hydrogen bond and the methyl group in the N-1 position of **47.III** is implicated in π-hydrogen bonds. So, from the results of docking studies and X-ray crystal analysis of compounds **46.III** and **47.III**, it is currently impossible to explain beneficial effect on the introduction of a methyl group on the nitrogen atom of the indole. The biological data suggest that either **47.III** binds differently to the active site of MAO-B than **46.III** or that the structure of the complex between **46.III** and MAO-B simulated by docking is not correct. Indeed, if **47.III** had to bind to MAO-B in a similar way than **46.III**, this would imply loss of a hydrogen bond interaction with a conserved water molecule by replacement of the NH (H bond donor) of **46.III** by a N-methyl group in **47.III**. Consequently, one would expect a decrease in activity for **47.III**, unless extra stabilization of the methylated compound within the hydrophobic cage formed by Tyr398, Tyr435 and FAD is able to compensate the loss of stabilization by loss of hydrogen bond interaction. An alternative explanation of the increased activity of **47.III** could be displacement of the conserved water molecule that would lead to a beneficial entropic effect. This hypothesis could not be tested by classical modeling approaches. Therefore, efforts in trying to obtain a crystal structure of MAO-B in complex with **46.III** and/or **47.III** should be pursued.

## 2. CONCLUSION

In order to identify new potential MAO-A and −B inhibitors including an indole core, a series of indole analogues from the department of Pharmacy (Prof. Masereel, FUNDP, Belgium), was evaluated by a luminescent test on hMAO-A and −B. First, the results confirm that 680C91 (**40.III**) is inactive on MAO-A and −B in agreement with the literature. Secondly, compound **41.III** which is substituted in the N-1 position with a methyl group compared to 680C91 (**40.III**) is the most potent of this series on MAO-A although moderate with a $K_i$

value of 1.15 μM. The MAO-B inhibition results bring to light that the substitution at C-5 of the indole core by a lipophilic group (**44**-**47.III**) allows to appreciably increase the inhibition of MAO-B. The introduction of a benzyloxy group (**46.III**) instead of a vinyl pyridin group (**44**-**45.III**) increases both the inhibitory potency and the selectivity on MAO-B. Surprisingly, the 1-methyl-5-benzyloxyindole derivative (**47.III**, $K_i$ value of 0.12 μM) displays a significant increase in the selectivity and inhibitory potency on MAO-B compared to compound 5-benzyloxyindole (**46.III**, $K_i$ value of 2.91 μM). With the aim of trying to understand the crucial role played by the methyl group in the N-1 position, a comparative study of packing from crystallography structures of compounds **46.III** and **47.III** and molecular docking studies were performed. The X-ray structures of compounds **46.III** and **47.III** show that the NH and N-methyl groups are implicated in hydrogen bonds and π-hydrogen bonds respectively. Docking simulations of 5-benzyloxyindole (**46.III**) compared to **2f.III** ($K_i = 0.22$ μM) into the active site of hMAO-B suggest that the β-carboline and indole cores incorporate into the substrate cavity. The stability of both compounds differs mainly by the π-π interaction with the Gln206 side chain, and the stabilization of the lateral chain in the entrance cavity. Indeed, reduction to two cycles of the central aromatic linker leads to the loss of the π-π interaction between the amide group of the Gln206 side chain and **46.III**. The reduction of the cycle and hydrogen bond prevents the benzyloxy group to extend in the entrance cavity compared to the β-carboline derivative for which the cyclohexyl chain points to a hydrophobic pocket of the entrance cavity where it is stabilized. The beneficial effect of methyl group on the activity on MAO-B is difficult to rationalize since NH group of corresponding compound **46.III** is supposed to be implicated in a hydrogen bond with a conserved water molecule. Definite explanation of the enhanced activity of **47.III** versus **46.III** could benefit from crystal structures of those inhibitors with MAO-B. In the same time, it would be interesting to confirm the competitive-type inhibition of MAO-B by compounds **46-47.III** from the Lineweaver–Burk plots, such as performed previously for **30a.III** on MAO-B.

# GENERAL CONCLUSIONS AND PERSPECTIVES

The last generation of reversible and selective MAOIs has shown a great promise in a broad range of treatments against pathologies including depression, anxiety disorders, Parkinson's and Alzheimer's diseases. Due to their selective and reversible inhibition of MAO, this new generation of MAOIs displays a safer profile compared to the former irreversible MAOIs, particularly with regard to the cheese-effect and drug interaction. Most current MAOIs lead to side effects by a lack of affinity and selectivity towards one of the isoforms. Furthermore, the recent crystal structures of hMAO-A and −B in complex with inhibitors opened the way towards the discovery by structure-based drug design of new, more selective and potent inhibitors. The main objective of this work was therefore the design of new, more potent, reversible and selective MAO-A and −B inhibitors derived from β-carbolines, indoles and 5*H*-indeno[1,2-*c*]pyridazin-5-ones.

In order to design new and more potent MAO-A inhibitors related to harmine (**3.I**, Figure 1.IV), a series of 7-alkyloxy-β-carboline analogues (**2a-5.III**) has been synthesized.
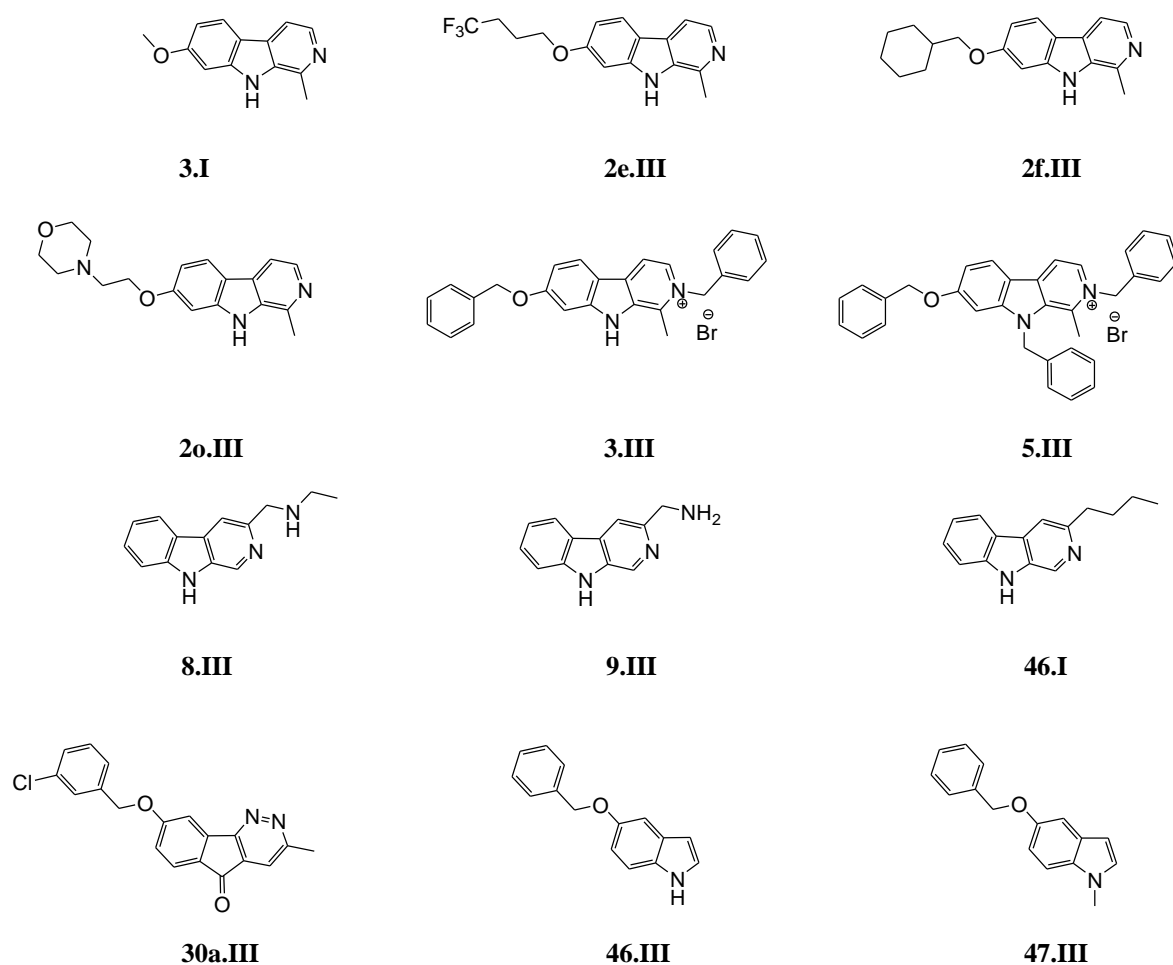


**Figure 1.IV.** Chemical structures of β-carboline (**3.I**, **2e-2f.III**, **2o.III**, **3.III**, **5.III**, **8-9.III** and **46.I**), 5*H*-indeno[1,2-*c*]pyridazin-5-one (**30a.III**) and indole (**46-47.III**) derivatives.

The **MAO** inhibitory potencies show that the replacement of the methoxy group of harmine (**3.I**) by a lipophilic group increases the inhibition for MAO-A (e.g., **2e.III**, $K_i$ hMAO-A = 3.6 nM, is the most active of this series, Figure 1.IV). Docking simulations into the active site of hMAO-A show that compound **2e.III** incorporates into the active site with harmine-like interactions (Figure 2.IV). The lateral chain points to the lipophilic pocket where it is stabilized in agreement with an enhanced inhibitory potency towards MAO-A. Interestingly, the compound **2o.III** ($K_i$ hMAO-A = 255.7 nM, Figure 1.IV) containing an ethylmorpholine group, although less active compared to **2e.III**, is a potent and selective inhibitor of MAO-A, and displays a higher solubility in buffer (pH 7.4) (totally soluble at >500 µM) compared to **2e.III** (<3 µM). Therefore, efforts in trying to obtain a crystal structure of hMAO-A in complex with **2o.III** could be pursued.
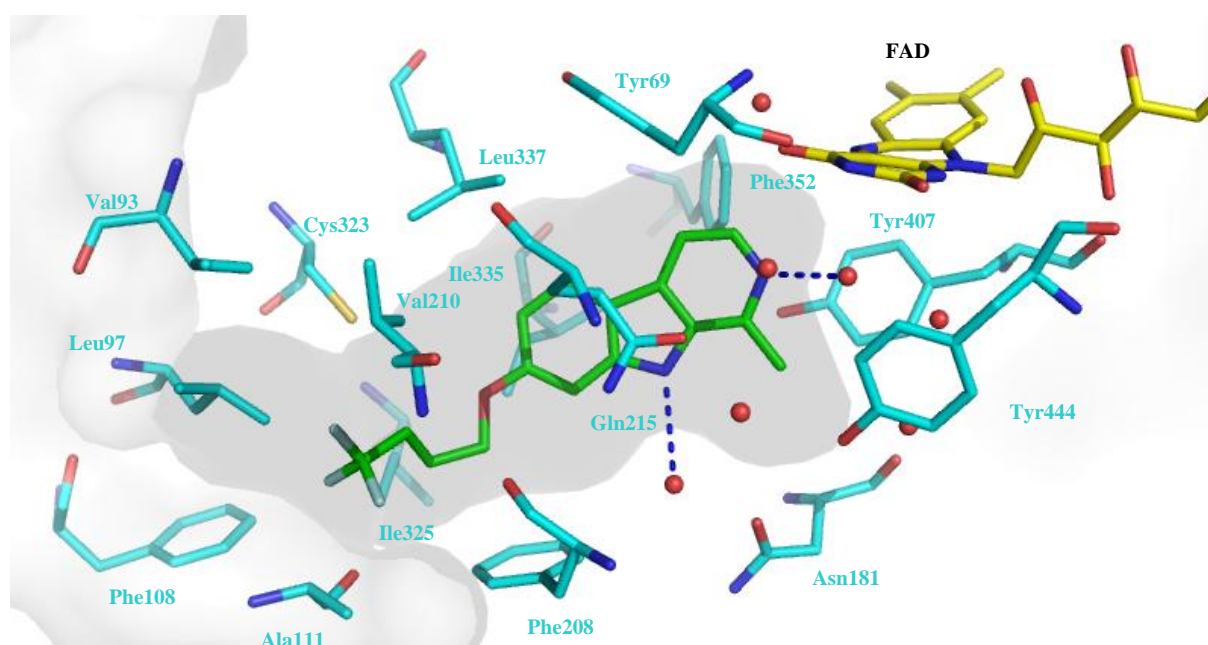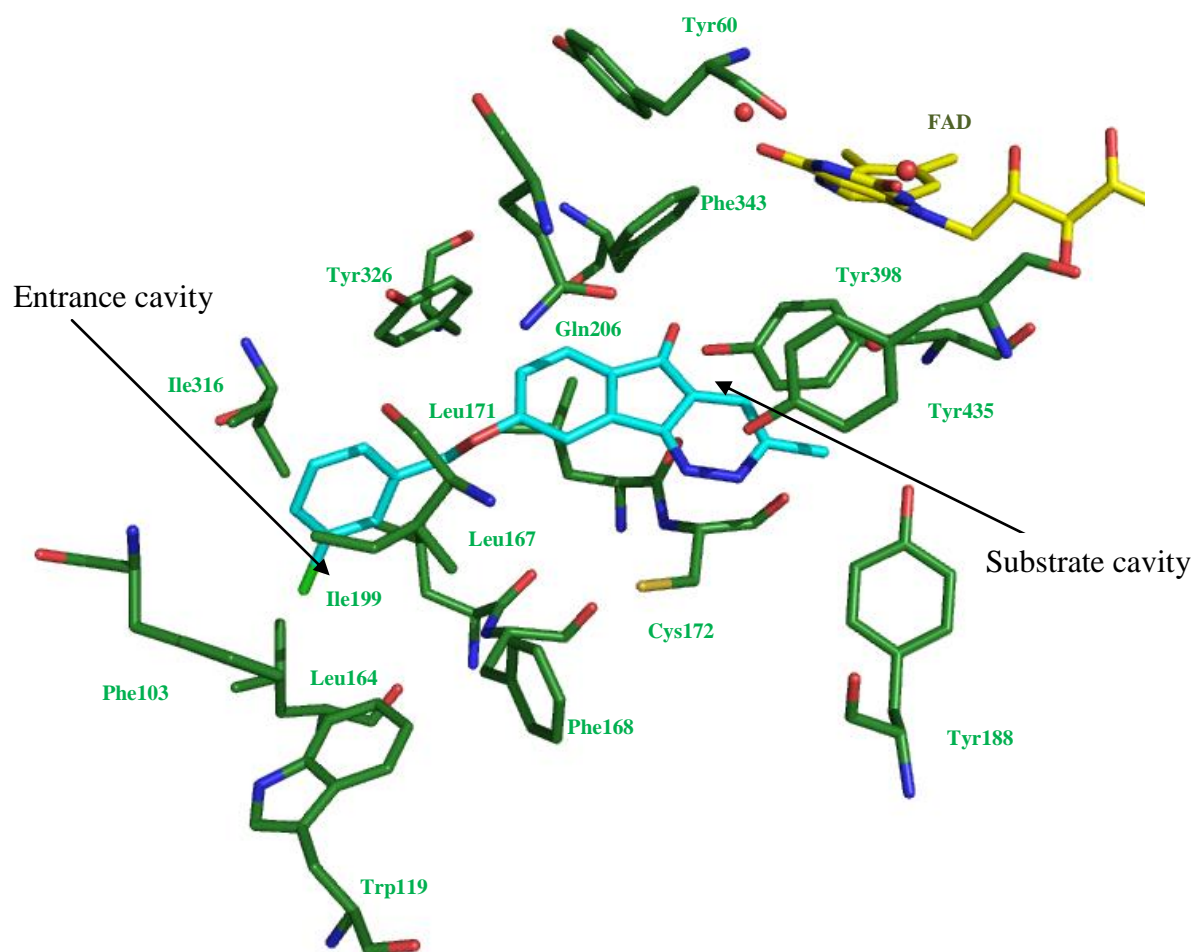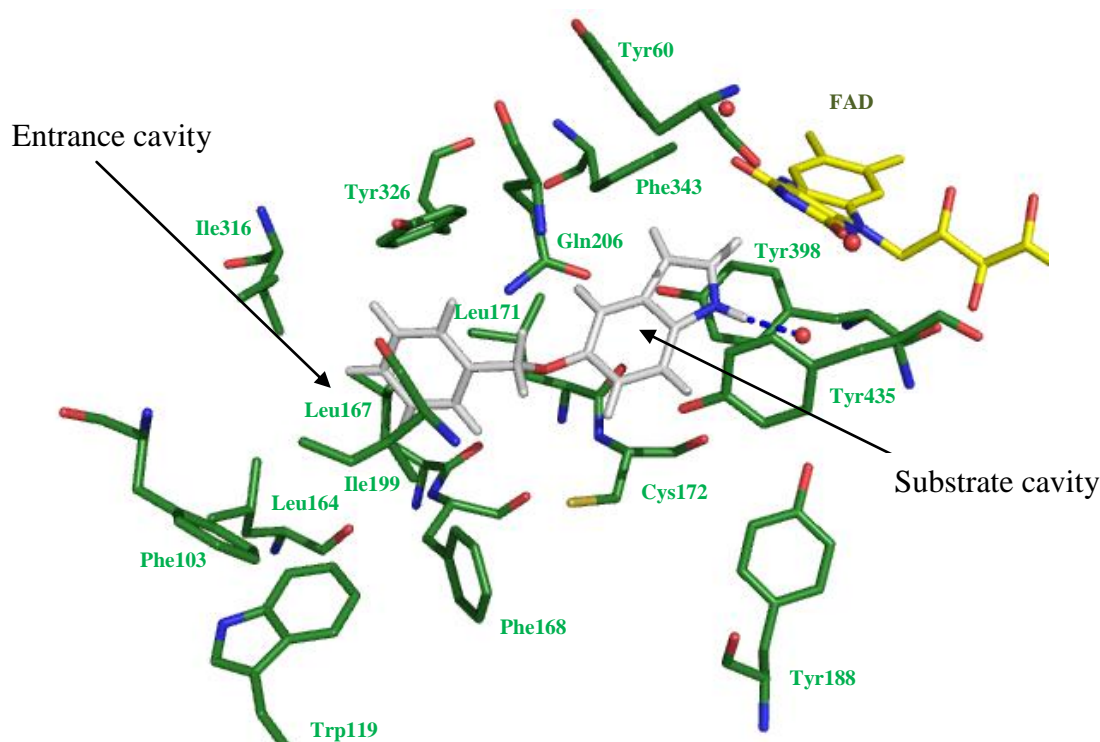


**Figure 2.IV.** Binding mode of compound **2e.III** in the active site of hMAO-A (2Z5X.pdb). Only amino acids directly implicated in the active site are displayed and labeled in cyan. Compound **2e.III** and FAD are in green and yellow respectively. The water molecules are displayed as red spheres. The hydrogen bonds discussed in the text are depicted as dashed blue lines.

All the synthesized compounds are selective of MAO-A but some of them show also a moderate MAO-B inhibition (e.g., **2f.III**, $K_i$ hMAO-B = 221.6 nM, Figure 1.IV) when compared to harmine (**3.I**). Docking simulations for compound **2f.III** performed in hMAO-B show that the β-carboline core incorporates into the substrate cavity (Figure 3.IV). A shift is observed for the β-carboline core orientation in MAO-B compared to MAO-A induced by the Tyr326 side chain in MAO-B which produces a restriction that is less pronounced in hMAO-

150

A where Ile335 occupies that position. In contrast to Gln215 in MAO-A, $\pi$-$\pi$ interaction of the β-carboline core with the equivalent amide group of the Gln206 in MAO-B is less favorable. In addition, the β-carboline core is stabilized by two hydrogen bonds with water molecules in MAO-A compared to only one hydrogen bond in MAO-B which may explain the selectivity of the β-carboline derivatives towards MAO-A compared to MAO-B. Interestingly, the cyclohexyl chain of compound **2f.III** points to a lipophilic pocket in the entrance cavity where it is stabilized in agreement with an enhanced inhibitory potency towards MAO-B compared to harmine (**3.I**).
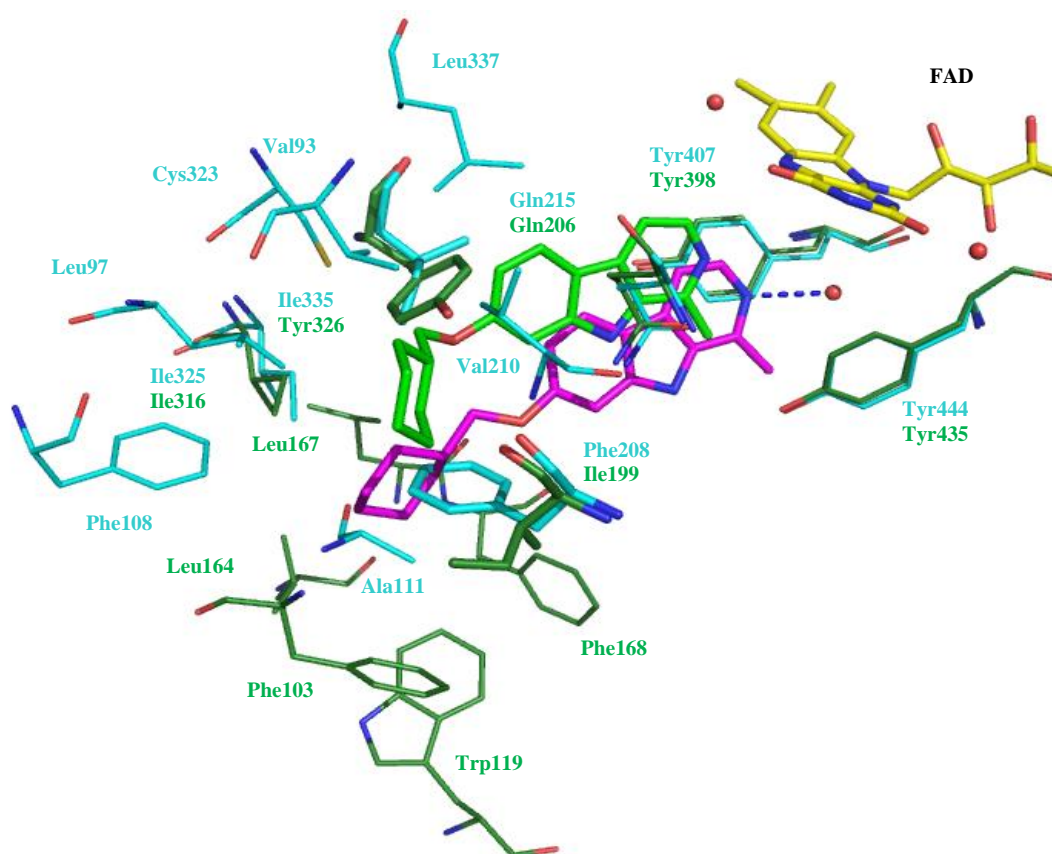


**Figure 3.IV.** Binding mode of compound **2f.III** in the active site of hMAO-A and –B. Only amino acids directly implicated in the active site are displayed and labeled in cyan (MAO-A) and in green (MAO-B). Compound **2f.III** is in green (MAO-A) and magenta (MAO-B). FAD is in yellow. The water molecules involved in MAO-B are displayed as red spheres. The hydrogen bond discussed in the text is depicted as a dashed blue line.

In order to design new, selective, and more potent MAO-B inhibitors, a series of 5*H*-indeno[1,2-*c*]pyridazin-5-one derivatives substituted both in the 3 and 8-positions by lipophilic groups has been synthesized (**22m.I**, **28a-b.III** and **30a-b.III**). Compounds display a higher activity and selectivity on MAO-B than MAO-A. Compound **30a.III** (Figure 1.IV),

is the most active and selective within this series, and displays a competitive-type inhibition with a $K_i$ on MAO-B of 0.11 µM. Replacement of the methyl moiety in the 3-position by a lipophilic group like a *meta*-CF$_3$-phenyl group abolishes the inhibitory potency on MAO-B. So, the substitution of the 5*H*-indeno[1,2-*c*]pyridazin-5-one core in the 3-position dramatically influences the MAO-inhibiting properties of these compounds. Docking simulations of compound **30a.III** in hMAO-B suggest that the 5*H*-indeno[1,2-*c*]pyridazin-5-one core incorporates into the substrate cavity with the *meta*-chlorobenzyloxy side chain extending towards a hydrophobic pocket of the entrance cavity space (Figure 4.IV).



**Figure 4.IV.** Binding mode of compound **30a.III** in the active site of hMAO-B (2V5Z.pdb). Only amino acids directly implicated in the active site are displayed and labeled (in green). Compound **30a.III** and FAD are in cyan and yellow respectively. The water molecules in the active site are displayed as red spheres.

Besides β-carbolines and 5*H*-indeno[1,2-*c*]pyridazin-5-ones, we were also interested in the identification of new potential MAO-A and –B inhibitors containing an indole core. Thus, a series of indole analogues including bulky and/or lipophilic groups in the 3 or 5-positions from the department of Pharmacy (Prof. Masereel, FUNDP, Belgium) was evaluated on

hMAO-A and –B. The MAO-B inhibition results bring to light that the substitution in the 5-position of the indole core by a lipophilic group allows to increase appreciably the inhibition of MAO-B. The introduction of a benzyloxy group (**46.III**, Figure 1.IV, $K_i$ hMAO-B = 2.91 µM) instead of a vinyl pyridin group increases both the inhibitory potency and the selectivity on MAO-B. Surprisingly, the 1-methyl-5-benzyloxyindole derivative (**47.III**, Figure 1.IV, $K_i$ hMAO-B = 0.12 µM) displays a significant increase in the selectivity and inhibitory potency on MAO-B compared to compound **46.III**. Docking simulations of **46.III** (Figure 5.IV) compared to **2f.III** ($K_i$ hMAO-B = 221.6 nM, Figure 3.IV) into the active site of hMAO-B suggest that the β-carboline and indole cores incorporate into the substrate cavity.



**Figure 5.IV.** Binding mode of **46.III** in the active site of hMAO-B (2V5Z.pdb). Only amino acids directly implicated in the active site are displayed and labeled (in green). Compound **46.III** is in gray. FAD is in yellow. The water molecules involved in MAO-B are displayed as red spheres. The hydrogen bond discussed in the text is depicted as a dashed blue line.

The stability of both compounds differs mainly by the π-π interaction with the Gln206 side chain and the stabilization of the lateral chain in the entrance cavity. Indeed, the reduction to two cycles of the central aromatic linker leads to the loss of the π-π interaction between the amide group of the Gln206 side chain and **46.III**. The reduction of the cycle and hydrogen bond prevents the benzyloxy group to extend in the entrance cavity compared to the β-carboline derivative **2f.III** for which the cyclohexyl chain points to a hydrophobic pocket of

153

the entrance cavity where it is stabilized. The beneficial effect of the methyl group on the activity on MAO-B is difficult to rationalize since the NH group of corresponding compound **46.III** is supposed to be implicated in a hydrogen bond with a conserved water molecule. Definite explanation of the enhanced activity of **47.III** versus **46.III** could benefit from crystal structures of those inhibitors with MAO-B.

Secondly, the involvement through a same metabolic pathway (the serotonergic pathways) for MAO-A and IDO, and the similarity in the structural properties of MAO and LSD1 led us to the investigation of the β-carboline and 5*H*-indeno[1,2-*c*]pyridazine-5-one derivatives as potential inhibitors of IDO and LSD1.

The **IDO** inhibitory potency of β-carbolines and 5*H*-indeno[1,2-*c*]pyridazin-5-ones revealed that, at 25 μM, the synthesized compounds display no inhibition of IDO. Thus, they are selective of MAO. However, 3-butyl-β-carboline (**46.I**) is known as inhibitor of IDO ($K_i$ hIDO = 3.3 μM, Figure 1.IV). Molecular docking studies of 3-butyl-β-carboline suggest that the β-carboline core is stabilized in the pocket A of IDO by Van der Waals interactions, complexation with the heme iron and a hydrogen bond (Figure 6.IV, top). Interestingly, the butyl side chain points to the pocket B of IDO lined with hydrophobic residues. This binding mode evidences that the substitutions in the 1, 2, 7 and 9-positions are not tolerated because of steric clashes within the active site of the enzyme. So, these substitutions lead to a new orientation of β-carboline scaffold which is not stabilized into the active site in agreement with weak obtained inhibition percentages. From results of synthesized β-carbolines, docking studies of 3-butyl-β-carboline (**46.I**) and the pharmacophore model developed on IDO by Rohrig et al, we were interested in the synthesis of two new 3-substituted-β-carbolines (*N*-ethyl-3-methylamino-β-carboline (**8.III**) and 3-methylamino-β-carboline (**9.III**), Figure 1.IV) potentially more potent compared to 3-butyl-β-carboline (**46.I**). These new derivatives should incorporate in the active site of IDO with 3-butyl-β-carboline-like interactions but the side chain would display also a positive charge at physiological pH which might establish a coulomb interaction with the 7-propionate of the heme present in the pocket B, in agreement with docking studies performed (Figure 6.IV, bottom). The synthesis of compounds **8.III** and **9.III** was performed in two and four steps, respectively from the ethyl β-carboline-3-carboxylate (**10.III**) intermediate in modest yields (22-38% yield). Surprisingly, first results on **8.III** revealed that it displays no inhibition on IDO at 100 μM. Although it was impossible to test the compound **9.III** due to a lack of availability of this latter, the absence of inhibition

154

observed for **8.III** tends to show that the introduction of a positive charge is not tolerated. The result of **8.III** must be yet confirmed again but this inactivity maybe explained by a more hydrophobic character of the pocket B. So, from the result of **8.III** and the pharmacophore model developed on IDO by Rohrig et al [126], it can be also interesting to explore the possibility to synthesize of new 3-substituted-β-carbolines with a negatively charged group such as a carboxylate that can form a salt bridge with Arg231.
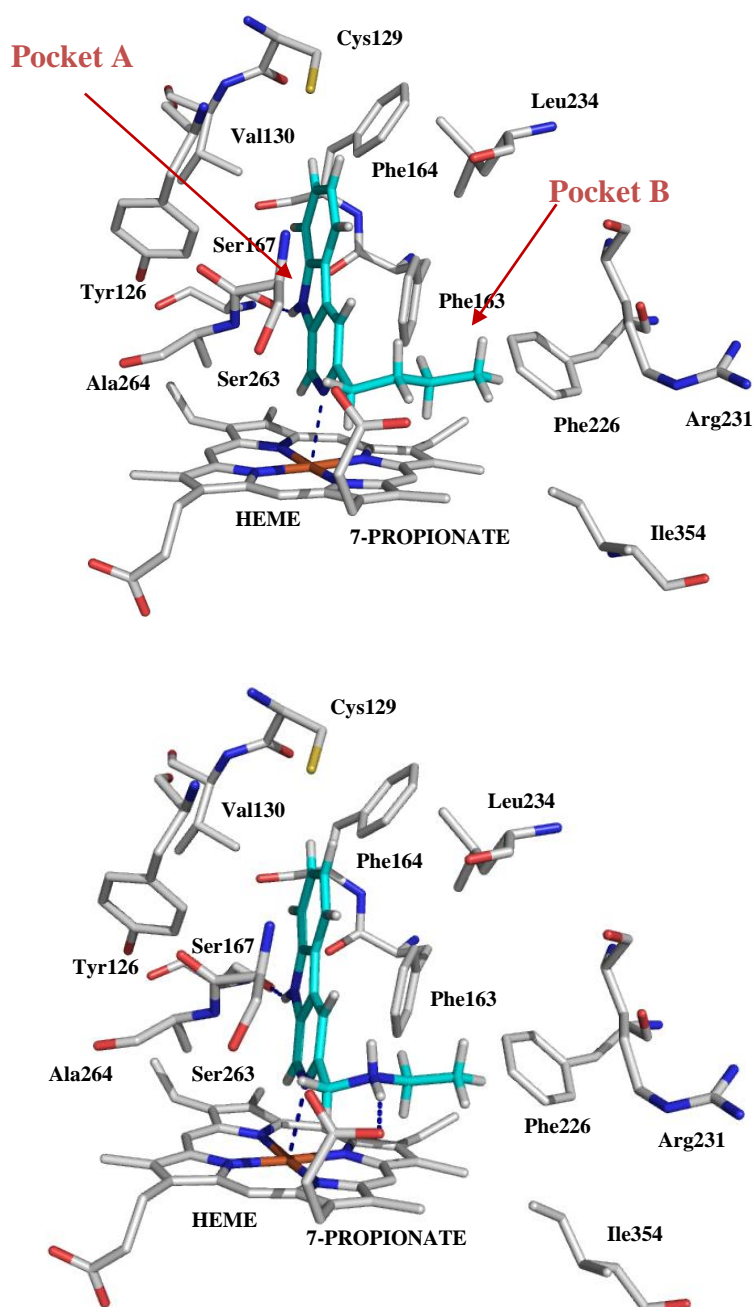


**Figure 6.IV.** Simulated binding mode of 3-butyl-β-carboline (**46.I**, top) and *N*-ethyl-3-methylamino-β-carboline (**8.III**, bottom) in the active site of hIDO (2D0T.pdb). Only amino acids directly implicated in the active site are displayed and labeled.

The **LSD1** inhibitory potency of β-carbolines shows that, at 25 μM, the synthesized β-carbolines are weak inhibitors of LSD1 and consequently, are selective of MAO-A. However, the introduction of lipophilic and bulky groups allows to increase the inhibitory potency of β-carboline scaffold on LSD1 compared to harmine (**3.I**, inactive at 50 μM). Furthermore, to date, no small, potent and non-irreversible inhibitor of LSD1 is known. Although the β-carboline analogues display moderate activities on LSD1, compound **3.III** (IC$_{50}$ = 31.5 μM, Figure 1.IV) could be an interesting scaffold for the design of new more potent and selective inhibitors of LSD1. In perspective, it would be interesting to overexpress directly the enzyme in the laboratory to monitor the activity of the enzyme in the LSD1 inhibitor screening assay. The 5*H*-indeno[1,2-*c*]pyridazine-5-ones could be then evaluated on LSD1. The purification of the enzyme could be performed and thus, efforts in trying to obtain a crystal structure of LSD1 in complex with analogues of compound **3.III** could be pursued.

## NEW PERSPECTIVES

A large number of cancer cells such as glioblastomas (brain cancers), brain metastases, melanomas, pancreatic cancers, lung cancers of the NSCLC-type (non-small-cell lung cancer), refractory prostate cancers and breast cancers are naturally resistant to apoptosis and cannot be treated by the many known drugs and chemotherapeutics. Development of new compounds having cytotoxic and/or cytostatic effects in tumour and cancer cells which are resistant to apoptosis is of considerable importance. Harmine (**3.I**) and certain of its derivatives exhibit anti-tumour and anti-cancer properties [210-214]. However, previous reports demonstrated that harmine and its derivatives caused remarkable acute neurotoxicity characterized by tremble, twitch, and jumping in experimental mice model [215]. By structural analogy, the novel synthesized β-carboline analogues were assessed for their anti-tumour and anti-cancer activity by the team of Professor Kiss (ULB, Brussels, Belgium). The anti-proliferative effects of the present compounds were evaluated by means of the colorimetric MTT assay in several human cancer cell-lines including a) U373, T98G and Hs683 glioblastoma cells, and b) OE21 and OE33 oesophageal cancer cells. It was unexpectedly found that the compounds had important cytostatic and/or anti-cancer effects. Whereas the compounds showed mean anti-proliferative effect on glioma cell lines in the low micromolar range, the highly effective compound **5.III** (Figure 1.IV) displayed mean anti-

proliferative effect on the glioma cell lines in the submicromolar range (0.7 μM compared to harmine (**3.I**, 28 μM)). Even more promisingly, it was found that the present compound exerted its effect via a non-apoptosis-related mechanism, which makes it particularly good candidate as anti-proliferative drugs for treating apoptosis-resistant tumours and cancers, and for reducing or overcoming problems linked to known anti-cancer drugs, such as acquisition of resistance, non-specific cytotoxicity, etc.

The promising result leads to the synthesis of novel tri-substituted β-carboline **5.III** analogues, which was performed in the department of Pharmacy (Prof. Masereel, FUNDP, Belgium). The new compounds displayed mean anti-proliferative effects on the glioma cell lines in the same range compared to **5.III**. Thus, a patent including the results was deposited « Beta-carbolines derivatives useful in the treatment of proliferative disorders » (PCT/EP2010/059083 and US/61/358,609).

Harmine (**3.I**) is a high affinity inhibitor of the dual specificity tyrosine phosphorylation regulated kinase 1A (DYRK1A) protein. The DYRK1A gene is located within the Down Syndrome Critical Region (DSCR) on chromosome 21 [216]. DYRK1A is a dual-specificity protein kinase that autophosphorylates a conserved tyrosine residue (Tyr321) in the activation loop but phosphorylates exogenous substrates only at serine or threonine residues [217]. DYRK1A is implicated in the neuronal development and thus depicts a target of first importance in certain tumoral pathologies of neurological origin [217-218]. In addition to its function in neuronal development, recent evidence has also implicated DYRK1A in the pathology of neurodegenerative disorders such as Alzheimer's disease, dementia with Lewy bodies and Parkinson's disease [216-217]. Harmine (**3.I**) is a potent and specific inhibitor of DYRK1A both *in vitro* and in cultured cells [217]. *In vitro*, harmine inhibits DYRK1A substrate phosphorylation ($IC_{50}$ = 33 nM) more potently than it inhibits tyrosine autophosphorylation ($IC_{50}$ = 1.9 μM). Importantly, harmine inhibits the phosphorylation of a specific substrate by DYRK1A in cultured cells with a potency similar to that observed *in vitro* ($IC_{50}$ = 48 nM), without negative effects on the viability of the cells [217].

Consequently, it would be interesting to design by a rational approach, new DYRK1A inhibitors derived from β-carbolines and to characterize their binding mode with the active site following a classical strategy including theoretical (molecular modeling) and experimental (synthesis, biological evaluation and crystal assays) approaches to establish

structure-activity relationships. As a starting point, we could study the ability of our β-carbolines to inhibit DYRK1A compared to harmine (**3.I**).

Previously, it has been proposed that the use of a molecule which both would be a MAO-B inhibitor and an acetyl- and butyrylcholinesterase (AChE and BChE) inhibitor is expected to have therapeutic benefit for the treatment of Alzheimer's disease (AD) [219]. Moreover, a series of varied 6-hydroxylated and 6-methoxylated harman and norharman derivatives, including the corresponding quaternary *N*-methyl-carbolinium salts were tested *in vitro* for their ability to inhibit AChE and BChE, respectively [67]. Particularly the carbolinium salts (quaternary β-carboline, i.e., **2.IV**, $IC_{50}$ AChE = 0.8 μM; $IC_{50}$ BChE = 1.2 μM, Figure 7.IV), which can be formed by intracerebral methylation out of the tertiary-β-carboline prodrugs, show inhibitory activity levels reaching those of the reference drugs (galantamine ($IC_{50}$ AChE = 0.6 μM; $IC_{50}$ BChE = 8.4 μM), physostigmine ($IC_{50}$ AChE = 0.5 μM; $IC_{50}$ BChE = 1.2 μM) and rivastigmine ($IC_{50}$ AChE = 48 μM; $IC_{50}$ BChE = 54 μM).



**1.IV**          **2.IV**          **3.IV**
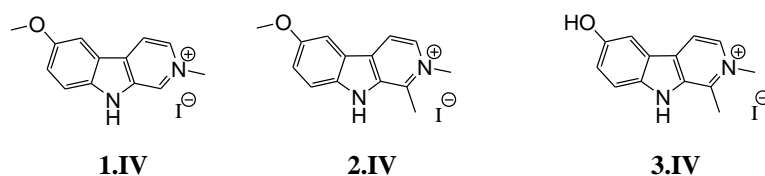
**Figure 7.IV.** Chemical structures of β-carboline derivatives (**1-3.IV**).

The activity increase between this class of quaternary compounds with tertiary compounds could be well explained by the resemblance of quaternary compounds to the natural substrate acetylcholine. Interestingly, there was also no prominent difference in inhibitory activity for 6-methoxylated (**2.IV**, $IC_{50}$ AChE = 0.8 μM; $IC_{50}$ BChE = 1.2 μM) compared to 6-hydroxylated compounds (**3.IV**, $IC_{50}$ AChE = 1.0 μM; $IC_{50}$ BChE = 1.6 μM, Figure 7.IV). Quaternary harmanium salts showed increased inhibitory activity for **2.IV** compared to **1.IV** ($IC_{50}$ AChE = 2.2 μM; $IC_{50}$ BChE = 17.5 μM, Figure 7.IV).

In contrast to the tertiary compounds, which can penetrate the blood–brain barrier, the quaternary compounds show strong levels of inhibitory activity. Therefore tertiary compounds might act as pro-drugs for the quaternary β-carbolines that are formed *in vivo* in the brain, representing a novel and target-specific approach for the therapy of AD. So, by structural

analogy, it would be interesting to study the ability of our β-carbolines including the corresponding quaternary *N*-methyl-carbolinium salts to inhibit AChE and BChE.

# MATERIALS AND METHODS

# 1. CHEMISTRY

## 1.1 Analytical techniques

**X-Ray Diffraction: XRD**

The compounds studied by X-ray crystallography were synthesized in the Bioorganic chemistry laboratory (Prof. Vincent, FUNDP, Belgium). All crystals were obtained by slow evaporation from an appropriate solution (*see experimental details in the section 1.5*) at room temperature. X-ray intensities were collected at room temperature on a Gemini Ultra R system (4-circle kappa platform, Ruby CCD detector) using Mo $K_\alpha$ radiation ($\lambda = 0.71073$ Å) or Cu $K_\alpha$ radiation ($\lambda = 1.54178$ Å). The structures were solved by direct-methods using Sir92 [220] and refined by full matrix least squares on $F^2$ using the program Shelxl97 [221]. All non-hydrogen atoms were treated anisotropically while a riding model was applied for the hydrogens. The molecular geometry analysis and ORTEP representations were carried out by PLATON [222]. For the trifluoromethyl groups which present large thermal displacements, a disordered model with the trifluoromethyl group distributed over two sites has been defined. The disordered model was constrained to have chemically reasonable geometry, whereas restraints on the anisotropic displacement parameters were used for trifluoromethyl group.

**Nuclear Magnetic Resonance: NMR**

$^1$H, $^{13}$C and $^{19}$F NMR spectra were obtained from a JEOL JNM EX 400 spectrometer (400 MHz for $^1$H, 100 MHz for $^{13}$C and 376 MHz for $^{19}$F). Chemical shifts are reported in ppm from tetramethylsilane (TMS, singulet, $\delta = 0.0$ ppm) for $^1$H NMR and from the solvent (CDCl$_3$, DMSO-d$_6$, CD$_3$OD) for $^{13}$C NMR as internal standard. NMR spectra are treated with the DELTA software. The coupling constants ($J$) are reported in Hertz. The following abbreviations are used: s, singlet; d, doublet; t, triplet; q, quadruplet; m, multiplet; dd, doublet of doublet; dt, doublet of triplet; C$_q$, quaternary carbon.

**Mass Spectrometry: MS**

Mass spectra were recorded on an Agilent 1100 series LC/MSD Trap spectrometer equipped with a C18-3,5 µm column (ZORBAX SB C18, 100 x 3 mm) and an electron spray ionization (ESI) source which was used in positive ion mode (MS+). The pressure of the atomizer was

40 psi with a flow of nitrogen of 8 L.min$^{-1}$. The voltage of the capillary was 3.5 kV. The scanning MS was performed between 300 and 2200 m/z.

HPLC method: By analysis, 10 µL of the studied samples are injected at a concentration of 20 µg.mL$^{-1}$ in acetonitrile. Compounds were separated by means of a gradient (flow of 0.5 mL.min$^{-1}$) which begins with a mixture of water/acetic acid (0.1%) of 95% and 5% of acetonitrile. In 5 min, the percentage of acetonitrile reaches 95% during 3 min and comes down again in 5% in 10 seconds during 5 min. Compounds are detected at 254 and 360 nm.

### Elemental analyses

Elemental analyses (C, H, N) were performed on a Thermo Finnigan Flash EA 1112 elemental analyzer.

### Melting point

Melting points were determined with a Totolli-Buchi melting point B-545 apparatus.

### Thin-Layer Chromatography (TLC)

Analytical thin-layer chromatography (TLC) was performed on Merck silica gel 60 F254 plates. Compounds were visualized by UV illumination at 254 nm.

### Reverse Phase High Performance Liquid Chromatography: RP-HPLC (analytical chromatography)

To study the purity of synthesized β-carboline derivatives (**2a.III**-**5.III**), RP-HPLC analyses were performed on a Varian 940-LC apparatus equipped with a C18-10 µm column (OmniSpher C18, 250 x 4.6 mm) and a Varian 380-LC detector. By analysis, 10 µL of the studied samples in methanol are injected. Compounds were analyzed during 8 min by means of an isocratic elution of 20% in water and 80% in methanol (flow of 1.0 mL.min$^{-1}$). Compounds are detected at 254 nm.

## 1.2 Purification techniques

**Column chromatography**

Column chromatographies were performed on Merck silica gel 60 (40–63 µm). Chromatography eluents are expressed in terms of volume fractions (v/v).

**Reverse Phase High Performance Liquid Chromatography: RP-HPLC (Semi-preparative chromatography)**

To purify the synthesized *N*-ethyl-3-methylamino-β-carboline (**8.III**), RP-HPLC analyses were performed on a Waters 2487 Dual λ Absorbance Detector equipped with a C18-10 µm column (OmniSpher C18, 250 x 21.4 mm). By analysis, 2.5 mL of the crude product (100 mg) in methanol (0.1% trifluoroacetic acid (TFA)) are injected. Compound was separated by means of a gradient (flow of 10 mL.min$^{-1}$) which begins with a mixture water/TFA (0.1%) of 85% and 15% of a methanol/TFA (0.1%) solution during 10 min. In 5 min, the percentage of methanol/TFA (0.1%) reaches 30% during 15 min. In 10 min, the percentage of methanol/TFA (0.1%) reaches 50% during 10 min. Finally, in 5 min, the percentage of methanol/TFA (0.1%) reaches 98% during 5 min. Compounds are detected at 254 nm.

## 1.3 Solvents and reagents

Anhydrous solvents are distilled under argon atmosphere. The dry solvents are obtained by the standard procedures described below;

- Tetrahydrofurane (THF) is distilled on sodium and benzophenone.
- Dichloromethane (DCM) is distilled on calcium hydride (CaH$_2$).
- Dimethylformamide (DMF) is keeped on molecular sieve 4 Å.
- Diethyl ether is distilled on sodium and benzophenone.

All reagents were purchased from Sigma–Aldrich, Acros Organics and Fluorochem Co.

## 1.4 Synthesis

**Notes.** For the synthesis of compounds **2e.III** and **25a.III**, 4,4,4-trifluoro-1-butanol is first transformed to 1-tosyl-4,4,4-trifluorobutane [7]. To a solution of 4,4,4-trifluoro-1-butanol (2.000 g, 15.61 mmol) in 20 mL of anhydrous dichloromethane, 2.360 g of triethylamine (23.32 mmol), 2.976 g of *p*-toluenesulfonyl chloride (15.61 mmol) and 0.010 g of 4-(dimethylamino)pyridine (0.08 mmol) are added. The mixture is stirred for 4 h under argon atmosphere. The crude is washed twice with water (10 mL) and once with hydrochloric acid (HCl 10%, 10 mL). The organic layer is concentrated under reduced pressure and the crude product was used without further purification for the following steps.

*Yield:* 83%

*Physical and spectral characteristics:*

- **Chemical Formula**      $C_{11}H_{13}F_3O_3S$
- **M.W. (g/mol)**      282.28
- **Aspect**      Colorless liquid
- **TLC** (DCM/EtOH: 8/2)      $R_f = 0.92$
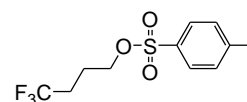


$^1$**H NMR (400 MHz, CDCl$_3$)** $\delta$ (ppm): 1.89-1.93 (m, 2H, CF$_3$-CH$_2$-C$H_2$), 2.10-2.20 (m, 2H, CF$_3$-CH$_2$), 2.45 (s, 3H, Ph-CH$_3$), 4.08 (t, $J$ = 6.1 Hz, 2H, SO$_3$-CH$_2$), 7.35 (d, $J$ = 8.5 Hz, 2H, ArH), 7.78 (d, $J$ = 8.2 Hz, 2H, ArH).

### 1.4.1. Synthesis of β-carbolines

a) Synthesis of harmol hydrobromide dihydrate (**1.III**)

Hydrobromic acid 47% aqueous (100 mL) was added to a solution of harmine (5.000 g, 23.35 mmol) in glacial acetic acid (100 mL). The solution was heated to reflux for 15 h and then allowed to cool to room temperature. The mixture was diluted in water (1000 mL), concentrated under reduced pressure and was used without further purification for the following steps. The molecular structure of compound **1.III** was determined by X-ray crystallographic analysis (*details are reported in section 1.5*).

*Yield:* 100%

*Physical and spectral characteristics:*

- **Chemical Formula**     $C_{12}H_{15}BrN_2O_3$
- **M.W. (g/mol)**          315.16
- **Aspect**                 White solid
- **TLC** (DCM/EtOH: 8/2)    $R_f = 0.35$
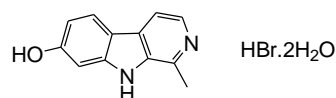


**$^1$H NMR (400 MHz, DMSO-d$_6$)** δ (ppm): 2.92 (s, 3H, CH$_3$), 6.88 (dd, $J_{6-5}$ = 8.7 Hz, $J_{6-8}$ = 2.1 Hz, 1H, H-6), 6.99 (d, $J_{8-6}$ = 2.1 Hz, 1H, H-8), 8.23 (d, $J_{5-6}$ = 8.7 Hz, 1H, H-5), 8.33 (d, $J_{3-4}$ = 6.4 Hz, 1H, H-3), 8.37 (d, $J_{4-3}$ = 6.2 Hz, 1H, H-4), 10.43 (s, 1H, O-H), 12.45 (s, 1H, N-H).

**$^{13}$C NMR (100 MHz, DMSO-d$_6$)** δ (ppm): 16.30 (CH$_3$), 96.95 (C-8), 113.18 (C$_q$), 113.31 (C-6), 114.04 (C-4), 125.10 (C-5), 128.96 (C-3), 132.79 (C$_q$), 133.93 (C$_q$), 136.78 (C$_q$), 146.13 (C$_q$), 161.75 (C$_q$).

**MS**: [M + H]$^+$ 199.1 m/z

**Mp**: 247.9°C

b) General procedure for the synthesis of 7-alkoxy-1-methyl-β-carbolines (**2a-o.III**)

The 7-alkoxy-1-methyl-*β*-carbolines (**2a-o.III**) were synthesized according to a previously reported procedure [193]. The appropriate alkyl halide (by portion) or 1-tosyl-4,4,4-trifluorobutane (for compound **2e.III**) and cesium carbonate were added to harmol (**1.III**) dissolved in anhydrous dimethylformamide (DMF). Then, the reaction mixture was stirred at room temperature or heated for several hours. At the end of the reaction, the mixture was cooled and diluted with dichloromethane, washed once with water and three times with brine. The organic layer was dried over $MgSO_4$ and concentrated. The crude product was purified by liquid chromatography.

**7-(Allyloxy)-1-methyl-β-carboline (2a.III)**

The title compound was prepared from a solution of harmol (0.250 g, 0.80 mmol), cesium carbonate (0.804 g, 2.47 mmol) and 3-bromo-1-propene (0.119 g, 0.98 mmol) in 5 mL of DMF. The reaction mixture was stirred at room temperature for 24 h. The crude product was purified by column chromatography (dichloromethane/ethanol 95: 5% v/v).

*Yield:* 75%

*Physical and spectral characteristics:*

- **Chemical Formula**     $C_{15}H_{14}N_2O$
- **M.W. (g/mol)**          238.28
- **Aspect**                White solid
- **TLC** (DCM/EtOH: 8/2)  **$R_f$** = 0.63
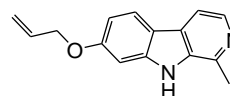
**$^1$H NMR (400 MHz, CDCl$_3$)** δ (ppm): 2.79 (s, 3H, C$H_3$), 4.63 (dt, $J$ = 1.4 Hz, $J$ = 5.3 Hz, 2H, O-C$H_2$), 5.30-5.34 (m, 1H, O-CH$_2$CH=C$H_2$), 5.43-5.48 (m, 1H, O-CH$_2$CH=C$H_2$), 6.05-6.15 (m, 1H, O-CH$_2$C$H$), 6.92 (dd, $J_{6-5}$ = 8.7 Hz, $J_{6-8}$ = 2.3 Hz, 1H, H-6), 6.97 (d, $J_{8-6}$ = 2.1 Hz, 1H, H-8), 7.71 (d, $J_{4-3}$ = 5.5 Hz, 1H, H-4), 7.96 (d, $J_{5-6}$ = 8.7 Hz, 1H, H-5), 8.31 (d, $J_{3-4}$= 5.5 Hz, 1H, H-3), 8.39 (s, 1H, N-H).

**$^{13}$C NMR (100 MHz, CDCl$_3$)** δ (ppm): 20.23 (CH$_3$), 69.31 (O-CH$_2$), 95.93 (C-8), 110.34 (C-6), 112.36 (C-4), 116.05 (C$_q$), 118.05 (O-CH$_2$CH=$C$H$_2$), 122.79 (C-5), 128.77 (C$_q$), 133.14 (O-CH$_2$$C$H), 134.72 (C$_q$), 138.81 (C-3), 141.00 (C$_q$), 141.72 (C$_q$), 159.87 (C$_q$).

**MS**: [M + H]$^+$ 239.1 m/z

**Mp**: 173.9°C

**Anal. calcd for** $C_{15}H_{14}N_2O+\frac{1}{2}H_2O$: C, 72.85%; H, 6.11%; N, 11.33%

**Found**: C, 73.76%; H, 5.82%; N, 11.14%

**Purity by HPLC**: 99%

## 7-(Isobutyloxy)-1-methyl-β-carboline (2b.III)

The title compound was prepared from a solution of harmol (0.307 g, 0.98 mmol), cesium carbonate (1.764 g, 5.41 mmol) and 1-bromo-2-methylpropane (0.283 g, 2.06 mmol) in 6 mL of DMF. The reaction mixture was heated at 60°C for 24 h. The crude product was purified by column chromatography (dichloromethane/ethanol 95: 5% v/v).

*Yield:* 87%

*Physical and spectral characteristics:*

- **Chemical Formula**        $C_{16}H_{18}N_2O$
- **M.W. (g/mol)**              254.33
- **Aspect**                          White solid
- **TLC** (DCM/EtOH: 8/2)        $R_f = 0.65$
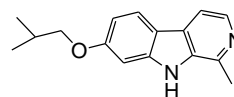
**¹H NMR (400 MHz, CDCl₃)** δ (ppm): 1.02 (d, *J* = 6.9 Hz, 6H, CH-(C*H₃*)₂), 2.05-2.15 (m, 1H, C*H*-(CH₃)₂), 2.78 (s, 3H, CH₃), 3.74 (d, *J* = 6.4 Hz, 2H, O-CH₂), 6.88-6.90 (m, 2H, H-8 + H-6), 7.74 (d, $J_{4-3}$ = 5.3 Hz, 1H, H-4), 7.95 (d, $J_{5-6}$ = 9.4 Hz, 1H, H-5), 8.34 (d, $J_{3-4}$ = 5.3 Hz, 1H, H-3), 10.05 (s, 1H, N-H).

**¹³C NMR (100 MHz, CDCl₃)** δ (ppm): 19.39 (CH-(*C*H₃)₂), 20.25 (CH₃), 28.40 (*C*H-(CH₃)₂), 74.87 (O-CH₂), 95.51 (C-8), 110.26 (C-6), 112.37 (C-4), 115.65 (C_q), 122.65 (C-5), 128.86 (C_q), 134.93 (C_q), 138.47 (C-3), 141.09 (C_q), 142.15 (C_q), 160.58 (C_q).

**MS**: [M + H]⁺ 255.1 m/z

**Mp**: 202.9°C

**Anal. calcd for** $C_{16}H_{18}N_2O$: C, 75.56%; H, 7.13%; N, 11.01%

**Found**: C, 75.54%; H, 7.19%; N, 10.75%

**Purity by HPLC**: 98%

**7-(2-Methoxyethoxy)-1-methyl-β-carboline (2c.III)**

The title compound was prepared from a solution of harmol (0.258 g, 0.82 mmol), cesium carbonate (1.135 g, 3.48 mmol) and 2-chloroethyl methyl ether (0.140 g, 1.48 mmol) in 5 mL of DMF. The reaction mixture was heated at 60°C for 24 h. The crude product was purified by column chromatography (dichloromethane/ethanol 95: 5% v/v).

*Yield:* 70%

*Physical and spectral characteristics:*

- **Chemical Formula**    $C_{15}H_{16}N_2O_2$
- **M.W. (g/mol)**    256.30
- **Aspect**    Brown solid
- **TLC** (DCM/EtOH: 8/2)    $R_f = 0.55$
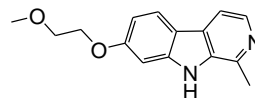


**$^1$H NMR (400 MHz, CDCl$_3$) δ** (ppm): 2.82 (s, 3H, CH$_3$), 3.45 (s, 3H, O-CH$_3$), 3.76 (t, $J = 4.6$ Hz , 2H, CH$_2$), 4.15 (t, $J = 4.6$ Hz , 2H, CH$_2$), 6.91 (dd, $J_{6-8} = 1.8$ Hz, $J_{6-5} = 8.7$ Hz, 1H, H-6), 7.00 (d, $J_{8-6} = 1.4$ Hz, 1H, H-8), 7.73 (d, $J_{4-3} = 5.5$ Hz, 1H, H-4), 7.93 (d, $J_{5-6} = 8.7$ Hz, 1H, H-5), 8.26 (d, $J_{3-4} = 5.3$ Hz, 1H, H-3), 9.78 (s, 1H, N-H).

**$^{13}$C NMR (100 MHz, CDCl$_3$) δ** (ppm): 19.66 (CH$_3$), 59.34 (O-CH$_3$), 67.72 (-CH$_2$-), 71.06 (-CH$_2$-), 95.75 (C-8), 110.68 (C-6), 112.54 (C-4), 115.72 (C$_q$), 122.80 (C-5), 129.32 (C$_q$), 134.88 (C$_q$), 137.00 (C-3), 140.56 (C$_q$), 142.59 (C$_q$), 160.37 (C$_q$).

**MS**: [M + H ]$^+$ 257.1 m/z

**Mp**: 175.8°C

**Anal. calcd for** $C_{15}H_{16}N_2O_2+\frac{1}{2}H_2O$: C, 67.91%; H, 6.46%; N, 10.56%

**Found**: C, 67.85%; H, 6.31%; N, 10.48%

**Purity by HPLC**: 99%

## 7-(2-Hydroxyethyloxy)-1-methyl-β-carboline (2d.III)

The title compound was prepared from a solution of harmol (0.845 g, 2.69 mmol), cesium carbonate (3.070 g, 9.42 mmol) and 2-chloroethanol (0.600 g, 7.46 mmol) in 8 mL of DMF. The reaction mixture was refluxed for 15 h. The crude product was purified by column chromatography (toluene/ethanol 80: 20% v/v).

*Yield:* 58%

*Physical and spectral characteristics:*

- **Chemical Formula**     $C_{14}H_{14}N_2O_2$
- **M.W. (g/mol)**          242.27
- **Aspect**                Brown solid
- **TLC** (DCM/EtOH: 8/2)   **$R_f$ = 0.33**
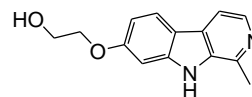


**$^1$H NMR (400 MHz, DMSO-d$_6$)** δ (ppm): 2.68 (s, 3H, CH$_3$), 3.75 (dt, *J* = 4.6 Hz, *J* = 5.1 Hz, 2H, C*H$_2$*-OH), 4.06 (t, *J* = 4.6 Hz, 2H, O-CH$_2$), 4.89 (t, *J* = 5.1 Hz, 1H, CH$_2$-O*H*), 6.81 (dd, $J_{6-5}$ = 8.7 Hz, $J_{6-8}$ = 2.1 Hz, 1H, H-6), 6.97 (d, $J_{8-6}$ = 2.1 Hz, 1H, H-8), 7.77 (d, $J_{4-3}$= 5.3 Hz, 1H, H-4), 8.01 (d, $J_{5-6}$ = 8.7 Hz, 1H, H-5), 8.11 (d, $J_{3-4}$= 5.3 Hz, 1H, H-3), 11.37 (s, 1H, N-H).

**$^{13}$C NMR (100 MHz, DMSO-d$_6$)** δ (ppm): 18.16 (CH$_3$), 60.06 (CH$_2$-OH), 70.58 (O-CH$_2$), 95.62 (C-8), 112.01 (C-6), 113.78 (C-4), 114.64 (C$_q$), 124.42 (C-5), 130.81 (C$_q$), 132.81 (C-3), 134.56 (C$_q$), 139.32 (C$_q$), 144.57 (C$_q$), 161.69 (C$_q$).

**MS**: [M + H]$^+$ 243.0 m/z

**Mp**: 264.4°C

**Anal. calcd for** $C_{14}H_{14}N_2O_2$: C, 69.41%; H, 5.82%; N, 11.56%

**Found**: C, 68.70%; H, 5.59%; N, 10.77%

**Purity by HPLC**: 97%

**7-(4,4,4-Trifluorobutoxy)-1-methyl-β-carboline (2e.III)**

The title compound was prepared from a solution of harmol (0.100 g, 0.32 mmol), cesium carbonate (0.330 g, 1.01 mmol) and 1-tosyl-4,4,4-trifluorobutane (0.150 g, 0.53 mmol) in 7 mL of DMF. The reaction mixture was heated at 90°C for 7 h. The crude product was purified by column chromatography (dichloromethane/ethanol 90: 10% v/v).

*Yield:* 72%

*Physical and spectral characteristics:*

- **Chemical Formula**        $C_{16}H_{15}F_3N_2O$
- **M.W. (g/mol)**             308.30
- **Aspect**                        White solid
- **TLC** (DCM/EtOH: 8/2)    **$R_f$ = 0.67**
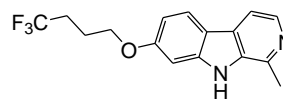


**$^1$H NMR (400 MHz, DMSO-d$_6$)** δ (ppm): 1.94-2.01 (m, 2H, CF$_3$-CH$_2$-C*H*$_2$), 2.39-2.52 (m, 2H, CF$_3$-CH$_2$, overlap with DMSO), 2.68 (s, 3H, CH$_3$), 4.12 (t, *J* = 6.2 Hz, 2H, O-CH$_2$), 6.82 (dd, $J_{6-5}$ = 8.7 Hz, $J_{6-8}$ = 2.1 Hz, 1H, H-6), 6.97 (d, $J_{8-6}$ = 2.1 Hz, 1H, H-8), 7.77 (d, $J_{4-3}$ = 5.3 Hz, 1H, H-4), 8.02 (d, $J_{5-6}$ = 8.7 Hz, 1H, H-5), 8.11 (d, $J_{3-4}$= 5.3 Hz, 1H, H-3), 11.38 (s, 1H, N-H).

**$^{13}$C NMR (100 MHz, DMSO-d$_6$)** δ (ppm): 20.88 (CH$_3$), 22.25 (d, *J* = 2.9 Hz, CF$_3$-CH$_2$-*C*H$_2$), 30.13 (q, *J* = 27.8 Hz, CF$_3$-*C*H$_2$), 66.55 (O-CH$_2$), 95.88 (C-8), 109.85 (C-6), 112.49 (C-4), 115.56 (C$_q$), 123.21 (C-5), 127.69 (C$_q$), 135.06 (C$_q$), 138.29 (C-3), 141.83 (C$_q$), 142.36 (C$_q$), 159.59 (C$_q$).

**$^{19}$F NMR (376 MHz, DMSO-d$_6$)** δ (ppm): -64.67 (t, *J* = 11.5 Hz).

**MS**: [M + H]$^+$ 309.1 m/z

**Mp**: 284.3°C

**Anal. calcd for** $C_{16}H_{15}F_3N_2O$: C, 62.33%; H, 4.90%; N, 9.09%

**Found**: C, 62.68%; H, 4.75%; N, 9.09%

**Purity by HPLC**: 98%

**7-(Cyclohexylmethoxy)-1-methyl-β-carboline (2f.III)**

The title compound was prepared from a solution of harmol (0.200 g, 0.64 mmol), cesium carbonate (0.911 g, 2.80 mmol) and (bromomethyl)cyclohexane (0.286 g, 1.61 mmol) in 5 mL of DMF. The reaction mixture was stirred at room temperature for 30 h. The crude product was purified by column chromatography (dichloromethane/ethanol 95: 5% v/v).

*Yield:* 85%

*Physical and spectral characteristics:*

- **Chemical Formula**   $C_{19}H_{22}N_2O$
- **M.W. (g/mol)**   294.39
- **Aspect**   White solid
- **TLC** (DCM/EtOH: 8/2)   $R_f = 0.65$
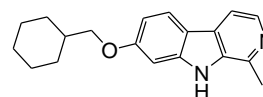


**$^1$H NMR (400 MHz, CDCl$_3$)** δ (ppm): 1.03-1.37 (m, 5H, CH (cyclohexyl)), 1.70-1.92 (m, 6H, CH (cyclohexyl)), 2.79 (s, 3H, CH$_3$), 3.84 (d, $J$ = 6.2 Hz, 2H, O-CH$_2$), 6.89 (dd, $J_{6\text{-}8}$ = 2.1 Hz, $J_{6\text{-}5}$ = 8.7 Hz , 1H, H-6), 6.93 (d, $J_{8\text{-}6}$ = 2.1 Hz, 1H, H-8), 7.70 (d, $J_{4\text{-}3}$ = 5.3 Hz, 1H, H-4), 7.94 (d, $J_{5\text{-}6}$ = 8.7 Hz, 1H, H-5), 8.19 (s, 1H, N-H), 8.31 (d, $J_{3\text{-}4}$ = 5.5 Hz, 1H, H-3).

**$^{13}$C NMR (100 MHz, CDCl$_3$)** δ (ppm): 20.36 (CH$_3$), 25.91 (CH (cyclohexyl)), 26.61 (CH (cyclohexyl)), 30.04 (CH (cyclohexyl)), 37.79 (CH (cyclohexyl)), 73.99 (O-CH$_2$), 95.44 (C-8), 110.29 (C-6), 112.27 (C-4), 115.72 (C$_q$), 122.68 (C-5), 128.73 (C$_q$), 134.63 (C$_q$), 139.12 (C-3), 140.98 (C$_q$), 141.67 (C$_q$), 160.61 (C$_q$).

**MS**: [M + H]$^+$ 295.2 m/z

**Mp**: 231.8°C

**Anal. calcd for** $C_{19}H_{22}N_2O$: C, 77.52%; H, 7.53%; N, 9.52%

**Found**: C, 76.59%; H, 7.03%; N, 8.87%

**Purity by HPLC**: 97%

**7-(Benzyloxy)-1-methyl-β-carboline (2g.III)**

The title compound was prepared from a solution of harmol (0.500 g, 1.59 mmol), cesium carbonate (1.410 g, 4.33 mmol) and 1-bromomethylbenzene (0.432 g, 2.53 mmol) in 10 mL of DMF. The reaction mixture was stirred at room temperature for 5 h. The crude product was purified by column chromatography (dichloromethane/ethanol 95: 5% v/v).

*Yield:* 70%

*Physical and spectral characteristics:*

- **Chemical Formula**     $C_{19}H_{16}N_2O$
- **M.W. (g/mol)**     288.34
- **Aspect**     White solid
- **TLC** (DCM/EtOH: 8/2)     $R_f = 0.69$
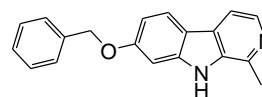
**¹H NMR (400 MHz, CDCl₃)** δ (ppm): 2.78 (s, 3H, CH₃), 5.17 (s, 2H, O-CH₂), 6.98 (dd, $J_{6-5}$ = 8.7 Hz, $J_{6-8}$ = 2.3 Hz, 1H, H-6), 7.01 (d, $J_{8-6}$ = 2.1 Hz, 1H, H-8), 7.32-7.47 (m, 5H, ArH), 7.71 (d, $J_{4-3}$ = 5.5 Hz, 1H, H-4), 7.97 (d, $J_{5-6}$ = 8.5 Hz, 1H, H-5), 8.28 (s, 1H, N-H), 8.32 (d, $J_{3-4}$ = 5.3 Hz, 1H, H-3).

**¹³C NMR (100 MHz, CDCl₃)** δ (ppm): 20.31 (CH₃), 70.50 (O-CH₂), 96.11 (C-8), 110.39 (C-6), 112.34 (C-4), 116.16 (C_q), 122.82 (C-5), 127.56 (C-ArH), 128.18 (C-ArH), 128.64 (C_q), 128.77 (C-ArH), 134.74 (C_q), 136.84 (C_q), 139.06 (C-3), 141.12 (C_q), 141.60 (C_q), 159.96 (C_q).

**MS**: [M + H]⁺ 289.1 m/z

**Mp**: 212.3°C

**Anal. calcd for** $C_{19}H_{16}N_2O$: C, 79.14%; H, 5.59%; N, 9.72%

**Found**: C, 78.99%; H, 5.60%; N, 9.60%

**Purity by HPLC**: 99%

**7-(Phenethoxy)-1-methyl-β-carboline (2h.III)**

The title compound was prepared from a solution of harmol (0.280 g, 0.89 mmol), cesium carbonate (3.010 g, 9.24 mmol) and (2-chloroethyl)benzene (0.363 g, 2.58 mmol) in 5 mL of DMF. The reaction mixture was refluxed for 30 h. The crude product was purified by column chromatography (dichloromethane/ethanol 95: 5% v/v).

*Yield:* 72%

*Physical and spectral characteristics:*

- **Chemical Formula**     $C_{20}H_{18}N_2O$
- **M.W. (g/mol)**         302.37
- **Aspect**               White solid
- **TLC** (DCM/EtOH: 8/2)  $R_f = 0.67$
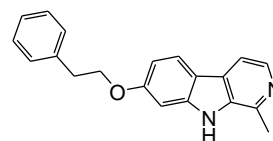


**$^1$H NMR (400 MHz, CDCl$_3$)** δ (ppm): 2.78 (s, 3H, CH$_3$), 3.14 (t, $J$ = 7.1 Hz, 2H, O-CH$_2$-C*H$_2$*), 4.24 (t, $J$ = 7.1 Hz, 2H, O-CH$_2$), 6.89 (dd, 1H, $J_{6-5}$ = 8.7 Hz, $J_{6-8}$ = 2.3 Hz, H-6), 6.93 (d, $J_{8-6}$ = 2.1 Hz, 1H, H-8), 7.22-7.34 (m, 5H, ArH), 7.71 (d, $J_{4-3}$ = 5.3 Hz, 1H, H-4), 7.94 (d, $J_{5-6}$ = 8.5 Hz, 1H, H-5), 8.30 (d, $J_{3-4}$ = 5.5 Hz, 1H, H-3), 8.89 (s, 1H, N-H).

**$^{13}$C NMR (100 MHz, CDCl$_3$)** δ (ppm): 20.16 (CH$_3$), 35.85 (CH$_2$), 69.16 (O-CH$_2$), 95.64 (C-8), 110.27 (C-6), 112.37 (C-4), 115.89 (C$_q$), 122.78 (C-5), 126.68 (C-ArH), 128.63 (C-ArH), 128.84 (C$_q$), 129.12 (C-ArH), 134.80 (C$_q$), 138.20 (C$_q$), 138.52 (C-3), 140.98 (C$_q$), 141.94 (C$_q$), 160.12 (C$_q$).

**MS**: [M + H]$^+$ 303.1 m/z

**Mp**: 139.7°C

**Anal. calcd for** $C_{20}H_{18}N_2O$: C, 79.44%; H, 6.00%; N, 9.26%

**Found**: C, 78.33%; H, 5.94%; N, 8.88%

**Purity by HPLC**: 99%

**7-(Pyridin-2-ylmethoxy)-1-methyl-β-carboline (2i.III)**

The title compound was prepared from a solution of harmol (0.362 g, 1.15 mmol), cesium carbonate (1.771 g, 5.44 mmol) and 2-(bromomethyl)pyridine hydrobromide (0.363 g, 1.43 mmol) in 7 mL of DMF. The reaction mixture was stirred at room temperature for 24 h. The crude product was purified by column chromatography (dichloromethane/ethanol 90: 10% v/v).

*Yield:* 90%

*Physical and spectral characteristics:*

- **Chemical Formula**      $C_{18}H_{15}N_3O$
- **M.W. (g/mol)**            289.33
- **Aspect**                     White solid
- **TLC** (DCM/EtOH: 8/2)      $R_f = 0.56$
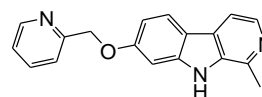
**$^1$H NMR (400 MHz, CDCl$_3$)** δ (ppm): 2.76 (s, 3H, CH$_3$), 5.29 (s, 2H, O-CH$_2$), 6.97-7.00 (m, 2H, H-6 + H-8), 7.23 (dd, $J = 5.5$ Hz, $J = 7.1$ Hz, 1H, ArH), 7.55 (d, $J = 8.0$ Hz, 1H, ArH), 7.69-7.73 (m, 2H, H-4 + ArH), 7.97 (d, $J_{5-6} = 9.2$ Hz, 1H, H-5), 8.31 (d, $J_{3-4} = 5.5$ Hz, 1H, H-3), 8.59 (d, $J = 4.8$ Hz, 1H, ArH), 8.94 (s, 1H, N-H).

**$^{13}$C NMR (100 MHz, CDCl$_3$)** δ (ppm): 20.33 (CH$_3$), 71.01 (O-CH$_2$), 96.01 (C-8), 110.36 (C-6), 112.36 (C-4), 116.26 (C$_q$), 121.56 (C-ArH), 122.87 (C-ArH), 122.90 (C-5), 128.58 (C$_q$), 134.88 (C$_q$), 137.09 (C-ArH), 138.83 (C-3), 141.24 (C$_q$), 141.74 (C$_q$), 149.29 (C-ArH), 157.12 (C$_q$), 159.46 (C$_q$).

**MS**: [M + H]$^+$ 290.1 m/z

**Mp**: 187.5°C

**Anal. calcd for** C$_{18}$H$_{15}$N$_3$O: C, 74.72%; H, 5.23%; N, 14.52%

**Found**: C, 74.23%; H, 5.23%; N, 14.22%

**Purity by HPLC**: 99%

**7-(Pyridin-3-ylmethoxy)-1-methyl-β-carboline (2j.III)**

The title compound was prepared from a solution of harmol (0.355 g, 1.13 mmol), cesium carbonate (1.550 g, 4.76 mmol) and 3-(bromomethyl)pyridine hydrobromide (0.342 g, 1.35 mmol) in 7 mL of DMF. The reaction mixture was stirred at room temperature for 24 h. The crude product was purified by column chromatography (dichloromethane/ethanol 90: 10% v/v).

*Yield:* 91%

*Physical and spectral characteristics:*

- **Chemical Formula**         $C_{18}H_{15}N_3O$
- **M.W. (g/mol)**             289.33
- **Aspect**                   Brown solid
- **TLC** (DCM/EtOH: 8/2)      $R_f = 0.44$
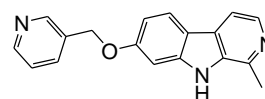
**$^1$H NMR (400 MHz, CDCl$_3$)** δ (ppm): 2.78 (s, 3H, CH$_3$), 5.15 (s, 2H, O-CH$_2$), 6.96 (dd, $J_{6-5}$ = 8.7 Hz, $J_{6-8}$ = 2.1 Hz, 1H, H-6), 6.99 (d, $J_{8-6}$ = 2.1 Hz, 1H, H-8), 7.33 (dd, $J$ = 4.8 Hz, $J$ = 7.8 Hz, 1H, ArH), 7.73 (d, 1H, $J_{4-3}$ = 5.5 Hz, 1H, H-4), 7.80 (dt, $J$ = 1.8 Hz, $J$ = 8.0 Hz, 1H, ArH), 7.99 (d, $J_{5-6}$ = 8.7 Hz, 1H, H-5), 8.32 (d, $J_{3-4}$ = 5.3 Hz, 1H, H-3), 8.59 (dd, $J$ = 1.4 Hz, $J$ = 4.6 Hz, 1H, ArH), 8.71 (d, $J$ = 1.6 Hz, 1H, ArH), 9.22 (s, 1H, N-H).

**$^{13}$C NMR (100 MHz, CDCl$_3$)** δ (ppm): 20.29 (CH$_3$), 68.00 (O-CH$_2$), 96.25 (C-8), 110.08 (C-6), 112.41 (C-4), 116.47 (C$_q$), 122.96 (C-5), 123.74 (C-ArH), 128.61 (C$_q$), 132.53 (C$_q$), 134.96 (C$_q$), 135.49 (C-ArH), 138.78 (C-3), 141.28 (C$_q$), 141.81 (C$_q$), 149.02 (C-ArH), 149.56 (C-ArH), 159.47 (C$_q$).

**MS**: [M + H]$^+$ 290.1 m/z

**Mp**: 226.6°C

**Anal. calcd for** $C_{18}H_{15}N_3O+\frac{1}{2}H_2O$: C, 72.47%; H, 5.41%; N, 14.08%

**Found**: C, 72.66%; H, 5.32%; N, 14.01%

**Purity by HPLC**: 99%

**7-(Pyridin-4-ylmethoxy)-1-methyl-β-carboline (2k.III)**

The title compound was prepared from a solution of harmol (0.355 g, 1.13 mmol), cesium carbonate (1.695 g, 5.20 mmol) and 4-(bromomethyl)pyridine hydrobromide (0.378 g, 1.49 mmol) in 7 mL of DMF. The reaction mixture was stirred at room temperature for 24 h. The crude product was purified by column chromatography (dichloromethane/ethanol 90: 10% v/v).

*Yield:* 62%

*Physical and spectral characteristics:*

- **Chemical Formula**      $C_{18}H_{15}N_3O$
- **M.W. (g/mol)**      289.33
- **Aspect**      Brown solid
- **TLC** (DCM/EtOH: 8/2)      $R_f = 0.39$
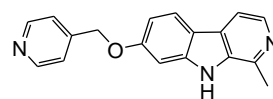
**¹H NMR (400 MHz, CDCl₃)** δ (ppm): 2.77 (s, 3H, CH₃), 5.20 (s, 2H, O-CH₂), 6.95-6.99 (m, 2H, H-6 + H-8), 7.39 (d, $J$ = 5.5 Hz, 2H, ArH), 7.72 (d, $J_{4-3}$ = 5.3 Hz, 1H, H-4), 8.00 (d, $J_{5-6}$ = 9.2 Hz, 1H, H-5), 8.32 (d, $J_{3-4}$ = 5.5 Hz, 1H, H-3), 8.48 (s, 1H, N-H), 8.62 (d, $J$ = 5.7 Hz, 2H, ArH).

**¹³C NMR (100 MHz, CDCl₃)** δ (ppm): 20.34 (CH₃), 68.65 (O-CH₂), 96.21 (C-8), 110.05 (C-6), 112.39 (C-4), 116.60 (C_q), 121.58 (C-ArH), 123.04 (C-5), 128.49 (C_q), 134.82 (C_q), 139.16 (C-3), 141.28 (C_q), 141.51 (C_q), 146.19 (C_q), 150.14 (C-ArH), 159.24 (C_q).

**MS**: [M + H]⁺ 290.1 m/z

**Mp**: 232.5°C

**Anal. calcd for** $C_{18}H_{15}N_3O + \frac{1}{2}H_2O$: C, 72.47%; H, 5.41%; N, 14.08%

**Found**: C, 72.05%; H, 5.34%; N, 14.11%

**Purity by HPLC**: 99%

**7-(Naphthalen-2-ylmethoxy)-1-methyl-β-carboline (2l.III)**

The title compound was prepared from a solution of harmol (0.500 g, 1.59 mmol), cesium carbonate (1.555 g, 4.77 mmol) and 2-(bromomethyl)naphthalene (0.540 g, 2.44 mmol) in 10 mL of DMF. The reaction mixture was stirred at room temperature for 6 h. The crude product was purified by column chromatography (dichloromethane/ethanol 95: 5% v/v).

*Yield:* 82%

*Physical and spectral characteristics:*

- **Chemical Formula**     $C_{23}H_{18}N_2O$
- **M.W. (g/mol)**     338.40
- **Aspect**     White solid
- **TLC** (DCM/EtOH: 8/2)     $R_f = 0.70$
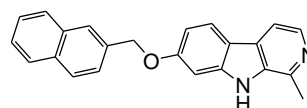


**$^1$H NMR (400 MHz, DMSO-d$_6$)** δ (ppm): 2.67 (s, 3H, CH$_3$), 5.38 (s, 2H, O-CH$_2$), 6.94 (dd, $J_{6-8}$ = 2.1 Hz, $J_{6-5}$ = 8.5 Hz , 1H, H-6), 7.09 (d, $J_{8-6}$ = 2.3 Hz, 1H, H-8), 7.47-7.53 (m, 2H, ArH), 7.61 (dd, $J$ = 1.6 Hz, $J$ = 8.5 Hz, 1H, ArH), 7.77 (d, $J_{4-3}$ = 5.3 Hz, 1H, H-4), 7.89-7.95 (m, 3H, ArH), 8.01 (s, 1H, ArH), 8.04 (d, $J_{5-6}$ = 8.7 Hz, 1H, H-5), 8.11 (d, $J_{3-4}$ = 5.3 Hz, 1H, H-3), 11.38 (s, 1H, N-H).

**$^{13}$C NMR (100 MHz, DMSO-d$_6$)** δ (ppm): 20.86 (CH$_3$), 70.19 (O-CH$_2$), 96.49 (C-8), 110.24 (C-6), 112.49 (C-4), 115.61 (C$_q$), 123.22 (C-5), 126.18 (C-ArH), 126.68 (C-ArH), 126.72 (C-ArH), 126.90 (C-ArH), 127.67 (C$_q$), 128.17 (C-ArH), 128.33 (C-ArH), 128.66 (C-ArH), 133.09 (C$_q$), 133.35 (C$_q$), 135.10 (C$_q$), 135.33 (C$_q$), 138.29 (C-3), 141.85 (C$_q$), 142.30 (C$_q$), 159.60 (C$_q$).

**MS**: [M + H]$^+$ 339.2 m/z

**Mp**: 238.6°C

**Anal. calcd for** $C_{23}H_{18}N_2O$: C, 81.63%; H, 5.36%; N, 8.28%

**Found**: C, 81.50%; H, 5.29%; N, 7.99%

**Purity by HPLC**: 99%

**7-(*N*,*N*-dimethylaminoethyloxy)-1-methyl-β-carboline (2m.III)**

The title compound was prepared from a solution of harmol (0.440 g, 1.40 mmol), cesium carbonate (2.060 g, 6.32 mmol) and 2-chloro-*N*,*N*-dimethylethylamine hydrochloride (0.330 g, 2.29 mmol) in 10 mL of DMF. The reaction mixture was heated at 110°C for 7 h. The crude product was purified by column chromatography (dichloromethane/ethanol/triethylamine 78: 20: 2% v/v/v). Finally, the final product is diluted with dichloromethane (10 mL), washed once with water (5 mL) to eliminate the triethylammonium salt. The organic layer was dried over $MgSO_4$ and concentrated.

*Yield:* 44%

*Physical and spectral characteristics:*

- **Chemical Formula**     $C_{16}H_{19}N_3O$
- **M.W. (g/mol)**           269.34
- **Aspect**                    Brown solid
- **TLC** (DCM/EtOH/NEt$_3$:     **R$_f$** = 0.26
  8/2/0.2)
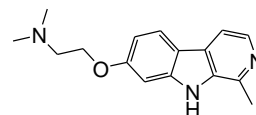


**¹H NMR (400 MHz, CDCl₃)** δ (ppm): 2.35 (s, 6H, 2CH₃), 2.77 (t, *J* = 5.7 Hz, 2H, O-CH₂-C*H₂*), 2.78 (s, 3H, CH₃), 4.12 (t, *J* = 5.7 Hz, 2H, O-CH₂), 6.90 (dd, $J_{6-5}$ = 8.5 Hz, $J_{6-8}$ = 2.1 Hz, 1H, H-6), 6.94 (d, $J_{8-6}$ = 2.1 Hz, 1H, H-8), 7.71 (d, $J_{4-3}$= 5.5 Hz, 1H, H-4), 7.94 (d, $J_{5-6}$ = 8.7 Hz, 1H, H-5), 8.31 (d, $J_{3-4}$= 5.3 Hz, 1H, H-3), 8.94 (s, 1H, N-H).

**¹³C NMR (100 MHz, CDCl₃)** δ (ppm): 20.34 (CH₃), 46.06 (2CH₃), 58.39 (O-CH₂-*C*H₂), 66.43 (O-CH₂), 95.65 (C-8), 110.11 (C-6), 112.34 (C-4), 115.96 (C$_q$), 122.69 (C-5), 128.69 (C$_q$), 134.87 (C$_q$), 138.79 (C-3), 141.16 (C$_q$), 141.85 (C$_q$), 160.05 (C$_q$).

**MS**: [M + H]⁺ 270.1 m/z

**Mp:** 218.3°C

**Anal. calcd for** $C_{16}H_{19}N_3O$+½$H_2O$: C, 69.04%; H, 7.24%; N, 15.10%

**Found**: C, 68.95%; H, 6.79%; N, 14.50%

**Purity by HPLC**: 99%

**7-(*N*,*N*-dimethylaminopropyloxy)-1-methyl-β-carboline (2n.III)**

The title compound was prepared from a solution of harmol (0.400 g, 1.27 mmol), cesium carbonate (1.450 g, 4.45 mmol) and 3-chloro-*N*,*N*-dimethylpropylamine hydrochloride (0.440 g, 2.78 mmol) in 10 mL of DMF. The reaction mixture was heated at 110°C for 7 h. The crude product was purified by column chromatography (dichloromethane/ethanol/triethylamine 78: 20: 2% v/v/v). Finally, the final product is diluted with dichloromethane (10 mL), washed once with water (5 mL) to eliminate the triethylammonium salt. The organic layer was dried over $MgSO_4$ and concentrated.

*Yield:* 52%

*Physical and spectral characteristics:*

- **Chemical Formula**    $C_{17}H_{21}N_3O$
- **M.W. (g/mol)**    283.37
- **Aspect**    Brown solid
- **TLC** (DCM/EtOH/NEt$_3$:    $R_f = 0.22$
  8/2/0.2)
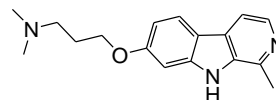
$^1$**H NMR (400 MHz, CDCl$_3$)** δ (ppm): 2.00-2.07 (m, 2H, O-CH$_2$-C*H$_2$*), 2.30 (s, 6H, 2CH$_3$), 2.53 (t, $J$ = 7.2 Hz, 2H, O-CH$_2$-CH$_2$-C*H$_2$*), 2.79 (s, 3H, CH$_3$), 4.12 (t, $J$ = 6.4 Hz, 2H, O-CH$_2$), 6.89 (dd, $J_{6-5}$ = 8.6 Hz, $J_{6-8}$ = 2.1 Hz, 1H, H-6), 6.96 (d, $J_{8-6}$ = 2.0 Hz, 1H, H-8), 7.70 (d, $J_{4-3}$ = 5.5 Hz, 1H, H-4), 7.94 (d, $J_{5-6}$ = 8.7 Hz, 1H, H-5), 8.12 (s, 1H, N-H), 8.31 (d, $J_{3-4}$ = 5.3 Hz, 1H, H-3).

$^{13}$**C NMR (100 MHz, CDCl$_3$)** δ (ppm): 20.38 (CH$_3$), 27.59 (O-CH$_2$-*C*H$_2$), 45.65 (2CH$_3$), 56.52 (O-CH$_2$-CH$_2$-*C*H$_2$), 66.54 (O-CH$_2$), 95.54 (C-8), 109.91 (C-6), 112.39 (C-4), 115.71 (C$_q$), 122.60 (C-5), 128.76 (C$_q$), 135.23 (C$_q$), 138.23 (C-3), 141.32 (C$_q$), 142.37 (C$_q$), 160.17 (C$_q$).

**MS**: [M + H]$^+$ 284.1 m/z

**Mp**: 179.5°C

**Anal. calcd for** $C_{17}H_{21}N_3O$+½H$_2$O: C, 69.84%; H, 7.58%; N, 14.37%

**Found**: C, 69.82%; H, 7.42%; N, 14.06%

**Purity by HPLC**: 98%

**7-(Ethyloxymorpholine)-1-methyl-β-carboline (2o.III)**

The title compound was prepared from a solution of harmol (0.440 g, 1.40 mmol), cesium carbonate (3.000 g, 9.21 mmol) and 4-(2-chloroethyl)morpholine hydrochloride (0.650 g, 3.49 mmol) in 10 mL of DMF. The reaction mixture was heated at 60°C for 24 h. The crude product was purified by column chromatography (dichloromethane/methanol 90: 10% v/v).

*Yield:* 38%

*Physical and spectral characteristics:*

- **Chemical Formula**     $C_{18}H_{21}N_3O_2$
- **M.W. (g/mol)**          311.38
- **Aspect**                Brown solid
- **TLC** (DCM/EtOH/NEt₃:   $R_f = 0.42$
  8/2/0.2)
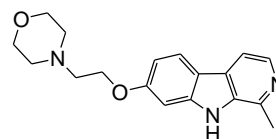


**¹H NMR (400 MHz, CDCl₃)** δ (ppm): 2.61 (t, $J$ = 4.6 Hz, 4H, CH₂ (morpholine)), 2.79 (s, 3H, CH₃), 2.86 (t, $J$ = 5.7 Hz, 2H, O-CH₂-C$H_2$), 3.75 (t, $J$ = 4.6 Hz, 4H, CH₂ (morpholine)), 4.20 (t, $J$ = 5.7 Hz, 2H, O-CH₂), 6.90 (dd, $J_{6-5}$ = 8.7 Hz, $J_{6-8}$ = 2.3 Hz, 1H, H-6), 6.96 (d, $J_{8-6}$ = 2.1 Hz, 1H, H-8), 7.70 (d, $J_{4-3}$= 5.3 Hz, 1H, H-4), 7.95 (d, $J_{5-6}$ = 8.7 Hz, 1H, H-5), 8.31 (d, $J_{3-4}$= 5.5 Hz, 1H, H-3), 8.40 (s, 1H, N-H).

**¹³C NMR (100 MHz, CDCl₃)** δ (ppm): 20.21 (CH₃), 54.22 (2 CH₂ (morpholine)), 57.71 (O-CH₂-C$H_2$), 66.33 (O-CH₂), 67.01 (2 CH₂ (morpholine)), 95.73 (C-8), 110.19 (C-6), 112.33 (C-4), 116.10 (C_q), 122.80 (C-5), 128.71 (C_q), 134.72 (C_q), 138.93 (C-3), 141.03 (C_q), 141.68 (C_q), 159.96 (C_q).

**MS**: [M + H]⁺ 312.1 m/z

**Mp**: 174.3°C

**Anal. calcd for** $C_{18}H_{21}N_3O_2$+2H₂O: C, 62.23%; H, 7.25%; N, 12.10%

**Found**: C, 62,72%; H, 7.22%; N, 11.82%

**Purity by HPLC**: 99%

c) Synthesis of 2-benzyl-7-benzyloxy-1-methyl-β-carboline (**3.III**)

The title compound was prepared from a solution of **2g.III** (0.140 g, 0.49 mmol) and benzyl bromide (0.831 g, 4.86 mmol) in 15 mL of anhydrous THF. The reaction mixture was heated to reflux for 48 h under argon atmosphere. At the end of the reaction, the mixture was cooled and THF is evaporated under reduced pressure to give the crude product which is purified by column chromatography (dichloromethane/ethanol 95: 5% v/v).

*Yield:* 31%

*Physical and spectral characteristics:*

- **Chemical Formula** $C_{26}H_{23}BrN_2O$
- **M.W. (g/mol)** 459.38
- **Aspect** Yellow solid
- **TLC** (DCM/EtOH: 8/2) $R_f = 0.73$
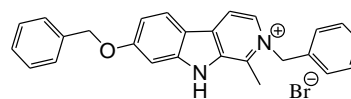


**$^1$H NMR (400 MHz, DMSO-d$_6$)** δ (ppm): 2.94 (s, 3H, CH$_3$), 5.30 (s, 2H, O-CH$_2$), 5.94 (s, 2H, N-CH$_2$), 7.12-7.20 (m, 4H, H-8 + H-6 + 2ArH), 7.30-7.50 (m, 8H, 8ArH), 8.34 (d, $J_{5-6} = 8.7$ Hz, 1H, H-5), 8.55 (d, $J_{4-3} = 6.4$ Hz, 1H, H-4), 8.70 (d, $J_{3-4} = 6.4$ Hz, 1H, H-3).

**$^{13}$C NMR (100 MHz, DMSO-d$_6$)** δ (ppm): 15.89 (CH$_3$), 59.54 (N-CH$_2$), 70.37 (O-CH$_2$), 96.07 (C-8), 113.93 (C-6), 114.32 (C$_q$), 115.21 (C-4), 125.40 (C-5), 127.49 (2C-ArH), 128.36 (2C-ArH), 128.61 (C-ArH), 128.99 (C-ArH), 129.10 (2C-ArH), 129.70 (2C-ArH), 132.03 (C$_q$), 135.19 (C-3), 135.84 (C$_q$), 136.98 (C$_q$), 139.71 (C$_q$), 146.43 (C$_q$), 162.53 (C$_q$).

**MS**: [M]$^+$ 379.14 m/z

**Mp**: 257.3°C

**Anal. calcd for** $C_{26}H_{23}BrN_2O + \frac{1}{2}H_2O$: C, 66.67%; H, 5.16%; N, 5.98%

**Found**: C, 66.12%; H, 5.48%; N, 6.00%

**Purity by HPLC**: 98%

d) Synthesis of 9-benzyl-7-benzyloxy-1-methyl-β-carboline (**4.III**)

The benzyl bromide (0.461 g, 2.69 mmol), potassium hydroxide (0.228 g, 4.06 mmol) were added to harmol (0.400 g, 1.27 mmol) dissolved in anhydrous in DMF (8 mL). The reaction mixture was stirred at room temperature for 4h. The reaction mixture was diluted in dichloromethane (40 mL), washed once with water (10 mL) and three times with brine (10 mL). The organic layer was dried over $MgSO_4$ and concentrated under reduced pressure. The crude product was purified by column chromatography (dichloromethane/ethanol 99: 1% v/v).

*Yield:* 84%

*Physical and spectral characteristics:*

- **Chemical Formula**      $C_{26}H_{22}N_2O$
- **M.W. (g/mol)**          378.47
- **Aspect**                White solid
- **TLC** (DCM/EtOH: 8/2)   **$R_f$ = 0.70**
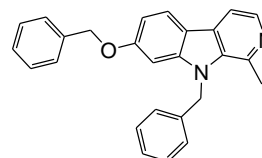
**$^1$H NMR (400 MHz, DMSO-d$_6$)** δ (ppm): 2.70 (s, 3H, CH$_3$), 5.14 (s, 2H, O-CH$_2$), 5.84 (s, 2H, N-CH$_2$), 6.88 (d, 2H, 2ArH), 6.94 (dd, $J_{6-5}$ = 8.7 Hz, $J_{6-8}$ = 2.1 Hz, 1H, H-6), 7.17-7.43 (m, 9H, H-8 + 8ArH), 7.89 (d, $J_{4-3}$ = 5.0 Hz, 1H, H-4), 8.11 (d, $J_{5-6}$ = 8.7 Hz, 1H, H-5), 8.14 (d, $J_{3-4}$ = 5.0 Hz, 1H, H-3).

**$^{13}$C NMR (100 MHz, DMSO-d$_6$)** δ (ppm): 23.21 (CH$_3$), 47.78 (N-CH$_2$), 70.24 (O-CH$_2$), 95.46 (C-8), 110.44 (C-6), 112.93 (C-4), 114.96 (C$_q$), 123.11 (C-5), 125.86 (2C-ArH), 127.63 (C-ArH), 128.41 (C-ArH), 128.48 (2C-ArH), 128.93 (2C-ArH), 129.08 (C$_q$), 129.34 (2C-ArH), 135.52 (C$_q$), 137.38 (C$_q$), 138.68 (C-3), 139.51 (C$_q$), 141.35 (C$_q$), 143.78 (C$_q$), 160.25 (C$_q$).

**MS**: [M + H]$^+$ 379.2 m/z

**Mp**: 155.7°C

**Anal. calcd for** $C_{26}H_{22}N_2O$: C, 82.51%; H, 5.86%; N, 7.40%

**Found**: C, 81.97%; H, 5.89%; N, 7.34%

**Purity by HPLC**: 97%

e) Synthesis of 2,9-dibenzyl-7-(benzyloxy)-1-methyl-β-carboline (**5.III**)

The title compound was prepared and purified according to procedure described for **3.III** from **4.III** (0.070 g, 0.18 mmol) and benzyl bromide (0.320 g, 1.85 mmol).

*Yield:* 36%

*Physical and spectral characteristics:*

- **Chemical Formula**    $C_{33}H_{29}BrN_2O$
- **M.W. (g/mol)**    549.50
- **Aspect**    White solid
- **TLC** (DCM/EtOH: 8/2)    $R_f = 0.73$
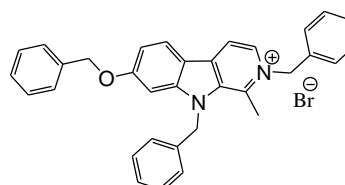
**$^1$H NMR (400 MHz, DMSO-d$_6$)** δ (ppm): 2.81 (s, 3H, CH$_3$), 5.23 (s, 2H, O-CH$_2$), 5.96 (s, 2H, N-CH$_2$), 5.98 (s, 2H, N-CH$_2$), 6.94 (d, $J$ = 7.1 Hz, 2H, 2ArH), 7.07 (d, $J$ = 7.1 Hz, 2H, 2ArH), 7.18-7.45 (m, 12H, 11 ArH + H-6), 7.53 (s, 1H, H-8), 8.45 (d, $J_{5-6}$ = 8.7 Hz, 1H, H-5), 8.69 (d, $J_{4-3}$ = 6.4 Hz, 1H, H-4), 8.82 (d, $J_{3-4}$ = 6.2 Hz, 1H, H-3).

**$^{13}$C NMR (100 MHz, DMSO-d$_6$)** δ (ppm): 16.57 (CH$_3$), 48.84 (N-CH$_2$), 60.33 (N-CH$_2$), 70.67 (O-CH$_2$), 95.55 (C-8), 113.39 (C$_q$), 114.28 (C-6), 115.23 (C-4), 125.44 (C-5), 125.98 (2C-ArH), 127.13 (2C-ArH), 128.05 (C-ArH), 128.65 (3C-ArH), 128.86 (C-ArH), 129.01 (2C-ArH), 129.56 (2C-ArH), 129.63 (2C-ArH), 133.99 (C$_q$), 135.28 (C$_q$), 135.89 (C$_q$), 136.75 (C-3), 136.77 (C$_q$), 138.10 (C$_q$), 140.14 (C$_q$), 148.51 (C$_q$), 163.38 (C$_q$).

**MS**: [M]$^+$ 469.3 m/z

**Mp**: 261.8°C

**Anal. calcd for** $C_{33}H_{29}BrN_2O + \frac{1}{2}H_2O$: C, 70.97%; H, 5.41%; N, 5.02%

**Found**: C, 69.65%; H, 5.28%; N, 4.83%

**Purity by HPLC**: 98%

f) Synthesis of *N*-ethyl-3-methylamino-β-carboline (**8.III**)

**N-Ethyl-3-carboxamide-β-carboline (11.III)**

Ethylamine solution (2.0 M in THF, 2.860 g, 63.44 mmol) was added to a solution of ethyl β-carboline-3-carboxylate (**10.III**) (0.508 g, 2.11 mmol) in methanol (15 mL). The resulting mixture was then stirred under reflux for 72h. After cooling, the solution was concentrated under reduced pressure and was used without further purification for the following step.

*Yield:* 100%

*Physical and spectral characteristics:*

- **Chemical Formula**   $C_{14}H_{13}N_3O$
- **M.W. (g/mol)**    239.27
- **Aspect**      Brown solid
- **TLC** (DCM/EtOH: 95/5)   **R$_f$** = 0.51
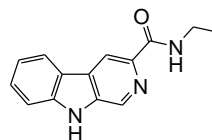


**$^1$H NMR (400 MHz, CDCl$_3$)** δ (ppm): 1.31 (t, *J* = 7.3 Hz, 3H, NH-CH$_2$-C*H$_3$*), 3.58 (q, *J* = 7.3 Hz, 2H, NH-C*H$_2$*-CH$_3$), 7.34 (dd, *J$_{6-5}$* = 7.8 Hz, *J$_{6-7}$* = 6.9 Hz, 1H, H-6), 7.54 (d, J$_{8-7}$ = 7.8 Hz, 1H, H-8), 7.56 (dd, *J$_{7-6}$* = 7.3 Hz, *J$_{7-8}$* = 7.8 Hz, 1H, H-7), 8.13 (s, 1H, N-H), 8.19 (d, *J$_{5-6}$* = 7.8 Hz, 1H, H-5), 8.72 (s, 1H, N-H), 8.79 (s, 1H, H-4), 8.93 (s, 1H, H-1).

**MS**: [M + H]$^+$ 240.0 m/z

**N-Ethyl-3-methylamino-β-carboline (8.III)**

A solution of the amide **11.III** (0.157 g, 0.66 mmol) in anhydrous THF (5 mL) was added dropwise to a suspension of lithium aluminium hydride (0.125 g, 3.29 mmol) in anhydrous THF (2.5 mL) at -50°C. The reaction mixture was then refluxed overnight, chilled once again to -50°C and treated with $H_2O$ (2 mL) in order to destroy the excess of lithium aluminium hydride. The resulting suspension was stirred for 30 min and filtered through celite. The filtrate was diluted with $Et_2O$ (45 mL), washed twice with water (20 mL) and twice with brine (25 mL), and dried over $MgSO_4$. The solvent was removed under reduced pressure to give the crude product which is purified by *RP-HPLC* semi-preparative (*see purification techniques in the section 1.2*). The derivative **8.III** is then deprotonated with a NaOH solution (2N, 5 mL) and extracted three times with dichloromethane (20 mL). The organic layer was dried over $MgSO_4$ and concentrated under reduced pressure.

*Yield:* 22%

*Physical and spectral characteristics:*

- **Chemical Formula**    $C_{14}H_{15}N_3$
- **M.W. (g/mol)**    225.29
- **Aspect**    Brown solid
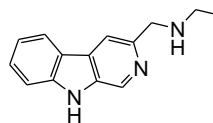


**$^1$H NMR (400 MHz, CD$_3$OD)** δ (ppm): 1.19 (t, $J$ = 7.3 Hz, 3H, NH-CH$_2$-C*H$_3$*), 2.78 (q, $J$ = 7.1 Hz, 2H, NH-C*H$_2$*-CH$_3$), 4.08 (s, 2H, -C*H$_2$*-NH-), 7.21-7.28 (m, 1H, H-6), 7.52-7.56 (m, 2H, H-7 + H-8), 8.11 (s, 1H, H-4), 8.17 (d, $J_{5-6}$ = 8.0 Hz, 1H, H-5), 8.77 (s, 1H, H-1).

**$^{13}$C NMR (100 MHz, CD$_3$OD)** δ (ppm): 12.81 (NH-CH$_2$-*C*H$_3$), 43.0 (NH-*C*H$_2$-CH$_3$), 53.0 (-*C*H$_2$-NH-), 111.56 (C-8), 113.71 (C-4), 119.49 (C-6), 120.83 (C$_q$), 121.93 (C-5), 128.49 (C-7), 129.75 (C$_q$), 132.49 (C-1), 135.65 (C$_q$), 141.80 (C$_q$), 145.36 (C$_q$).

**MS**: [M + H]$^+$ 226.1 m/z

**Anal. calcd for** $C_{14}H_{15}N_3$+2H$_2$O: C, 64.35%; H, 7.33%; N, 16.08%

**Found**: C, 65.79%; H, 7.06%; N, 14.29%

g) Synthesis of 3-methylamino-β-carboline (**9.III**)

**3-Hydroxymethyl-β-carboline (13.III)**

A solution of ethyl β-carboline-3-carboxylate (**10.III**) (0.570 g, 2.37 mmol) in anhydrous THF (20 mL) was added dropwise to a suspension of lithium aluminium hydride (0.450 g, 11.86 mmol) in anhydrous THF (10 mL) at -50°C. The reaction mixture was then stirred at room temperature for 24h, chilled once again to -50°C and treated with $H_2O$ (8 mL) in order to destroy the excess of lithium aluminium hydride. The resulting suspension was stirred for 30 min and filtered through celite. The aqueous suspension was extracted with dichloromethane (40 mL) and washed once with $H_2O$ (10 mL). The solution was dried over $MgSO_4$, concentrated under reduced pressure and was used without further purification for the following steps.

*Yield:* 52%

*Physical and spectral characteristics:*

- **Chemical Formula**       $C_{12}H_{10}N_2O$
- **M.W. (g/mol)**           198.22
- **Aspect**                 Yellow solid
- **TLC** (DCM/EtOH: 8/2)    $R_f$ = 0.41
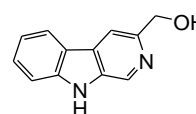


**$^1$H NMR (400 MHz, DMSO-d$_6$)** δ (ppm): 4.61 (s, 2H, -C$H_2$), 6.66 (dd, $J_{6-5}$ = 7.3 Hz, $J_{6-7}$ = 7.1 Hz, 1H, H-6), 7.07 (dd, $J_{7-8}$ = 8.0 Hz, $J_{7-6}$ = 7.1 Hz, 1H, H-7), 7.39 (d, $J_{8-7}$ = 8.2 Hz, 1H, H-8), 7.78 (s, 1H, H-4), 7.90 (d, $J_{5-6}$ = 7.8 Hz, 1H, H-5), 8.62 (s, 1H, H-1).

**MS**: $[M + H]^+$ 199.0 m/z

**3-Azidomethyl-β-carboline (16.III)**

    A) Via 3-chloromethyl-β-carboline (**14.III**)

3-Hydroxymethyl-β-carboline (**13.III**) (0.097 g, 0.49 mmol) was added to an excess of thionyl chloride (15 mL) and the mixture was refluxed for 1 h. The excess thionyl chloride was then evapored and the crude product was used without further purification for the following step. NaN$_3$ (0.035 g, 0.540 mmol) was added to the crude product (0.100 g) containing **14.III** dissolved in anhydrous DMF (5 mL). The reaction mixture was heated at 100°C for 1 h and then diluted in Et$_2$O (10 mL), washed twice with water (5 mL) and three times with brine (5 mL). The organic layer was dried over MgSO$_4$ and concentrated under reduced pressure.

    B) Via 3-(trifluoromethanesulfonate)methyl-β-carboline (**15.III**)

To a solution of 3-hydroxymethyl-β-carboline (**13.III**) (0.081 g, 0.41 mmol) in anhydrous pyridine (3 mL), trifluoromethanesulfonic anhydride (0.128 g, 0.45 mmol) was added dropwise over 15 min, while the mixture was gently stirred at 0°C. The mixture was then stirred for 3 h at room temperature. After completion of the reaction, the reaction mixture was diluted in chloroform (15 mL), washed twice with water (5 mL). The organic layer was dried over MgSO$_4$ and concentrated under reduced pressure. The crude product was used without further purification for the following step. NaN$_3$ (0.043 g, 0.66 mmol) was added to the crude product (0.200 g) containing **15.III** dissolved in anhydrous DMF (5 mL). The reaction mixture was heated at 100°C for 1 h and then diluted in Et$_2$O (10 mL), washed twice with water (5 mL) and three times with brine (5 mL). The organic layer was dried over MgSO$_4$ and concentrated under reduced pressure.

*Yield:* 24% (via B)

*Physical and spectral characteristics:*

- **Chemical Formula**      C$_{12}$H$_9$N$_5$
- **M.W. (g/mol)**      223.23
- **Aspect**      Brown solid
- **TLC** (DCM/EtOH: 9/1)      **R$_f$** = 0.60
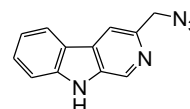
**$^1$H NMR (400 MHz, CDCl$_3$)** δ (ppm): 4.66 (s, 2H, CH$_2$-N$_3$), 7.31 (dd, $J_{6\text{-}7}$ = 7.1 Hz, $J_{6\text{-}5}$ = 7.6 Hz, 1H, H-6), 7.52 (d, $J_{8\text{-}7}$ = 8.0 Hz, 1H, H-8), 7.56 (dd, $J_{7\text{-}8}$ = 8.0 Hz, $J_{7\text{-}6}$ = 7.1 Hz,

1H, H-7), 7.99 (s, 1H, H-4), 8.13 (d, $J_{5-6}$ = 8.2 Hz, 1H, H-5), 8.78 (s, 1H, NH), 8.88 (s, 1H, H-1).

$^{13}$**C NMR (100 MHz, CDCl$_3$)** δ (ppm): 56.32 (CH$_2$-N$_3$), 111.80 (C-8), 113.70 (C-4), 120.49 (C-6), 121.41 (C$_q$), 121.96 (C-5), 128.96 (C-7), 129.96 (C$_q$), 133.44 (C-1), 135.39 (C$_q$), 140.94 (C$_q$), 144.90 (C$_q$).

**MS**: [M + H]$^+$ 224.0 m/z

**Mp**: 138-140°C

### 3-Methylamino-β-carboline (9.III)

Triphenylphosphine (0.025 g, 0.09 mmol) was added to a solution of **16.III** (0.021 g, 0.09 mmol) in THF (3 mL) and water (0.5 mL). The mixture was stirred at room temperature overnight. After the solvents were evaporated, the residue was purified by an acid-base extraction.

*Yield:* 38% (via B)

*Physical and spectral characteristics:*

- **Chemical Formula**    C$_{12}$H$_{11}$N$_3$
- **M.W. (g/mol)**         197.24
- **Aspect**                Brown solid
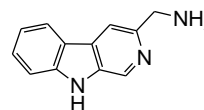


$^1$**H NMR (400 MHz, CD$_3$OD)** δ (ppm): 4.15 (s, 2H, CH$_2$-NH$_2$), 7.22-7.28 (m, 1H, H-6), 7.52-7.56 (m, 2H, H-7 + H-8), 8.11 (s, 1H, H-4), 8.17 (d, $J_{5-6}$ = 8.0 Hz, 1H, H-5), 8.78 (s, 1H, H-1).

$^{13}$**C NMR (100 MHz, CD$_3$OD)** δ (ppm): 44.74 (CH$_2$-NH$_2$), 111.63 (C-8), 113.12 (C-4), 119.57 (C-6), 120.97 (C$_q$), 121.40 (C-5), 128.58 (C-7), 128.43 (C$_q$), 132.81 (C-1), 135.85 (C$_q$), 139.99 (C$_q$), 141.80 (C$_q$).

**MS**: [M + H]$^+$ 198.0 m/z

h) Synthesis of 3-butyl-β-carboline (**46.I**)


**3-Carbaldehyde-β-carboline (18.III)**

To a stirred solution of ethyl β-carboline-3-carboxylate (**10.III**) (0.107 g, 0.44 mmol) in anhydrous dichloromethane (8 mL) was added DIBAL-H solution (1.0 M in hexane, 3.10 mL, 3.10 mmol) at -50°C. The mixture was stirred at -50°C for 45 min and quenched by sequential addition of MeOH (1 mL) and NaOH (0.1 M, 3 mL) at -50°C. Then the mixture was stirred at room temperature for an additional 1h. The precipitates were removed through a celite and washed with methanol-chloroforme (50/50 v/v). The combined filtrate was washed once with brine (2 mL), dried over MgSO$_4$, concentrated under reduced pressure and was used without further purification for the following steps.

*Yield:* 93%

*Physical and spectral characteristics:*


- **Chemical Formula**    $C_{12}H_8N_2O$
- **M.W. (g/mol)**    196.20
- **Aspect**    Brown solid
- **TLC** (DCM/EtOH: 9/1)    **R$_f$** = 0.19
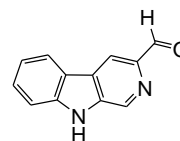
**1-Phenylbutan-1-ol (22.III)**

A solution of 1-bromopropane (0.90 mL, 9.91 mmol) in anhydrous diethyl ether (2 mL) was added dropwise to a suspension of magnesium (0.240 g, 9.87 mmol) in anhydrous diethyl ether (1 mL) at room temperature. The reaction mixture was then stirred at room temperature for 30 min. To a stirred solution of benzaldehyde (0.80 mL, 7.87 mmol) in anhydrous diethyl ether (2 mL) was added dropwise the n-propylmagnesium bromide solution at -8°C. The mixture was stirred at room temperature for 3 h, quenched by addition of sat. $NH_4Cl$ (10 mL) and extracted with diethyl ether (30 mL). The combined organic phases were washed once with brine (10 mL), dried over $MgSO_4$ and concentrated under reduced pressure.

*Yield:* 65%

*Physical and spectral characteristics:*

- **Chemical Formula**    $C_{10}H_{14}O$
- **M.W. (g/mol)**    150.10
- **Aspect**    Colorless oil
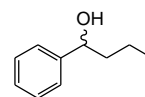


**¹H NMR (400 MHz, CDCl₃)** δ (ppm): 0.95 (t, *J* = 7.3 Hz, 3H, CH₃), 1.25-1.47 (m, 2H, CH₂), 1.61-1.81 (m, 2H, CH₂), 3.33 (s, 1H, OH), 4.59 (t, *J* = 6.6 Hz, 1H, CH), 7.26-7.37 (m, 5H, ArH).

**MS**: $[M + H]^+$ 151.0 m/z

**1.4.2 Synthesis of 5*H*-indeno[1,2-*c*]pyridazin-5-ones**

a) Synthesis of 8-(4,4,4-trifluorobutyloxy)-3-(3'-(trifluoromethyl)phenyl)-5*H*-indeno [1,2-*c*]pyridazin-5-one (**28a.III**) [74]

**5-(4,4,4-Trifluorobutyloxy)-1-indanone (25a.III)**

1-Tosyl-4,4,4-trifluorobutane (3.480 g, 12.33 mmol) was added to a solution of 5-hydroxy-1-indanone (**24.III**, 1.660 g, 11.20 mmol) in anhydrous acetonitrile (15 mL) containing potassium carbonate (3.380 g, 24.46 mmol). The resulting mixture was stirred for 4 h at 90 °C under an argon atmosphere and then cooled to room temperature. After evaporation of the solvents, the residue was poured into ethyl acetate (30 mL), washed twice with water (5 mL), dried over magnesium sulfate, filtered, and evaporated to dryness. The crude product was purified by column chromatography (pentane/ethyl acetate 70: 30% v/v).

*Yield:* 96%

*Physical and spectral characteristics:*

- **Chemical Formula**       $C_{13}H_{13}F_3O_2$
- **M.W. (g/mol)**            258.24
- **Aspect**                 Brown solid
- **TLC** (pentane/AcOEt: 7/3)   $R_f = 0.41$
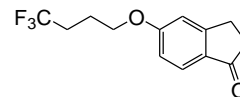


**¹H NMR (400 MHz, CDCl₃)** δ (ppm): 2.06-2.13 (m, 2H, CF₃-CH₂-C*H₂*), 2.27-2.39 (m, 2H, CF₃-CH₂), 2.67 (t, *J* = 5.7 Hz, 2H, CH₂), 3.08 (t, *J* = 5.7 Hz, 2H, CH₂), 4.08 (t, *J* = 6.0 Hz, 2H, O-CH₂), 6.86-6.90 (m, 2H, H-4 + H-6), 7.67 (d, *J₇₋₆* = 9.2 Hz, 1H, H-7).

**¹⁹F NMR (376 MHz, CDCl₃)** δ (ppm): -66.15 (t, *J* = 11.6 Hz).

**5-(4,4,4-Trifluorobutyloxy)ninhydrin (26a.III)**

5-(4,4,4-Trifluorobutyloxy)-1-indanone (**25a.III**, 1.800 g, 6.97 mmol) was added to a suspension of selenium dioxide (3.870 g, 34.88 mmol) in anhydrous dioxane (10 mL). The suspension was stirred for 3 h to reflux under an argon atmosphere, filtered, and the solvents evaporated. The residue was poured into dichloromethane (30 mL) into which the unreacted $SeO_2$ precipitated. The $SeO_2$ was filtered off and the filtrate evaporated to dryness. The crude product was purified by column chromatography (dichloromethane/ethyl acetate 80: 20% v/v).

*Yield:* 76%

*Physical and spectral characteristics:*

- **Chemical Formula** $C_{13}H_{11}F_3O_5$
- **M.W. (g/mol)** 304.22
- **Aspect** Brown solid
- **TLC** (DCM/AcOEt: 3/1) **$R_f$ = 0.41**
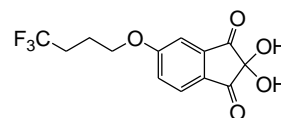


**$^1$H NMR (400 MHz, CDCl$_3$)** δ (ppm): 2.10-2.22 (m, 2H, CF$_3$-CH$_2$-C*H$_2$*), 2.28-2.40 (m, 2H, CF$_3$-CH$_2$), 4.18 (t, *J* = 5.8 Hz, 2H, O-CH$_2$), 7.31 (d, $J_{4-6}$ = 2.3 Hz, 1H, H-4), 7.36 (dd, $J_{6-4}$ = 2.3 Hz, $J_{6-7}$ = 8.5 Hz, 1H, H-6), 7.90 (d, $J_{7-6}$ = 8.5 Hz, 1H, H-7).

**$^{19}$F NMR (376 MHz, CDCl$_3$)** δ (ppm): -66.13 (t, *J* = 11.6 Hz).

**8-(4,4,4-Trifluorobutyloxy)-3-(3'-(trifluoromethyl)phenyl)-5*H*-indeno[1,2-*c*]pyridazin-5-one (28a.III)**

3'-(Trifluoromethyl)acetophenone (0.310 g, 1.65 mmol) was added to a solution of 5-(4,4,4-trifluorobutyloxy)ninhydrin (**26a.III**, 0.500 g, 1.64 mmol) in glacial acetic acid (10 mL) which was stirred under reflux for 3 h. After cooling, the solution was concentrated (2 mL), and hydrazine monohydrate (0.079 g, 2.48 mmol) added. After stirring vigorously overnight at room temperature, the solvent was evaporated. The crude product was purified by column chromatography (dichloromethane 100% v).

*Yield:* 44%

*Physical and spectral characteristics:*

- **Chemical Formula**      $C_{22}H_{14}F_6N_2O_2$
- **M.W. (g/mol)**      452.35
- **Aspect**      Yellow solid
- **TLC** (DCM)      **$R_f$** = 0.52
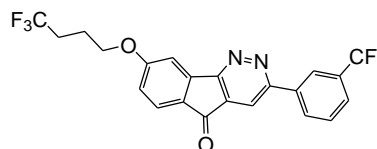


**$^1$H NMR (400 MHz, CDCl$_3$)** δ (ppm): 2.13-2.20 (m, 2H, CF$_3$-CH$_2$-C*H$_2$*), 2.31-2.43 (m, 2H, CF$_3$-CH$_2$), 4.25 (t, *J* = 6.1 Hz, 2H, O-CH$_2$), 7.04 (dd, $J_{7-9}$ = 2.3 Hz, $J_{7-6}$ = 8.2 Hz, 1H, H-7), 7.65 (d, $J_{9-7}$ = 2.1 Hz, 1H, H-9), 7.69 (t, $J_{5'-6'}$ = $J_{5'-4'}$ = 7.8 Hz, 1H, H-5'), 7.80 (d, $J_{4'-5'}$ = 8.5 Hz, 1H, H-4'), 7.83 (d, $J_{6-7}$ = 8.5 Hz, 1H, H-6), 8.00 (s, 1H, H-4), 8.31 (d, $J_{6'-5'}$ = 7.8 Hz, 1H, H-6'), 8.42 (s, 1H, H-2').

**$^{13}$C NMR (100 MHz, CDCl$_3$)** δ (ppm): 22.10 (d, *J* = 3.8 Hz, CF$_3$-CH$_2$-*C*H$_2$), 30.69 (q, *J* = 29.7 Hz, CF$_3$-*C*H$_2$), 67.18 (O-CH$_2$), 107.38 (C-9), 117.27 (C-4), 118.95 (C-7), 123.94 (q, *J* = 272.2 Hz, C$_q$), 124.14 (q, *J* = 3.8 Hz, C-2'), 127.32 (q, *J* = 3.8 Hz, C-4'), 127.61 (C-6), 128.27 (C$_q$), 129.83 (C-5'), 130.31 (C-6'), 131.83 (q, *J* = 33.6 Hz, C-3'), 132.67 (C$_q$), 136.81 (C$_q$), 145.23 (C$_q$), 159.11 (C$_q$), 160.71 (C$_q$), 165.77 (C$_q$), 188.11 (C$_q$).

**$^{19}$F NMR (376 MHz, CDCl$_3$)** δ (ppm): -66.12 (t, *J* = 11.6 Hz), -62.63 (s).

**MS**: [M + H]$^+$ 453.2 m/z

**Mp**: 173.1°C

**Anal. calcd for** $C_{22}H_{14}F_6N_2O_2$: C, 58.41%; H, 3.12%; N, 6.19%

**Found**: C, 58.47%; H, 3.21%; N, 6.10%

b) Synthesis of 8-(benzyloxy)-3-(3'-(trifluoromethyl)phenyl)-5*H*-indeno[1,2-*c*]pyridazin-5-one (**28b.III**)

**5-Benzyloxy-1-indanone (25b.III)**

Benzyl bromide (1.904 g, 11.13 mmol) was added to a solution of 5-hydroxy-1-indanone (**24.III**, 1.500 g, 10.12 mmol) in anhydrous DMF (15 mL) containing potassium carbonate (3.077 g, 22.26 mmol) is suspended. The resulting mixture was stirred for 5 h at room temperature under an argon atmosphere. The mixture was diluted with ethyl acetate (30 mL), washed once with water (10 mL) and three times with brine (10 mL). The organic layer was dried over MgSO$_4$ and concentrated. The crude product was purified by liquid chromatography (pentane/ethyl acetate 85: 15% v/v).

*Yield:* 90%

*Physical and spectral characteristics:*

- **Chemical Formula** $C_{16}H_{14}O_2$
- **M.W. (g/mol)** 238.28
- **Aspect** Brown solid
- **TLC**(pentane/AcOEt: 7/3) **R$_f$** = 0.64
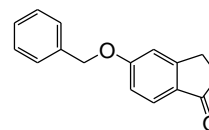


**$^1$H NMR (400 MHz, CDCl$_3$)** $\delta$ (ppm): 2.66 (t, *J* = 5.7 Hz, 2H, CH$_2$), 3.07 (t, *J* = 5.7 Hz, 2H, CH$_2$), 5.13 (s, 2H, O-CH$_2$), 6.96-6.98 (m, 2H, H-4 + H-6), 7.33-7.44 (m, 5H, ArH), 7.69 (d, *J$_{7-6}$* = 8.9 Hz, 1H, H-7).

**5-Benzyloxyninhydrin (26b.III)**

The title compound was prepared from 5-benzyloxy-1-indanone (**25b.III**, 1.800 g, 7.56 mmol) and selenium dioxide (4.193 g, 37.79 mmol) according to the same procedure than that described for **26a.III**. The crude product was purified by column chromatography (dichloromethane/ethyl acetate 90: 10% v/v).

*Yield:* 81%

*Physical and spectral characteristics:*

- **Chemical Formula** $C_{16}H_{12}O_5$
- **M.W. (g/mol)** 284.26
- **Aspect** Brown solid
- **TLC** (DCM/AcOEt: 7/3) $R_f = 0.60$
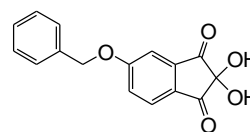
$^{1}$**H NMR (400 MHz, CDCl$_3$)** δ (ppm): 5.20 (s, 2H, O-CH$_2$), 7.30-7.52 (m, 7H, H-4 + H-6 + 5 ArH), 7.93 (d, $J_{7-6} = 8.2$ Hz, 1H, H-7).

**8-(Benzyloxy)-3-(3'-(trifluoromethyl)phenyl)-5*H*-indeno[1,2-*c*]pyridazin-5-one (28b.III)**

The title compound was prepared and purified according to procedure described for **28a.III** from 3'-(trifluoromethyl)acetophenone (0.331 g, 1.76 mmol) and 5-benzyloxyninhydrin (**26b.III**, 0.500 g, 1.76 mmol).

*Yield:* 46%

*Physical and spectral characteristics:*

- **Chemical Formula**  $C_{25}H_{15}F_3N_2O_2$
- **M.W. (g/mol)**  432.39
- **Aspect**  Yellow solid
- **TLC** (DCM)  **$R_f$** = 0.56
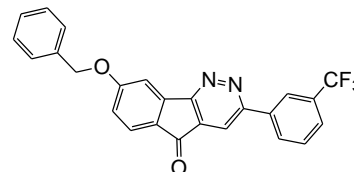


**¹H NMR (400 MHz, CDCl₃)** δ (ppm): 5.29 (s, 2H, O-CH₂), 7.11 (dd, $J_{7-9}$ = 2.3 Hz, $J_{7-6}$ = 8.2 Hz, 1H, H-7), 7.36-7.49 (m, 5H, ArH), 7.69 (t, $J_{5'-6'}$ = $J_{5'-4'}$ = 7.8 Hz, 1H, H-5'), 7.75 (d, $J_{9-7}$ = 2.3 Hz, 1H, H-9), 7.79 (d, $J_{4'-5'}$ = 8.5 Hz, 1H, H-4'), 7.82 (d, $J_{6-7}$ = 8.5 Hz, 1H, H-6), 8.00 (s, 1H, H-4), 8.31 (d, $J_{6'-5'}$ = 8.0 Hz, 1H, H-6'), 8.42 (s, 1H, H-2').

**¹³C NMR (100 MHz, CDCl₃)** δ (ppm): 71.01 (O-CH₂), 107.92 (C-9), 117.20 (C-4), 119.39 (C-7), 123.94 (q, $J$ = 273.2 Hz, C_q), 124.13 (q, $J$ = 3.8 Hz, C-2'), 127.29 (q, $J$ = 3.8 Hz, C-4'), 127.59 (C-6), 127.72 (2C-ArH), 128.17 (C_q), 128.69 (C-ArH), 128.96 (2C-ArH), 129.81 (C-5'), 130.29 (C-6'), 131.83 (q, $J$ = 32.6 Hz, C-3'), 132.72 (C_q), 135.43 (C_q), 136.83 (C_q), 145.15 (C_q), 159.08 (C_q), 160.77 (C_q), 165.98 (C_q), 188.16 (C_q).

**¹⁹F NMR (376 MHz, CDCl₃)** δ (ppm): -62.63 (s).

**MS**: [M + H]⁺ 433.2 m/z

**Mp**: 209.3°C

**Anal. calcd for** $C_{25}H_{15}F_3N_2O_2$: C, 69.44%; H, 3.50%; N, 6.48%.

**Found**: C, 69.76%; H, 3.62%; N, 6.37%.

c) Synthesis of 8-(methoxy)-3-(3'-(trifluoromethyl)phenyl)-5*H*-indeno[1,2-*c*]pyridazin-5-one (**22m.I**) [74]

**5-Methoxyninhydrin (26c.III)**

The title compound was prepared from 5-(methoxy)-1-indanone (**25c.III**, 1.000 g, 6.17 mmol) and selenium dioxide (3.420 g, 30.82 mmol) according to the same procedure than that described for **26a.III**. The crude product was purified by column chromatography (dichloromethane/ethyl acetate 70: 30% v/v).

*Yield:* 73%

*Physical and spectral characteristics:*

- **Chemical Formula**      $C_{10}H_8O_5$
- **M.W. (g/mol)**          208.17
- **Aspect**                Brown solid
- **TLC** (DCM/AcOEt: 7/3)   $\mathbf{R_f} = 0.45$
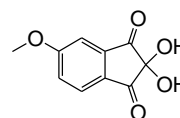
**$^1$H NMR (400 MHz, CDCl₃)** δ (ppm): 3.99 (s, 3H, O-CH₃), 7.40 (d, $J_{4-6}$ = 2.3 Hz, 1H, H-4), 7.44 (dd, $J_{6-4}$ = 2.3 Hz, $J_{6-7}$ = 8.5 Hz, 1H, H-6), 7.99 (d, $J_{7-6}$ = 8.2 Hz, 1H, H-7).

**8-(Methoxy)-3-(3'-(trifluoromethyl)phenyl)-5*H*-indeno[1,2-*c*]pyridazin-5-one (22m.I)**

The title compound was prepared and purified according to procedure described for **28a.III** from 3'-(trifluoromethyl)acetophenone (0.452 g, 2.40 mmol) and 5-methoxyninhydrin (**31c**, 0.500 g, 2.40 mmol).

*Yield:* 39%

*Physical and spectral characteristics:*

- **Chemical Formula**    $C_{19}H_{11}F_3N_2O_2$
- **M.W. (g/mol)**    356.30
- **Aspect**    Yellow solid
- **TLC** (pentane/AcOEt 7/3)    **$R_f$ = 0.48**
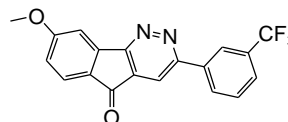


**¹H NMR (400 MHz, CDCl₃)** δ (ppm): 4.01 (s, 3H, O-CH₃), 7.03 (dd, $J_{7-9}$ = 2.3 Hz, $J_{7-6}$ = 8.5 Hz, 1H, H-7), 7.66 (d, $J_{9-7}$ = 2.1 Hz, 1H, H-9), 7.68 (t, $J_{5'-6'}$ = $J_{5'-4'}$ = 7.8 Hz, 1H, H-5'), 7.78 (d, $J_{4'-5'}$ = 7.6 Hz, 1H, H-4'), 7.80 (d, $J_{6-7}$ = 8.5 Hz, 1H, H-6), 7.98 (s, 1H, H-4), 8.31 (d, $J_{6'-5'}$ = 7.8 Hz, 1H, H-6'), 8.41 (s, 1H, H-2').

**¹³C NMR (100 MHz, CDCl₃)** δ (ppm): 56.35 (O-CH₃), 107.06 (C-9), 117.20 (C-4), 118.65 (C-7), 123.95 (q, *J* = 272.2 Hz, C$_q$), 124.11 (q, *J* = 3.8 Hz, C-2'), 127.28 (q, *J* = 3.8 Hz, C-4'), 127.54 (C-6), 128.00 (C$_q$), 129.81 (C-5'), 130.30 (C-6'), 131.80 (q, *J* = 32.6 Hz, C-3'), 132.75 (C$_q$), 136.83 (C$_q$), 145.16 (C$_q$), 159.09 (C$_q$), 160.77 (C$_q$), 166.91 (C$_q$), 188.15 (C$_q$).

**¹⁹F NMR (376 MHz, CDCl₃)** δ (ppm): -62.63 (s).

**MS**: [M + H]⁺ 357.2 m/z

**Mp**: 216.3°C

**Anal. calcd for** $C_{19}H_{11}F_3N_2O_2$: C, 64.05%; H, 3.11%; N, 7.86%.

**Found**: C, 64.19%; H, 3.21 %; N, 7.73%.

d) Synthesis of 3-methyl-8-*meta*-chlorobenzyloxy-5*H*-indeno[1,2-*c*]pyridazin-5-one (**30a.III**, performed by Fabrice Camus, Biological Structural Chemistry Laboratory, FUNDP, Belgium)

Silver oxide (2.320 g, 10.01 mmol) was added at room temperature to a solution of 3-methyl-8-ol-5*H*-indeno[1,2-*c*]pyridazin-5-one (**29.III**) (0.500 g, 2.36 mmol) and 1-(bromomethyl)-3-chlorobenzene (2.050 g, 9.98 mmol) in anhydrous DMF (10 mL). The mixture was stirred for 4 h. The crude suspension was then filtered and washed with ethyl acetate (30 mL). The filtrate was evaporated and the crude product was purified by column chromatography (ethyl acetate 100%).

*Yield:* 15%

*Physical and spectral characteristics:*

- **Chemical Formula**     $C_{19}H_{13}ClN_2O_2$
- **M.W. (g/mol)**         336.77
- **Aspect**               Yellow solid
- **TLC** (DCM/AcOEt: 3/1)  **R$_f$** = 0.32
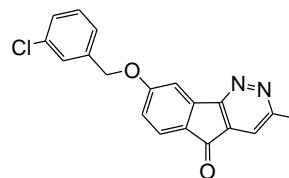


**$^1$H NMR (400 MHz, CDCl$_3$)** δ (ppm): 2.78 (s, 3H, CH$_3$), 5.22 (s, 2H, O-CH$_2$), 7.05 (dd, $J_{7-9}$ = 2.3 Hz, $J_{7-6}$ = 8.5 Hz, 1H, H-7), 7.31-7.35 (m, 3H, ArH), 7.40 (s, 1H, H-4), 7.46 (s, 1H, ArH), 7.67 (d, $J_{9-7}$ = 2.3 Hz, 1H, H-9), 7.77 (d, $J_{6-7}$ = 8.5 Hz, 1H, H-6).

**$^{13}$C NMR (100 MHz, CDCl$_3$)** δ (ppm): 23.05 (CH$_3$), 69.97 (O-CH$_2$), 107.36 (C-9), 119.04 (C-7), 120.23 (C-4), 125.54 (C-ArH), 127.32 (C-6), 127.59 (C-ArH), 128.21 (C$_q$), 128.74 (C-ArH), 130.19 (C-ArH), 131.89 (C$_q$), 134.86 (C$_q$), 137.58 (C$_q$), 145.71 (C$_q$), 159.70 (C$_q$), 161.52 (C$_q$), 165.42 (C$_q$), 188.75 (C$_q$).

**MS**: [M + H]$^+$ 337.0 m/z

**Mp**: 145°C

**Anal. calcd for** $C_{19}H_{13}ClN_2O_2$: C, 67.76%; H, 3.89%; N, 8.32%.

**Found**: C, 66.90%; H, 3.96%; N, 7.86%.

e) Synthesis of 3-methyl-8-*meta*-methylbenzyloxy-5*H*-indeno[1,2-*c*]pyridazin-5-one (**30b.III**, performed by Fabrice Camus, Biological Structural Chemistry Laboratory, FUNDP, Belgium)

The title compound was prepared and purified according to procedure described for **30a.III** from 3-methyl-8-ol-5*H*-indeno[1,2-*c*]pyridazin-5-one (**29.III**) (0.500 g, 2.36 mmol), silver oxide (2.320 g, 10.01 mmol) and 1-(bromomethyl)-3-methylbenzene (2.320 g, 12.54 mmol).

*Yield:* 6%

*Physical and spectral characteristics:*

- **Chemical Formula** $C_{20}H_{16}N_2O_2$
- **M.W. (g/mol)** 316.35
- **Aspect** Yellow solid
- **TLC** (DCM/AcOEt: 3/1) **$R_f$ = 0.42**
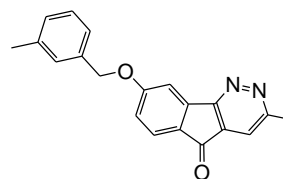
**$^1$H NMR (400 MHz, CDCl$_3$)** δ (ppm): 2.39 (s, 3H, CH$_3$), 2.78 (s, 3H, CH$_3$), 5.21 (s, 2H, O-CH$_2$), 7.06 (dd, $J_{7-9}$ = 2.3 Hz, $J_{7-6}$ = 8.5 Hz, 1H, H-7), 7.17-7.32 (m, 4H, ArH), 7.40 (s, 1H, H-4), 7.69 (d, $J_{9-7}$ = 2.3 Hz, 1H, H-9), 7.76 (d, $J_{6-7}$ = 8.5 Hz, 1H, H-6).

**$^{13}$C NMR (100 MHz, CDCl$_3$)** δ (ppm): 21.52 (CH$_3$), 23.05 (CH$_3$), 71.01 (O-CH$_2$), 107.46 (C-9), 119.07 (C-7), 120.17 (C-4), 124.80 (C-ArH), 127.27 (C-6), 127.96 (C$_q$), 128.42 (C-ArH), 128.80 (C-ArH), 129.39 (C-ArH), 131.97 (C$_q$), 135.40 (C$_q$), 138.65 (C$_q$), 145.64 (C$_q$), 159.80 (C$_q$), 161.49 (C$_q$), 165.86 (C$_q$), 188.75 (C$_q$).

**MS**: [M + H]$^+$ 317.1 m/z

**Mp**: 146°C

**Anal. calcd for** $C_{20}H_{16}N_2O_2$: C, 75.93%; H, 5.10%; N, 8.86%.

**Found**: C, 75.05%; H, 4.97%; N, 8.44%.

## 1.5 Experimental details for the compounds studied by X-ray crystallography

| | 1.III | 2e.III | 2f.III |
|---|---|---|---|
| **Crystal data** | | | |
| Chemical Formula | $C_{12}H_{15}BrN_2O_3$ | $C_{16}H_{15}F_3N_2O$ | $C_{19}H_{22}N_2O$ |
| Formula weight | 315.16 | 308.30 | 294.21 |
| Crystal system | Orthorhombic | Trigonal | Trigonal |
| Space group | Pnma | $R\bar{3}$ | $R\bar{3}$ |
| a (Å) | 13.320(3) | 25.400(2) | 25.698(2) |
| b (Å) | 6.679(3) | 25.400(2) | 25.698(2) |
| c (Å) | 13.895(4) | 12.703(1) | 13.360(1) |
| α (°) | 90.00 | 90.00 | 90.00 |
| β (°) | 90.00 | 90.00 | 90.00 |
| γ (°) | 90.00 | 120.00 | 120.00 |
| V (Å³) | 1236.2(7) | 7097.5(10) | 7640.8(9) |
| Z | 4 | 18 | 18 |
| $\mu$ (mm$^{-1}$) | 3.316 | 0.106 | 0.072 |
| $D_{calc}$ (g.cm$^{-3}$) | 1.591 | 1.298 | 1.152 |
| $F$(000) | 596 | 2880 | 2844 |
| Crystal Size (mm) | 0.13 x 0.17 x 0.40 | 0.14 x 0.20 x 0.30 | 0.10 x 0.10 x 0.30 |
| | | | |
| **Data collection** | | | |
| Temperature (K) | 293 | 293 | 293 |
| Radiation (Å) | Mo Kα 0.71073 Å | Mo Kα 0.71073 Å | Mo Kα 0.71073 Å |
| θ Min-Max (°) | 3.3, 32.6 | 3.3, 28.0 | 3.2, 32.7 |
| No. of measured reflections | 6084 | 9332 | 11109 |
| No. of independent reflections | 2236 | 3321 | 5628 |
| $R_{int}$ | 0.0227 | 0.0273 | 0.0423 |
| No. of observed reflections (I>2σ(I)) | 1220 | 1639 | 1666 |
| | | | |
| **Refinement** | | | |
| Refinement on | F² | F² | F² |
| No. of reflections used in refinement | 2236 | 3321 | 5628 |
| No. of parameters used | 104 | 208 | 206 |
| R[F²>2σ (F²)] | 0.0302 | 0.0617 | 0.0642 |
| wR[F²] | 0.0757 | 0.1810 | 0.2066 |
| S | 0.814 | 0.978 | 0.785 |

|                                      | **2g.III**            | **3.III**             | **4.III**             |
|--------------------------------------|-----------------------|-----------------------|-----------------------|
| **Crystal data**                     |                       |                       |                       |
| Chemical Formula                     | $C_{19}H_{16}N_2O$    | $C_{26}H_{23}BrN_2O$  | $C_{26}H_{22}N_2O$    |
| Formula weight                       | 288.34                | 459.37                | 378.46                |
| Crystal system                       | Trigonal              | Monoclinic            | Triclinic             |
| Space group                          | $R\bar{3}$            | P21/c                 | P-1                   |
| a (Å)                                | 25.588(2)             | 10.189(1)             | 5.410(1)              |
| b (Å)                                | 25.588(2)             | 29.543(1)             | 9.667(2)              |
| c (Å)                                | 12.844(1)             | 14.822(1)             | 19.125(3)             |
| α (°)                                | 90.00                 | 90.00                 | 87.44(1)              |
| β (°)                                | 90.00                 | 103.08(2)             | 88.83(1)              |
| γ (°)                                | 120.00                | 90.00                 | 87.34(1)              |
| V (Å³)                               | 7282.9(10)            | 4345.6(4)             | 998.0(3)              |
| Z                                    | 18                    | 8                     | 2                     |
| $\mu$ (mm$^{-1}$)                    | 0.074                 | 1.912                 | 0.077                 |
| $D_{calc}$ (g.cm$^{-3}$)             | 1.183                 | 1.404                 | 1.259                 |
| $F$(000)                             | 2736                  | 1888                  | 400                   |
| Crystal Size (mm)                    | 0.15 x 0.20 x 0.30    | 0.10 x 0.18 x 0.25    | 0.09 x 0.14 x 0.38    |
|                                      |                       |                       |                       |
| **Data collection**                  |                       |                       |                       |
| Temperature (K)                      | 293                   | 293                   | 293                   |
| Radiation (Å)                        | Mo Kα 0.71073 Å       | Mo Kα 0.71073 Å       | Mo Kα 0.71073 Å       |
| θ Min-Max (°)                        | 3.2, 32.5             | 3.4, 28.0             | 2.9, 27.9             |
| No. of measured reflections          | 10872                 | 26126                 | 10380                 |
| No. of independent reflections       | 5366                  | 9093                  | 4128                  |
| $R_{int}$                            | 0.0311                | 0.0772                | 0.0567                |
| No. of observed reflections (I>2σ(I))| 1239                  | 2591                  | 2009                  |
|                                      |                       |                       |                       |
| **Refinement**                       |                       |                       |                       |
| Refinement on                        | F²                    | F²                    | F²                    |
| No. of reflections used in refinement| 5366                  | 9093                  | 4128                  |
| No. of parameters used               | 182                   | 526                   | 262                   |
| R[F²>2σ (F²)]                        | 0.0765                | 0.0489                | 0.0532                |
| wR[F²]                               | 0.3128                | 0.1519                | 0.1386                |
| S                                    | 0.779                 | 0.584                 | 0.881                 |

| | 5.III | 28a.III | 28b.III |
|---|---|---|---|
| **Crystal data** | | | |
| Chemical Formula | $C_{33}H_{29}BrN_2O$ | $C_{22}H_{14}F_6N_2O_2$ | $C_{25}H_{15}F_3N_2O_2$ |
| Formula weight | 549.49 | 452.35 | 432.39 |
| Crystal system | Monoclinic | Monoclinic | Monoclinic |
| Space group | P21/c | $C2_C$ | $C_C$ |
| a (Å) | 10.073(3) | 9.765(1) | 6.365(1) |
| b (Å) | 12.673(6) | 14.631(1) | 40.848(3) |
| c (Å) | 22.987(1) | 27.968(4) | 7.600(1) |
| α (°) | 90.00 | 90.00 | 90.00 |
| β (°) | 110.10(4) | 96.96(1) | 94.96(1) |
| γ (°) | 90.00 | 90.00 | 90.00 |
| V (Å³) | 2755.8(2) | 3966.5(8) | 1968.6(4) |
| Z | 4 | 8 | 4 |
| $\mu$ (mm$^{-1}$) | 1.520 | 0.136 | 0.113 |
| $D_{calc}$ (g.cm$^{-3}$) | 1.324 | 1.515 | 1.459 |
| *F*(000) | 1136 | 1840 | 888 |
| Crystal Size (mm) | 0.06 x 0.07 x 0.30 | 0.06 x 0.19 x 0.40 | 0.02 x 0.25 x 0.40 |
| | | | |
| **Data collection** | | | |
| Temperature (K) | 293 | 293 | 293 |
| Radiation (Å) | Mo Kα 0.71073 Å | Mo Kα 0.71073 Å | Mo Kα 0.71073 Å |
| θ Min-Max (°) | 3.2, 28.0 | 3.0, 30.6 | 3.3, 30.7 |
| No. of measured reflections | 19358 | 12585 | 12165 |
| No. of independent reflections | 5849 | 5461 | 2869 |
| $R_{int}$ | 0.0892 | 0.0549 | 0.0351 |
| No. of observed reflections (I>2σ(I)) | 2080 | 1690 | 1570 |
| | | | |
| **Refinement** | | | |
| Refinement on | F² | F² | F² |
| No. of reflections used in refinement | 5849 | 5461 | 2869 |
| No. of parameters used | 335 | 299 | 299 |
| R[F²>2σ (F²)] | 0.0474 | 0.0611 | 0.0627 |
| wR[F²] | 0.1024 | 0.1768 | 0.1708 |
| S | 0.769 | 0.854 | 0.964 |

|  | **30a.III** | **46.III** | **47.III** |
|---|---|---|---|
| **Crystal data** | | | |
| Chemical Formula | $C_{19}H_{13}ClN_2O_2$ | $C_{15}H_{13}NO$ | $C_{16}H_{15}NO$ |
| Formula weight | 336.76 | 223.27 | 237.29 |
| Crystal system | Orthorhombic | Hexagonal | Monoclinic |
| Space group | $P2_12_12_1$ | $R\bar{3}$ | $P2_1$ |
| a (Å) | 4.021(1) | 26.670(2) | 6.509(2) |
| b (Å) | 9.681(2) | 26.670(2) | 7.918(3) |
| c (Å) | 39.832(5) | 9.696(1) | 12.348(5) |
| α (°) | 90.00 | 90.00 | 90.00 |
| β (°) | 90.00 | 90.00 | 93.85(4) |
| γ (°) | 90.00 | 120.00 | 90.00 |
| V (Å³) | 1550.6(5) | 5972.5(7) | 635.0(4) |
| Z | 4 | 6 | 2 |
| $\mu$ (mm$^{-1}$) | 0.260 | 0.077 | 0.606 |
| $D_{calc}$ (g.cm$^{-3}$) | 1.443 | 1.171 | 1.241 |
| $F(000)$ | 696 | 2220 | 252 |
| Crystal Size (mm) | 0.10 x 0.15 x 0.30 | 0.07 x 0.08 x 0.50 | 0.01 x 0.15 x 0.45 |
| | | | |
| **Data collection** | | | |
| Temperature (K) | 293 | 293 | 293 |
| Radiation (Å) | Mo Kα 0.71073 Å | Mo Kα 0.71073 Å | Cu Kα 1.54178 Å |
| θ Min-Max (°) | 3.3, 32.5 | 3.8, 32.5 | 3.6, 67.7 |
| No. of measured reflections | 7090 | 9690 | 2966 |
| No. of independent reflections | 4895 | 4295 | 1695 |
| $R_{int}$ | 0.0370 | 0.0415 | 0.0192 |
| No. of observed reflections (I>2σ(I)) | 2797 | 1065 | 1603 |
| | | | |
| **Refinement** | | | |
| Refinement on | F² | F² | F² |
| No. of reflections used in refinement | 4895 | 4295 | 1695 |
| No. of parameters used | 218 | 209 | 164 |
| R[F²>2σ (F²)] | 0.0841 | 0.0972 | 0.0354 |
| wR[F²] | 0.2093 | 0.3660 | 0.1103 |
| S | 1.115 | 0.840 | 1.159 |

# 2. MOLECULAR MODELING

The structures of ligands are built and geometry minimized at physiological pH using the CHARMm force field implemented in Discovery studio® 2.5 (Accelrys Software Inc., San Diego, USA) software. Docking of ligands in the active site of the hMAO-A, hMAO-B and hIDO structures obtained through X-ray crystallography (2Z5X [3], 2V5Z [4] and 2D0T [144], respectively), was carried out using GOLD (version 3.2) software (Cambridge Crystallographic Data Centre, Cambridge, U.K.).

The interaction sphere in the docking was centered on the N5 atom of the flavin (FAD) in the catalytic site of the protein (**MAO-A** and **–B**) and delimited by a 20Å radius. Seven water molecules which occupy the space between harmine (**3.I**) and FAD were conserved from X-ray crystallography (2Z5X.pdb) into the MAO-A model. Into the MAO-B model, three conserved water molecules have been identified, which are buried in the vicinity of FAD and proved to be important for docking simulation of MAO-B selective ligand [73]. So these water molecules are kept inside the binding site as an integral part of the protein structure during the whole computational procedure.

The interaction sphere in the docking was centered on the heme in the catalytic site of **IDO** and delimited by a 7Å radius. In addition to PIM (**37.I**), there are two molecules of CHES bound at the entrance of the binding site which were removed for docking studies. A total of twenty-five docking solutions were generated using GOLD (version 3.2) software. For the 25 genetic algorithm (GA) runs performed, a total of 100 000 genetic operations were carried out on five islands, each containing 100 individuals. The niche size was set to 2, and the value for the selection pressure was set to 1.1. Genetic operator weights for crossover, mutation, and migration were set to 95, 95 and 10, respectively. The scoring function used to rank the docking was Goldscore. The binding mode of ligands on hMAO-A, –B and hIDO was selected from Goldscore and/or as a plausible solution in agreement with literature.

# 3. MOLECULAR ELECTROSTATIC POTENTIAL

The starting geometry for compound **30a.III** was obtained from X-ray crystallography. The geometry of the system was first optimized at the PBE1PBE level using the 6-311G** basis sets. Secondly, using the Gaussian09 program, a first cube file is generated for the total

electron density and then a second cube file is produced for the electrostatic potential. Mapping of the MEP onto the molecular surface was performed with Gaussview 5.0.8.

## 4. ENZYMATIC ASSAYS

### 4.1 MAO-A and –B

Inhibition of hMAO-A and –B was evaluated according to a published two steps methodology [194]. The MAO enzymes were produced from insect cells infected with recombinant baculovirus containing complementary DNA inserts for hMAO-A and –B (Sigma–Aldrich, M7316 and M7441, respectively). The recombinant MAO enzymes were provided under microsomes at a protein concentration of 5 mg.mL$^{-1}$.

The MAO-Glo$^{TM}$ two-step bioluminescent assay from Promega Corporation was performed in 96-wells plates at 37°C. Recombinant MAO enzyme (25.0 µL, final concentration of 0.5 U.mg$^{-1}$) were first incubated with the test compound (12.5 µL) for 2.5 min. Then, the substrate (12.5 µL, final concentration of 120 µM and 15 µM for MAO-A and –B, respectively) was added to the mixture. Finally, after 1 h of reaction, 50.0 µL of luciferin detection reaction (LDR) was added to the wells. The luminescent signal was measured 20 min after the addition of the LDR with a 96-wells luminometer Fluoroskan FL (Thermo Fisher Scientific). Test compounds were assessed in triplicate for each concentration on hMAO-A and –B. IC$_{50}$ and $K_i$ values of the most active compounds were evaluated. DMSO (12.5% final concentration) was used as cosolvant to dissolve the test compounds in buffer (100 mM Hepes (pH 7.5) and 5% glycerol). Inhibition percentages at each concentration were calculated as follows: I (%) = 100 x {1 − (luminescent signal with test compound/luminescent signal without test compound)}. The inhibition percentages were plotted against the logarithms of the compound molar concentrations. The IC$_{50}$ values were calculated from normalized sigmoidal dose-response non-linear regression curves using the GraphPad Prism 5.01 software and were expressed as mean ± SD from triplicate experiments. $K_i$ values were determined from the IC$_{50}$ values using the Cheng–Prusoff equation: $K_i = IC_{50}/(1 + [S]/K_m)$ [192]. The aminopropylether analogue of methyl ester luciferin exhibited $K_m$ values of 116.1 µM and 14.6 µM for MAO-A and MAO-B, respectively. $K_i$ values were expressed as mean with 95% confidence intervals in brackets. Lineweaver-Burk plots on MAO-B by **30a.III**

208

were obtained from incubations at four substrate concentrations (5, 15, 50 and 75 μM), without or with three different inhibitor concentrations (2, 5 and 15 μM). The inverse values of the reaction velocities were then represented as a function of the inverse value of substrate concentration. $K_i$ value was calculated from the x-axis intercept (y = 0) using the equation $1/[S] = -1/(K_m \cdot (1 + [I]/K_i))$ where $K_m$ was obtained in the absence of inhibitor I [223].

## 4.2 IDO

The IDO inhibition assay was performed as described by Takikawa et al [198] with some modifications. It is based on the conversion of L-tryptophan to *N*-formylkynurenine, followed by hydrolysis to produce kynurenine. The measurement of IDO activity in this method relies on quantifying the amount of kynurenine produced in the assay through an indirect mean. It relies on absorption of the imine (Schiff base) produced by the reaction of the aromatic amino group of kynurenine with *para*-dimethylaminobenzaldehyde (p-DMAB) at 490 nm. The measurements are carried out in 96-wells plates at 37°C.

Plasmid was obtained from Van Den Eynde's team of the UCL university (Woluwe-Saint-Lambert, Belgium). The recombinant plasmid, phIDO, encodes a histidine tag at the N-terminus of IDO. *Escherichia coli* strain BL21 (DE3) (Invitrogen) was used for overexpression of IDO and transformed with the phIDO plasmid. The enzyme was purified by IMAC using $Ni^{2+}$ as a ligand and an IMAC Hitrap column (GE Healthcare).

Briefly, the reaction mixture (200.0 μL) contains a premix solution (100.0 μL of a solution containing ascorbic acid (20 mM) and methylene blue (17 μM) in potassium phosphate buffer (50 mM, pH 6.5)), potassium phosphate buffer (60.0 μL, 50 mM, pH 6.5), L-tryptophan (10.0 μL, 2 mM), hIDO (20.0 μL, 50 μg.mL$^{-1}$) and the inhibitor dissolved in DMSO (10.0 μL, 25 μM final concentration).

The reaction was initiated by the addition of the substrate to the premix mixture maintained at 37°C. After 10 min, the reaction was stopped by addition of 30% (w/v) trichloroacetic acid (40.0 μL). To convert *N*-formylkynurenine to kynurenine, the reaction was incubated at 37°C for 30 min. Lastly, 100.0 μL of reaction mixture were transferred to 100.0 μL of a solution of p-DMAB 2% in a 96-wells plate to form a yellow schiff base. So, the absorption of the Schiff base is detected at $\lambda = 490$ nm with a 96-wells microplate absorbance reader (BIO-RAD). Test compounds were assessed in triplicate for each concentration on hIDO. The inhibitory

percentage was calculated for each compound as follows: I (%) = 100 x {1 − (absorbance signal with test compound/absorbance signal without test compound)}. The data were expressed as mean ± SD from triplicate experiments.

## 4.3 LSD1

The LSD1 inhibition assay was performed as described by Cayman's LSD1 inhibitor screening assay (Cayman) with some modifications. The assay is based on the multistep enzymatic reaction in which LSD1 first produces $H_2O_2$ during the demethylation of the substrate peptide. In the presence of horseradish peroxidase (HRP), $H_2O_2$ reacts with ADHP (10-acetyl-3,7-dihydroxyphenoxazine) to produce the highly fluorescent compound resorufin. The measurement of LSD1 activity is quantified by the amount of resorufin produced which is detected by fluorescence ($\lambda_{ex}$ 535 nm; $\lambda_{em}$ 595 nm). The measurements are carried out in a black 96-wells plate at 37°C.

Briefly, the reaction mixture (200.0 µL) contains a buffer solution (105.0 µL, 50 mM Hepes, pH 7.5), HRP (20.0 µL), ADHP (10.0 µL), recombinant hLSD1 (20.0 µL), LSD1 peptide (20.0 µL, 1 mM) and the test compound dissolved in DMSO (25.0 µL, final DMSO percentage of 12.5%).

The reaction was initiated by the addition of the substrate peptide at 37 °C. After stirring, the fluorescent signal of resorufin was detected for 30 min at 37°C by measuring emited fluorescence ($\lambda_{ex}$ 535 nm; $\lambda_{em}$ 595 nm) with a 96-wells Beckman Coulter DTX 880 Multimode Detector. Test compounds were assessed in triplicate for each concentration on hLSD1. $IC_{50}$ value of the most active compound was evaluated. Inhibition percentages at each concentration were calculated as follows: I (%) = 100 x {1 − (fluorescent signal with test compound/fluorescent signal without test compound)}. The inhibition percentages were plotted against the logarithms of the compound molar concentrations. The $IC_{50}$ value was calculated from normalized sigmoidal dose-response non-linear regression curve using the GraphPad Prism 5.01 software and was expressed as mean ± SD from triplicate experiments.

# REFERENCES

[1] N. Gokhan-Kelekci, S. Koyunoglu, S. Yabanoglu, K. Yelekci, O. Ozgen, G. Ucar, K. Erol, E. Kendi, A. Yesilada, New pyrazoline bearing 4(3*H*)-quinazolinone inhibitors of monoamine oxidase: synthesis, biological evaluation, and structural determinants of MAO-A and MAO-B selectivity, Bioorg. Med. Chem. 17 (2009) 675-689.

[2] D.E. Edmondson, C. Binda, J. Wang, A.K. Upadhyay, A. Mattevi, Molecular and mechanistic properties of the membrane-bound mitochondrial monoamine oxidases, Biochemistry 48 (2009) 4220-4230.

[3] S.Y. Son, J. Ma, Y. Kondou, M. Yoshimura, E. Yamashita, T. Tsukihara, Structure of human monoamine oxidase A at 2.2-A resolution: the control of opening the entry for substrates/inhibitors, Proc. Natl. Acad. Sci. U.S.A. 105 (2008) 5739-5744.

[4] C. Binda, J. Wang, L. Pisani, C. Caccia, A. Carotti, P. Salvati, D.E. Edmondson, A. Mattevi, Structures of human monoamine oxidase B complexes with selective noncovalent inhibitors: safinamide and coumarin analogs, J. Med. Chem. 50 (2007) 5848-5852.

[5] F. Chimenti, D. Secci, A. Bolasco, P. Chimenti, B. Bizzarri, A. Granese, S. Carradori, M. Yanez, F. Orallo, F. Ortuso, S. Alcaro, Synthesis, molecular modeling, and selective inhibitory activity against human monoamine oxidases of 3-carboxamido-7-substituted coumarins, J. Med. Chem. 52 (2009) 1935-1942.

[6] W. Weyler, Y.P. Hsu, X.O. Breakefield, Biochemistry and genetics of monoamine oxidase, Pharmacol. Ther. 47 (1990) 391-417.

[7] F. Ooms, Rational approach of the reversible inhibition of type A and B MAO. Design and synthesis of original 5*H*-indeno[1,2-*c*]pyridazin-5-one derivatives, Presses universitaires de Namur (2000).

[8] D.E. Edmondson, A. Mattevi, C. Binda, M. Li, F. Hubalek, Structure and mechanism of monoamine oxidase, Curr. Med. Chem. 11 (2004) 1983-1993.

[9] M. Bortolato, K. Chen, J.C. Shih, Monoamine oxidase inactivation: from pathophysiology to therapeutics, Adv. Drug Deliv. Rev. 60 (2008) 1527-1533.

[10] M.B. Youdim, D. Edmondson, K.F. Tipton, The therapeutic potential of monoamine oxidase inhibitors, Nat. Rev. Neurosci. 7 (2006) 295-309.

[11] H.L. White, A.T. Glassman, Multiple binding sites of human brain and liver monoamine oxidase: substrate specificities, selective inhibitions, and attempts to separate enzyme forms, J. Neurochem. 29 (1977) 987-997.

[12] P.L. Dostert, M. Strolin Benedetti, K.F. Tipton, Interactions of monoamine oxidase with substrates and inhibitors, Med. Res. Rev. 9 (1989) 45-89.

[13] H. Blaschko, Oxidation of tertiary amines by monoamine oxidases, J. Pharm. Pharmacol. 41 (1989) 664.

[14] L. De Colibus, M. Li, C. Binda, A. Lustig, D.E. Edmondson, A. Mattevi, Three-dimensional structure of human monoamine oxidase A (MAO A): relation to the structures of rat MAO A and human MAO B, Proc. Natl. Acad. Sci. U.S.A. 102 (2005) 12684-12689.

[15] C. Binda, P. Newton-Vinson, F. Hubalek, D.E. Edmondson, A. Mattevi, Structure of human monoamine oxidase B, a drug target for the treatment of neurological disorders, Nat. Struct. biol. 9 (2002) 22-26.

[16] C. Binda, F. Hubalek, M. Li, D.E. Edmondson, A. Mattevi, Crystal structure of human monoamine oxidase B, a drug target enzyme monotopically inserted into the mitochondrial outer membrane, FEBS Lett. 564 (2004) 225-228.

[17] C. Binda, M. Li, F. Hubalek, N. Restelli, D.E. Edmondson, A. Mattevi, Insights into the mode of inhibition of human mitochondrial monoamine oxidase B from high-resolution crystal structures, Proc. Natl. Acad. Sci. U.S.A. 100 (2003) 9750-9755.

[18] J.N. Sachs, D.M. Engelman, Introduction to the membrane protein reviews: the interplay of structure, dynamics, and environment in membrane protein function, Annu. Rev. Biochem. 75 (2006) 707-712.

[19] A.K. Upadhyay, P.P. Borbat, J. Wang, J.H. Freed, D.E. Edmondson, Determination of the oligomeric states of human and rat monoamine oxidases in the outer mitochondrial membrane and octyl beta-D-glucopyranoside micelles using pulsed dipolar electron spin resonance spectroscopy, Biochemistry 47 (2008) 1554-1566.

[20] D.E. Edmondson, L. DeColibus, C. Binda, M. Li, A. Mattevi, New insights into the structures and functions of human monoamine oxidases A and B, J. Neural Transm. 114 (2007) 703-705.

[21] F. Hubalek, C. Binda, A. Khalil, M. Li, A. Mattevi, N. Castagnoli, D.E. Edmondson, Demonstration of isoleucine 199 as a structural determinant for the selective inhibition of human monoamine oxidase B by specific reversible inhibitors, J. Biol. Chem. 280 (2005) 15761-15766.

[22] D.E. Edmondson, C. Binda, A. Mattevi, Structural insights into the mechanism of amine oxidation by monoamine oxidases A and B, Arch. Biochem. Biophys. 464 (2007) 269-276.

[23] M. Li, Comparative mechanistic and structural approaches to investigate the membrane-bound enzymes monoamine oxidase A and monoamine oxidase B, Ph.D. Dissertation, Emory University, Atlanta, (2006).

[24] J.R. Miller, D.E. Edmondson, Structure-activity relationships in the oxidation of para-substituted benzylamine analogues by recombinant human liver monoamine oxidase A, Biochemistry 38 (1999) 13670-13683.

[25] F.G. Bordwell, J.-P. Cheng, A.V. Satish, C.L. Twyman, Acidities and homolytic bond dissociation energies (BDEs) of benzyl-type carbon-hydrogen bonds in sterically congested substrates, J. Org. Chem. 57 (1992) 6542–6546.

[26] P. Macheroux, S. Ghisla, C. Sanner, H. Ruterjans, F. Muller, Reduced flavin: NMR investigation of N5-H exchange mechanism, estimation of ionisation constants and assessment of properties as biological catalyst, BMC Biochem. 6 (2005) 26.

[27] W. Eisenreich, K. Kemter, A. Bacher, S.B. Mulrooney, C.H. Williams, Jr., F. Muller, $^{13}$C-, $^{15}$N- and $^{31}$P-NMR studies of oxidized and reduced low molecular mass thioredoxin reductase and some mutant proteins, Eur. J. Biochem. / FEBS 271 (2004) 1437-1452.

[28] X. Lu, H. Ji, R.B. Silverman, in: S. Chapman, R. Perham, N. Scrutton (Eds.), Flavins and Flavoproteins 2002, Agency for Scientific Publications, Berlin, 2002, pp. 817–830.

[29] S.S. Erdem, O. Karahan, I. Yildiz, K. Yelekci, A computational study on the amine-oxidation mechanism of monoamine oxidase: insight into the polar nucleophilic mechanism, Org. Biomol. Chem. 4 (2006) 646-658.

[30] C.W. Kay, H. El Mkami, G. Molla, L. Pollegioni, R.R. Ramsay, Characterization of the covalently bound anionic flavin radical in monoamine oxidase a by electron paramagnetic resonance, J. Am. Chem. Soc. 129 (2007) 16091-16097.

[31] A. Pletscher, The discovery of antidepressants: a winding path, Experientia 47 (1991) 4-8.

[32] S. Zisook, A clinical overview of monoamine oxidase inhibitors, Psychosomatics 26 (1985) 240-251.

[33] A.M. Cesura, A. Pletscher, The new generation of monoamine oxidase inhibitors, Prog. Drug Res. 38 (1992) 171-297.

[34] P. Gareri, U. Falconi, P. De Fazio, G. De Sarro, Conventional and new antidepressant drugs in the elderly, Prog. Neurobiol. 61 (2000) 353-396.

[35] L. Oreland, Monoamine oxidase, dopamine and Parkinson's disease, Acta Neurol. Scand. Suppl. 136 (1991) 60-65.

[36] T. Nagatsu, Isoquinoline neurotoxins in the brain and Parkinson's disease, Neurosci. Res. 29 (1997) 99-111.

[37] T.P. Singer, R.R. Ramsay, Mechanism of the neurotoxicity of MPTP. An update, FEBS Lett. 274 (1990) 1-8.

[38] D. van den Berg, K.R. Zoellner, M.O. Ogunrombi, S.F. Malan, G. Terre'Blanche, N. Castagnoli, J.J. Bergh, J.P. Petzer, Inhibition of monoamine oxidase B by selected benzimidazole and caffeine analogues, Bioorg. Med. Chem. 15 (2007) 3692-3702.

[39] C. Binda, F. Hubalek, M. Li, Y. Herzig, J. Sterling, D.E. Edmondson, A. Mattevi, Crystal structures of monoamine oxidase B in complex with four inhibitors of the N-propargylaminoindan class, J. Med. Chem. 47 (2004) 1767-1774.

[40] C. Caccia, R. Maj, M. Calabresi, S. Maestroni, L. Faravelli, L. Curatolo, P. Salvati, R.G. Fariello, Safinamide: from molecular targets to a new anti-Parkinson drug, Neurology 67 (2006) S18-23.

[41] J.N. Octave, The amyloid peptide and its precursor in Alzheimer's disease, Rev. Neurosci. 6 (1995) 287-316.

[42] H.P. Volz, C.H. Gleiter, Monoamine oxidase inhibitors. A perspective on their use in the elderly, Drugs aging 13 (1998) 341-355.

[43] J. Saura, J.M. Luque, A.M. Cesura, M. Da Prada, V. Chan-Palay, G. Huber, J. Loffler, J.G. Richards, Increased monoamine oxidase B activity in plaque-associated astrocytes of Alzheimer brains revealed by quantitative enzyme radioautography, Neuroscience 62 (1994) 15-30.

[44] Y. Avramovich-Tirosh, T. Amit, O. Bar-Am, H. Zheng, M. Fridkin, M.B. Youdim, Therapeutic targets and potential of the novel brain- permeable multifunctional iron chelator-monoamine oxidase inhibitor drug, M-30, for the treatment of Alzheimer's disease, J. Neurochem. 100 (2007) 490-502.

[45] S.V. Patel, P.N. Tariot, J. Asnis, L-Deprenyl augmentation of fluoxetine in a patient with Huntington's disease, Ann. Clin. Psychiatry 8 (1996) 23-26.

[46] J. Sivenius, T. Sarasoja, H. Aaltonen, E. Heinonen, O. Kilkku, K. Reinikainen, Selegiline treatment facilitates recovery after stroke, Neurorehabil. Neural Repair 15 (2001) 183-190.

[47] J. Knoll, (-)Deprenyl (Selegiline): past, present and future, Neurobiology 8 (2000) 179-199.

[48] H. Carageorgiou, A. Zarros, S. Tsakiris, Selegiline long-term effects on brain acetylcholinesterase, (Na+,K+)-ATPase activities, antioxidant status and learning performance of aged rats, Pharmacol. Res. 48 (2003) 245-251.

[49] A. Maurel, C. Hernandez, O. Kunduzova, G. Bompart, C. Cambon, A. Parini, B. Frances, Age-dependent increase in hydrogen peroxide production by cardiac monoamine oxidase A in rats, Am. J. Physiol. Heart Circ. Physiol. 284 (2003) H1460-1467.

[50] P. Bianchi, O. Kunduzova, E. Masini, C. Cambon, D. Bani, L. Raimondi, M.H. Seguelas, S. Nistri, W. Colucci, N. Leducq, A. Parini, Oxidative stress by monoamine oxidase mediates receptor-independent cardiomyocyte apoptosis by serotonin and postischemic myocardial injury, Circulation 112 (2005) 3297-3305.

[51] F. Gentili, N. Pizzinat, C. Ordener, S. Marchal-Victorion, A. Maurel, R. Hofmann, P. Renard, P. Delagrange, M. Pigini, A. Parini, M. Giannella, 3-[5-(4,5-dihydro-1$H$-imidazol-2-yl)-furan-2-yl]phenylamine (Amifuraline), a promising reversible and selective peripheral MAO-A inhibitor, J. Med. Chem. 49 (2006) 5578-5586.

[52] E.J. Houtsmuller, J.A. Thornton, M.L. Stitzer, Effects of selegiline (L-deprenyl) during smoking and short-term abstinence, Psychopharmacology 163 (2002) 213-220.

216

[53] I. Berlin, H.J. Aubin, A.M. Pedarriosse, A. Rames, S. Lancrenon, G. Lagrue, Lazabemide, a selective, reversible monoamine oxidase B inhibitor, as an aid to smoking cessation, Addiction 97 (2002) 1347-1354.

[54] I. Berlin, S. Said, O. Spreux-Varoquaux, J.M. Launay, R. Olivares, V. Millet, Y. Lecrubier, A.J. Puech, A reversible monoamine oxidase A inhibitor (moclobemide) facilitates smoking cessation and abstinence in heavy, dependent smokers, Clin. Pharmacol. Ther. 58 (1995) 444-452.

[55] T. Herraiz, C. Chaparro, Human monoamine oxidase is inhibited by tobacco smoke: beta-carboline alkaloids act as potent and reversible inhibitors, Biochem. Biophys. Res. Commun. 326 (2005) 378-386.

[56] S. Alcaro, A. Gaspar, F. Ortuso, N. Milhazes, F. Orallo, E. Uriarte, M. Yanez, F. Borges, Chromone-2- and -3-carboxylic acids inhibit differently monoamine oxidases A and B, Bioorg. Med. Chem. Lett. 20 (2010) 2709-2712.

[57] D. Balsa, E. Fernandez-Alvarez, K.F. Tipton, M. Unzeta, Inhibition of MAO by substituted tryptamine analogues, J. Neural Transm. Suppl. 32 (1990) 103-105.

[58] D. Balsa, E. Fernandez-Alverez, K.F. Tipton, M. Unzeta, Monoamine oxidase inhibitory potencies and selectivities of 2-[*N*-(2-propynyl)-aminomethyl]-1-methyl indole derivatives, Biochem. Soc. Trans. 19 (1991) 215-218.

[59] C. Fernández García, J.L. Marco, E. Fernández-Álvarez, Acetylenic and allenic derivatives of 2-(5-methoxy-1-methylindolyl) alkylamines: Synthesis and evaluation as selective inhibitors of the monoamine oxidases A and B, Eur. J. Med. Chem. 27 (1992) 909-918.

[60] J.A. Moron, M. Campillo, V. Perez, M. Unzeta, L. Pardo, Molecular determinants of MAO selectivity in a series of indolylmethylamine derivatives: biological activities, 3D-QSAR/CoMFA analysis, and computational simulation of ligand recognition, J. Med. Chem. 43 (2000) 1684-1691.

[61] G. La Regina, R. Silvestri, V. Gatti, A. Lavecchia, E. Novellino, O. Befani, P. Turini, E. Agostinelli, Synthesis, structure-activity relationships and molecular modeling studies of new indole inhibitors of monoamine oxidases A and B, Bioorg. Med. Chem. 16 (2008) 9729-9740.

[62] L.H. Prins, J.P. Petzer, S.F. Malan, Inhibition of monoamine oxidase by indole and benzofuran derivatives, Eur. J. Med. Chem. 45 (2010) 4458-4466.

[63] E.M. Van der Walt, E.M. Milczek, S.F. Malan, D.E. Edmondson, N. Castagnoli, Jr., J.J. Bergh, J.P. Petzer, Inhibition of monoamine oxidase by (*E*)-styrylisatin analogues, Bioorg. Med. Chem. Lett. 19 (2009) 2509-2513.

[64] C.I. Manley-King, J.J. Bergh, J.P. Petzer, Inhibition of monoamine oxidase by selected C5- and C6-substituted isatin analogues, Bioorg. Med. Chem. 19 (2011) 261-274.

[65] N. Eguchi, Y. Watanabe, K. Kawanishi, Y. Hashimoto, O. Hayaishi, Inhibition of indoleamine 2,3-dioxygenase and tryptophan 2,3-dioxygenase by beta-carboline and indole derivatives, Arch. Biochem. Biophys. 232 (1984) 602-609.

[66] T. Herraiz, C. Chaparro, Analysis of monoamine oxidase enzymatic activity by reversed-phase high performance liquid chromatography and inhibition by beta-carboline alkaloids occurring in foods and plants, J. Chromatogr. A 1120 (2006) 237-243.

[67] Y. Schott, M. Decker, H. Rommelspacher, J. Lehmann, 6-Hydroxy- and 6-methoxy-beta-carbolines as acetyl- and butyrylcholinesterase inhibitors, Bioorg. Med. Chem. Lett. 16 (2006) 5840-5843.

[68] N.S. Buckholtz, W.O. Boggan, Monoamine oxidase inhibition in brain and liver produced by beta-carbolines: structure-activity relationships and substrate specificity, Biochem. Pharmacol. 26 (1977) 1991-1996.

[69] H. Kim, S.O. Sablin, R.R. Ramsay, Inhibition of monoamine oxidase A by beta-carboline derivatives, Arch. Biochem. Biophys. 337 (1997) 137-142.

[70] T. Herraiz, C. Chaparro, Human monoamine oxidase enzyme inhibition by coffee and beta-carbolines norharman and harman isolated from coffee, Life Sci. 78 (2006) 795-802.

[71] S. Kneubuhler, V. Carta, C. Altomare, A. Carotti, B. Testa, Synthesis and monoamine oxidase inhibitory activity of 3-substituted 5*H*-indeno[1,2-*c*]pyridazines, Helv. Chim. Acta 76 (1993) 1956-1963.

[72] S. Kneubuhler, U. Thull, C. Altomare, V. Carta, P. Gaillard, P.A. Carrupt, A. Carotti, B. Testa, Inhibition of monoamine oxidase-B by 5*H*-indeno[1,2-*c*]pyridazines: biological activities, quantitative structure-activity relationships (QSARs) and 3D-QSARs, J. Med. Chem. 38 (1995) 3874-3883.

[73] L. Novaroli, A. Daina, E. Favre, J. Bravo, A. Carotti, F. Leonetti, M. Catto, P.A. Carrupt, M. Reist, Impact of species-dependent differences on screening, design, and development of MAO B inhibitors, J. Med. Chem. 49 (2006) 6264-6272.

[74] R. Frederick, W. Dumont, F. Ooms, L. Aschenbach, C.J. Van der Schyf, N. Castagnoli, J. Wouters, A. Krief, Synthesis, structural reassignment, and biological activity of type B MAO inhibitors based on the 5*H*-indeno[1,2-*c*]pyridazin-5-one core, J. Med. Chem. 49 (2006) 3743-3747.

[75] F. Ooms, R. Frederick, F. Durant, J.P. Petzer, N. Castagnoli, C.J. Van der Schyf, J. Wouters, Rational approaches towards reversible inhibition of type B monoamine oxidase. Design and evaluation of a novel 5*H*-indeno[1,2-*c*]pyridazin-5-one derivative, Bioorg. Med. Chem. Lett. 13 (2003) 69-73.

[76] A. Carotti, M. Catto, F. Leonetti, F. Campagna, R. Soto-Otero, E. Mendez-Alvarez, U. Thull, B. Testa, C. Altomare, Synthesis and monoamine oxidase inhibitory activity of new pyridazine-, pyrimidine- and 1,2,4-triazine-containing tricyclic derivatives, J. Med. Chem. 50 (2007) 5364-5371.

218

[77] C. Gnerre, M. Catto, F. Leonetti, P. Weber, P.A. Carrupt, C. Altomare, A. Carotti, B. Testa, Inhibition of monoamine oxidases by functionalized coumarin derivatives: biological activities, QSARs, and 3D-QSARs, J. Med. Chem. 43 (2000) 4747-4758.

[78] F. Chimenti, D. Secci, A. Bolasco, P. Chimenti, A. Granese, O. Befani, P. Turini, S. Alcaro, F. Ortuso, Inhibition of monoamine oxidases by coumarin-3-acyl derivatives: biological activity and computational study, Bioorg. Med. Chem. Lett. 14 (2004) 3697-3703.

[79] M. Catto, O. Nicolotti, F. Leonetti, A. Carotti, A.D. Favia, R. Soto-Otero, E. Mendez-Alvarez, A. Carotti, Structural insights into monoamine oxidase inhibitory potency and selectivity of 7-substituted coumarins from ligand- and target-based approaches, J. Med. Chem. 49 (2006) 4912-4925.

[80] F. Chimenti, D. Secci, A. Bolasco, P. Chimenti, A. Granese, S. Carradori, O. Befani, P. Turini, S. Alcaro, F. Ortuso, Synthesis, molecular modeling studies, and selective inhibitory activity against monoamine oxidase of *N*,*N*'-bis[2-oxo-2*H*-benzopyran]-3-carboxamides, Bioorg. Med. Chem. Lett. 16 (2006) 4135-4140.

[81] L. Santana, H. Gonzalez-Diaz, E. Quezada, E. Uriarte, M. Yanez, D. Vina, F. Orallo, Quantitative structure-activity relationship and complex network approach to monoamine oxidase A and B inhibitors, J. Med. Chem. 51 (2008) 6740-6751.

[82] M.J. Matos, D. Vina, C. Picciau, F. Orallo, L. Santana, E. Uriarte, Synthesis and evaluation of 6-methyl-3-phenylcoumarins as potent and selective MAO-B inhibitors, Bioorg. Med. Chem. Lett. 19 (2009) 5053-5055.

[83] L. Pisani, G. Muncipinto, T.F. Miscioscia, O. Nicolotti, F. Leonetti, M. Catto, C. Caccia, P. Salvati, R. Soto-Otero, E. Mendez-Alvarez, C. Passeleu, A. Carotti, Discovery of a novel class of potent coumarin monoamine oxidase B inhibitors: development and biopharmacological profiling of 7-[(3-chlorobenzyl)oxy]-4-[(methylamino)methyl]-2*H*-chromen-2-one methanesulfonate (NW-1772) as a highly potent, selective, reversible, and orally active monoamine oxidase B inhibitor, J. Med. Chem. 52 (2009) 6685-6706.

[84] L. Novaroli, M. Reist, E. Favre, A. Carotti, M. Catto, P.A. Carrupt, Human recombinant monoamine oxidase B as reliable and efficient enzyme source for inhibitor screening, Bioorg. Med. Chem. 13 (2005) 6212-6217.

[85] F. Chimenti, R. Fioravanti, A. Bolasco, P. Chimenti, D. Secci, F. Rossi, M. Yanez, F. Orallo, F. Ortuso, S. Alcaro, R. Cirilli, R. Ferretti, M.L. Sanna, A new series of flavones, thioflavones, and flavanones as selective monoamine oxidase-B inhibitors, Bioorg. Med. Chem. 18 (2010) 1273-1279.

[86] C. Gnerre, U. Thull, P. Gaillard, P.A. Carrupt, B. Testa, E. Fernandes, F. Silva, M. Pinto, M.M.M. Pinto, J.L. Wolfender, K. Hostettmann, G. Cruciani, Natural and synthetic xanthones as monoamine oxidase inhibitors: Biological assay and 3D-QSAR, Helv. Chim. Acta 84 (2001) 552-570.

[87] F. Chimenti, R. Fioravanti, A. Bolasco, P. Chimenti, D. Secci, F. Rossi, M. Yanez, F. Orallo, F. Ortuso, S. Alcaro, Chalcones: a valid scaffold for monoamine oxidases inhibitors, J. Med. Chem. 52 (2009) 2818-2824.

[88] J.F. Chen, K. Xu, J.P. Petzer, R. Staal, Y.H. Xu, M. Beilstein, P.K. Sonsalla, K. Castagnoli, N. Castagnoli, Jr., M.A. Schwarzschild, Neuroprotection by caffeine and $A_{2A}$ adenosine receptor inactivation in a model of Parkinson's disease, J. Neurosci. 21 (2001) RC143.

[89] J.P. Petzer, S. Steyn, K.P. Castagnoli, J.F. Chen, M.A. Schwarzschild, C.J. Van der Schyf, N. Castagnoli, Inhibition of monoamine oxidase B by selective adenosine $A_{2A}$ receptor antagonists, Bioorg. Med. Chem. 11 (2003) 1299-1310.

[90] N. Castagnoli, Jr., J.P. Petzer, S. Steyn, K. Castagnoli, J.F. Chen, M.A. Schwarzschild, C.J. Van der Schyf, Monoamine oxidase B inhibition and neuroprotection: studies on selective adenosine $A_{2A}$ receptor antagonists, Neurology 61 (2003) S62-68.

[91] N. Vlok, S.F. Malan, N. Castagnoli, Jr., J.J. Bergh, J.P. Petzer, Inhibition of monoamine oxidase B by analogues of the adenosine $A_{2A}$ receptor antagonist (*E*)-8-(3-chlorostyryl)caffeine (CSC), Bioorg. Med. Chem. 14 (2006) 3512-3521.

[92] L.H. Prins, J.P. Petzer, S.F. Malan, Synthesis and in vitro evaluation of pteridine analogues as monoamine oxidase B and nitric oxide synthase inhibitors, Bioorg. Med. Chem. 17 (2009) 7523-7530.

[93] B. Strydom, S.F. Malan, N. Castagnoli, Jr., J.J. Bergh, J.P. Petzer, Inhibition of monoamine oxidase by 8-benzyloxycaffeine analogues, Bioorg. Med. Chem. 18 (2010) 1018-1028.

[94] C. Binda, F. Hubalek, M. Li, N. Castagnoli, D.E. Edmondson, A. Mattevi, Structure of the human mitochondrial monoamine oxidase B: new chemical implications for neuroprotectant drug design, Neurology 67 (2006) S5-7.

[95] R. Silvestri, G. La Regina, G. De Martino, M. Artico, O. Befani, M. Palumbo, E. Agostinelli, P. Turini, Simple, potent, and selective pyrrole inhibitors of monoamine oxidase types A and B, J. Med. Chem. 46 (2003) 917-920.

[96] G. La Regina, R. Silvestri, M. Artico, A. Lavecchia, E. Novellino, O. Befani, P. Turini, E. Agostinelli, New pyrrole inhibitors of monoamine oxidase: synthesis, biological evaluation, and structural determinants of MAO-A and MAO-B selectivity, J. Med. Chem. 50 (2007) 922-931.

[97] F. Manna, F. Chimenti, A. Bolasco, D. Secci, B. Bizzarri, O. Befani, P. Turini, B. Mondovi, S. Alcaro, A. Tafi, Inhibition of amine oxidases activity by 1-acetyl-3,5-diphenyl-4,5-dihydro-(1*H*)-pyrazole derivatives, Bioorg. Med. Chem. Lett. 12 (2002) 3629-3633.

[98] F. Chimenti, A. Bolasco, F. Manna, D. Secci, P. Chimenti, A. Granese, O. Befani, P. Turini, S. Alcaro, F. Ortuso, Synthesis and molecular modelling of novel substituted-4,5-dihydro-(1*H*)-pyrazole derivatives as potent and highly selective monoamine oxidase-A inhibitors, Chem. Biol. Drug Des. 67 (2006) 206-214.

[99] F. Chimenti, E. Maccioni, D. Secci, A. Bolasco, P. Chimenti, A. Granese, O. Befani, P. Turini, S. Alcaro, F. Ortuso, R. Cirilli, F. La Torre, M.C. Cardia, S. Distinto, Synthesis, molecular modeling studies, and selective inhibitory activity against monoamine oxidase of 1-
220

thiocarbamoyl-3,5-diaryl-4,5-dihydro-(1*H*)-pyrazole derivatives, J. Med. Chem. 48 (2005) 7113-7122.

[100] F. Chimenti, R. Fioravanti, A. Bolasco, F. Manna, P. Chimenti, D. Secci, F. Rossi, P. Turini, F. Ortuso, S. Alcaro, M.C. Cardia, Synthesis, molecular modeling studies and selective inhibitory activity against MAO of *N*1-propanoyl-3,5-diphenyl-4,5-dihydro-(1*H*)-pyrazole derivatives, Eur. J. Med. Chem. 43 (2008) 2262-2267.

[101] V. Jayaprakash, B.N. Sinha, G. Ucar, A. Ercan, Pyrazoline-based mycobactin analogues as MAO-inhibitors, Bioorg. Med. Chem. Lett. 18 (2008) 6362-6368.

[102] E. Palaska, F. Aydin, G. Ucar, D. Erol, Synthesis and monoamine oxidase inhibitory activities of 1-thiocarbamoyl-3,5-diphenyl-4,5-dihydro-1*H*-pyrazole derivatives, Arch. Pharm. 341 (2008) 209-215.

[103] N. Gokhan-Kelekci, O.O. Simsek, A. Ercan, K. Yelekci, Z.S. Sahin, S. Isik, G. Ucar, A.A. Bilgin, Synthesis and molecular modeling of some novel hexahydroindazole derivatives as potent monoamine oxidase inhibitors, Bioorg. Med. Chem. 17 (2009) 6761-6772.

[104] F. Chimenti, S. Carradori, D. Secci, A. Bolasco, B. Bizzarri, P. Chimenti, A. Granese, M. Yanez, F. Orallo, Synthesis and inhibitory activity against human monoamine oxidase of *N*1-thiocarbamoyl-3,5-di(hetero)aryl-4,5-dihydro-(1*H*)-pyrazole derivatives, Eur. J. Med. Chem. 45 (2010) 800-804.

[105] M. Karuppasamy, M. Mahapatra, S. Yabanoglu, G. Ucar, B.N. Sinha, A. Basu, N. Mishra, A. Sharon, U. Kulandaivelu, V. Jayaprakash, Development of selective and reversible pyrazoline based MAO-A inhibitors: Synthesis, biological evaluation and docking studies, Bioorg. Med. Chem. 18 (2010) 1875-1881.

[106] A. Sahoo, S. Yabanoglu, B.N. Sinha, G. Ucar, A. Basu, V. Jayaprakash, Towards development of selective and reversible pyrazoline based MAO-inhibitors: Synthesis, biological evaluation and docking studies, Bioorg. Med. Chem. Lett. 20 (2010) 132-136.

[107] F. Chimenti, E. Maccioni, D. Secci, A. Bolasco, P. Chimenti, A. Granese, S. Carradori, S. Alcaro, F. Ortuso, M. Yanez, F. Orallo, R. Cirilli, R. Ferretti, F. La Torre, Synthesis, stereochemical identification, and selective inhibitory activity against human monoamine oxidase-B of 2-methylcyclohexylidene-(4-arylthiazol-2-yl)hydrazones, J. Med. Chem. 51 (2008) 4874-4880.

[108] F. Chimenti, A. Bolasco, D. Secci, P. Chimenti, A. Granese, S. Carradori, M. Yanez, F. Orallo, F. Ortuso, S. Alcaro, Investigations on the 2-thiazolylhydrazyne scaffold: synthesis and molecular modeling of selective human monoamine oxidase inhibitors, Bioorg. Med. Chem. 18 (2010) 5715-5723.

[109] F. Chimenti, D. Secci, A. Bolasco, P. Chimenti, A. Granese, S. Carradori, M. Yanez, F. Orallo, M.L. Sanna, B. Gallinella, R. Cirilli, Synthesis, stereochemical separation, and biological evaluation of selective inhibitors of human MAO-B: 1-(4-arylthiazol-2-yl)-2-(3-methylcyclohexylidene)hydrazines, J. Med. Chem. 53 (2010) 6516-6520.

[110] L.P. Quinn, B. Crook, M.E. Hows, M. Vidgeon-Hart, H. Chapman, N. Upton, A.D. Medhurst, D.J. Virley, The PPARgamma agonist pioglitazone is effective in the MPTP mouse model of Parkinson's disease through inhibition of monoamine oxidase B, Br. J. Pharmacol. 154 (2008) 226-233.

[111] N. Schintu, L. Frau, M. Ibba, P. Caboni, A. Garau, E. Carboni, A.R. Carta, PPAR-gamma-mediated neuroprotection in a chronic mouse model of Parkinson's disease, Eur. J. Neurosci. 29 (2009) 954-963.

[112] W.J. Geldenhuys, A.S. Darvesh, M.O. Funk, C.J. Van der Schyf, R.T. Carroll, Identification of novel monoamine oxidase B inhibitors by structure-based virtual screening, Bioorg. Med. Chem. Lett. 20 (2010) 5295-5298.

[113] S.N. Khattab, S.Y. Hassan, A.A. Bekhit, A.M. El Massry, V. Langer, A. Amer, Synthesis of new series of quinoxaline based MAO-inhibitors and docking studies, Eur. J. Med. Chem. 45 (2010) 4479-4489.

[114] L. Shi, Y. Yang, Z.L. Li, Z.W. Zhu, C.H. Liu, H.L. Zhu, Design of novel nicotinamides as potent and selective monoamine oxidase a inhibitors, Bioorg. Med. Chem. 18 (2010) 1659-1664.

[115] A. Fierro, M. Osorio-Olivares, B.K. Cassels, D.E. Edmondson, S. Sepulveda-Boza, M. Reyes-Parada, Human and rat monoamine oxidase-A are differentially inhibited by (*S*)-4-alkylthioamphetamine derivatives: insights from molecular modeling studies, Bioorg. Med. Chem. 15 (2007) 5198-5206.

[116] S. Luhr, M. Vilches-Herrera, A. Fierro, R.R. Ramsay, D.E. Edmondson, M. Reyes-Parada, B.K. Cassels, P. Iturriaga-Vasquez, 2-Arylthiomorpholine derivatives as potent and selective monoamine oxidase B inhibitors, Bioorg. Med. Chem. 18 (2010) 1388-1395.

[117] F. Leonetti, C. Capaldi, L. Pisani, O. Nicolotti, G. Muncipinto, A. Stefanachi, S. Cellamare, C. Caccia, A. Carotti, Solid-phase synthesis and insights into structure-activity relationships of safinamide analogues as potent and selective inhibitors of type B monoamine oxidase, J. Med. Chem. 50 (2007) 4909-4916.

[118] T. Petersen, G.I. Papakostas, M.A. Posternak, A. Kant, W.M. Guyker, D.V. Iosifescu, A.S. Yeung, A.A. Nierenberg, M. Fava, Empirical testing of two models for staging antidepressant treatment resistance, J. Clin. Psychopharmacol. 25 (2005) 336-341.

[119] S. Hruschka, T.C. Rosen, S. Yoshida, K.L. Kirk, R. Frohlich, B. Wibbeling, G. Haufe, Fluorinated phenylcyclopropylamines. Part 5: Effects of electron-withdrawing or -donating aryl substituents on the inhibition of monoamine oxidases A and B by 2-aryl-2-fluoro-cyclopropylamines, Bioorg. Med. Chem. 16 (2008) 7148-7166.

[120] C. Binda, S. Valente, M. Romanenghi, S. Pilotto, R. Cirilli, A. Karytinos, G. Ciossani, O.A. Botrugno, F. Forneris, M. Tardugno, D.E. Edmondson, S. Minucci, A. Mattevi, A. Mai, Biochemical, structural, and biological evaluation of tranylcypromine derivatives as inhibitors of histone demethylases LSD1 and LSD2, J. Am. Chem. Soc. 132 (2010) 6827-6833.

[121] K. Matsuno, K. Takai, Y. Isaka, Y. Unno, M. Sato, O. Takikawa, A. Asai, S-benzylisothiourea derivatives as small-molecule inhibitors of indoleamine-2,3-dioxygenase, Bioorg. Med. Chem. Lett. 20 (2010) 5126-5129.

[122] D. Batabyal, S.R. Yeh, Human tryptophan dioxygenase: a comparison to indoleamine 2,3-dioxygenase, J. Am. Chem. Soc. 129 (2007) 15690-15701.

[123] G.J. Maghzal, S.R. Thomas, N.H. Hunt, R. Stocker, Cytochrome b5, not superoxide anion radical, is a major reductant of indoleamine 2,3-dioxygenase in human cells, J. Biol. Chem. 283 (2008) 12014-12025.

[124] M. Sono, M.P. Roach, E.D. Coulter, J.H. Dawson, Heme-Containing Oxygenases, Chem. Rev. 96 (1996) 2841-2888.

[125] T. Shimizu, S. Nomiyama, F. Hirata, O. Hayaishi, Indoleamine 2,3-dioxygenase. Purification and some properties, J. Biol. Chem. 253 (1978) 4700-4706.

[126] U.F. Rohrig, L. Awad, A. Grosdidier, P. Larrieu, V. Stroobant, D. Colau, V. Cerundolo, A.J. Simpson, P. Vogel, B.J. Van den Eynde, V. Zoete, O. Michielin, Rational design of indoleamine 2,3-dioxygenase inhibitors, J. Med. Chem. 53 (2010) 1172-1189.

[127] T.W. Stone, L.G. Darlington, Endogenous kynurenines as targets for drug discovery and development, Nat. Rev. Drug Discov. 1 (2002) 609-620.

[128] M. Salter, Selective Inhibitors of tryptophan 2,3-dioxygenase and combined inhibitors of tryptophan 2,3-dioxygenase and 5-HT reuptake as novel serotonergic antidepressants, CNS Drug Reviews 2 (1996) 127-143.

[129] O. Takikawa, Biochemical and medical aspects of the indoleamine 2,3-dioxygenase-initiated L-tryptophan metabolism, Biochem. Biophys. Res. Commun. 338 (2005) 12-19.

[130] M.W. Taylor, G.S. Feng, Relationship between interferon-gamma, indoleamine 2,3-dioxygenase, and tryptophan catabolism, Faseb J. 5 (1991) 2516-2522.

[131] A.L. Mellor, D.H. Munn, IDO expression by dendritic cells: tolerance and tryptophan catabolism, Nat. Rev. Immunol. 4 (2004) 762-774.

[132] E.R. Pfefferkorn, Interferon gamma blocks the growth of Toxoplasma gondii in human fibroblasts by inducing the host cells to degrade tryptophan, Proc. Natl. Acad. Sci. U.S.A. 81 (1984) 908-912.

[133] D.H. Munn, E. Shafizadeh, J.T. Attwood, I. Bondarev, A. Pashine, A.L. Mellor, Inhibition of T cell proliferation by macrophage tryptophan catabolism, J. Exp. Med. 189 (1999) 1363-1372.

[134] G. Frumento, R. Rotondo, M. Tonetti, G.B. Ferrara, T cell proliferation is blocked by indoleamine 2,3-dioxygenase, Transplant. Proc. 33 (2001) 428-430.

[135] D.H. Munn, M. Zhou, J.T. Attwood, I. Bondarev, S.J. Conway, B. Marshall, C. Brown, A.L. Mellor, Prevention of allogeneic fetal rejection by tryptophan catabolism, Science 281 (1998) 1191-1193.

[136] J.F. Baurain, P. Van der Bruggen, B.J. Van den Eynde, P.G. Coulie, N. Van Baren, General principles and first clinical trials of therapeutic vaccines against cancer, Bull. Cancer 95 (2008) 327-335.

[137] C. Uyttenhove, L. Pilotte, I. Theate, V. Stroobant, D. Colau, N. Parmentier, T. Boon, B.J. Van den Eynde, Evidence for a tumoral immune resistance mechanism based on tryptophan degradation by indoleamine 2,3-dioxygenase, Nat. Med. 9 (2003) 1269-1274.

[138] A.J. Muller, G.C. Prendergast, Marrying immunotherapy with chemotherapy: why say IDO?, Cancer Res. 65 (2005) 8065-8068.

[139] A.J. Muller, J.B. DuHadaway, P.S. Donover, E. Sutanto-Ward, G.C. Prendergast, Inhibition of indoleamine 2,3-dioxygenase, an immunoregulatory target of the cancer suppression gene Bin1, potentiates cancer chemotherapy, Nat. Med. 11 (2005) 312-319.

[140] G.J. Guillemin, B.J. Brew, C.E. Noonan, O. Takikawa, K.M. Cullen, Indoleamine 2,3 dioxygenase and quinolinic acid immunoreactivity in Alzheimer's disease hippocampus, Neuropathol. Appl. Neur. 31 (2005) 395-404.

[141] F. Leblhuber, J. Walli, K. Jellinger, G.P. Tilz, B. Widner, F. Laccone, D. Fuchs, Activated immune system in patients with Huntington's disease, Clin. Chem. Lab. Med. 36 (1998) 747-750.

[142] A.M. Myint, Y.K. Kim, Cytokine-serotonin interaction through IDO: a neurodegeneration hypothesis of depression, Med. Hypotheses 61 (2003) 519-525.

[143] S.J. Kerr, P.J. Armati, L.A. Pemberton, G. Smythe, B. Tattam, B.J. Brew, Kynurenine pathway inhibition reduces neurotoxicity of HIV-1-infected macrophages, Neurology 49 (1997) 1671-1681.

[144] H. Sugimoto, S.I. Oda, T. Otsuki, T. Hino, T. Yoshida, Y. Shiro, Crystal structure of human indoleamine 2,3-dioxygenase: Catalytic mechanism of $O_2$ incorporation by a heme-containing dioxygenase, Proc. Natl. Acad. Sci. U.S.A. 103 (2006) 2611-2616.

[145] A. Macchiarulo, R. Nuti, D. Bellocchi, E. Camaioni, R. Pellicciari, Molecular docking and spatial coarse graining simulations as tools to investigate substrate recognition, enhancer binding and conformational transitions in indoleamine-2,3-dioxygenase (IDO), Biochim. Biophys. Acta 1774 (2007) 1058-1068.

[146] D.Y. Hou, A.J. Muller, M.D. Sharma, J. DuHadaway, T. Banerjee, M. Johnson, A.L. Mellor, G.C. Prendergast, D.H. Munn, Inhibition of indoleamine 2,3-dioxygenase in dendritic cells by stereoisomers of 1-methyl-tryptophan correlates with antitumor responses, Cancer Res. 67 (2007) 792-801.

[147] J.B. Katz, A.J. Muller, G.C. Prendergast, Indoleamine 2,3-dioxygenase in T-cell tolerance and tumoral immune escape, Immunol. Rev. 222 (2008) 206-221.
224

[148] S.G. Cady, M. Sono, 1-Methyl-DL-tryptophan, $\beta$-(3-benzofuranyl)-DL-alanine (the oxygen analog of tryptophan), and beta-[3-benzo(*b*)thienyl]-DL-alanine (the sulfur analog of tryptophan) are competitive inhibitors for indoleamine 2,3-dioxygenase, Arch. Biochem. Biophys. 291 (1991) 326-333.

[149] R. Metz, J.B. Duhadaway, U. Kamasani, L. Laury-Kleintop, A.J. Muller, G.C. Prendergast, Novel tryptophan catabolic enzyme IDO2 is the preferred biochemical target of the antitumor indoleamine 2,3-dioxygenase inhibitory compound D-1-methyl-tryptophan, Cancer Res. 67 (2007) 7082-7087.

[150] S. Lob, A. Konigsrainer, Is IDO a key enzyme bridging the gap between tumor escape and tolerance induction?, Langenbecks Arch. Chir. 393 (2008) 995-1003.

[151] S. Lob, A. Konigsrainer, R. Schafer, H.G. Rammensee, G. Opelz, P. Terness, Levo- but not dextro-1-methyl tryptophan abrogates the IDO activity of human dendritic cells, Blood 111 (2008) 2152-2154.

[152] S. Lob, A. Konigsrainer, H.G. Rammensee, G. Opelz, P. Terness, Inhibitors of indoleamine-2,3-dioxygenase for cancer therapy: can we see the wood for the trees?, Nat. Rev. Cancer 9 (2009) 445-452.

[153] P. Gaspari, T. Banerjee, W.P. Malachowski, A.J. Muller, G.C. Prendergast, J. DuHadaway, S. Bennett, A.M. Donovan, Structure-activity study of brassinin derivatives as indoleamine 2,3-dioxygenase inhibitors, J. Med. Chem. 49 (2006) 684-692.

[154] E. Dolusic, P. Larrieu, S. Blanc, F. Sapunaric, J. Pouyez, L. Moineaux, D. Colette, V. Stroobant, L. Pilotte, D. Colau, T. Ferain, G. Fraser, M. Galleni, J.M. Frere, B. Masereel, B. Van den Eynde, J. Wouters, R. Frederick, Discovery and preliminary SARs of keto-indoles as novel indoleamine 2,3-dioxygenase (IDO) inhibitors, Eur. J. Med. Chem. 46 (2011) 3058-3065.

[155] E. Dolusic, P. Larrieu, S. Blanc, F. Sapunaric, B. Norberg, L. Moineaux, D. Colette, V. Stroobant, L. Pilotte, D. Colau, T. Ferain, G. Fraser, M. Galleni, J.M. Frere, B. Masereel, B. Van den Eynde, J. Wouters, R. Frederick, Indol-2-yl ethanones as novel indoleamine 2,3-dioxygenase (IDO) inhibitors, Bioorg. Med. Chem. 19 (2011) 1550-1561.

[156] A.C. Peterson, A.J. La Loggia, L.K. Hamaker, R.A. Arend, P.L. Fisette, Y. Ozaki, J.A. Will, R.R. Brown, J.M. Cook, Evaluation of substituted beta-carbolines as noncompetitive indoleamine 2,3-dioxygenase inhibitors, Med. Chem. Res. 7 (1993) 473-482.

[157] S. Kumar, D. Jaller, B. Patel, J.M. LaLonde, J.B. DuHadaway, W.P. Malachowski, G.C. Prendergast, A.J. Muller, Structure based development of phenylimidazole-derived inhibitors of indoleamine 2,3-dioxygenase, J. Med. Chem. 51 (2008) 4968-4977.

[158] S. Kumar, W.P. Malachowski, J.B. DuHadaway, J.M. LaLonde, P.J. Carroll, D. Jaller, R. Metz, G.C. Prendergast, A.J. Muller, Indoleamine 2,3-dioxygenase is the anticancer target for a novel series of potent naphthoquinone-based inhibitors, J. Med. Chem. 51 (2008) 1706-1718.

[159] G. Carr, M.K. Chung, A.G. Mauk, R.J. Andersen, Synthesis of indoleamine 2,3-dioxygenase inhibitory analogues of the sponge alkaloid exiguamine A, J. Med. Chem. 51 (2008) 2634-2637.

[160] E.W. Yue, B. Douty, B. Wayland, M. Bower, X. Liu, L. Leffet, Q. Wang, K.J. Bowman, M.J. Hansbury, C. Liu, M. Wei, Y. Li, R. Wynn, T.C. Burn, H.K. Koblish, J.S. Fridman, B. Metcalf, P.A. Scherle, A.P. Combs, Discovery of potent competitive inhibitors of indoleamine 2,3-dioxygenase with in vivo pharmacodynamic activity and efficacy in a mouse melanoma model, J. Med. Chem. 52 (2009) 7364-7367.

[161] Y. Zhang, D. Reinberg, Transcription regulation by histone methylation: interplay between different covalent modifications of the core histone tails, Genes Dev. 15 (2001) 2343-2360.

[162] R. Margueron, P. Trojer, D. Reinberg, The key to development: interpreting the histone code?, Curr. Opin. Genet. Dev. 15 (2005) 163-176.

[163] C. Martin, Y. Zhang, The diverse functions of histone lysine methylation, Nat. Rev. Mol. Cell Biol. 6 (2005) 838-849.

[164] F. Forneris, C. Binda, M.A. Vanoni, A. Mattevi, E. Battaglioli, Histone demethylation catalysed by LSD1 is a flavin-dependent oxidative process, FEBS Lett. 579 (2005) 2203-2207.

[165] F. Forneris, E. Battaglioli, A. Mattevi, C. Binda, New roles of flavoproteins in molecular cell biology: histone demethylase LSD1 and chromatin, FEBS J. 276 (2009) 4304-4312.

[166] X. Zhou, H. Ma, Evolutionary history of histone demethylase families: distinct evolutionary patterns suggest functional divergence, BMC Evol. Biol. 8 (2008) 294.

[167] J.C. Culhane, P.A. Cole, LSD1 and the chemistry of histone demethylation, Curr. Opin. Chem. Biol. 11 (2007) 561-568.

[168] S. Mimasu, T. Sengoku, S. Fukuzawa, T. Umehara, S. Yokoyama, Crystal structure of histone demethylase LSD1 and tranylcypromine at 2.25 A, Biochem. Biophys. Res. Commun. 366 (2008) 15-22.

[169] E. Metzger, M. Wissmann, N. Yin, J.M. Muller, R. Schneider, A.H. Peters, T. Gunther, R. Buettner, R. Schule, LSD1 demethylates repressive histone marks to promote androgen-receptor-dependent transcription, Nature 437 (2005) 436-439.

[170] J. Huang, R. Sengupta, A.B. Espejo, M.G. Lee, J.A. Dorsey, M. Richter, S. Opravil, R. Shiekhattar, M.T. Bedford, T. Jenuwein, S.L. Berger, p53 is regulated by the lysine demethylase LSD1, Nature 449 (2007) 105-108.

[171] J. Wang, S. Hevi, J.K. Kurash, H. Lei, F. Gay, J. Bajko, H. Su, W. Sun, H. Chang, G. Xu, F. Gaudet, E. Li, T. Chen, The lysine demethylase LSD1 (KDM1) is required for maintenance of global DNA methylation, Nat. Genet. 41 (2009) 125-129.

226

[172] Y. Wang, H. Zhang, Y. Chen, Y. Sun, F. Yang, W. Yu, J. Liang, L. Sun, X. Yang, L. Shi, R. Li, Y. Li, Y. Zhang, Q. Li, X. Yi, Y. Shang, LSD1 is a subunit of the NuRD complex and targets the metastasis programs in breast cancer, Cell 138 (2009) 660-672.

[173] Y. Huang, E. Greene, T. Murray Stewart, A.C. Goodwin, S.B. Baylin, P.M. Woster, R.A. Casero, Jr., Inhibition of lysine-specific demethylase 1 by polyamine analogues results in reexpression of aberrantly silenced genes, Proc. Natl. Acad. Sci. U.S.A. 104 (2007) 8023-8028.

[174] Y. Huang, T.M. Stewart, Y. Wu, S.B. Baylin, L.J. Marton, B. Perkins, R.J. Jones, P.M. Woster, R.A. Casero, Jr., Novel oligoamine analogues inhibit lysine-specific demethylase 1 and induce reexpression of epigenetically silenced genes, Clin. Cancer Res. 15 (2009) 7217-7228.

[175] Y. Liang, J.L. Vogel, A. Narayanan, H. Peng, T.M. Kristie, Inhibition of the histone demethylase LSD1 blocks alpha-herpesvirus lytic replication and reactivation from latency, Nat. Med. 15 (2009) 1312-1317.

[176] P. Stavropoulos, G. Blobel, A. Hoelz, Crystal structure and mechanism of human lysine-specific demethylase-1, Nat. Struct. Mol. Biol. 13 (2006) 626-632.

[177] M. Yang, C.B. Gocke, X. Luo, D. Borek, D.R. Tomchick, M. Machius, Z. Otwinowski, H. Yu, Structural basis for CoREST-dependent demethylation of nucleosomes by the human LSD1 histone demethylase, Mol. Cell 23 (2006) 377-387.

[178] Y. Chen, Y. Yang, F. Wang, K. Wan, K. Yamane, Y. Zhang, M. Lei, Crystal structure of human histone lysine-specific demethylase 1 (LSD1), Proc. Natl. Acad. Sci. U.S.A. 103 (2006) 13956-13961.

[179] F. Forneris, C. Binda, A. Adamo, E. Battaglioli, A. Mattevi, Structural basis of LSD1-CoREST selectivity in histone H3 recognition, J. Biol. Chem. 282 (2007) 20070-20074.

[180] R. Baron, C. Binda, M. Tortorici, J.A. McCammon, A. Mattevi, Molecular mimicry and ligand recognition in binding and catalysis by the histone demethylase LSD1-CoREST complex, Structure 19 (2011) 212-220.

[181] M. Yang, J.C. Culhane, L.M. Szewczuk, P. Jalili, H.L. Ball, M. Machius, P.A. Cole, H. Yu, Structural basis for the inhibition of the LSD1 histone demethylase by the antidepressant trans-2-phenylcyclopropylamine, Biochemistry 46 (2007) 8058-8065.

[182] S. Mimasu, N. Umezawa, S. Sato, T. Higuchi, T. Umehara, S. Yokoyama, Structurally designed trans-2-phenylcyclopropylamine derivatives potently inhibit histone demethylase LSD1/KDM1, Biochemistry 49 (2010) 6494-6503.

[183] M. Yang, J.C. Culhane, L.M. Szewczuk, C.B. Gocke, C.A. Brautigam, D.R. Tomchick, M. Machius, P.A. Cole, H. Yu, Structural basis of histone demethylation by LSD1 revealed by suicide inactivation, Nat. Struct. Mol. Biol. 14 (2007) 535-539.

[184] H. Hou, H. Yu, Structural insights into histone lysine demethylation, Curr. Opin. Struct. Biol. 20 (2010) 739-748.
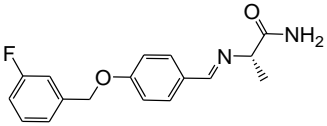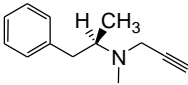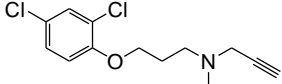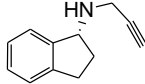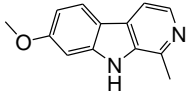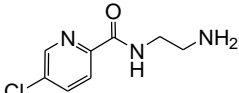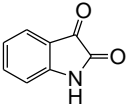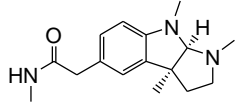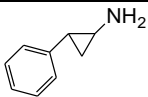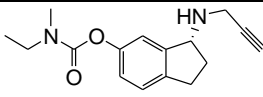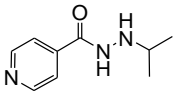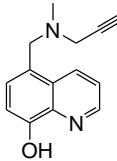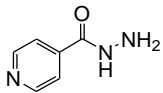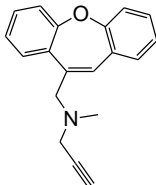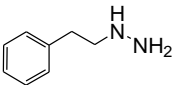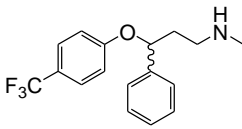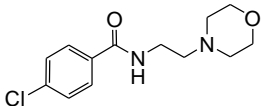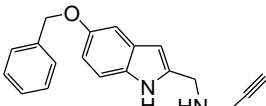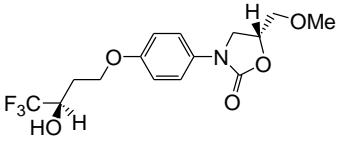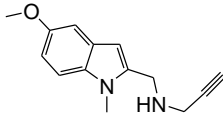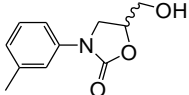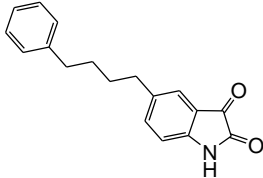
[185] D.M. Gooden, D.M. Schmidt, J.A. Pollock, A.M. Kabadi, D.G. McCafferty, Facile synthesis of substituted *trans*-2-arylcyclopropylamine inhibitors of the human histone demethylase LSD1 and monoamine oxidases A and B, Bioorg. Med. Chem. Lett. 18 (2008) 3047-3051.

[186] R.J. Klose, Y. Zhang, Regulation of histone methylation by demethylimination and demethylation, Nat. Rev. Mol. Cell Biol. 8 (2007) 307-318.

[187] F. Forneris, C. Binda, E. Battaglioli, A. Mattevi, LSD1: oxidative chemistry for multifaceted functions in chromatin regulation, Trends Biochem. Sci. 33 (2008) 181-189.

[188] M.G. Lee, C. Wynder, D.M. Schmidt, D.G. McCafferty, R. Shiekhattar, Histone H3 lysine 4 demethylation is a target of nonselective antidepressive medications, Chem. Biol. 13 (2006) 563-567.

[189] J.C. Culhane, L.M. Szewczuk, X. Liu, G. Da, R. Marmorstein, P.A. Cole, A mechanism-based inactivator for histone demethylase LSD1, J. Am. Chem. Soc. 128 (2006) 4536-4537.

[190] J.C. Culhane, D. Wang, P.M. Yen, P.A. Cole, Comparative analysis of small molecules and histone substrate analogues as LSD1 lysine demethylase inhibitors, J. Am. Chem. Soc. 132 (2010) 3164-3176.

[191] R. Ueda, T. Suzuki, K. Mino, H. Tsumoto, H. Nakagawa, M. Hasegawa, R. Sasaki, T. Mizukami, N. Miyata, Identification of cell-active lysine specific demethylase 1-selective inhibitors, J. Am. Chem. Soc. 131 (2009) 17536-17537.

[192] Y. Cheng, W.H. Prusoff, Relationship between the inhibition constant ($K_i$) and the concentration of inhibitor which causes 50 per cent inhibition ($I_{50}$) of an enzymatic reaction, Biochem. Pharmacol. 22 (1973) 3099-3108.

[193] Y. Song, J. Wang, S.F. Teng, D. Kesuma, Y. Deng, J. Duan, J.H. Wang, R.Z. Qi, M.M. Sim, Beta-carbolines as specific inhibitors of cyclin-dependent kinases, Bioorg. Med. Chem. Lett. 12 (2002) 1129-1132.

[194] M.P. Valley, W. Zhou, E.M. Hawkins, J. Shultz, J.J. Cali, T. Worzella, L. Bernad, T. Good, D. Good, T.L. Riss, D.H. Klaubert, K.V. Wood, A bioluminescent assay for monoamine oxidase activity, Anal. Biochem. 359 (2006) 238-246.

[195] A. Holt, D.F. Sharman, G.B. Baker, M.M. Palcic, A continuous spectrophotometric assay for monoamine oxidase and related enzymes in tissue homogenates, Anal. Biochem. 244 (1997) 384-392.

[196] M. Zhou, N. Panchuk-Voloshina, A one-step fluorometric method for the continuous measurement of monoamine oxidase activity, Anal. Biochem. 253 (1997) 169-174.

[197] E. Dolusic, P. Larrieu, L. Moineaux, V. Stroobant, L. Pilotte, D. Colau, L. Pochet, B. Van den Eynde, B. Masereel, J. Wouters, R. Frederick, Tryptophan 2,3-Dioxygenase (TDO) Inhibitors. 3-(2-(Pyridyl)ethenyl)indoles as Potential Anticancer Immunomodulators, J. Med. Chem. 54 (2011) 5320-5334.

228

[198] O. Takikawa, T. Kuroiwa, F. Yamazaki, R. Kido, Mechanism of interferon-gamma action. Characterization of indoleamine 2,3-dioxygenase in cultured human cells induced by interferon-gamma and evaluation of the enzyme-mediated tryptophan degradation in its anticellular activity, J. Biol. Chem. 263 (1988) 2041-2048.

[199] J.C. Pinkert, R.W. Clark, J.N. Burstyn, Modeling proline ligation in the heme-dependent CO sensor, CooA, using small-molecule analogs, J. Biol. Inorg. Chem. 11 (2006) 642-650.

[200] R.T. Coutts, R.G. Micetich, G.B. Baker, A. Benderly, T. Dewhurst, T.W. Hall, A.R. Locock, J. Pyrozko, Some 3-carboxamides of beta-carboline and tetrahydro-beta-carboline, Heterocycles 22 (1984) 131-142.

[201] A. Tsotinis, A. Eleutheriades, K.A. Hough, K. Davidson, D. Sugden, Design, synthesis and melatoninergic potency of new *N*-acyl 8,9-dihydro-4-methoxy-7*H*-2-benzo[de]quinolinalkanamines, Bioorg. Chem. 35 (2007) 189-204.

[202] V. Kogan, Preparation of pyrido[3,4-*b*]indoles and pyrimido[4,5-*b*]benzo[*d*]thiophen-4-ones as serotonergic and dopaminergic agents, PCT Int. Appl., (2008).

[203] M.S. Allen, Y.C. Tan, M.L. Trudell, K. Narayanan, L.R. Schindler, M.J. Martin, C. Schultz, T.J. Hagen, K.F. Koehler, P.W. Codding, et al., Synthetic and computer-assisted analyses of the pharmacophore for the benzodiazepine receptor inverse agonist site, J. Med. Chem. 33 (1990) 2343-2357.

[204] K. Takasu, T. Shimogama, C. Saiin, H.S. Kim, Y. Wataya, R. Brun, M. Ihara, Synthesis and evaluation of beta-carbolinium cations as new antimalarial agents based on pi-delocalized lipophilic cation (DLC) hypothesis, Chem. Pharm. Bull. 53 (2005) 653-661.

[205] M. Node, M. Ozeki, L. Planas, M. Nakano, H. Takita, D. Mori, S. Tamatani, T. Kajimoto, Efficient asymmetric synthesis of abeo-abietane-type diterpenoids by using the intramolecular Heck reaction, J. Org. Chem. 75 (2010) 190-196.

[206] M. Congreve, D. Aharony, J. Albert, O. Callaghan, J. Campbell, R.A. Carr, G. Chessari, S. Cowan, P.D. Edwards, M. Frederickson, R. McMenamin, C.W. Murray, S. Patel, N. Wallis, Application of fragment screening by X-ray crystallography to the discovery of aminopyridines as inhibitors of beta-secretase, J. Med. Chem. 50 (2007) 1124-1132.

[207] D.K. Tiwari, V.K. Gumaste, A.R.A.S. Deshmukh, Azetidinedione synthon for stereoselective synthesis of *cis*- and *trans*-C-3-alkyl/aryl azetidin-2-ones, Synthesis 1 (2006) 115-122.

[208] M. Salter, R. Hazelwood, C.I. Pogson, R. Iyer, D.J. Madge, The effects of a novel and selective inhibitor of tryptophan 2,3-dioxygenase on tryptophan and serotonin metabolism in the rat, Biochem. Pharmacol. 49 (1995) 1435-1442.

[209] V. Perez, J.L. Marco, E. Fernandez-Alvarez, M. Unzeta, Relevance of benzyloxy group in 2-indolyl methylamines in the selective MAO-B inhibition, Br. J. Pharmacol. 127 (1999) 869-876.
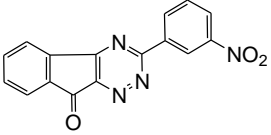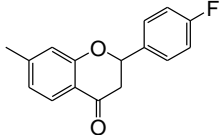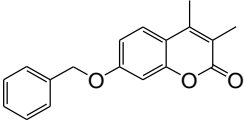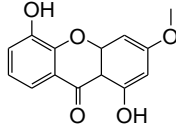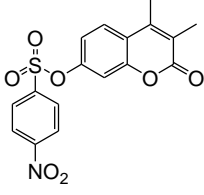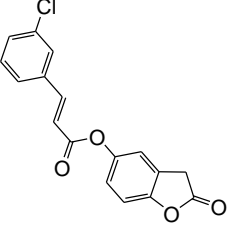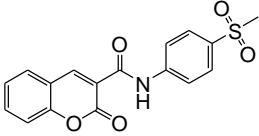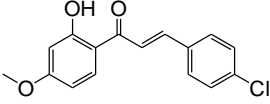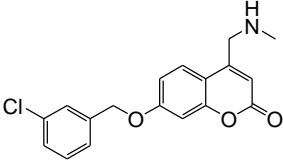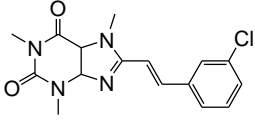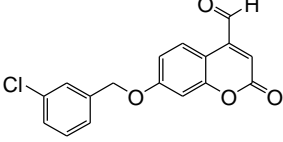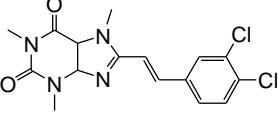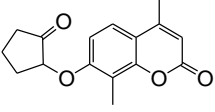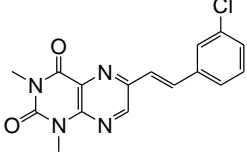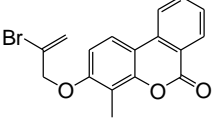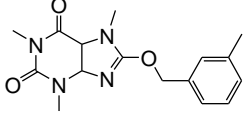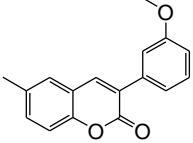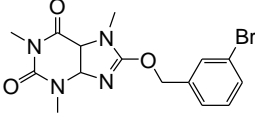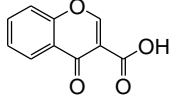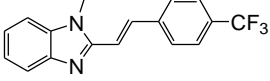
[210] T.A.K. Al-Allaf, L.J. Rashan, Synthesis and cytotoxic evaluation of the first *trans*-palladium(II) complex with naturally occurring alkaloid harmine, Eur. J. Med. Chem. 33 (1998) 817-820.

[211] J. Ishida, H.K. Wang, K.F. Bastow, C.Q. Hu, K.H. Lee, Antitumor agents 201. Cytotoxicity of harmine and beta-carboline analogs, Bioorg. Med. Chem. Lett. 9 (1999) 3319-3324.

[212] R. Cao, W. Peng, H. Chen, Y. Ma, X. Liu, X. Hou, H. Guan, A. Xu, DNA binding properties of 9-substituted harmine derivatives, Biochem. Biophys. Res. Commun. 338 (2005) 1557-1563.

[213] R. Cao, W. Yi, Q. Wu, X. Guan, M. Feng, C. Ma, Z. Chen, H. Song, W. Peng, Synthesis and cytotoxic activities of 1-benzylidine substituted beta-carboline derivatives, Bioorg. Med. Chem. Lett. 18 (2008) 6558-6561.

[214] T.P. Hamsa, G. Kuttan, Harmine inhibits tumour specific neo-vessel formation by regulating VEGF, MMP, TIMP and pro-inflammatory mediators both in vivo and in vitro, Eur. J. Pharmacol. 649 (2010) 64-73.

[215] R. Cao, Q. Chen, X. Hou, H. Chen, H. Guan, Y. Ma, W. Peng, A. Xu, Synthesis, acute toxicities, and antitumor effects of novel 9-substituted beta-carboline derivatives, Bioorg. Med. Chem. 12 (2004) 4613-4623.

[216] D. Frost, B. Meechoovet, T. Wang, S. Gately, M. Giorgetti, I. Shcherbakova, T. Dunckley, β-carboline compounds, including harmine, inhibit DYRK1A and tau phosphorylation at multiple Alzheimer's disease-related sites, PLoS One 6 (2011) e19264.

[217] N. Gockler, G. Jofre, C. Papadopoulos, U. Soppa, F.J. Tejedor, W. Becker, Harmine specifically inhibits protein kinase DYRK1A and interferes with neurite formation, FEBS J. 276 (2009) 6324-6337.

[218] A. Seifert, L.A. Allan, P.R. Clarke, DYRK1A phosphorylates caspase 9 at an inhibitory site and is potently inhibited in human cells by harmine, FEBS J. 275 (2008) 6268-6280.

[219] M.B. Youdim, M. Weinstock, Molecular basis of neuroprotective activities of rasagiline and the anti-Alzheimer drug TV3326 [(*N*-propargyl-(3*R*)aminoindan-5-YL)-ethyl methyl carbamate], Cell. Mol. Neurobiol. 21 (2001) 555-573.

[220] A. Altomare, G. Cascarano, C. Giacovazzo, A. Guagliardi, Completion and refinement of crystal-structures with Sir92, J. Appl. Crystal. 26 (1993) 343-350.

[221] G.M. Sheldrick, A short history of SHELX, Acta Crystallogr A 64 (2008) 112-122.

[222] A.L. Spek, PLATON, A multipurpose crystallographic tool, Utrecht University, The Netherlands, (2004).

[223] R.A. Copeland, Evaluation of enzyme inhibitors in drug discovery: a guide for medicinal chemists and pharmacologists (Methods of Biochemical Analysis), Wiley, Hoboken, New Jersey (2005).

230

# APPENDIX
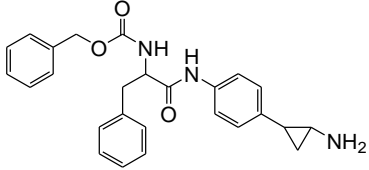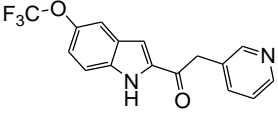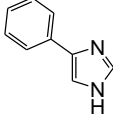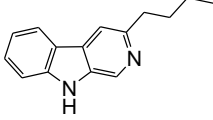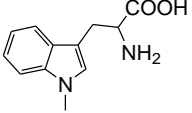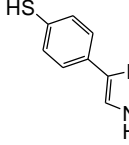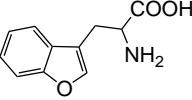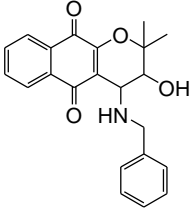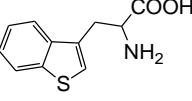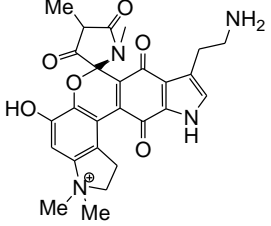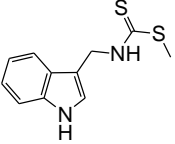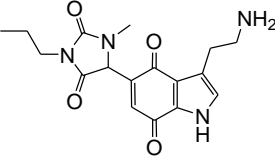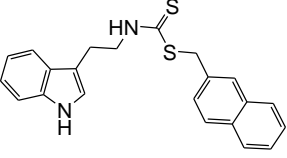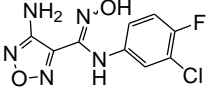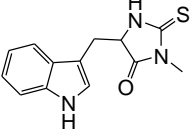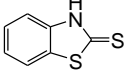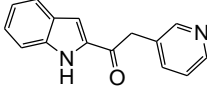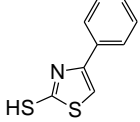
## LISTING OF COMPOUNDS
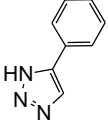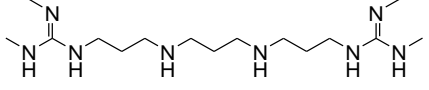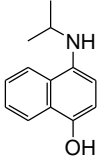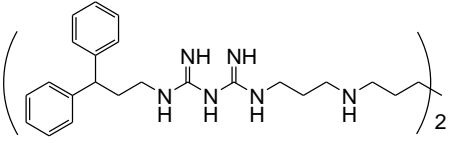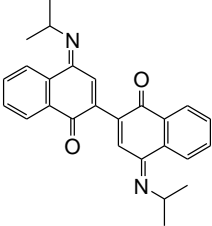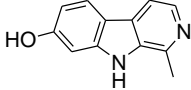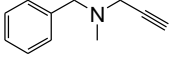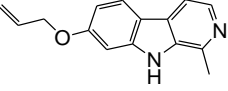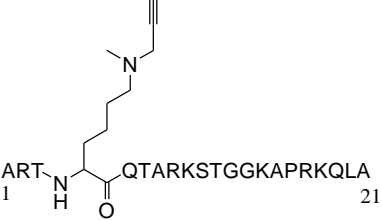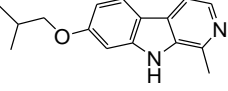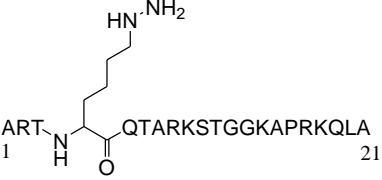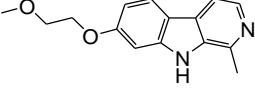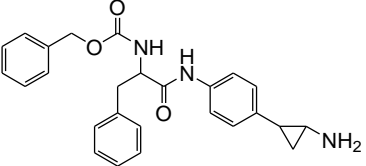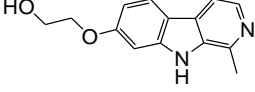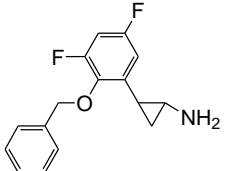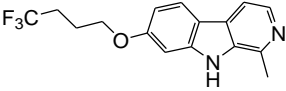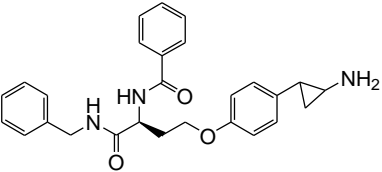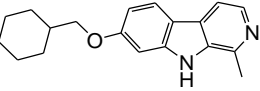
| | | | |
|---|---|---|---|
| **1.I** |  | **12.I** |  |
| **2.I** |  | **13.I** |  |
| **3.I** |  | **14.I** |  |
| **4.I** |  | **15.I** |  |
| **5.I** |  | **16.I** |  |
| **6.I** |  | **17.I** |  |
| **7.I** |  | **18.I** |  |
| **8.I** |  | **19.I** |  |
| **9.I** |  | **20a.I** |  |
| **10.I** |  | **20b.I** |  |
| **11.I** |  | **20c.I** |  |

| | | | |
|---|---|---|---|
| **20d.I** |  | **22e.I** |  |
| **20e.I** |  | **22f.I** |  |
| **20f.I** |  | **22g.I** |  |
| **21a.I** |  | **22h.I** |  |
| **21b.I** |  | **22i.I** |  |
| **21c.I** |  | **22j.I** |  |
| **21d.I** |  | **22k.I** |  |
| **22a.I** |  | **22l.I** |  |
| **22b.I** |  | **22m.I** |  |
| **22c.I** |  | **23a.I** |  |
| **22d.I** |  | **23b.I** |  |

| | | | |
|---|---|---|---|
| **23c.I** |  | **25b.I** |  |
| **24a.I** |  | **25c.I** |  |
| **24b.I** |  | **26.I** |  |
| **24c.I** |  | **27.I** |  |
| **24d.I** |  | **28a.I** |  |
| **24e.I** |  | **28b.I** |  |
| **24f.I** |  | **28c.I** |  |
| **24g.I** |  | **28d.I** |  |
| **24h.I** |  | **28e.I** |  |
| **25a.I** |  | **28f.I** |  |

| | | | |
|---|---|---|---|
| **29a.I** | | **31c.I** | |
| **29b.I** | | **32.I** | |
| **29c.I** | | **33a.I** | |
| **29d.I** | | **33b.I** | |
| **29e.I** | | **34a.I** | |
| **29f.I** | | **34b.I** | |
| **29g.I** | | **35a.I** | |
| **30a.I** | | **35b.I** | |
| **30b.I** | | **36a.I** | |
| **31a.I** | | **36b.I** | |
| **31b.I** | | **36c.I** | |

| | | | |
|---|---|---|---|
| **36d.I** | NH, O, H, N, O, NH₂ | **45.I** | F₃C-O, N, H, O, N |
| **37.I** | Phenyl, N, N, H | **46.I** | N, H |
| **38.I** | COOH, NH₂, N, Me | **47.I** | HS, N, H |
| **39.I** | COOH, NH₂, O | **48.I** | O, O, OH, O, HN |
| **40.I** | COOH, NH₂, S | **49.I** | Me, O, N, O, O, O, HO, N, H, O, NH₂, Me, N⁺, Me |
| **41.I** | S, S, NH, N, H | **50.I** | O, N, Me, O, O, O, N, H, NH₂ |
| **42.I** | HN, S, S, N, H | **51.I** | NH₂, N·OH, N, O, N, H, F, Cl |
| **43.I** | H, N, S, N, Me, O, N, H | **52.I** | H, N, S, S |
| **44.I** | N, H, O, N | **53.I** | N, HS, S |

| | | | |
|---|---|---|---|
| **54.I** |  | **63.I** |  |
| **55.I** |  | **64.I** |  |
| **56.I** |  | **1.III** | <br>HBr. 2H$_2$O |
| **57.I** |  | **2a.III** |  |
| **58.I** | <br>ART—NH ... QTARKSTGGKAPRKQLA<br>1 ... 21 | **2b.III** |  |
| **59.I** | <br>ART—NH ... QTARKSTGGKAPRKQLA<br>1 ... 21 | **2c.III** |  |
| **60.I** |  | **2d.III** |  |
| **61.I** |  | **2e.III** |  |
| **62.I** |  | **2f.III** |  |

| | | | |
|---|---|---|---|
| **2g.III** |  | **5.III** |  |
| **2h.III** |  | **6.III** |  |
| **2i.III** |  | **7.III** |  |
| **2j.III** |  | **8.III** |  |
| **2k.III** |  | **9.III** |  |
| **2l.III** |  | **10.III** |  |
| **2m.III** |  | **11.III** |  |
| **2n.III** |  | **12.III** |  |
| **2o.III** |  | **13.III** |  |
| **3.III** |  | **14.III** |  |
| **4.III** |  | **15.III** |  |

| | | | |
|---|---|---|---|
| **16.III** |  | **25b.III** |  |
| **17.III** |  | **25c.III** |  |
| **18.III** |  | **26a.III** |  |
| **19.III** |  | **26b.III** |  |
| **20.III** |  | **26c.III** |  |
| **21.III** |  | **27a.III** |  |
| **22.III** |  | **27b.III** |  |
| **23.III** |  | **27c.III** |  |
| **24.III** |  | **28a.III** |  |
| **25a.III** |  | **28b.III** |  |

| | | | |
|---|---|---|---|
| 29.III | | 37.III | |
| 30a.III | | 38.III | |
| 30b.III | | 39.III | |
| 31.III | | 40.III | |
| 32.III | | 41.III | |
| 33.III | | 42.III | |
| 34.III | | 43.III | |
| 35.III | | 44.III | |
| 36.III | | 45.III | |

| 46.III |  | 1.IV |  |
|---|---|---|---|
| 47.III |  | 2.IV |  |
| 48.III |  | 3.IV |  |
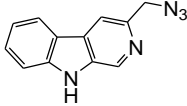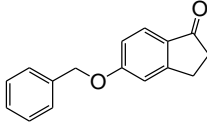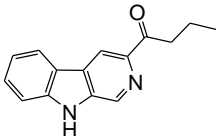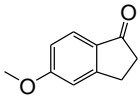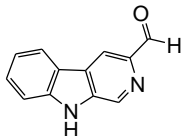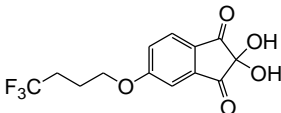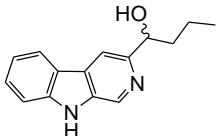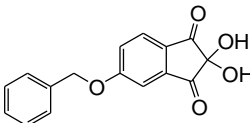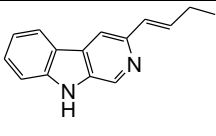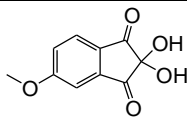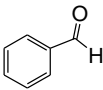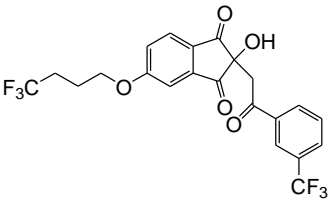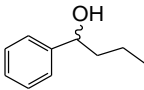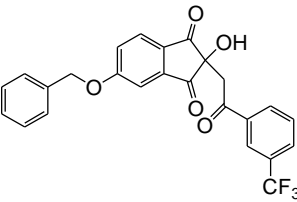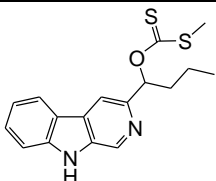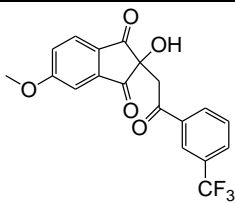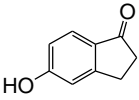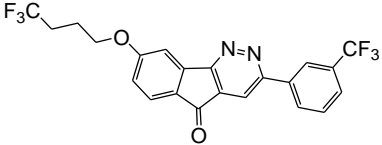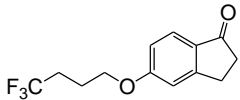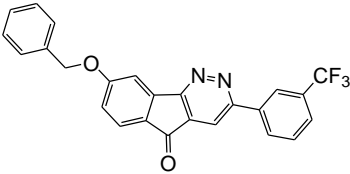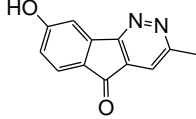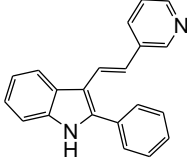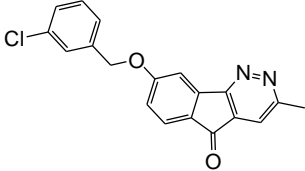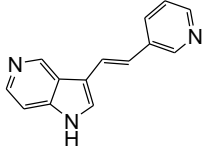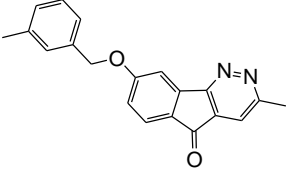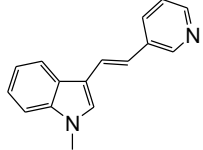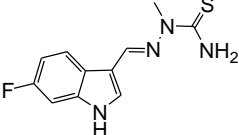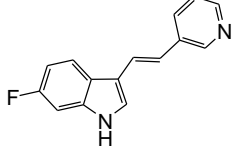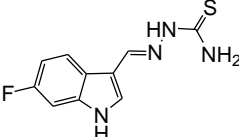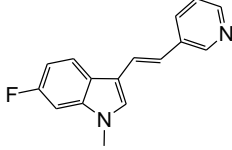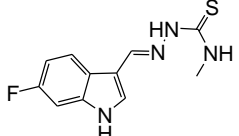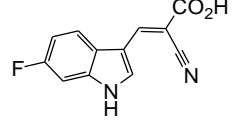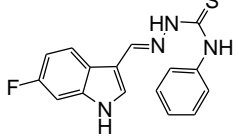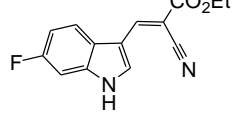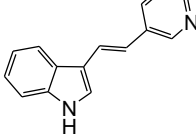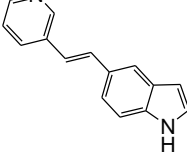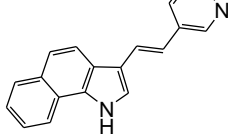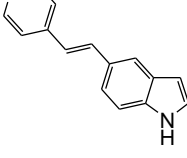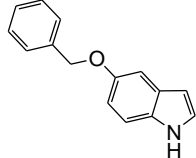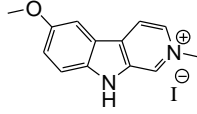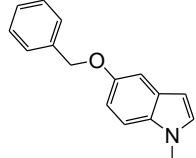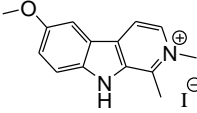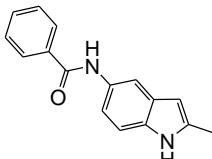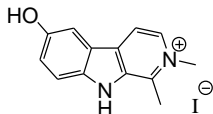
The studies performed during this thesis led to the publication of an article in *Bioorganic and Medicinal Chemistry* relating the results of β-carbolines on MAO and a patent including the results of β-carbolines in the treatment of proliferative disorders ;

- J. Reniers, S. Robert, R. Frederick, B. Masereel, S. Vincent, J. Wouters, Synthesis and evaluation of β-carboline derivatives as potential monoamine oxidase inhibitors, Bioorg. Med. Chem. 19 (2011) 134-144.

- R. Frederick, B. Masereel, J. Reniers, J. Wouters, C. Bruyere, R. Kiss, Beta-carbolines derivatives useful in the treatment of proliferative disorders, PCT/EP2010/059083 and US/61/358,609.

Another article relating the results of 5*H*-indeno[1,2-*c*]pyridazin-5-one derivatives on MAO and IDO is on revision in *European Journal of Medicinal Chemistry* ;

- J. Reniers, C. Meinguet, L. Moineaux, B. Masereel, S. P. Vincent, R. Frederick, J. Wouters, Synthesis and inhibition study of monoamine oxidase, indoleamine 2,3-dioxygenase and tryptophan 2,3-dioxygenase by 3,8-substituted 5*H*-indeno[1,2-*c*]pyridazin-5-one derivatives, Eur. J. Med. Chem, article in revision.